Regulation of chemokine receptor expression and function on $CD4^+$ T lymphocytes during central nervous system inflammation

Rachel Elizabeth Kohler, B.Sc. (Hons.)

Discipline of Microbiology and Immunology,
School of Molecular and Biomedical Sciences,
University of Adelaide

A thesis submitted to University of Adelaide in fulfillment of the requirements for the degree of Doctor of Philosophy

November 2003

THE UNIVERSITY OF ADELAIDE
AUSTRALIA

SUB CRUCE LUMEN

This thesis is dedicated to my mother Margaret and to my sister Jacqui

I feel privileged to have such admirable women guide me through life

Statement of originality

This thesis contains no material which has been accepted for the award of any other degree or diploma in any university or other tertiary institution, and to the best of my knowledge, contains no material previously published or written by another person, except where due reference has been made.

I consent to this copy of my thesis, when deposited in the University Library, being made available for photocopying and loan.

Rachel Elizabeth Kohler, B.Sc. (Hons)

11th November 2003

Abstract

Chemokines are a family of cytokines that exhibit selective chemoattractant properties for target leukocytes, including $CD4^+$ T lymphocytes, and play a significant role leukocyte migration. However, a target leukocyte can only respond to a chemokine if it expresses the cognate receptor(s). Recent studies have demonstrated alterations in both chemokine and chemokine receptor expression patterns in the CNS during experimental autoimmune encephalomyelitis (EAE), a model for Multiple Sclerosis. Accordingly, the aim of the research presented in this thesis was to investigate chemokine receptor regulation and function on $CD4^+$ T lymphocytes during T cell-mediated central nervous system (CNS) inflammation *in vivo*. In the proteolipid protein (PLP)-induced model of EAE, two inflammatory (CXCR3 and CCR5) and one supposedly homeostatic (CXCR4) chemokine receptors were upregulated on $CD4^+$ T cells during antigen-dependent clonal selection in the draining lymph nodes. As the $CD4^+$ T cells migrated through the blood and into the CNS tissue, expression of these receptors remained elevated such that, at the peak of clinical disease, the majority of neuroantigen-specific $CD4^+$ T cells in the CNS expressed elevated levels of CXCR4, CXCR3 and CCR5. Detailed characterisation of these receptors revealed that upregulation occurred in co-ordination with cellular division.

Subsequent experiments were performed in order to determine the biological consequences of specific chemokine/receptor interactions during EAE. Amino terminal modifications of chemokines, which convert agonists to antagonists, have previously been shown to interfere with ligand/receptor interactions during inflammation. Therefore, a series of synthetic N-terminal chemokine mutants were initially tested *in vitro* for their ability to act as antagonists in preventing the migration of neuroantigen-activated lymphocytes to ligands of the receptors CXCR4, CXCR3 and CCR5. These analyses revealed that the synthetic mutants SDF-1 P2G, I-TAC 4-79 and RANTES 9-68 possessed potent antagonistic capacities. Following EAE induction, treatment every second day with the antagonists until day 15 resulted in a significant decrease in the severity of the neurological symptoms of EAE. Histological analyses demonstrated that the reduction in disease severity corresponded with a reduced number of inflammatory infiltrates in the spinal cords of antagonist-treated mice at peak clinical disease compared with control-treated mice.

The ability to separate the disease process into two separate phases (sensitisation and effector) using adoptive transfer experiments provided a means to investigate the temporal and spatial control that specific chemokine/receptor interactions exerted during the pathogenesis of EAE. Accordingly, a series of *ex vivo* proliferation assays and adoptive transfer experiments were conducted. From these experiments, a potential role for the SDF-1/CXCR4 interaction was identified in the sensistisation phase of the disease. These results indicated that SDF-1/CXCL12 and CXCR4 interactions not only play a role in homeostasis, but may also provide costimulatory signals to antigen-stimulated $CD4^+$ T cells. Converely, roles for I-TAC/CXCR3 and RANTES/CCR5 interactions, but not SDF-1/CXCR4 interactions were identified in the effector phase of EAE. Collectively, the results generated in the present thesis, together with those from other studies, enabled the construction of a model detailing the temporal and spatial parameters of chemokine/chemokine receptor regulation of $CD4^+$ T cell activation and migration during a $CD4^+$ T cell-mediated immune response in the CNS.

Acknowledgements

I would firstly like to extend my sincere gratitude to Associate Professor Shaun McColl for providing me the opportunity to undertake such an interesting project. Your scientific knowledge, support and encouragement have been invaluable and have allowed me to grow as a scientist in the most enjoyable of environments. Thank you also for the amount of time that you have spent editing this thesis. Many thanks also to the laboratory of Pr. Ian Clark-Lewis at the University of British Columbia, Vancouver. Without the collaboration, this work would not have been possible. From the Neuroscience Research Unit at Woden Hospital, Canberra, I extend my thanks to Drs. David Willenborg and Maria Staykova. Your expert advice over the years has been greatly appreciated (now you can officially call me Dr. Rachet!).

A big thank you must also go to my fellow lab members, both past and present: Dr. Lisa Ebert (my Yoda); Dr. Sumone Chakravarti (my confidant and friend); Dr. Olivier Fahy (the crazy Frenchman! Thank you for our daily conversations- scientific discussions, of course- and for your friendship); and to my fellow PhD students, Kate (my editor, personal IT technician and friend, words cannot say how grateful I am for all of your help) and Jane (thank you for making me laugh, even in the most stressful of times), good luck in the future girls! To Adriana, Felicity, Jeremy, Scott, Marina, Koi and Sharon, thank you for your technical help, your constructive criticism and for allowing me to take over the computer for the last 3 months- you can definitely have it back now- I don't want it anymore!!! From the department of Molecular Biosciences I wish to acknowledge Gail Bezuidenhoudt, Tony Richardson, Shelley Pezy, and Sharon Koltze for always being willing to help, even when I have left matters to the last minute.

To all of my magnificent friends, Jo, Elaine, Mikey, Tiff, Justin, Natasha, Olivia, Ben, Bec, Ned, Trudy, Mason, Sumone, Kieran, Kath, Steve, Frenchie, Rache, Ollie and Annika - thank you for all your wonderful support over the years – it's finally over!!! But do we really need an excuse to party?!!!

To my greatest supporters – my family. To Mum and John, I thank you unconditionally for everything. Thankyou for teaching me, by example, how to explore my own interests with strength and determination. To Dad and Lancia, you may not live in this country, but I feel the support and love through the phone lines every time we speak, and for this I thank you both. To Jacqui and Mark, thank you for the daily conversations when writing up and keeping me sane in the direst of times. Good luck for your thesis Jac, I'm sure you will blitz it! (By the way, my thesis is 200 pages ------ double-spaced!!!!).

Finally, the biggest thanks of all are reserved for Tom (Duth). I thank you for helping me far beyond the call of duty, for making no demands on my time, for looking after me, and for your unwavering support and faith in my ability. Your exuding charisma and wealth of knowledge are characteristics to which I can only endeavour. You are my inspiration. THANK YOU for being you.

Publications arising from this thesis

Rachel E. Kohler, Adriana C. Caon, David O. Willenborg, Ian Clark-Lewis & Shaun R. McColl. 2003. A role for Macrophage Inflammatory Protein (MIP)-3α/CC Chemokine Ligand 20 in Immune Priming during T Cell-Mediated Inflammation of the Central Nervous System. *J. Immunol., 170: 6298-6306.*

Rachel E. Kohler, Ian Clark-Lewis & Shaun R. McColl. Distinct Roles for Chemokine Receptors CXCR3 and CXCR4 in the Generation of T cell- Dependent Inflammation of the Central Nervous System. *Manuscript in preparation.*

Rachel E. Kohler, Ian Clark-Lewis & Shaun R. McColl. Antagonism of Chemokine Receptors CCR1 and CCR5 Inhibits the Effector Phase of Experimental Autoimmune Encephalomyelitis. *Manuscript in preparation.*

List of abbreviations

a.a.	amino acid
APC	antigen presenting cell
BBB	blood brain barrier
BSA	bovine serum albumin
CCL	CC chemokine ligand
CCR	CC chemokine receptor
CFA	complete Freund's adjuvant
CNS	central nervous system
Con A	Concanavalin A
CSF	cerebral spinal fluid
CXCL	CXC chemokine ligand
CXCR	CXC chemokine receptor
DC	dendritic cell
EAE	experimental autoimmune encephalomyelitis
ELISA	Enzyme-linked immunosorbent assay
HEVs	high endothelial venules
hu	human
i.p.	intraperitoneal
i.v.	intravenous

IP-10	γ-interferon-inducible protein-10
I-TAC	Interferon-inducible T cell α-chemoattractant
LN	lymph node
m	murine
MCP	Monocyte chemoattractant protein
MHC	major histocompatibilty complex
MHV	mouse hepatitis virus
Mig	Monokine induced by γ-interferon
MIP	Macrophage inflammatory protein
MS	multiple sclerosis
PBS	phosphate buffered saline
PCR	polymerase chain reaction
PLP	proteolipid protein
RANTES	Regulated on activation normal T cell expressed and secreted
RT	reverse transcription
s.c.	subcutaneous
SC	spinal cord
SDF-1	Stromal cell derived factor-1
WT	wild-type

Table of Contents

Chapter 1

Introduction

1.1 Overview

In a normal immune response, leukocytes are summoned to the site of infection in order to defend the body from disease-bearing organisms. Numerous studies investigating directed leukocyte migration and activation have demonstrated that chemokines are central orchestrators during the immune response mounted against pathogens. However, under certain circumstances, when tolerance breaks down, the immune response can be inappropriately activated and targeted toward normal healthy tissue leading to autoimmunity and disease. Chemokines have also been shown to be involved in a number of autoinflammatory diseases mediated by T lymphocytes (T cells) including multiple sclerosis (MS), rheumatoid arthritis (RA) and diabetes, to name a few (1).

The expression of an appropriate chemokine receptor on the surface of a T cell is a critical factor in determining the chemokines to which that T cell is able to respond. Accordingly, the patterns of chemokine receptors expressed by autoaggressive T cells are likely to have a major impact on their migratory properties during disease pathogenesis. This study aims to identify specific chemokine receptors that are expressed by neuroantigen-specific (encephalitogenic) $CD4^+$ T cells, and to investigate their potential role in central nervous system (CNS) inflammation.

1.2 T cell biology

1.2.1 The importance of controlled T cell trafficking in adaptive immunity

Adaptive immunity in higher organisms is maintained by lymphocytes. These cells differ from other haematopoietic cells in that they have the ability to recirculate throughout the body. Lymphocyte recirculation enables the adaptive immune system to achieve three main functions: (1) retention of cells that are critical for initiation of an adaptive immune response; (2) localisation of lymphocytes to centres of antigen presentation; and (3) a distinction between naïve and effector/memory lymphocytes that enables secondary immune responses to occur in peripheral tissues outside of secondary lymphoid organs. For this system to function effectively, lymphocytes must be able to migrate to the correct location.

Central to these patterns of migration is the ability of naïve and effector/memory T cells to differentially traffic through lymphoid tissues versus peripheral tissues (2, 3). Naïve T cells do not readily enter peripheral tissues, and instead traffic continuously between the blood and lymphatic circulation systems. From the bloodstream, naïve T cells enter secondary lymphoid tissues such as the lymph nodes and Peyer's patches by passing through high endothelial venules (HEV), which are regions of endothelium specialised for the passage of naïve lymphocytes. If a dendritic cell (DC) presenting cognate antigen is not located, the naïve T cells then leave the lymphoid tissue via the efferent lymphatics and enter the general lymphoid circulation, eventually returning to the bloodstream via the

thoracic duct. This process is then repeated. If a DC presenting cognate antigen is located, the naïve T cells clonally expand into effector and memory cells.

Compared with naïve cells, effector and memory T cells have a reduced ability to pass through HEV. Instead, they preferentially leave the bloodstream by passing through endothelium within peripheral tissues during an ongoing immune response, thereby enabling them to migrate to infected tissues and to survey these sites for antigen in the absence of infection. If antigen is not present, they exit the peripheral tissues by draining into the afferent lymphatics and subsequently enter secondary lymphoid tissues via this route. They then continue this trafficking pattern by entering the efferent lymphatic vessels and returning to the bloodstream via the thoracic duct, similarly to naïve T cells.

1.2.2 Differential trafficking properties of effector T cell sub-populations

More recently, it has been demonstrated that the entry of effector/memory T cells into peripheral tissues is non-random. First, there is considerable evidence that memory T cells show a preference for returning to the region serviced by the lymph nodes in which they were first activated. For example, T cells activated in the mucosal lymphoid tissue demonstrate preferential homing to the intestines, while T cells activated in skin-draining lymph nodes home to the skin (4, 5). Second, T cells of the T-helper 1 (Th1) and T-helper 2 (Th2) subsets also display differential migratory properties (6). Th1 cells promote immune responses directed toward intracellular pathogens, through the secretion of cytokines such as interferon-γ (IFN-γ), interleukin (IL)-2 and tumour necrosis factor (TNF)-β; together these cytokines promote cytotoxic T lymphocyte (CTL) activity, macrophage activation and the production of immunoglobulins that bind Fc receptors and

fix complement. In addition, Th1 cells have been implicated in acute and chronic inflammatory diseases, such as RA, MS, diabetes and transplant rejection (1). Conversely, Th2 cells promote immune responses toward extracellular pathogens via the secretion of cytokines such as IL-4, IL-5 and IL-13, which together promote strong humoral immune responses and class-switching toward immunoglobulins of the IgE isotype, as well as inducing eosinophil and mast cell accumulation and activation (7-9). In addition, Th2 cells have been implicated in inflammatory diseases, such as asthma (10, 11). Thus, considering their divergent effector functions, it is important that Th1 and Th2 cells can specifically migrate to those sites in the periphery where they are likely to be most useful. Accordingly, there is now evidence that these two subsets display divergent migratory properties *in vivo*, as Th1 cells show greatly enhanced homing to inflamed sites in the periphery, such as rheumatoid joints and sites of DTH, compared to Th2 cells (12, 13).

1.2.3 Molecular mechanisms of T cell extravasation

At the molecular level, the process of T lymphocyte migration into lymph nodes and peripheral tissues appears to follow the multistep paradigm proposed and validated for leukocyte extravasation in general (Fig 1.1). Within this multistep schematic, the first step is mediated by selectins. These are a group of adhesion molecules involved in leukocyte rolling along the vasculature. Selectin binding to carbohydrate ligands are weak interactions that allow rapid attachment to, and detachment from, the endothelium. The second step depends upon the interaction between integrins expressed on activated leukocytes (eg. leukocyte function associated antigen (LFA)-1) and Ig-related molecules expressed on endothelial cells. Examples of the latter are intracellular adhesion molecules (ICAMs) and vascular CAMs (VCAMs). The integrins serve as counter receptors and are

generally constitutively expressed but must undergo conformational changes mediated by chemotactic factors prior to adhesion molecule binding. The interaction between activated integrins and CAMs arrests the rolling and allows firm adhesion of the leukocyte to the vascular endothelium. Tethering to the endothelial cell wall is followed by extravasation, where leukocytes diapedeze through the junctions between endothelial cells. Once through the basement membrane, leukocytes follow chemotactic gradients through the extracellular matrix to localize at the site of inflammation.

Collectively, the processes of T cell migration and extravasation are controlled by an intricate molecular network (5, 14, 15), which enables naïve, effector and memory T cells, and their subsets, to display the differential migratory patterns discussed previously. Included in this network are chemokines and their receptors.

1.3 Overview of the chemokine system

1.3.1 Chemokine structure and function

The chemokines (*chemo*tactic cyto*kines*) are a large family of chemotactic factors that play a central role in the trafficking of leukocytes throughout the body. All members of this family are low molecular weight (~8kDa), secreted proteins (with the exception of two membrane-bound members) and can be divided into distinct groups on the basis of structure and function (16, 17).

Assignment of molecules to the chemokine gene superfamily is based on homology at the primary amino acid sequence level and the presence of a highly conserved cysteine signature. Based on the spacing of their amino-terminus cysteine residues, chemokines are structurally divided into 4 different subfamilies (Fig 1.2). The majority of chemokines belong to the major CXC and CC subfamilies, while the minor C and CX_3C subfamilies have only two and one member, respectively (Table 1.1). The CXC family can be further divided on the basis of the presence of a glutamine-leucine-arginine (ELR) motif located upstream of the CXC sequence. The presence of an ELR motif appears to influence the action of CXC chemokines in at least one respect – ELR containing chemokines are angiogenic, whilst non-ELR chemokines are angiostatic (18).

The organisation of chemokines into structurally-based subfamilies correlates moderately well with their biological function (16, 17). In general, members of the C, CC and CX_3C subfamilies are chemotactic for monocytes and lymphocyte subsets, with some members also active on dendritic cells (DC) and granulocytes other than neutrophils. In contrast, C-X-C chemokines are active on neutrophils, T cells and monocytes, depending upon the presence or absence of the ELR motif. However, it is important to note that the classification of chemokine function according to the cysteine-containing and ELR motifs is highly generalised, and there is considerable variation within the sub-families with regard to target cell specificity.

Due to the numerous inconsistencies in the original chemokine nomenclature, a new classification system was recently devised, whereby each chemokine was named according to its sub-family classification (CC, CXC, C or CX_3C) and given a number (19). For example, the chemokine previously known as I-309 is now known as CCL1 (CC

ligand 1). Whilst this nomenclature is beginning to gain widespread use, several synthetic molecules used in the present study were characterised prior to the new nomenclature. Therefore, both the old and new nomenclature will be used subsequently throughout this text.

By far the best understood biological action of chemokines is that of chemotaxis, however emerging data also shows that various members of the chemokine gene superfamily exert a range of biological effects beyond chemotaxis. These include organogenesis, hematopoiesis, angiogenesis/angiostasis, and cellular activation other than chemotaxis including adhesion, apoptosis, proliferation and differentiation (16). The latter will be discussed in further detail below.

1.3.2 Regulation of chemokine production

1.3.2.1 Homeostatic and inflammatory chemokines

Chemokines are produced by a wide variety of cell types, of both haematopoietic and non-haematopoietic origin (20). Because of the difficulty in associating chemokine structure with function (mentioned above), a more intuitive classification has recently been adopted. In this system, the chemokines are commonly grouped into two broad categories on the basis of production and function – homeostatic (alternatively called constitutive) and inflammatory (alternatively called inducible) (Table 1.2) (21-23). Homeostatic chemokines are produced constitutively in discrete microenvironments within lymphoid and non-lymphoid tissue such as the mucosa and skin (22). They are believed to drive the

homeostatic, basal trafficking of leukocytes throughout the body, and localisation within these tissues, and are therefore critical for the maintenance of homeostatic immunosurveillance. The majority of chemokines are inflammatory chemokines, which are upregulated, or induced, as part of the immune response – these chemokines direct the recruitment of specialised effector cell populations to sites of infection/inflammation. More recently, the distinction between these different classes of chemokines has become less separate, with a new class emerging that are capable of being homeostatic or inflammatory.

1.3.2.2 Patterns of homeostatic chemokine expression

Homeostatic chemokines are generally produced in primary and secondary lymphoid tissues such as bone marrow, thymus, spleen and lymph nodes (22, 24-26), although the expression of MEC/CCL28 has thus far only been demonstrated at sites associated with epithelial mucosa (27). SDF-1/CXCL12 is also unusual, in that it shows a much broader pattern of expression throughout the body than other homeostatic chemokines (28, 29), which may be related to its important functions outside of the immune system (30). Nonetheless, prominent expression of SDF-1/CXCL12 by endothelial cells has led to the suggestion of a role in leukocyte homeostasis (22). Often, the expression of homeostatic chemokines is microenvironment-specific, such that production may be limited to T cell or B cell zones, and in most cases is thought to be relatively stable. However, recent exception to this theory was documented by Alt *et al.* (2002) who demonstrated functional expression of ELC/CCL19 and SLC/CCL21 at the blood brain barrier (BBB) in mice experiencing CNS inflammation (31).

1.3.2.3 Patterns of inflammatory chemokine expression

Examples of increased inflammatory chemokine expression in response to human pathological conditions, or experimentally induced pathology in animals, are extensive in the literature. The range of human pathologies that have been associated with altered chemokine gene or protein expression include MS, transplant rejection, inflammatory bowel disease, asthma, rheumatoid arthritis, glomerulonephritis and vascular disease (1, 17, 32, 33). With regard to animal studies, altered patterns of chemokine expression have been observed during the rejection of various foreign grafted tissues, in rodent models of airway hypersensitivity and arthritis, and in the rodent model of MS, experimental autoimmune encephalomyelitis (EAE), to name a few (1, 33-36). Patterns of chemokine expression in EAE will be discussed in more detail below (Section 1.4.7)

Patterns of inflammatory chemokines produced in a particular tissue have also been shown to depend upon the nature of the immune response occurring there, for example, a type 1 or type 2 immune response. In particular, a local environment dominated by either Th1 cytokines (IFN-γ, TNF-α, IL-12, etc) or Th2 cytokines (IL-4, IL-10, etc) has been suggested to influence the production of a number of chemokines. For example, the production of chemokines such as RANTES/CCL5, MIP-1α/CCL3 and MIP-1β/CCL4 has been associated with a type 1 immune response (37, 38), while the production of MCP-1/CCL2, MDC/CCL22 and eotaxin/CCL11 is often equated with a type 2 immune response (39-41). Of note, these differential expression patterns may be due, at least in part, to differential production of chemokines by Th1 and Th2 effector cells themselves, as these populations have been shown to secrete distinct subsets of chemokines *in vitro* (42).

1.3.2.4 Expression of chemokines that have both homeostatic and inflammatory functions

Included in this third class of chemokines is CCL20/MIP-3α, which is expressed constitutively in secondary lymphoid organs, but is also induced in peripheral tissues, such as the CNS (43). In addition, Mig/CXCL9 and IP-10/CXCL10 are constitutively expressed in the colon (44), but are induced in the skin only under inflammatory conditions (45-47). Similarly, a number of chemokines are upregulated at peripheral sites of inflammation, thereby classifying them as inflammatory, but in addition are constitutively expressed in secondary lymphoid tissue. For example, while eotaxin expression is induced in the lung under inflammatory conditions such as OVA-induced eosinophilia (48), it is also constitutively expressed in secondary lymphoid tissues such as the thymus and lymph nodes (49).

1.3.3 Chemokine receptors

1.3.3.1 Overview

Chemokines exert their actions on target cells via cell surface receptors that are members of the G-protein coupled receptor superfamily. Engagement of these seven transmembrane spanning, G-protein-linked molecules induces a variety of downstream intracellular signalling mechanisms including intracellular calcium mobilisation, cytoskeletal rearrangement and transcription factor activation. Together, these culminate in the expression of biological effects (21). Chemokine receptors are closely related in structure and signal transduction-coupling mechanisms to other seven transmembrane domain

receptors from a wide range of biological systems, including the cardiovascular system (β-adrenergic receptors) and the central nervous system (receptors for vision, olfaction and taste). While there is an extensive body of literature on chemokine receptor signal transduction pathways, this is not a major focus of this thesis and will not be discussed further. For further information, refer to (50).

1.3.3.2 Structure and specificity

Eighteen chemokine receptors have be cloned so far including, six receptors for CXC chemokines, eleven receptors for CC chemokines, and one receptor each for the C and CX_3C chemokines (Table 1.3). One notable feature of chemokine receptors is the remarkable degree of promiscuity with regard to ligand binding (Table 1.3). Although some chemokine receptors bind to only one chemokine, others are able to bind as many as seven different chemokine ligands, often with varying affinity and sometimes with distinct signalling outcomes. Generally, chemokine receptors bind members of only one chemokine sub-family (and do so with high affinity) although exceptions do exist. For example, the CXC chemokines Mig/CXCL9, IP-10/CXCL10 and I-TAC/CXCL11 have been shown to bind to CCR3, but act as antagonists rather than agonists (51). In addition, murine SLC/CCL21 (a CC chemokine) binds to and activates CXCR3 (52, 53). Finally, the Duffy Antigen Receptor for Chemokines (DARC), an apparently non-functional chemokine binding protein expressed on erythrocytes and endothelial cells, has been shown to bind chemokines from both the CXC and CC sub-families with equal affinity (54).

Given their role in host defense, it is not surprising that chemokine receptors are also gateways for the entry of at least two important human pathogens into target cells. First, CCR5 and CXCR4 act as co-receptors, in conjunction with CD4, for the cellular entry of human immunodeficiency virus (HIV) and accordingly, are currently considered excellent potential anti-HIV targets (55, 56). Second, the promiscuous chemokine binding protein DARC is the surface receptor used by *Plasmodium vivax* (a causative agent of malaria), to gain entry into erythrocytes (57).

1.4 Chemokines and chemokine receptors in T cell biology

1.4.1 Chemokines, chemokine receptors and T cells: in vitro studies

1.4.1.1 Chemotaxis

Most of our current understanding of the role of chemokines in T cell biology comes from *in vitro* studies. Chemotaxis assays have identified at least 25 chemokines capable of attracting certain types of T cells *in vitro* (Table 1.4). In general, chemokines that are active on naïve T cells are homeostatic, whereas those chemokines that attract only effector/memory T cells are generally inflammatory. Thus far, the only chemokines identified that possess the ability to recruit naïve T cells are SDF-1/CXCL12, ELC/CCL19, SLC/CCL21 and DC-CK1/CCL18 (29, 58-61). The remainder of those listed are active only on effector/memory T cell sub-populations, with very little or no

activity on naïve cells. This distinction is what defines the former group as homeostatic chemokines, which through their ability to recruit and induce the adhesion of naïve T cells, play a role in the recirculation of naïve T cells under conditions of homeostasis. Conversely, inflammatory chemokines, which are able to attract and stimulate effector/memory T cells to adhere to vascular endothelium, are thought to play an important role in the specific recruitment of effector T cells to sites of inflammation in the periphery (21-23).

Some of these inflammatory chemokines, such as MCP-1/CCL2, are active on a broad range of effector/memory T cells, with little preference for $CD4^+$ or $CD8^+$ cells (62), or Th1 or Th2 subsets (63). Accordingly, the level of expression of the MCP-1/CCL2 receptor CCR2 is similar in populations of $CD4^+$ and $CD8^+$ (64, 65) and Th1 and Th2 (64, 66) cells. In contrast, other chemokines demonstrate preferential recruitment of particular T cell subsets. For example, MIP-1β/CCL4 and IP-10/CXCL10 demonstrate a higher degree of activity on Th1 cells compared with Th2 cells (63, 66, 67). Correspondingly, receptors for these ligands are preferentially expressed on Th1 cells compared with Th2 cells (22, 64). On the other hand, some chemokines such as TARC/CCL17, MDC/CCL22 and eotaxin/CCL11 demonstrate preferential recruitment of Th2 cells expressing CCR3 and CCR4 (64, 66-69). Regulation of chemokine receptors on T cells will be dicsussed in more detail below.

1.4.1.2 Adhesion

In addition to stimulating the directional migration of T cells, *in vitro* studies have identified a number of chemokines that also have the capacity to enhance T cell adhesion

under conditions that mimic the shear stresses of blood flow. SDF-1/CXCL12, ELC/CCL19 and SLC/CCL21, three of the chemokines that are capable of attracting T cells of a naïve phenotype, also stimulate the rapid firm adhesion of naïve T cells to endothelial cells or endothelial cell adhesion molecules (70, 71). The chemokines Mig/CXCL9, IP-10/CXCL10, TARC/CCL17 and MIP-3α/CCL20 have similar effects on T cell adhesion, but are only active on effector/memory T cell populations, consistent with their chemotaxis profiles (70, 72, 73). The ability of these chemokines to increase the adhesion of T cells to endothelial cells suggests an important role for chemokines in the induction of firm adhesion of T cells prior to transmigration through the endothelial barrier. Other chemokines such as MCP-1/CCL2, RANTES/CCL5 and MIP-1β/CCL4 enhance the binding of T cells to components of the extracellular matrix and fibronectin (74), implicating these chemokines in the movement of T cells post-extravasation.

1.4.1.3 T cell activation and differentiation

In addition to chemotaxis and adhesion, further functions for chemokines in the control of T cell behaviour have also been proposed. A number of *in vitro* studies have suggested that some chemokines may play a co-stimulatory role during the T cell activation process. Of particular interest is a study demonstrating that SDF-1/CXCL12 has a co-stimulatory effect on $CD4^+$ T cells (75), while lymphotactin/XCL1 has divergent effects on $CD4^+$ and $CD8^+$ T cell activation, acting as an inhibitor of the former and a co-stimulator of the latter (76). In addition, emerging evidence indicates that some chemokines can contribute to the polarisation of T cells into Th1 or Th2 effector cells (77, 78). For example, MIP-1α/CCL3 and MCP-1/CCL2 appear to enhance the development of Th1 and Th2 responses, respectively (40, 79-81).

1.5 Chemokine/chemokine receptor control of $CD4^+$ T cell migration

1.5.1 Overview

Chemokines demonstrate remarkable diversity and redundancy in their ability to attract particular subsets of T cells. Most notable is the differential activity of chemokines on naïve versus effector/memory T cells. As discussed above and summarised in Table 1.4, a large number of chemokines demonstrate no activity with respect to naïve T cells, yet are able to attract effector/memory T cell populations. On the other hand, a small number of chemokines are able to induce the chemotaxis of naïve T cells, but demonstrate reduced activity on effector T cells. These findings, together with documented expression of chemokine receptors on specific T cells subsets, and early intervention studies, including gene knockout studies, have provided some important insights into the migratory patterns of T cells during both homeostasis and inflammation.

1.5.2 Evidence for chemokine/chemokine receptor control $CD4^+$ T cell migration

As described above, an increasing body of evidence characterising the migratory phenotypes of the various $CD4^+$ T cell subsets has begun to identify chemokines and chemokine receptors that may play critical roles in directing their trafficking. Table 1.5 summarises the expression of chemokine receptors by $CD4^+$ T cells. Differential patterns

of chemokine receptor expression have been documented on a wide variety of functional T ccll subsets, however in most cases the functional consequences of the expression of many chemokine receptors have yet to be determined.

As discussed previously, the prevailing theory of $CD4^+$ T cell migration suggests that the migratory pattern of $CD4^+$ T cells is determined by their state of differentiation - naïve, effector or memory – with each subset's migratory pattern reflecting its functional role (Figure 1.3). Naïve T cells re-circulate through the blood and secondary lymphoid organs (regional centres for antigen presentation), surveying the body for novel foreign antigens (82). The trafficking pattern of naïve cells (blood - secondary lymphoid organ - efferent lymphatics – blood) maximises the chances of a naïve clone encountering its specific antigen, and differentiating into effector and memory type cells (ie. undergoing clonal selection). Naïve T cells express high levels of CCR7, and respond chemotactically to SLC/CCL21 and ELC/CCL19 (83). The high endothelial venules (HEV) and stromal cells in the T cell zones of the lymph node secrete SLC/CCL21 and ELC/CCL19, facilitating the exit of naïve cells from the blood and into the lymph node, where they interact with antigen-presenting cells (84). The importance of CCR7 and its ligands in the trafficking of naïve cells is clearly demonstrated in the plt/plt (paucity of lymphoid tissue) mouse, which lacks both SLC/CCL21 and ELC/CCL19, and in CCR7 knockout mice. These mice have severe defects in the micro-architecture of non-splenic secondary lymphoid organs, lacking clearly defined T and B cell zones (85). In addition to CCR7, CXCR4 (the receptor for SDF-1/CXCL12) is expressed at high levels on the naïve T cell population in humans, which respond chemotactically to SDF-1/CXCL12. However, no such functional role has been documented in the mouse since deletion of CXCR4 is embryologically lethal

and produces serious developmental effects in the immune system (86, 87). Therefore other approaches must be taken to determine the role of CXCR4 *in vivo*.

Upon encountering antigen, naïve $CD4^+$ T cells differentiate into effector and memory cells. Effector $CD4^+$ T cells increase inflammatory cytokine production and acquire the ability to exit the blood and enter peripheral tissues, where they participate in the immune response against invading microorganisms (82). The observed changes in the migratory properties between naïve and effector T cells corresponds with a change in chemokine receptor profile. Expression of CCR7 and CXCR4, which drive trafficking to secondary lymphoid organs, is reduced. In contrast to the naïve T cell population, effector T cells have the capacity to express numerous inflammatory chemokine receptors, which explains the ability of these cells to respond to inflammatory chemokines. These chemokine receptors include CCR2, CCR3, CCR4, CCR5, CCR6, CCR8, CXCR3, CXCR4 and CXCR6. With respect to the polarity of the effector $CD4^+$ T cell (Th1 or Th2), the upregulation of specific chemokine receptors appears to be divergent. Th1 cells have been shown to express higher levels of CCR5, CXCR3 and CXCR6 compared with Th2 cells (23, 64, 88, 89). Conversely, Th2 cells appear to express higher levels of CCR3, CCR4, and CCR8 (23, 66-68, 90). These distinct groupings of chemokine receptors are likely to be responsible for the differential migratory patterns of Th1 and Th2 cells discussed previously.

Some chemokine receptors appear to control the migration of effector $CD4^+$ T cells into specialised microenvironments or tissues. Members of this group include CXCR5, which is expressed on a subset of follicular B helper T cells (T_{FH}). These cells are localised in the B cell areas of secondary lymphoid tissue and are uniquely adapted to provide help to B

cells for antibody production (91-93). Other members are CCR4 and CCR9, which are expressed on skin- and gut-homing T cells, respectively (94, 95). Additionally, the cerebral spinal fluid (CSF) is enriched in $CD4^+$ T cells expressing CXCR3, CCR5 and CCR6, suggesting that these receptors may be involved in extravasation across the BBB (96).

Although many chemokine receptors have been demonstrated to be upregulated on activated $CD4^+$ T cells, the significance of the expression of individual receptors, and their contributions to migratory properties have only recently begun to be the subject of detailed *in vivo* investigations.

Memory $CD4^+$ T cells are long-lived, antigen-experienced cells generated during primary antigen exposure that mediate rapid responses to recurring antigen (recall responses). Expression of the chemokine receptor CCR7 has been proposed to divide memory T cells into two functional subsets – central memory cells (T_{CM}) and peripheral memory cells (T_{EM}) (83, 97). T_{CM} cells recirculate through secondary lymphoid organs, whilst T_{EM} cells recirculate through peripheral tissues. T_{CM} cells express CCR7, which theoretically allows them to efficiently home to the secondary lymphoid organs in order to aid in the rapid initiation of a secondary response (83, 97). T_{EM} cells, which recirculate through the peripheral, non-lymphoid tissues lack expression of CCR7. As a function of cell division, these cells have been demonstrated to progressively acquire chemokine receptors such as CCR2, CCR3, CCR4, CCR5 and CXCR6, depending on the polarising conditions (64). This chemokine receptor expression pattern is believed to facilitate the trafficking of peripheral memory cells throughout the peripheral tissues, where they are ready for immediate participation in recall responses.

It is therefore clear that T cell subsets express unique patterns of chemokine receptors on their surface. What is not well understood, however, are the mechanisms by which the various functional subsets of T cells come to acquire such a divergent range of chemokine receptors and the location and timing of such changes. Such an understanding can only come from analyses of chemokine receptor expression during the process of T cell activation *in vivo*, or the acquisition of a defined effector function, such as that which occurs during organ-specific inflammation.

1.6 Inflammation of the central nervous system

1.6.1 The healthy central nervous system

The healthy CNS is surrounded by the blood-brain barrier (BBB), which regulates the entry of large molecules and cells into the sensitive environment of the CNS (Fig 1.4). Consisting of microvessel endothelial cells (EC), the underlying basement membrane, and associated cells (smooth muscle/pericytes and astrocytes), the BBB highly restricts passage from the blood into the CNS. This is due to the tight junctions present between the cerebral ECs (98). Behind the BBB, the CNS is composed of impulse-conducting neurons and four glial cell types - oligodendrocytes, astrocytes, microglia and ependymal cells. Oligodendrocytes are responsible for producing the myelin sheaths that surround and insulate neurons and that are essential for conductivity. The myelin sheaths produce by oligodendrocytes are composed of lipids and proteins, including myelin basic protein (MBP), proteolipid protein (PLP) and myelin oligodendrocyte glycoprotein (MOG).

Astrocytes, as well as forming part of the BBB, are critical for synaptic maintenance and regulation of extracellular pH and K^+ levels. Microglia are the resident macrophage population of the CNS, and are involved in immune surveillance of the CNS, as well as playing other homeostatic roles in the maintenance of the CNS environment. The function of ependymal cells remains speculative, although they may be important for the formation of another protective barrier of the CNS, the cerebrospinal fluid (CSF)-brain barrier (CBB). In addition to the BBB, the chance of immune activation is reduced by allowing only low numbers of activated T cells and macrophages to enter the CNS, and much lower expression of MHC on antigen presenting cells (APCs) within the CNS (99). This results in the tissue having multiple levels of control to restrict inflammation (100).

1.6.2 Neuroinflammation

While the CNS is buffered against immunological activation, under certain circumstances inflammation can occur. Under inflammatory conditions, the BBB becomes more permeable, allowing an increased number of activated lymphocytes to enter the CNS. Initially, this influx does not require antigen-specificity. However, infiltrating cells that recognise their cognate antigen presented in the context of MHC molecules by microglia are retained in the CNS and antigen re-stimulation occurs (100). Generally antigen recognition results in amplification of inflammation, leading to the production of inflammatory mediators by both resident cells (36) and infiltrating cells (101), causing a further influx of lymphocytes, monocytes and granulocytes (101).

1.6.3 Multiple sclerosis pathology

Inflammatory cell recruitment into the CNS is a critical step in the development of pathological processes such as multiple sclerosis (MS) (32). MS is a common neurological syndrome in young adults, which results in permanent neurological dysfunction, due to the destruction and impaired regenerative capacity of the myelin sheath of the oligodendroglial cells surrounding the axons. Notable symptoms of MS include visual, motor and sensory disturbances, ataxia and incontinence. Most patients (~85%) initially have a relapsing-remitting form of MS (RRMS), which is characterised by discrete clinical 'attacks' or 'relapses' followed by subsequent improvement (102). Over many years, slow neurological deterioration develops in the majority of these patients, which has been termed secondary-progressive MS (SPMS). Primary-progressive MS (PPMS) occurs in a minority of patients (~15%). This form is characterised by a progressive course of symptoms from onset, with an absence of clinically evident relapses (102). Whilst it has been postulated that MS is caused by a number of genetic, environmental and infectious factors, which result in an autoimmune response (103), the primary cause of the disease remains an enigma (104). Magnetic resonance shows that BBB disruption is an early event in MS lesion formation although what mediates this effect is unknown. Histologically, MS lesions are characterised by chronic inflammation, glial cell activation, myelin destruction and axon loss. Studies have shown that demyelination and oligodendrocyte death are mediated by the infiltration of blood-derived cells and by activated parenchymal cells, such as activated microglia and astrocytes (105). Though mediated by blood-derived cells, it remains uncertain how demyelination is initiated in MS. However, inflammatory products such as nitric oxide, proteases, IFN-γ and TNF-α have been implicated in this process (35). The central cellular effectors of the disease are

believed to be infiltrating Th1 $CD4^+$ cells, specific for one or more antigens in the CNS, followed closely by non-specific infiltrating macrophages (100).

1.6.4 $CD4^+$ T cells and MS

Genetic, histological, phenotypic and molecular studies have all implicated $CD4^+$ T cells in MS. Genetic association between MS susceptibility and the HLA (human leukocyte antigen) has been known for approximately 30 years. Extended MHC haplotype analysis has revealed that predisposition to the disease has been consistently associated with class II HLA-DR2 (includes DR and DQ) haplotype. Individuals with the DR2 (alternatively referred to as Dw2) phenotype are at a higher risk of developing the disease by a factor of 3 or 4 (106). Other MHC class II alleles have also been associated with varied clinical outcomes including increased and decreased disease likelihood (107). The mechanisms underlying the genetic association of DR2 with MS are not fully understood. However, based on the theoretical functions of MHC class II molecules, the DR2 phenotype may orchestrate the selection of a specific repertoire of T cell receptors (TCR) in the thymus that predispose to autoimmune activation. DR2 has been postulated to exert its influence by preferentially binding myelin-derived antigen and clonally selecting encephalitogenic cells (cells capable of inducing myelitis). Support for this has been demonstrated. In patients who are HLA DR2-positive, there are T cell receptor arrangements characteristic of T cell clones reactive to MBP_{83-99} bound to HLA DR2 at sites of MS brain plaques (reviewed in (108)). Thus, the observed association of MS with particular MHC class II haplotypes suggests that presentation of neural antigens to $CD4^+$ T cells may be an important pathogenic event.

Evidence for a pathogenic role of $CD4^+$ T cells in MS was provided by the finding of increased frequencies of activated myelin-reactive $CD4^+$ T cells in the CSF compared with peripheral blood of MS patients or in the CSF or peripheral blood of patients with other neurological diseases (109). This indicates that these $CD4^+$ T cells are capable of traversing the BBB, entering the CNS and accumulating there. Histologically, $CD4^+$ T cells have been observed in actively demyelinating lesions (105). $CD8^+$ T cells are also present, however the majority of cells comprising the lesion are macrophages and microglia displaying enhance expression of MHC class II antigen (110). Whilst macrophages tend to accumulate at the leading edge of the lesion, $CD4^+$ T cells penetrate from the active edge deeply into the periplaque area (111). Consistent with that mentioned previously naïve $CD4^+$ T cells are a rare occurrence in a MS lesion (111). Whilst recent evidence has shown that clonal expansions of $CD8^+$ T cells predominate in MS lesions, expansions of $CD4^+$ T cell clones were also identified, although the population was shown to be more heterogeneous (112). Oligoclonal expansions of $CD4^+$ T cells have also been detected in the CSF of MS patients (113).

Several reports have suggested that myelin-reactive T cells from RRMS patients have a Th1 bias. This is based on cytokine expression and chemokine receptor patterns on T cells in both the CSF and lesions of MS patients (114-116). Both $CD4^+$ and $CD8^+$ T cells in the CSF of MS patients expressed the Th1-associated chemokine receptors CXCR3 and CCR5. Ligands of these receptors and others have also been documented in the MS lesion and CSF during MS. Interactions between encephalitogenic T cells with resident APCs can trigger expression of MIP-1α/CCL3, MIP-1β/CCL4, RANTES/CCL5, MCP-1/CCL2 and IP-10/CXCL10 in MS lesions (114, 116). IP-10/CXCL10, Mig/CXCL9 and RANTES/CCL5 have also been documented in the CSF of MS patients (115). Co-

localisation of these chemokines (with the exception of MCP-1/CCL2) and the $CCR5^+$ and $CXCR3^+$ $CD4^+$ T cells has been documented (114-116).

In vitro studies have provided evidence that myelin-reactive cells from MS patients appear to be in an enhanced state of activation. In those studies, transfected cells expressing MHC class II DR2 molecules with or without B7 molecules were used to present MBP_{85-99} to $CD4^+$ T cells from DR2 patients or controls. Whilst both DR2 and B7 were required for activation of $CD4^+$ T cells from control individuals, DR2 alone could expand MBP-reactive T cells from MS patients (117). It is important to note that T cells reactive to the major constituents of myelin are also detectable within the periphery of normal individuals, however have more stringent stimulation requirements (117).

Taken together, the outlined evidence indicates that $CD4^+$ T cells: a) are linked genetically to MS susceptibility through association with certain MHC class II alleles; b) are present in the CNS during the course of MS; c) localise to lesions and in some instances are clonally-related; d) accumulate in the CNS in response to expression of Th1-associated chemokines; and e) have less stringent stimulation requirements when they are re-exposed to myelin antigens. These properties implicate $CD4^+$ T cells as potential effectors in the pathogenesis of MS.

1.6.5 EAE- A model for MS

Improved understanding of the immunopathological mechanisms underlying MS has developed from the study of experimental models of demyelination, such as experimental autoimmune encephalomyelitis (EAE). EAE is an inflammatory demyelinating disease of

the CNS characterised by progressive ascending paralysis due to central nervous system (CNS) infiltration of antigen-specific and non-specific $CD4^+$ and $CD8^+$ T cells as well as macrophages (118).

Studies in EAE have shown that many proteins of the nervous system are potentially encephalitogenic (ie, have the ability to cause encephalitis). Accordingly, EAE can be induced in genetically susceptible mice by two main strategies. Firstly, active disease is induced by direct injection of myelin antigens such as myelin basic protein (MBP), myelin proteolipid protein (PLP) or myelin oligodendrocyte protein (MOG), or peptides derived from these proteins, emulsified in complete Freund's adjuvant (CFA). Many studies have shown that for efficient induction, treatment with extracts of *Bordatella pertussis* is also required. One such extract is pertussigen (119, 120). While the requirement for pertussigen is not understood, it may be necessary for appropriate immune stimulation, increased vascular permeability of the BBB, Th1/Th2 deviation, or a combination of these (or other) factors. Infection with neurotrophic viruses also elicits a form of active disease. Secondly, passive disease is induced by adoptively transferring encephalitogenic T cells from immunised donor mice to naïve recipients. Accordingly, the different disease models afford researchers the opportunity to study both the sensitisation and effector phases of the disease independently.

Depending upon the immunising antigen, and animal in which disease is induced, the course of disease varies. In the SJL/J mouse strain, following immunisation with $PLP_{139-151}$, the clinical course closely parallels that observed in relapsing, remitting MS. MOG_{35-55}-induced EAE in C57Bl/6 mice exhibits a chronic sustained disease with fewer relapses but extensive demyelination and inflammation in the CNS (121). MOG-induced EAE has

frequently been employed by gene-targeting experiments due to the C57Bl/6 background of many genetically modified mice (118).

1.6.6 $CD4^+$ T cell involvement in EAE

The mechanism by which inflammatory cells gain access to the CNS during the development of EAE is a long-studied issue, which has primarily been investigated in the adoptive transfer model of EAE (100, 122-126). These studies have demonstrated that activated T lymphocytes rapidly enter the CNS regardless of antigenic specificity (126, 127). In the absence of antigenic recognition the cells leave the CNS, but if antigenic recognition does occur, a population of T lymphocytes remains in the CNS and initiates an inflammatory response resulting in the recruitment and activation of non-specific inflammatory cells, such as macrophages and microglia, antigen non-specific T cells, and epitope spreading of the specific T cell population (122, 127). Reagents that block inflammatory cell recruitment into the CNS, such as anti-VLA-4 antibodies, strongly suppress EAE, further indicating a need for leukocyte migration into the CNS for clinical disease to occur (128). Concomitant with CNS mononuclear cell infiltration is breakdown of the BBB, which is essential for the development of EAE. However, the mechanisms responsible for this increased BBB permeability are not clear.

In order for $CD4^+$ T lymphocytes to initiate disease in the CNS, they must recognise their respective antigen in the context of major histocompatibility complex (MHC) class II molecules. It is believed that the most likely candidates in the CNS for antigen presentation to autoreactive T lymphocytes are the perivascular macrophages and microgial cells of the BBB. However, these cell types do not express MHC class II

molecules constitutively and require stimulation with regulatory cytokines to do so. Activated $CD4^+$ T lymphocytes produce a wealth of cytokines and it is possible that the cytokines responsible for upregulating MHC class II expression in the CNS, such as interferon (IFN)-γ and TNF-α, originate from infiltrating autoreactive T lymphocytes and later from other recruited inflammatory cells and from activated glial cells (129). In this scenario, the ability of IFN-γ-producing $CD4^+$ T cells to enter the CNS would play a critical role in the initiation and amplification of EAE.

Previous studies have shown that inflammatory $CD4^+$ T cells produce IFN-γ during EAE (129). IFN-γ induces MHC expression on a variety of cell types, including endothelial cells (130), and activates macrophages. TNF-α is a known inducer of the production of certain chemokines (RANTES/CCL5, MIP-1α/CCL3, MCP-1/CCL2, IP-10/CXCL10 as well as MIP-3α/CCL20). TNF-α has also been shown to activate the endothelium to increase expression of adhesion molecules. Whilst the expression studies suggest that these two cytokines play proinflammatory roles in the pathogenesis of EAE, studies using mice deficient in IFN-γ, or IFN-γR, or using anti-IFN-γ antibodies reveal that the role of IFN-γ in EAE is very complex. Deletion of IFN-γ, or IFN-γR, results in previously resistant animals becoming susceptible to EAE (131-133). Systemic administration of anti-IFN-γ antibodies also enhances disease severity (134). In addition, administration of this cytokine has been shown to either enhance inflammatory pathology or ameliorate disease, depending on concentration and route of administration (135). Collectively, these results suggest that IFN-γ may have dual effects during EAE, which, in part, are related to concentration. Conversely, antibodies against TNF-α block the development of EAE, indicating that this cytokine plays a pathogenic role in EAE (122). Together, these data

suggest that IFN-γ and TNF-α may act to facilitate cellular trafficking across the BBB. Nevertheless, a role for pro-inflammatory cytokines in the initiation of EAE is now well accepted.

1.6.7 Chemokines and chemokine receptors during EAE

In addition to the above cytokines, growing evidence supports a role for members of the chemokine superfamily in EAE (reviewed in (136)). During an immune response, inflammatory chemokines are rapidly increased to high levels in order to combat infection. Unfortunately, the same induction can contribute to autoimmune disorders if inappropriately directed towards self (such as during EAE), causing collateral damage (which further amplifies inflammation) (1).

Chemokine expression in the inflamed CNS during EAE shows a temporal and spatial relationship to disease activity and lesion architecture (36, 114, 115). There are numerous ways in which chemokines may influence disease progression. Most obviously, by activating integrin binding to endothelial adhesion molecules and providing a chemotactic gradient, they can mediate the recruitment/accumulation of leukocytes in the CNS (121). In addition, as discussed above, recent data indicate that some chemokines aid in the costimulation and activation of T cells, influence Th-1/2 differentiation and immunomodulatory cytokine production, and stimulate autocrine feedback enhancing inflammation (137).

When expression patterns of chemokines and receptors are compared in inflamed and healthy CNS tissue, several chemokines are consistently upregulated. However, the

expression patterns of many others vary considerably between different models/individuals, and with the techniques used for detection. Expression patterns for animal models are relatively comprehensive, while human data are still quite limited. The general expression of chemokines closely matches that seen with other CNS inflammation models, such as spinal cord injury (138). Those chemokines with the greatest correlation with disease progression are RANTES/CCL5, MIP-1α/CCL3, MIP-1β/CCL4 and MCP-1/CCL2 (137), however many other chemokines have also been detected in the CNS during EAE and MS (Table 1.6), including SDF-1/CXCL12 (139, 140), IP-10/CXCL10 (115, 116, 141, 142) and MIP-3α (43, 143). A recent study analysing chemokine receptor mRNA expression in the CNS of mice exhibiting chronic-relapsing EAE demonstrated an up-regulation in CCR1 and CCR5 mRNA expression during acute and relapsing attacks, which correlated with expression of the corresponding ligands (144). Another study revealed that the chemokine receptors CCR1, CCR2, CCR3, CCR5 and CXCR4 were up-regulated on MBP-specific T cells *in vivo* (140). Thus, while chemokines and receptors are expressed by both resident cells and activated infiltrating cells (34, 137, 140, 143, 144), the level of expression does not correlate sufficiently to demonstrate a role for these chemokines/chemokine receptors in the pathogenesis of MS or EAE. Therefore, functional analysis of the chemokine system by blockade with neutralising antibodies, examination of disease in knockout mice, or blockade with receptor antagonists is required in order to determine the roles of chemokines and their receptors in disease.

1.7 Roles for chemokines and their receptors *in vivo*

1.7.1 Overview

Data obtained *in vitro* and from expression studies indicate that chemokines have the potential to play a critical role in a number of aspects of T cell biology. However, the contribution of chemokines to the control of T cell behaviour during inflammation *in vivo* remains ill-defined. The genetic deletion of chemokine and chemokine receptor genes, and the use of agonists, antagonists or neutralising antibodies to block chemokine or chemokine receptor function, has provided significant insight into the role of these molecules *in vivo*.

1.7.2 Ligand/receptor knockout mice

Gene knockouts are a common method of deducing the biological role of particular proteins, including chemokines and chemokine receptors, in a range of processes. These studies have revealed potential roles for a number of inflammatory chemokines and their receptors in T cell-mediated immune responses (see Tables 1.7 and 1.8). However, in most instances, a direct effect of gene deletion on T cell migration has not been demonstrated. In addition, while useful information has been gained, there are problems associated with this approach, chiefly because gene knockouts can be lethal (as is the case with SDF-1/CXCL12- and CXCR4-null mice), or can cause developmental disturbances (including in the immune system), which reduce the usefulness of the knockout mouse in studies examining certain aspects of the immune system.

Several mice deficient in chemokines and chemokine receptors have been used to investigate EAE. The complexity of results indicates the intricate regulation of EAE by the chemokine system. Mice deficient in MIP-1α/CCL3 or CCR5 were as susceptible to MOG-induced disease as their wild-type counterparts (145). With respect to MIP-1α/CCL3, these results are in contrast to that observed following treatment with anti-MIP-1α/CCL3 neutralising antibodies (See section 1.7.4). Deletion of CCR1 in the mouse resulted in reduced disease incidence and severity in MOG-induced EAE (146). Two independent research groups demonstrated that deletion of CCR2 almost completely protected mice from MOG-induced EAE (101, 147). The protection afforded was due to reduced numbers of T cells as well as infiltrating macrophages in the CNS. Similar results were obtained in MCP-1/CCL2-deficient mice, in that the gene deletion decreased the severity of disease by reducing the number of macrophages that accumulated in the CNS (148). Mice deficient in IP-10/CXCL10 were also shown to be partially protected from the chronic demyelination and clinical paralysis following intrathecal injections of mouse hepatitis virus (MHV) (149). Finally, CX_3CR1-deficient mice develop similar levels of disease in MOG-induced EAE compared with their wild-type counterparts (150).

1.7.3 Intrakine studies

Intrakines are a means of blocking chemokine receptor surface expression without altering the receptor gene (151-153). The intrakine is a normal chemokine with an additional endoplasmic reticulum retention signal sequence (KDEL) at the C-terminus that causes the chemokine to remain within the cell in the ER. The intracellular chemokine is then able to bind newly synthesised cognate chemokine receptors, preventing their transport to the surface of the cell. Since chemokines bind with a high affinity, and chemokine receptors

are constantly turned over (i.e. cell surface expression relies on *de novo* synthesis), in principle this technique blocks receptor surface expression (as has been demonstrated with CCR5 and CXCR4 (151-153). This gives a phenotypic knockout without the complications of embryonically lethal effects and developmental impairment that can arise with knockout mice. This approach has only been used *in vitro* to date.

1.7.4 Antibody neutralisation studies

A number of chemokines have been implicated in the T cell recruitment process during the generation of pathological immune responses in animals through the use of neutralizing antibodies. For example, blocking the function of MCP-1/CCL2 with a neutralising antibody was shown to greatly reduce the accumulation of T cells in the lung during *Cryptococcus neoformans* infection (154) or at a site of delayed-type hypersensitivity (DTH) activity in the rat (155). Similarly, the recruitment of polarised Th2 effector cells to a site of allergic airways disease could be reduced following the administration of neutralising antibodies to MDC/CCL22 or eotaxin/CCL11 (156). Furthermore, the administration of antibodies to TARC/CCL17 was shown to diminish the accumulation of T cells in the liver during bacteria-induced hepatic failure (157). Several groups have also studied the effect of antibody neutralisation of chemokines during neuroinflammation. Anti-MIP-1α/CCL3 (123) and anti-IP-10/CXCL10 (141) treatment prevented adoptively-transferred EAE in SJL/J mice by reducing the number of infiltrating mononuclear cells in the CNS. With respect to the latter, concordance was found following treatment with antibodies against CXCR3 (158). Anti-IP-10/CXCL10 treatment was also shown to reduce the clinical and histological symptoms of mouse hepatitis virus (MHV)-induced neuroinflammation in C57Bl/6 mice, but only when treatment was delayed until day 10

post-infection (159). In contrast, anti-CXCL10 treatment was shown to exacerbate EAE induced in rats using whole brain homogenates (142). Anti-MCP-1/CCL2 and anti-RANTES/CCL5 treatment had no effect on the development of the acute phase of adoptively-transferred EAE in SJL/J mice. However, anti-MCP-1/CCL2 treatment suppressed relapses of disease in chronic EAE (36, 136). More recently, anti-MIP-3α/CCL20 treatment was demonstrated to ameliorate EAE induced in SJL/J mice using whole spinal cord homogenate and in PLP-induced EAE (43).

1.7.5 Chemokine receptor antagonism studies

Chemokines have two main sites of interaction with their receptors – one in the N-terminal region and another within an exposed loop of the backbone that extends between the second and third cysteine residues (160). The N-terminal region is essential for the triggering of the receptor, while the loop region is required for initial binding (allowing correct presentation of the N-terminal region for triggering) (21, 161). Therefore, N-terminal truncations still bind to the receptor efficiently, without activating signal transduction. This allows them to act as competitive antagonists (Figure 1.5). This principle has been used to successfully create several different chemokine receptor antagonists (160, 162-164). Investigations specifically examining T cell function *in vivo* are yet to be conducted, however, several synthetic antagonists have been successful in treating autoimmune disease in the MRL/*lpr* mouse (165), and have reduced kidney transplant rejection in rats (166).

1.7.6 Summary

Thus, while the literature to date provides evidence that some inflammatory chemokines are required for effector T cell recruitment *in vivo*, many chemokines have not been investigated, and the chemokine receptors on T cells that mediate these effects have not been clearly identified.

1.8 The research project

The central hypothesis of this research project is as follows:

"Upon antigen-specific activation, encephalitogenic $CD4^+$ T cells up-regulate inflammatory chemokine receptors. These receptors are required for the cells to accumulate in the CNS tissue and mediate disease pathogenesis."

In order to test this hypothesis, the following aims will be addressed:

To identify chemokine receptors that are specifically regulated on antigen-activated $CD4^+$ T cells during the induction of an immune response *in vivo*;

To perform a detailed analysis of the expression patterns of these chemokine receptors on encephalitogenic T cells accumulating in the CNS during CNS inflammation;

To assess the impact that changes in chemokine receptor expression have on the effector functions of encephalitogenic T cells *in vivo*;

To determine the mechanisms by which changes in chemokine receptor expression influence the capacity of encephalitogenic T cells to mediate disease.

These aims are each addressed in turn in each of the data chapters of this thesis.

Table 1.1: Nomenclature and subfamily classification of chemokines [1, 2]

Systematic Nomenclature	Human Nomenclature	Mouse Nomenclature	Major Receptors
ELR$^+$ group			
CXCL1	GROα/MGSA-α	GRO/KC?	CXCR2, CXCR1
CXCL2	GROβ/MSGA-β	GRO/KC?	CXCR2
CXCL3	GROγ/MSGA-γ	GRO/KC?	CXCR2
CXCL5	ENA-78	LIX?	CXCR2
CXCL6	GCP-2	CKα-3	CXCR1, CXCR2
CXCL7	NAP-2	*not identified in mouse*	CXCR2
CXCL8	IL-8	*not identified in mouse*	CXCR1, CXCR2
ELR$^-$ group			
CXCL4	PF4	PF4	*not identified*
CXCL9	Mig	Mig	CXCR3
CXCL10	IP-10	IP-10	CXCR3
CXCL11	I-TAC	I-TAC	CXCR3
CXCL12	SDF-1α/β	SDF-1	CXCR4
CXCL13	BLC/BCA-1	BLC/BCA-1	CXCR5
CXCL14	BRAK/bolekine	BRAK	*not identified*
CXCL15	*not identified in human*	Lungkine	*not identified*
CXCL16	Sexckine	Sexckine	CXCR6

[1] Continued on next page

Table 1.1: Nomenclature and subfamily classification of chemokines, continued [1, 2]

Systematic Nomenclature	Human Nomenclature	Mouse Nomenclature	Major Receptors
CCL1	I-309	TCA-3	CCR8
CCL2	MCP-1	JE	CCR2
CCL3	MIP-1α	MIP-1α	CCR1, CCR5
CCL4	MIP-1β	MIP-1β	CCR5
CCL5	RANTES	RANTES	CCR1, CCR3, CCR5
CCL6	*not identified in human*	C10	*not identified*
CCL7	MCP-3	MARC?	CCR1, CCR2, CCR3
CCL8	MCP-2	MCP-2?	CCR3
CCL9/10	*not identified in human*	CCF18 / MIP-1γ	*not identified*
CCL11	Eotaxin	Eotaxin	CCR3
CCL12	*not identified in human*	MCP-5	CCR2
CCL13	MCP-4	*not identified in mouse*	CCR2, CCR3
CCL14	HCC-1	*not identified in mouse*	CCR1
CCL15	HCC-2 / MIP-1δ	*not identified in mouse*	CCR1, CCR3
CCL16	HCC-4	LCC-1	CCR1
CCL17	TARC	TARC	CCR4
CCL18	DC-CK1 / PARC	*not identified in mouse*	*not identified*
CCL19	ELC / MIP-3β / exodus-3	MIP-3β / ELC / exodus-3	CCR7, CCR11
CCL20	MIP-3α / LARC / exodus-1	MIP-3α / LARC / exodus-1	CCR6
CCL21	SLC / 6Ckine / exodus-2	SLC / 6Ckine / exodus-2 / TCA-4	CCR7, CCR11
CCL22	MDC / STCP-1	ABCD-1	CCR4
CCL23	MPIF-1	*not identified in mouse*	CCR1
CCL24	Eotaxin-2 / MPIF-2	*not identified in mouse*	CCR3
CCL25	TECK	TECK	CCR9, CCR11
CCL26	Eotaxin-3	*not identified in mouse*	CCR3
CCL27	CTACK/ILC	CTACK / ESkine	CCR10
CCL28	MEC	CCL28	CCR10

[1] Continued on next page

Table 1.1: Nomenclature and subfamily classification of chemokines, continued [2]

Systematic Nomenclature	Human Nomenclature	Mouse Nomenclature	Major Receptors
C Family			
XCL1	Lymphotactin / SCM-1α	Lymphotactin	XCR1
XCL2	SCM-1β	*not identified in mouse*	XCR1
CX_3C Family			
CX_3CL1	Fractalkine	Neurotactin	CX_3CR1

[2] Adapted from Zlotnik & Yoshie (19). Only the more common alternative names are shown; the first in the list is the one that will be used subsequently throughout the text. A question mark in the third column indicates that the listed mouse homologue may not correspond to the listed human ligand. In the forth column, the major (but not only) receptors for each ligand are shown.

Table 1.2: Functional classification of chemokines into inflammatory and homeostatic groupings

Inflammatory chemokines	Homeostatic chemokines
CC chemokines	
CCL1 / I-309	CCL18 / DC-CK1
CCL2 / MCP-1	CCL19 / ELC
CCL3 / MIP-1α	CCL21 / SLC
CCL4 / MIP-1β	CCL25 / TECK
CCL5 / RANTES	CCL28 / MEC
CCL7 / MCP-3	
CCL8 / MCP-2	
CCL11 / eotaxin-1	
CCL12 / MCP-5	
CCL13 / MCP-4	
CCL17 / TARC	
CCL20 / MIP-3α	CCL20 / MIP-3α
CCL22 / MDC	
CCL24 / eotaxin-2	
CCL26 / eotaxin-3	
CCL27 / CTACK	
CXC chemokines	
CXCL1 / GROα	CXCL12 / SDF-1
CXCL2 / GROβ	CXCL13 / BLC
CXCL3 / GROγ	
CXCL5 / ENA-78	
CXCL6 / GCP-2	
CXCL7 / NAP-2	
CXCL8 / IL-8	
CXCL9 / Mig	
CXCL10 / IP-10	
CXCL11 / I-TAC	
CXCL16	
C and CX3C chemokines	
XCL1 / lymphotactin	
CX3CL1 / fractalkine	

[1] Adapted from Sallusto *et al* (67) and Moser and Loetscher (22). Chemokines for which expression patterns have not been characterized are not included.

Table 1.3: Promiscuous Chemokine Receptor-Ligand Interactions[1]

Receptor	Ligands
CXCR1	CXCL1, CXCL6, CXCL8
CXCR2	CXCL1, CXCL2, CXCL3, CXCL5, CXCL6, CXCL7, CXCL8
CXCR3	CXCL9, CXCL10, CXCL11
CXCR4	CXCL12
CXCR5	CXCL13
CXCR6	CXCL16
CCR1	CCL3, CCL5, CCL7, CCL14, CCL15, CCL16, CCL23
CCR2	CCL2, CCL7, CCL12, CCL13
CCR3	CCL5, CCL7, CCL8, CCL11, CCL13, CCL15, CCL24, CCL26
CCR4	CCL17, CCL22
CCR5	CCL3, CCL4, CCL5
CCR6	CCL20
CCR7	CCL19, CCL21
CCR8	CCL1, CCL17
CCR9	CCL25
CCR10	CCL27, CCL28
CCR11	CCL19, CCL21, CCL25
XCR1	XCL1, XCL2
CX_3CR1	CX_3CL1
DARC	CXCL1, CXCL8, CCL3, CCL4, CCL5

[1] Adapted from Proudfoot *et al* (164). Chemokine receptors are listed, along with their major ligands. Ligands that show only limited affinity for the receptor, or do not induce a significant agonistic response, are not shown.

Table 1.4: T cell-active chemokines: subset dependent chemotaxis

Chemokine	T cell chemotaxis profile
Inflammatory chemokines	
CCL1 / I-309	effector/memory (Th2 preference)
CCL2 / MCP-1	effector/memory
CCL3 / MIP-1a	effector/memory
CCL4 / MIP-1b	effector/memory (Th1 preference)
CCL5 / RANTES	effector/memory (Th1 preference)
CCL7 / MCP-3	effector/memory
CCL8 / MCP-2	effector/memory
CCL11 / eotaxin	effector/memory (Th2 preference)
CCL17 / TARC	effector/memory (Th2 and CLA+ preference)
CCL20 / MIP-3a	effector/memory
CCL22 / MDC	effector/memory (Th2 and CLA+ preference)
CCL25 / TECK	effector/memory, thymocytes
CCL27 / CTACK	effector/memory (CLA+ preference)
CXCL9 / mig	effector/memory (Th1 preference)
CXCL10 / IP-10	effector/memory (Th1 preference)
CXCL11 / I-TAC	effector/memory (Th1 preference)
CXCL16	effector/memory
XCL1 / lymphotactin	effector/memory, thymocytes
CX3CL1 / fractalkine	effector/memory
Homeostatic chemokines	
CCL18 / DC-CK1	naïve
CCL19 / ELC	naïve, effector/memory
CCL21 / SLC	naïve, effector/memory
CCL25 / TECK	effector/memory, thymocytes
CCL28 / MEC	effector/memory (CLA+ preference)
CXCL12 / SDF-1	naïve, effector/memory, thymocytes
CXCL13 / BLC	effector/memory

[1] Adapted from Moser and Loetscher (22). All chemokines listed have been demonstrated to be chemotactic for human T cells in *in vitro* assays. The differential responsiveness of various subsets has either been demonstrated in chemotaxis assays, or inferred through subset-restricted expression of the relevant receptors.

Table 1.5: Chemokine Receptor Expression on $CD4^+$ T Lymphocyte subsets [1]

Receptor	Expression on $CD4^+$ T Lymphocytes
CXCR1	Expressed on both naïve and memory $CD8^+$ T cells, with a greater with greater expression in the memory subset (human)
CXCR2	No data available
CXCR3	Expressed on effector/memory cells (Th1 preference)
CXCR4	Expressed on naïve cells, effector/memory cells and thymocytes
CXCR5	Expressed on effector/memory cells (Follicular B helper T cells (T_{FH}))
CXCR6	Expressed on effector/memory cells (Th1 preference)(167)
CCR1	Expressed on effector/memory cells
CCR2	Expressed on effector/memory cells
CCR3	Expressed on effector/memory cells (Th2 preference)
CCR4	Expressed on effector/memory cells (Th2 and CLA+ preference)
CCR5	Expressed on effector/memory cells (Th1 preference)
CCR6	Expressed on effector/memory cells
CCR7	Expressed on naïve and central memory T cells (T_{CM}), but not peripheral memory cells
CCR8	Expressed on effector/memory cells (Th2 preference)
CCR9	Expressed on effector/memory cells and thymocytes
CCR10	Expressed on effector/memory cells (CLA+ preference)
CCR11	No data available
XCR1	Expressed on effector/memory cells
CX3CR1	Expressed on effector/memory cells and thymocytes

[1] Adapted from Moser and Loetscher (22). The receptors listed have been demonstrated to be expressed on subsets of human T cells in *in vitro* assays. Additional information is referenced accordingly.

Table 1.6: Expression of chemokines and chemokine receptors in EAE/MS [1]

Chemokine	Detected in EAE	Detected in MS lesions	Detected in MS CSF
CCL1 / TCA-3	+ (168)		
CCL2 / MCP-1	+ (79, 126)	+ (169)	
CCL3 /MIP-1α	+ (79)	+ (114)	+ (170)
CCL4 / MIP-1β	+ (35, 168)	+ (114)	
CCL5 / RANTES	+ (36)	+ (114)	+ (115)
CCL6 / C10	+ (171)		
CCL7 / MCP-3	+ (35, 171)	+ (169)	
CCL8 / MCP-2		+ (169)	
CCL21 / SLC	+ (31)		
CCL19 / ELC	+ (31)		
CCL20 / MIP-3α	+ (43, 143)		
CXCL9 / Mig	+ (142)		+ (115)
CXCL10 / IP-10	+ (126, 141)	+ (114, 116)	+ (115)
CXCL11 / I-TAC	+ (142)		
CXCL12 / SDF-1			+ (139)
CX3CL1/ fractalkine	+ (172)		
Receptor			
CCR1	+ (140)		
CCR2	+ (140)		
CCR3	+ (140)		
CCR4	+ (137)		
CCR5	+ (140)	+ (114, 116)	+ (115)
CCR6	+ (143)		+ (96)
CCR8	+ (137)		
CXCR2	+ (173)		
CXCR3	+ (140, 141)	+ (114, 116)	+ (115)
CXCR4	+ (140)		

[1] Ligands and receptors are listed that have been detected in EAE or in multiple sclerosis (either through detection in brain lesions, or in the CSF).

Table 1.7: Phenotypes of chemokine receptor knock-out mice [1, 2]

Mouse	Summary of phenotype	Reference
CCR1	• defective myelopoiesis under conditions of homeostasis and LPS challenge • reduced immunity to *Aspergillus fumigatus* • reduced SEA-induced granuloma formation, associated with increased IFN-γ secretion resistance to EAE development	(174) (146)
CCR2	• reduced recruitment of macrophages to peritoneal cavity • decrease in size and macrophage content of *Mycobacterium bovis* PPD-induced granulomas • altered IL-2 and IFN-γ production by lymphocytes resistance to EAE development	(175) (101) (147)
CCR4	• resistance to high and low dose models of endotoxemia • reduced numbers of macrophages in LPS-stimulated peritoneal cavity	(176)
CCR5	• altered cytokine production by macrophages and T cells • reduced ability to clear *Listeria monocytogenes* infection • enhance resistance to endotoxemia • increased contact sensitivity response to FITC • increased IgG1 response to soluble protein antigens no significant difference to EAE development	(177) (145)
CCR6	• absence of $CD11b^+$ $CD11c^+$ dendritic cell sub-population within intestinal sub-epithelial dome • increased numbers of lymphocytes in intestinal epithelium • reduced intestinal humoral immune response to KLH and rotavirus • enhanced contact sensitivity response to DNFB • reduced DTH response to allogeneic splenocytes	(178) (179)
CCR7	• altered secondary lymphoid tissue architecture • altered frequencies of immunoglobulin isotypes • disrupted migration of DCs, T cells and B cells to secondary lymphoid tissue • impaired T cell and humoral immune responses	(180)
CCR8	• reduced eosinophil content in SEA-induced granulomas • Th2 cytokine production defect • reduced numbers of pulmonary and circulating eosinophils during allergic airways inflammation	(181)

[1] Continued next page

Table 1.7: Phenotypes of chemokine receptor knock-out mice, continued [2]

Mouse	Summary of phenotype	Reference
CXCR2	• enlarged lymph nodes and spleen due to increase in myelopoeisis and increased B cell numbers • defective neutrophil migration to peritoneum following thioglycollate injection	(182)
CXCR3	• decreased MLR response • increased acceptance of cardiac allografts	(33)
CXCR4	• embryonic lethal • defective haematopoiesis in bone marrow and liver • abnormal cardiac and cerebellum development	(87)
CXCR5	• absence of inguinal lymph nodes and Peyer's patches • disrupted primary and secondary follicle architecture in spleen • increased B cell numbers in blood and spleen • inability of transferred $CXCR5^{-/-}$ B cells to home to follicles	(183)
CX3CR1	• increased cardiac allograft survival in the presence of cyclosporin no change in MOG-induced EAE	(150)

[2] A summary of the differences between each genetically deficient mouse and its wild-type counterpart is given. In general, where numerous studies have used a particular knock-out mouse, only the basic characterisation of the phenotype is described. Additionally, where determined, the effect of the knock-out on the development of EAE is described. Negative results, in which the knock-out animal was not significantly different to the wild-type, are not described.

Table 1.8: Phenotypes of chemokine ligand knock-out mice [1]

Mouse	Summary of phenotype	Reference
CCL2 / MCP-1	• reduced recruitment of monocytes/macrophages to peritoneum and sites of DTH • defect in Th2-associated immune responses, and reduced lymphocyte production of Th2 cytokines resistance to EAE development	(81) (184) (148)
CCL3 / MIP-1α	• reduced autoimmune response to Coxsackie-virus • reduced clearance of influenza virus no significant effect on EAE development	(185) (145)
CCL11 / eotaxin	• lower numbers of circulating eosinophils • early reduction in eosinophil recruitment to the lung and cornea in models of eosinophil-associated inflammation	(186)
CXCL10 / IP-10	• cardiac allografts derived from CXCL10 $^{-/-}$ mice show increased survival in wild-type recipients resistance to MHV-induced EAE	(187) (149)
CXCL12 / SDF-1	• embryonic lethal • defective haematopoiesis in bone marrow and liver • abnormal cardiac development	(30)
CX_3CL1 / fractalkine	• lower numbers of circulating F4/80+ cells	(188)

[1] A summary of the differences between each genetically deficient mouse and its wild-type counterpart is given. In general, where numerous studies have used a particular knock-out mouse, only the basic characterisation of the phenotype is described. Negative results, whereby the knock-out animal was not significantly different to the wild-type, are not described.

Figure 1.1 – The molecular mechanisms of T cell extravasation. T cells flowing through the blood vessel lumen interact transiently with endothelial cells via the binding of selectins (and, to a lesser extent, α4 integrins) to their counter-receptors on endothelial cells. These interactions initially involve a loose tethering, mediated by clustered adhesion molecules on the tips of microvilli, which is followed by a more sustained rolling motion, which does not require adhesion molecule clustering. Rolling T cells are slowed down sufficiently to enable interactions of chemoattractant molecules (particularly chemokines) with their 7-transmembrane domain receptors on the T cell surface, leading to the activation of T cell-expressed integrins. The subsequent binding of activated integrins on T cells to their counter-receptors on endothelial cells allows for T cell arrest (firm adhesion), which is followed by diapedesis through inter-endothelial junctions and chemokine-guided movement through the tissues. From von Andrian & Mackay (5).

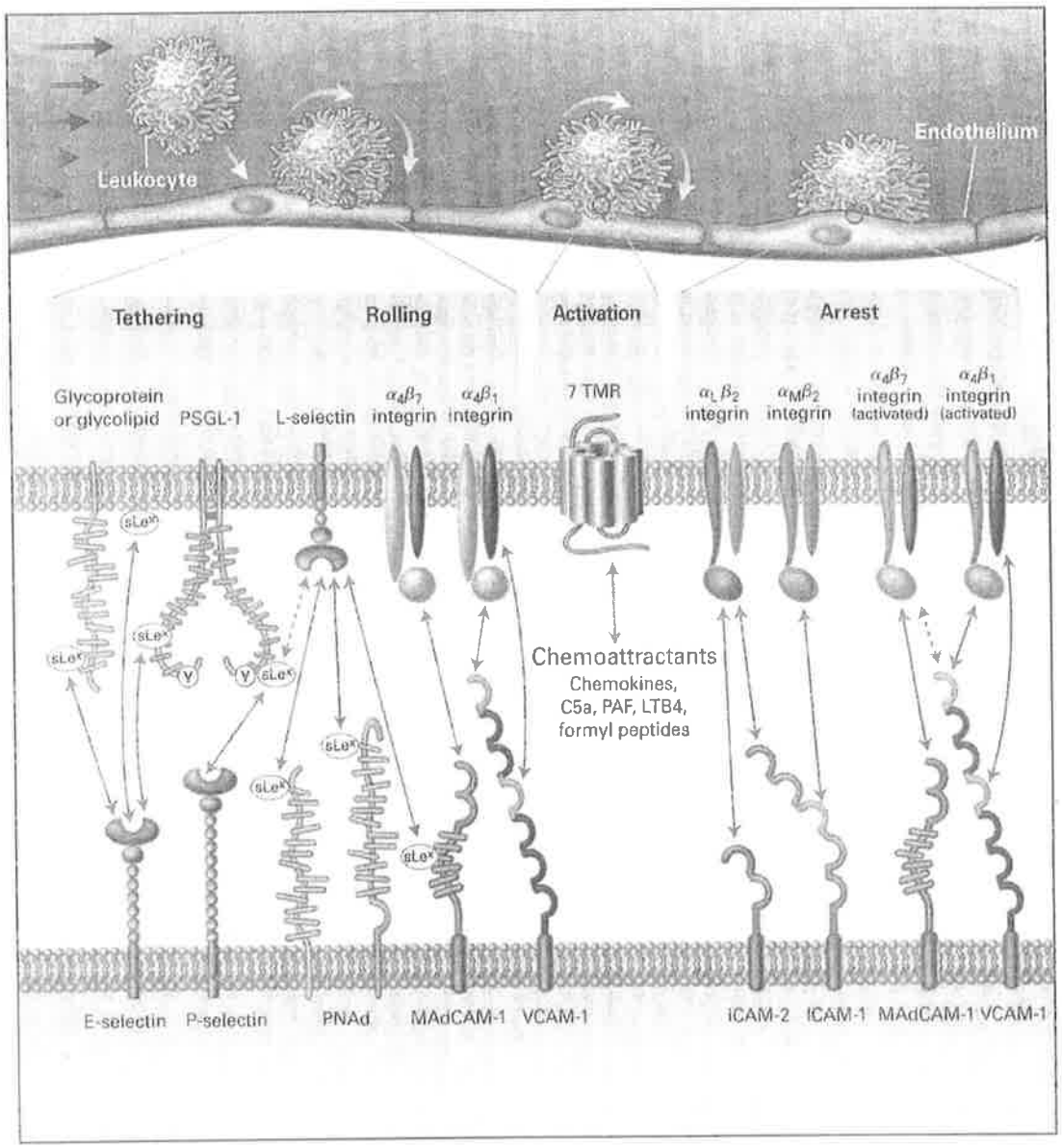
Leukocyte
Endothelium
Tethering
Rolling
Activation
Arrest
Glycoprotein or glycolipid
PSGL-1
L-selectin
$\alpha_4\beta_7$ integrin
$\alpha_4\beta_1$ integrin
7 TMR
$\alpha_L\beta_2$ integrin
$\alpha_M\beta_2$ integrin
$\alpha_4\beta_7$ integrin (activated)
$\alpha_4\beta_1$ integrin (activated)
sLe^x
Chemoattractants
Chemokines, C5a, PAF, LTB4, formyl peptides
E-selectin
P-selectin
PNAd
MAdCAM-1
VCAM-1
ICAM-2
ICAM-1
MAdCAM-1
VCAM-1

Figure 1.2 – The classification of chemokines according to primary amino acid sequence. Chemokines can be classified into two major (CXC / α and CC / β) and two minor (C / γ and CX3C / δ) sub-families, on the basis of a cysteine-containing motif. Members of the CXC sub-family have an intervening amino acid between the first two cysteines, and can be further sub-divided according to the presence or absence of the glutamine-leucine-asparagine (ELR) motif. This sub-family also contains one member with an extended, membrane-bound structure (CXCL16). Members of the CC sub-family are characterised by the juxtaposition of the first two cysteines, while the C sub-family members are missing two of the four cysteines normally found within the motif. The sole member of the CX3C sub-family has three intervening amino acids between the first two cysteines, and an extended, membrane-bound structure. Adapted from Gale & McColl (16).

CXC (α) sub-family

CC (β) sub-family

C (γ) sub-family

CX_3C (δ) sub-family

Figure 1.3 – Chemokine system involvement in the recruitment and localisation of T and B cells within secondary lymphoid organs and peripheral tissues. Naïve $CD4^+$ T cells expressing CCR7 and CXCR4 migrate across the HEVs along a gradient of ELC/CCL19 and SLC/CCL21 and into the T cell zone. Witin the T cell zone, interactions with dendritic cells (DCs) results in differentiation into memory and effector T cells. Effector Th1/Th2 T cells and effector memory cells (T_{EM}), which are distinguished by chemokine receptor expression, exit the secondary lymphoid organ to recirculate through peripheral tissues. CCR7-expressing central memory T cells circulate between the blood and secondary lymphoid tissues. BCA-1/CXCL13 present in B cell follicles positions $CXCR5^+$ T and B cells for generation of antibody producing plasma cells. Adapted from Moser & Loetscher (22) and Moser & Ebert (91).

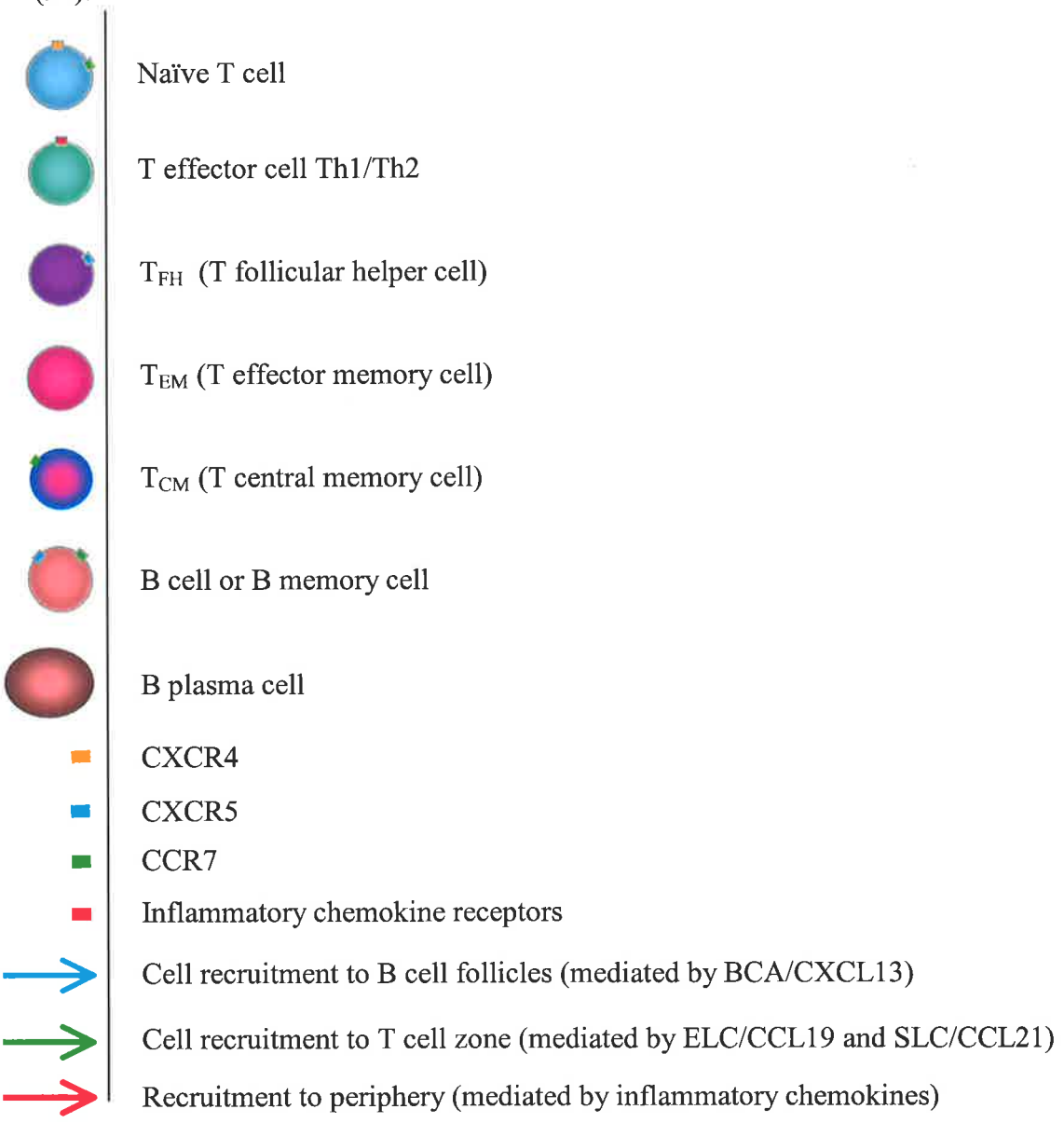

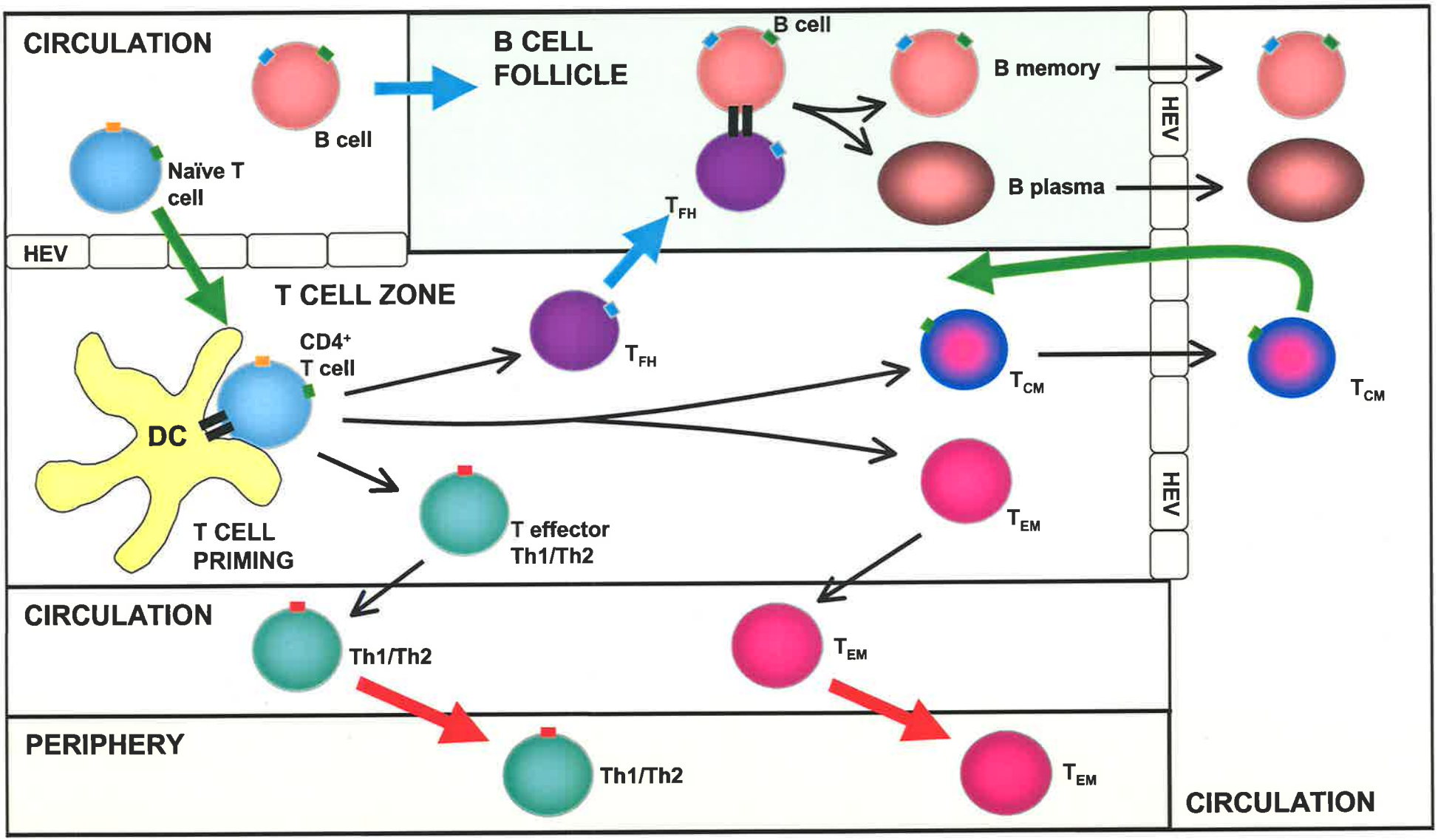
CIRCULATION
B cell
Naïve T cell
HEV
B CELL FOLLICLE
B cell
B memory
B plasma
HEV
T CELL ZONE
CD4+ T cell
DC
T CELL PRIMING
T effector Th1/Th2
T FH
T FH
T CM
T CM
T EM
HEV
CIRCULATION
Th1/Th2
T EM
PERIPHERY
Th1/Th2
T EM
CIRCULATION

Figure 1.4 – Schematic representation of the blood brain barrier and resident cells of the central nervous system. The healthy CNS is surrounded by the blood-brain barrier (BBB), which consists of microvessel endothelial cells with tight junctions, the perivascular space, the basement membrane, and associated cells including microglia and astrocytes. Behind the BBB, the CNS is composed of impulse-conducting neurons, oligodendrocytes, astrocytes, and microglia. Adapted from (270).

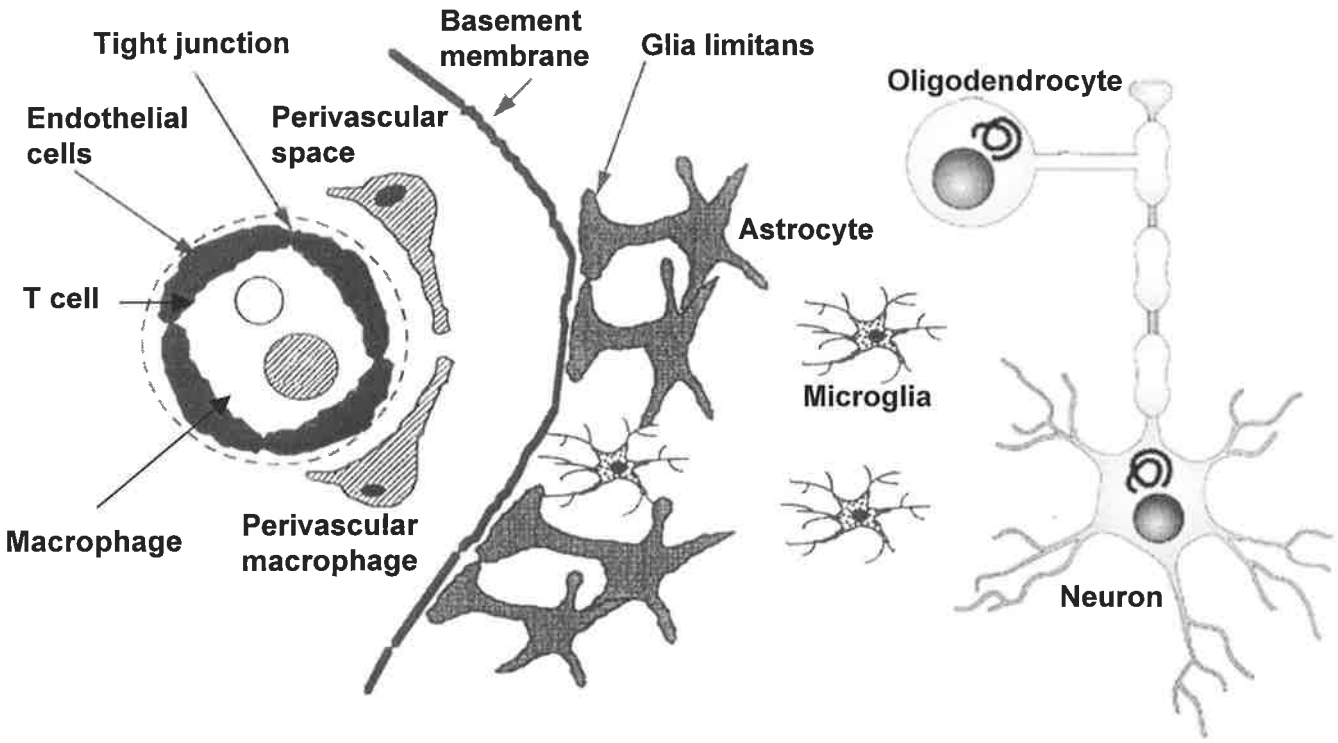
Tight junction
Basement membrane
Glia limitans
Endothelial cells
Perivascular space
Oligodendrocyte
Astrocyte
T cell
Microglia
Macrophage
Perivascular macrophage
Neuron
Blood Brain Barrier
Parenchyma

Figure 1.5 – Action of N-terminally modified chemokines as receptor antagonists. Presented in this figure is the proposed mechanism of antagonism of chemokine receptors by N-terminally modified chemokines.

(A) The wild-type chemokine binds to the 7 transmembrane-spanning chemokine receptor with the exposed loop of the backbone that extends between the second and third cysteine residues. This allows the flexible N-terminal region of the ligand to facilitate activation of the receptor for signal transduction.

(B) The N-terminally modified chemokine is able to bind to the chemokine receptor through the internal loop, but does not have the N-terminal sequence required to activate the receptor. Therefore, it is able to compete with the wild-type chemokine for receptor binding without subsequent activation, thus allowing it to act as a successful antagonist at high concentrations.

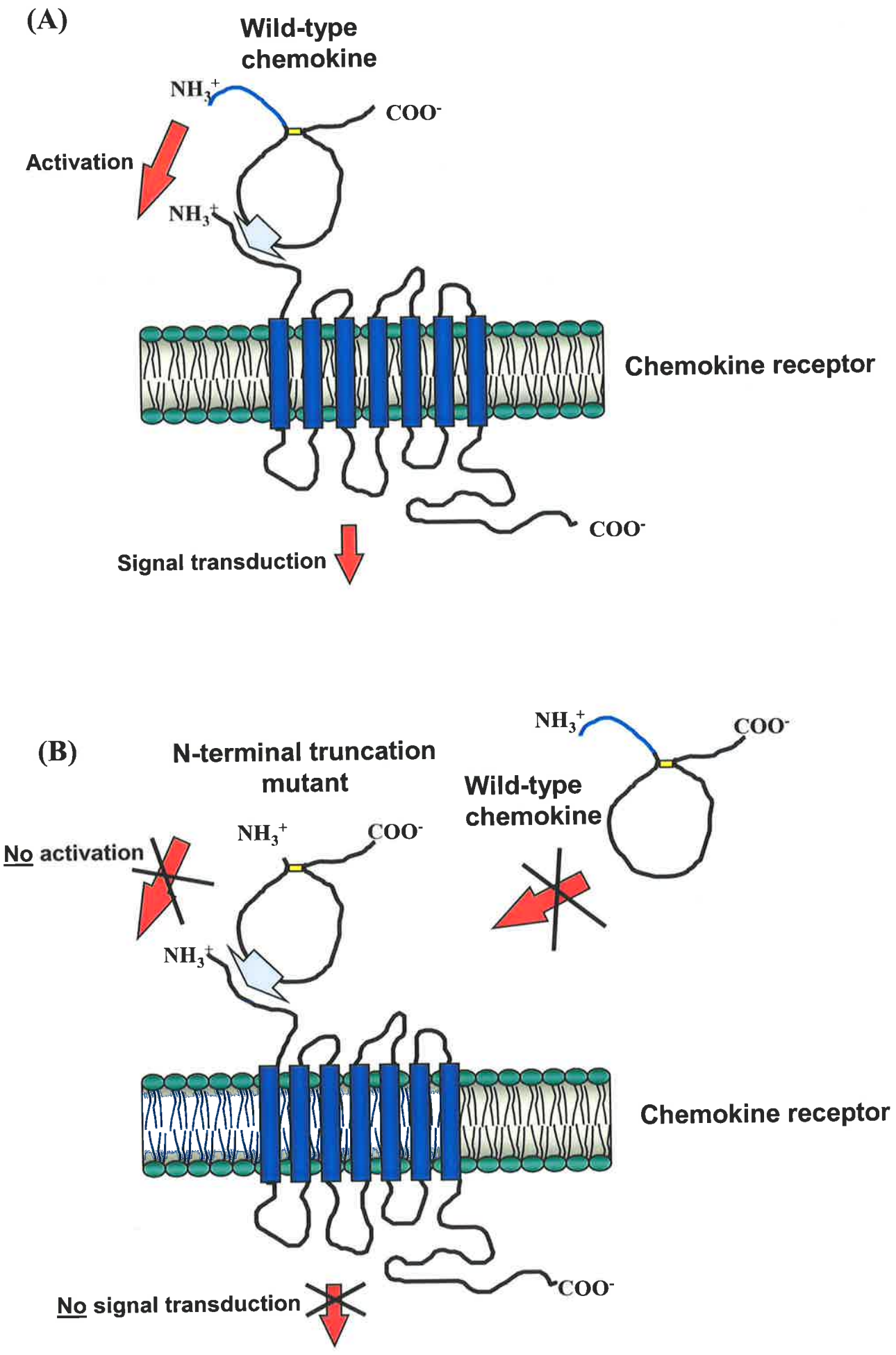
(A)
Wild-type chemokine
NH3+
COO-
Activation
NH3+
Chemokine receptor
COO-
Signal transduction
(B)
N-terminal truncation mutant
NH3+
COO-
No activation
NH3+
Wild-type chemokine
NH3+
COO-
Chemokine receptor
COO-
No signal transduction

Chapter 2

Materials and Methods

2.1 Animals and Reagents

2.1.1 Mouse strains and conditions

Female SJL/J mice (H-2^s) were purchased from the Animal Resource Centre (Perth, WA, Australia) or the Australian National University (Canberra, ACT, Australia). Female BALB/c mice (H-2^d) were purchased from the Adelaide University Animal House (Adelaide, SA, Australia). BALB/c mice were housed in the conventional rodent room and SJL/J mice were housed in the non-approved supplier room (Adelaide University Animal House). Mice were aged 6-9 weeks at the initiation of experiments. Mice were kept under standard temperature and light conditions, and afforded food and water *ad libitum*. Severely paralysed mice were hand fed and watered.

2.1.2 General chemicals

The following chemicals were obtained from Sigma Australia (Castle Hill, NSW, Australia): polyoxyethylene sorbitan monolaurate (Tween-20), p-phenylenediamine (PPD), β-Mercaptoethanol and diethylpyrocarbonate (DEPC).

The following chemicals were obtained from BDH Chemicals (Kilsyth, VIC, Australia): sodium chloride (NaCl), disodium hydrogen orthophosphate (Na_2HPO_4), ethylenediaminotetra-acetic acid (EDTA), potassium dihydrogen orthophosphate (KH_2PO_4), D-glucose, HEPES, calcium chloride ($CaCl_2$), paraformaldehyde (PFA),

sodium hydroxide (NaOH), ethanol, chloroform, propan-2-ol (isopropanol), glacial acetic acid and hydrochloric acid (HCl).

The following chemicals were obtained from Ajax Chemicals (Auburn, NSW): potassium chloride (KCl), magnesium chloride ($MgCl_2$), sodium azide (NaN_3) sodium carbonate (Na_2CO_3), sodium hydrogen carbonate ($NaHCO_3$), glycerol and acetone.

Tris hydrochloride (Tris-HCl) was obtained from ICN Biomedicals Australasia (Seven Hills, NSW) and agarose was obtained from Progen Biotechnik (Heidelburg, Germany).

The sources of specialised reagents are stated at the relevant place in the text.

2.1.3 Antigens and adjuvants used in vivo

2.1.3.1 Proteolipid protein (PLP) peptide 139-151

$PLP_{139-151}$ is the encephalitogenic peptide of proteolipid protein and was a kind gift from Pr Ian Clark-Lewis (Biomedical Research Centre, University of British Columbia, Vancouver, Canada). The sequence (N→ C Terminus) is as follows: HSLGKWLGHPDKF. $PLP_{139-151}$ was received in dessicated form and stored at 4°C.

2.1.3.2 Incomplete Freund's Adjuvant (IFA)

IFA was made up with 85% mineral oil and 15% Mannide monooleate (Sigma Chemical Co, St Louis, MO, USA). IFA was stored at 4°C.

2.1.3.3 Complete Freund's Adjuvant (CFA)

CFA contained 0.5 mg/ml *Mycobacterium butyricum* (Difco Laboratories, Detroit, MI, USA) and 8.33 mg/ml *M. tuberculosis* H37Ra (Difco Laboratories) in IFA (Section 2.1.3.1). The bacteria were ground using a mortar and pestle in incomplete Freund's adjuvant.

2.1.3.4 Pertussigen

Pertussigen, a crude extract of *Bordetella pertussis* cells, was a gift from Dr. David Willenborg (Neurosciences Research Unit, Canberra Hospital, Canberra, ACT). It was received in dessicated form and reconstituted to 100 µg/200 µl aliquots in endotoxin-free PBS then stored at -70°C.

2.1.4 Chemokine peptides

Synthetic peptides used were a kind gift from Pr Ian Clark-Lewis. A brief description of the chemokines, and their sequences is contained in Table 2.1.

2.1.5 Antibodies and conjugates

Primary antibodies used in flow cytometry and ELISA are listed in Table 2.2. Secondary detection reagents are listed in Table 2.3.

2.1.6 Enzymes and Oligonucleotides

2.1.6.1 Enzymes

All enzymes used are listed in Table 2.4.

2.1.6.2 Oligonucleotide primers

Primers used for PCR amplification and reverse transcription are listed in Table 2.5. All primers were purchased from GeneWorks (Adelaide, SA) and were of RPC purity. Primers were received in a lyophilised form, diluted in sterile Milli-Q water and stored at –20°C.

2.1.7 General Solutions

2.1.7.1 Hank's Balanced Salt Solution (HBSS)

The following reagents were dissolved in Milli-Q water to generate 10X stocks: 80 g/L NaCl, 4 g/L KCl, 0.32 g/L Na_2HPO_4, 0.6 g/L KH_2PO_4 and 10 g/L D-glucose and the

solution sterilised by autoclaving. When required for use, the solution was diluted to 1X in Milli-Q water, and HEPES buffer (pH 7.4) and $CaCl_2$ were added to a final concentration of 0.01 M and 1.6 mM, respectively.

2.1.7.2 Phosphate buffered saline (PBS)

The following reagents were dissolved in Milli-Q water: 8 g/L NaCl, 0.2 g/L KCl, 1.15 g/L Na_2HPO_4, 0.2 g/L KH_2PO_4 and the solution sterilised by autoclaving. Endotoxin-free PBS was obtained from the Media Production Unit of the Institute of Medical and Veterinary Sciences (IMVS; Adelaide, SA).

2.1.7.3 ELISA coating buffer

$NaHCO_3$ was dissolved in Milli-Q water to a concentration of 0.1 M, the pH was adjusted to 9.6 and the solution sterilised by autoclaving.

2.1.7.4 PBS/Tween

Tween-20 (polyoxyethylene sorbitan monolaurate) was added to PBS to a final concentration of 0.2% (w/v) and the solution mixed thoroughly.

2.1.7.5 Mowiol mounting medium

Mowiol mounting medium base was purchased from Calbiochem (La Jolla, CA, USA) and prepared as follows: 2.4 g of Mowiol was mixed with 6 g of glycerol, 6 ml of Milli-Q water and 12 ml of 0.2 M Tris-HCl (pH 8.5). The mixture was gently stirred at RT for 4 hours, incubated at RT for 2 hours without mixing, and then incubated in a 50°C water

bath for 10 minutes. Any undissolved powder was then pelleted by centrifuging for 15 minutes at 5000 *x g* and aliquots of the supernatant stored at –20°C). When required, an aliquot was thawed and PPD was added as an anti-fade agent (a saturated solution of PPD was prepared in absolute ethanol and this solution diluted 1:50 into the mounting medium just prior to use).

2.1.7.6 Standard Isotonic Percoll (SIP)

Standard isotonic percoll was prepared by mixing 1 part HBSS with 9 parts Percoll (Amersham Pharmacia Biotech Australia, Castle Hill, NSW).

2.1.7.7 Mouse Red Cell Removal Buffer (MRCRB)

MRCRB was prepared by mixing 9 parts Solution A (8.3 g NH_4Cl made up to 1 L with Milli-Q water) with 1 part Solution B (20.6 g Tris base made up to 1 L with Milli-Q water and adjusted to pH 7.65 with HCl). MRCRB was filter sterilized and stored at 4°C.

2.1.7.8 Staining buffer for flow cytometry

PBS was mixed with 1% Bovine serum albumin (BSA; Sigma) and 0.04% NaN_3 (both w/v) and stored at 4°C.

2.1.7.9 1% Paraformaldehyde (PFA)

1% paraformaldehyde (w/v) was prepared by dissolving paraformaldehyde in PBS (pH 7.4) at 55°C with stirring for approximately 30 minutes. PFA was stored at 4°C for up to one month.

2.1.7.10 DNase solution for BrdU labelling

Stock solutions of DNase were prepared by dissolving DNase I (Sigma) to 5000 U/ml in a solution of 4.2 mM $MgCl_2$ + 0.15 mM NaCl in Milli-Q water (pH 5.0). Aliquots of the stock solution were stored at –20°C. When required, an aliquot of stock solution was thawed and diluted to 50 units/ml in 4.2 mM $MgCl_2$ + 0.15 mM NaCl.

2.1.7.11 1% acid alcohol

In a large container, 10 ml of concentrated hydrochloric acid was added to 300 ml of distilled water. Seven hundred ml of commercial grade ethanol was added to the acid/water solution, then mixed thoroughly.

2.1.7.12 Scott's Tapwater substitute

The following reagents were dissolved in Milli-Q water: 2 g sodium bicarbonate and 20 g magnesium sulphate,then made up to 1 L with additional Milli-Q water. The solution was filter-sterilised and stored at RT.

2.1.7.13 DEPC-treated water

DEPC was diluted to 0.1% (vol/vol) in Milli-Q water, incubated overnight at RT and then autoclaved.

2.1.7.14 TAE

1x TAE consisted of 0.04 M Tris-acetate, 0.02 M Na acetate, 1 mM EDTA (pH 7.4).

2.1.7.15 DNA Loading buffer

6 x DNA loading buffer consisted of 30% sucrose (w/v) and 0.35% Orange G (Sigma) in sterile Milli-Q water.

2.2 *In vivo* techniques

2.2.1 Active induction of EAE with $PLP_{139-151}$ in CFA

Female SJL/J mice were immunised with 50 µg of $PLP_{139-151}$ (Section 2.1.3.1) in CFA (Section 2.1.3.3). The emulsion contained 50 µl of 50 µg $PLP_{139-151}$ in endotoxin free PBS and 50 µl of CFA (PLP/CFA). In the case of control immunisation, the emulsion contained 50 µl of endotoxin free PBS and 50 µl of CFA (PBS/CFA). Fifty microlitres of the emulsion were injected subcutaneously (s.c.) into each hind flank. Two hours prior to immunisation, and two days after, the mice were intravenously (i.v.) injected with 5 µg of pertussigen (Section 2.1.3.4) in 250 µl of endotoxin free PBS.

2.2.2 Adoptive transfer of EAE using $PLP_{139-151}$-activated cells

Donor SJL/J mice were primed by immunisation with 25 µg $PLP_{139-151}$ emulsified in CFA. Each mouse received 120 µl of the emulsion. Forty microlitres of the emulsion were injected s.c. into each hind footpad, 10 µl were injected s.c. into each front footpad, and 20

μl were injected s.c. into the nape of the neck. Ten days later, the mice were sacrificed by carbon dioxide asphyxiation. The draining lymph nodes (popliteal, axillary and brachial) were removed, and lymph node cells were pooled and cultured *in vitro* for 96 hours in RPMI-10% FCS at 4 X 10^6 viable cells/ml in the presence of 50 μg/ml $PLP_{139-151}$. Cells were incubated at 37°C in a humidified atmosphere containing 5% CO_2. The cells were harvested after 96 hours culture, washed, and $5x10^7$ viable cells were transferred i.v. into normal SJL/J recipients.

2.2.3 Clinical assessment of EAE

Mice were evaluated daily until day 21 post-immunisation or post-transfer, and scored for severity of clinical disease on a scale of 0-5, as follows; 0, no clinically detectable signs of EAE; 0.5, early symptoms of movement dysfunction; 1, slight weakness in the tail or agitated gait; 2, definite tail and partial hind limb paralysis or inability to turn over when placed on back; 3, complete hindquarter paralysis; 3.5, complete hindquarter paralysis with partial forelimb paralysis; 4, complete hindquarter and forelimb paralysis; 5, moribund.

2.2.4 Treatment of mice with chemokine antagonists

In experiments involving SDF-1 P2G and RANTES 9-68, mice were injected into the peritoneal cavity (i.p.) with 250 μl of endotoxin free PBS containing 100 μg of either SDF-1 P2G, RANTES 9-68 or the control peptide MCP-ala (Table 2.1). In experiments involving I-TAC 4-79, mice were injected i.p. with 250 μl of endotoxin free PBS

containing 250 µg of either I-TAC 4-79 or MCP-ala (Table 2.1). The antagonist was administered on Days 1, 3, 5, 7, 9, 11, 13 and 15 post-induction. In experiments involving the combined treatment of SDF-1 P2G and I-TAC 4-79, mice were injected i.p. with 250 µl of endotoxin free PBS containing 100 µg of SDF-1 P2G + 250 µg of I-TAC 4-79 or 350 µg of MCP-ala. In these experiments, the antagonists were administered on Days 1, 3, 5, 7, 9, 11, and 13 post-induction.

2.2.5 Passive immunisation with Salmonella enteriditis

BALB/c mice were injected i.p. with 3 x 10^5 colony forming units of *Salmonella enteriditis* in 500 µl of PBS. Five days later, the mice were sacrificed by carbon dioxide asphyxiation and peritoneal washouts were performed (see section 2.3.3).

2.2.6 Detection of cellular proliferation by BrdU incorporation

BrdU (Sigma) was dissolved to 0.8mg/ml in the drinking water of the animals starting at day 6 post-immunisation with $PLP_{139-151}$ in CFA. The drinking bottles were covered in aluminium foil to prevent light-induced degradation of BrdU. This procedure was carried out every second day until the day of experimental end-point.

2.3 Primary cell isolation and collection of tissues and serum

2.3.1 Preparation of single cell suspensions from lymphoid organs

Mice were sacrificed by carbon dioxide asphyxiation and LNs and/or thymi removed by blunt dissection. Organs were placed individually onto cell strainers (with 70 μm nylon mesh) resting in a 35 mm tissue culture dish (both from BD Falcon™, BD Biosciences, Franklin Lakes, NJ, USA) containing ~1ml of RPMI-1% FCS (see section 2.4.1.3). The capsule was cut with scissors and lymphocytes released into the dish by gentle homogenisation with the plunger of a 5 ml syringe. Cells were collected from the tissue culture dish, washed twice, and resuspended at the desired concentration.

2.3.2 Isolation of leukocytes from spinal cords

Mice were sacrificed by carbon dioxide asphyxiation, and perfused through the left ventricle with ice-cold PBS to remove circulating leukocytes. The spinal cord was extracted from the spinal column using scissors to cut the vertebrae and a scalpel to remove the cord. Following removal, the spinal cord was passed through a cell strainer (BD Falcon™). The cell suspension passing through the strainer was collected in 30 ml of RPMI supplemented with 1% FCS (see section 2.4.1.3), in a 50 ml tube (BD Falcon™). Twenty ml of SIP (see section 2.1.7.6) was added, and the tube inverted several times, before centrifuging at 1000 *x g* for 25 minutes at 4°C, with no brake. Following

centrifugation, the myelin cake was discarded, and the cell pellet resuspended in 5 ml MRCRB (see section 2.1.7.7) and allowed to sit for 5 minutes at 37°C. Twenty ml of RPMI-1% FCS was added to the tube, and centrifuged at 400 *x g* for 10 minutes. Cells were then washed twice, and resuspended at the desired concentration.

2.3.3 Isolation of leukocytes from mouse peritoneal cavities (peritoneal washouts)

Mice were sacrificed by carbon dioxide asphyxiation and the peritoneal cavity was exposed by blunt dissection. Five ml HBSS (see section 2.1.7.1) was injected into the peritoneal cavity and the cavity was gently massaged for 30 seconds without removing the needle. Using the same syringe, the injected fluid was carefully withdrawn and collected into a 50 ml tube. Twenty ml of HBSS was added to the tube, and centrifuged at 400 *x g* for 10 minutes. Following centrifugation, the cell pellet was resuspended in 5 ml MRCRB and allowed to sit for 5 mins at 37°C. Twenty ml of HBSS was added to the tube, and centrifuged at 400 *x g* for 10 minutes. Cells were then washed once, and resuspended at the desired concentration.

2.3.4 Nylon wool purification of T lymphocytes

Peritoneal cells were recovered as described in Section 2.3.3. Cell suspensions were further purified for T lymphocytes by passage through nylon wool columns. Each nylon wool column (NW; Robbins Scientific Corporation, Sunny Vale, CA) consisted of 0.62 g of sterile NW in a 10 ml syringe that was pre-warmed at 37°C in RPMI-1%FCS. A total of 1 x 10^8 peritoneal cells in 2 ml of warm RPMI-1% FCS were loaded onto each NW

column. After 1 hr incubation at 37°C in an atmosphere of 5% CO_2, the non-adherent cells were harvested by washing each column with 15-18 ml of pre-warmed RPMI-1%FCS. Cells were washed twice in RPMI-1% FCS then resuspended at the desired concentration.

2.3.5 Collection of tissues for RT-PCR analysis

Mice were sacrificed by carbon dioxide asphyxiation, and perfused through the left ventricle with ice-cold PBS to remove circulating leukocytes. The draining inguinal lymph nodes and spinal cord were removed as described above (see sections 2.3.1 and 2.3.2). Samples of tissue were then snap frozen in liquid nitrogen and stored at –70°C prior to use.

2.3.6 Collection of mouse serum

Mice were sacrificed by carbon dioxide asphyxiation. The rib cage was then immediately reflected back to expose the ascending aorta, which was perforated with surgical scissors. Blood was collected from the chest cavity into eppendorf tubes and allowed to clot at 37°C for 1 hour. Tubes were flicked several times to loosen the resulting clot, incubated at 4°C overnight, then centrifuged at 1000 *x g* for 10 minutes at 4°C. Serum was collected and the cell pellet discarded. Centrifugation was repeated, and serum finally stored at -20°C.

2.3.7 Isolation of leukocytes from peripheral blood

Mice were sacrificed by carbon dioxide asphyxiation. The rib cage was then immediately reflected back to expose the ascending aorta, which was perforated with surgical scissors. Blood was collected from the chest cavity into 15 ml tubes containing 1% EDTA (w/v) in 10 ml of HBSS. Tubes were inverted several times and centrifuged at 350 *x g* for 10 minutes at RT. Following centrifugation, the cell pellet was resuspended in 5 ml MRCRB and allowed to sit for 5 mins at 37°C. Ten ml of HBSS was added to the tube, and centrifuged at 350 *x g* for 10 minutes. Cells were then washed once, and resuspended at the desired concentration.

2.4 Cell culture

2.4.1 Culture media

2.4.1.1 Serum

Foetal calf serum (FCS) was obtained from Trace Scientific (Noble Park, VIC) and was heat-inactivated by incubation at 55°C for 1 hour.

2.4.1.2 RPMI-10% FCS

The culture medium referred to throughout the text as RPMI-10% FCS was as follows: RPMI supplemented with 10 mM HEPES, 2 mM L-glutamine, penicillin + gentamycin supplement (all obtained from the Infectious Diseases Laboratories Media Production Unit, IMVS), 50 μM β-mercaptoethanol and 10% heat-inactivated FCS.

2.4.1.3 RPMI-1% FCS

The culture medium referred to throughout the text as RPMI-1% FCS was as follows: RPMI supplemented with 10 mM HEPES, 2 mM L-glutamine, penicillin + gentamycin supplement (all obtained from the Infectious Diseases Laboratories Media Production Unit, IMVS), 50 μM β-mercaptoethanol and 1% heat-inactivated FCS.

2.4.1.4 RPMI-BSA

The culture medium used for Transwell chemotaxis assays was RPMI containing 0.5% (w/v) BSA.

2.4.2 Culturing primary lymph node cells

Lymph node cells were prepared from donor SJL/J mice, as described in Section 2.3.1, aliquoted into 6-well trays, in a 4 ml volume, and cultured at a concentration of 4 x 10^6 viable cells/ml in RPMI-10% FCS in the presence of 50 μg/ml $PLP_{139-151}$. Cells were incubated at 37°C in a humidified atmosphere containing 5% CO_2 for 96 hours. After 72 hours of culture, an additional 1 ml of RPMI-10% FCS was added to each well.

2.4.3 Concanavalin A (Con A) stimulation of lymphocytes

Lymph node cells were prepared from naïve SJL/J mice, as described in Section 2.3.1, aliquoted into 6-well trays, in a 4 ml volume, and cultured at a concentration of 4 x 10^6 viable cells/ml in RPMI-10% FCS in the presence of 2 µg/ml Con A (Amersham Pharmacia Biotech Australia). Cells were incubated at 37°C in a humidified atmosphere containing 5% CO_2 for 48 hours. Cells were then washed twice in RPMI-1% FCS, and resuspended at the desired concentration in RPMI-BSA (Section 2.4.1.4).

2.5 *In vitro* assays

2.5.1 Viable cell counts

Cells were routinely enumerated by diluting in 0.8% trypan blue (Sigma), followed by counting on a haemocytometer (Improved Neubauer, Weber, UK). At least 60 cells were counted per sample.

2.5.2 Analysis of cell division by carboxyfluorescein diacetate succinimidyl ester (CFSE) dye dilution

Cell division in the *in vitro* cultures (Section 2.4.2) and proliferation assay (Section 2.5.3) was assessed fluorometrically by labelling cells with CFSE prior to culture. Lymph node cells were resuspended to 2 x 10^7 cells/ml in RPMI-1% FCS, and CFSE (Molecular Probes, Eugene, OR, USA) was added to a final concentration of 10 μM. After incubation at 37°C for 10 minutes, the staining reaction was quenched by the addition of a large volume of complete medium (RPMI-10% FCS) for 5 minutes, followed by 2 washes in the same medium. After the required time in culture, cells were analysed by flow cytometry (in conjunction with surface phenotyping) and cell division detected as a progressive two-fold loss in CFSE fluorescence intensity.

2.5.3 Proliferation assay

Mice immunised with PLP peptide$_{139-151}$ in CFA (Section 2.2.1) were euthanased 9 days post-immunisation and the draining inguinal lymph nodes were taken for proliferation assays using a modification of previously published protocols involving CFSE (189, 190). Single cell suspensions were labelled with CFSE, as described in Section 2.5.2, and resuspended at a final concentration of 2.5 x 10^6 viable cells/ml. In a final volume of 200 μl, 2.5 x 10^5 cells were cultured in 96-well round-bottom trays with added PLP peptide$_{139-151}$ at a concentration of 0.5, 5.0, 25.0, or 50.0 μg/ml, or with 1.5 μg/ml Concanavalin A (ConA). After 4 days of culture at 37°C in a humidified atmosphere containing 5% CO_2, the cells were harvested, labelled for CD4 (see Table 2.2) and analysed by flow cytometry (see section 2.6.4). Cell division (proliferation) was determined as a progressive halving in CFSE fluorescence intensity.

2.5.4 Transwell chemotaxis and inhibition assay

For dose-response and inhibition studies, cells were first fluorescently labelled by incubating with Calcein-AM (Molecular Probes; 40 nM final concentration in RPMI-BSA) for 30 minutes at 37°C, followed by three washes in RPMI-BSA. Cells were resuspended to 1 x 10^7 viable cells/ml in RPMI-BSA and subjected to Transwell chemotaxis assays. Synthetic chemokines (Section 2.1.4, Table 2.1) were diluted to the required concentration in RPMI-BSA and 600 µl added to the lower chambers of a Transwell plate (6.5 mm diameter filter, 5 µm pore size; Corning, NY, USA). After adding 100 µl of cells to the upper chambers, the assay was incubated for 3 hours at 37°C and cells were collected from the lower chamber after extensive PBS washing of the filter underside with a plastic transfer pipette. The cells from the lower chamber were transferred to an eppendorf and pelleted by centrifuging at 400 *x g* for 5 minutes. The cell pellets were resuspended in 100 µl of PBS and transferred to a 96-well opaque microtitre tray for fluorescence analysis. Fluorescence levels were measured with a Molecular Imager FX (Biorad Laboratories, Hercules, CA) using Quantity One ™ software, with excitation at 488nm and emission at 494nm. The percentage migration of cells was calculated by inserting the fluorescence value from each chamber into the following formula: $[100 \times (Y-Y_{min})/(Y_{max})]$, where Y_{min} was the value obtained in the absence of chemokine, Y_{max} was the value obtained for 100 µl of cells added directly to the lower chamber of the Transwell and Y was the value obtained from the experimental sample. To correct for any variations in spontaneous migration, the data (cell migration) are expressed as a percentage of the total input cells.

For the inhibition studies using synthetic mutants, cells were subjected to identical conditions as above, however, mutants were diluted to the appropriate concentrations and added in combination with the agonists, as described above. To correct for any variations in migration between individual assays, the data (cell migration) was then converted to a percentage of the level of migration observed with agonist alone.

2.5.5 Direct ELISA for anti-chemokine antibody detection

Anti-chemokine, and anti-chemokine mutant, antibody levels in mouse serum were measured though a direct peroxidase ELISA. High protein-binding ELISA plates (Corning) were coated with 200 ng of specific peptide in (Section 2.1.4, Table 2.1) 100 µl of ELISA coating buffer (Section 2.1.7.3). Plates were incubated overnight at 4°C before being washed with PBS/Tween (Section 2.1.7.4). Plates were then blocked through incubation with PBS/3% BSA for 2 hours at 37°C. Serum samples, diluted 1 in 300 in PBS/1% BSA, were added to the wells, and were allowed to bind through incubation at 37°C for one hour. Plates were then washed with PBS/Tween, and the secondary antibody of rabbit anti-mouse :: HRP (Table 2.3), was added at a dilution of 1 in 20 000 in PBS/1% BSA. After incubation at 37°C for one hour, plates were thoroughly washed with PBS/Tween, and developed using o-Phenylenediamine dihydrochloride (Sigma Fast™ OPD; Sigma), as per the manufacturer's recommendations. Reactions were stopped with 50 µl 3M HCl, and the intensity was read at 490 nm with a Dynatech plate reader.

2.6 Immunostaining of cells and tissue sections

2.6.1 Preparation of spinal cord tissue sections

To prepare spinal cord tissue for immunohistological staining, mice were sacrificed by carbon dioxide asphyxiation, and perfused through the left ventricle with ice-cold PBS. The spinal cord was extracted from the spinal column using scissors to cut the vertebrae and a scalpel to remove the cord. Samples were immersed in a plastic mould containing Tissue-Tek® OCT embedding medium (Sakura Finetek, Torrance, CA) and frozen using the Gentle Jane snap-freezing system (Instrumedics Inc., Hackensack, NJ). Blocks were stored at –70°C until sectioning. Ten micron cryostat sections were cut from embedded tissue using a BRIGHT cryostat (Huntingdon, UK), air-dried onto microscope slides, fixed for 7 minutes in 60% acetone/40% methanol, air-dried and then frozen at -20°C with desiccant.

2.6.2 Immunofluorescence staining of tissue sections

Sections were isolated using a hydrophobic pen (Pap Pen, Zymed Laboratories, San Francisco, CA), and subsequently rehydrated in PBS for 5 minutes. Non-specific binding was then blocked by covering samples with Powerblock® (InnoGenex, San Ramon, CA) and incubating at RT for 1 hour. After rinsing off the blocking agent in PBS, 50 µl of primary antibody mix (the appropriate goat polyclonal antibody plus FITC-conjugated anti-CD4; see Table 2.2) was added to the samples. After overnight incubation at 4°C, the

sections were washed with 2 changes of PBS (2 minutes each), followed by the addition of the anti-goat secondary antibody conjugated to Alexa 594 (see Table 2.3). Any potential cross-reactivity of the anti-goat secondary for rat and mouse immunoglobulins was prevented by pre-blocking the secondary antibody with 400 µg/ml rat gamma-globulin and 200 µg/ml mouse gamma-globulin (Rockland Immunochemicals, Gilbertsville, PA, USA), in the presence of 2% normal mouse serum. Following a 1 hour incubation at 4°C, the sections were washed through 3 changes of PBS (2 minutes each) and coverslipped with Mowiol mounting medium + PPD (Section 2.1.7.5). All incubations were carried out in a humid chamber. Following staining, slides were viewed and photographed using an Olympus Provis AX reflected light fluorescence microscope (Melville, NY) equipped with a Photometrics CE 200A digital camera (Auckland, NZ), using V for Windows software (Photometrics; version 3.5r) for image capture.

2.6.3 Labelling cells for flow cytometry

2.6.3.1 Standard protocol

Cells were resuspended to 4 x 10^6 viable cells/ml in mouse staining buffer. Fc receptors were blocked by incubating for 30 minutes at room temperature with 50 µg of murine gamma-globulin (Rockland) per million cells, then 50 µl of cells aliquoted into round-bottomed polystyrene tube (BD Falcon™ #352008). For experiments in which goat primary antibodies were unlabelled (see Table 2.2), cells were mixed with saturating concentrations of the unlabelled primary antibodies, incubated for 30 minutes at room temperature and washed once with 3 ml of mouse staining buffer (ie, 3 ml of buffer was added to the tube, cells were pelleted by centrifuging for 7 minutes at 350 *x g*, the supernatant was poured off and the cells resuspended in the remaining liquid), prior to the

addition of biotin-conjugated anti-goat detection antibody (see Table 2.3). Following a 30 minute incubation on ice, cells were washed with mouse staining buffer and free binding sites on the detection antibody were blocked by incubation with 20 µg of goat IgG (Laboratory Animal Services, Adelaide, SA) per tube for 20 minutes at room temperature. Fluorochrome-conjugated primary antibodies, as well as fluorochrome-conjugated streptavidin, were then added and incubated for 30 minutes on ice (see Tables 2.2 and 2.3). Cells were washed with 3 ml of mouse staining buffer followed by 3 ml of protein-free staining buffer and fixed in 300 µl of PFA (1% in PBS).

A slightly different approach was adopted when all primary antibodies were directly labelled with fluorochromes or biotin; cells were mixed with all of the required primary antibodies, incubated at room temperature for 30 minutes, washed, incubated with fluorochrome-conjugated streptavidin, then washed and fixed as described above.

2.6.3.2 Modified protocol for the detection of 5-bromo-2-deoxyuridine (BrdU) incorporation

Cells were prepared, blocked with gamma-globulin and labelled for surface antigens, as for the standard protocol (Section 2.6.3.1). After washing in PBS, the cell pellets were resuspended in 500 µl of ice-cold NaCl (0.15 M). While gently vortexing, 1.2 ml of ice-cold 95% (vol/vol) ethanol was added in a dropwise manner, and the cells incubated on ice for 30 minutes. To wash, 2 ml of PBS were added and the cells pelleted by centrifuging at 450 *x g*. Cell pellets were resuspended in 500 µl of paraformaldehyde/Tween (1% paraformaldehyde + 0.01% Tween in PBS), incubated at room temperature for 30 minutes and subsequently pelleted by centrifugation. In order to generate single-stranded DNA (a

prerequisite for the detection of incorporated BrdU), cells were incubated in 1 ml of DNase solution at 37°C for 30 minutes, and then washed in 2 ml of PBS. After decanting the supernatant, cell pellets were resuspended in the remaining volume, and 10 µl of fluorescein-conjugated anti-BrdU (Becton Dickinson Immunocytometry, San Jose, CA) or isotype-matched control antibody was added. After incubation at RT for 30 minutes, the cells were washed in 2 ml of PBS and resuspended in 250 µl of PBS, prior to flow cytometric analysis.

2.6.4 Flow cytometric analysis

Labelled cells were analysed on a Becton Dickinson FACScan and data analysed using CellQuest Pro software (BD Biosciences). For most analyses, lymphocytes (or, in some experiments, monocytes) were gated using forward and side angle light scatter characteristics.

Positive events were defined on the basis of quadrant or histogram markers, which were set according to the level of background staining observed using isotype-matched control antibodies. All percentage values presented in the data have been corrected for background staining, by subtracting the percentage of events defined as positive by the markers in relevant control samples (generally <1% for monoclonal antibodies, <5% for polyclonal antibodies).

2.6.5 Haematoxylin and Eosin (H&E) staining

Sections were rehydrated in water for 2 minutes, before being immersed in Gill's Haematoxylin (Sigma) for 90 seconds. Following staining, the slides were immersed in a large bath of water to remove excess stain. After rinsing, sections were differentiated in 1% acid alcohol in 3 x 3 second dips (Section 2.1.7.11), then rinsed again. Following immersion in Scott's tapwater substitute for 2 minutes (Section 2.1.7.12), the sections were rinsed then immersed in eosin (Sigma) for 60 seconds. After eosin staining, the sections were rinsed twice and coverslipped with DAKO Glycergel mounting medium (DAKO Corporation, CA) and allowed to dry for 5 hours. Following staining, slides were viewed and photographed using a Zeiss Axiophot microscope (Oberkochen, Germany) equipped with a FUJIX HC-1000 3CCD digital camera, using Photograb software (Magi Consulting, CO) for image capture.

2.7 Analysis of chemokine receptor expression by reverse-transcriptase polymerase chain reaction (RT-PCR)

2.7.1 RNA extraction from lymphoid and spinal cord tissue

Following removal from animals, tissues were snap frozen and stored at -70°C until required (Section 2.3.5). To extract RNA, tissue was thawed and homogenized in 1 ml of Trizol (Life Technologies, Gilbertsville, PA, USA), then incubated at RT for 5 minutes

prior to the addition of 200 µl of chloroform. After vigorous shaking, the mixture was incubated for a further 2-3 minutes at RT. Centrifugation at 12 000 *x g* for 15 minutes at 4°C generated 2 phases. The upper aqueous phase was transferred to a clean reaction tube and the extraction of remaining RNA from the lower phase was repeated with 400 µl of DEPC-treated water. RNA from both extractions was precipitated separately by the addition of 500 µl of isopropanol, followed by a 10-minute incubation at RT. The precipitate was then centrifuged at 12 000 *x g* for 10 minutes at 4°C. The pellet was washed in 70% ethanol and air-dried for approximately 15 minutes. RNA was dissolved in 20 µl of DEPC-treated water and incubated at 55°C for 10 minutes to ensure complete resuspension. RNA purity was determined by measuring optical density at 260 nm and 280 nm, and calculated using the following formula:

[purity = OD_{260}/OD_{280}].

The concentration of RNA was calculated using the following formula:

[concentration (µg/µl) = OD_{260} x dilution factor x 0.04].

2.7.2 DNase I treatment of RNA

RNA was treated with DNase I to remove any contaminating chromosomal DNA. Each reaction was set up as follows, using RNase-free DNase I and the associated buffers as provided (Promega, Madison, WI, USA). RNA (5 µg) was diluted to a final volume of 17 µl in DEPC-treated water, to which 2 µl of 10X reaction buffer and 1 µl of enzyme were added. Following incubation at 37°C for 1 hour, the reaction was terminated by the addition of 2 µl of 10X stop buffer and heat-inactivation at 65°C for 20 minutes.

2.7.3 Reverse-transcription

Generation of first strand cDNA from RNA was conducted using Superscript II reverse-transcriptase and the associated buffer and dithiothreitol (DTT) reagent as provided (Life Technologies). Each reaction was set up as follows: 1 µl of random hexamer primers (500 µg/ml; Amersham Pharmacia Biotech) was combined with 2.5 µg of total RNA and the volume adjusted to 12 µl with DEPC-treated water. The mixture was heated to 70°C for 10 minutes, then immediately cooled to 4°C and the following reagents added: 4 µl of first strand buffer, 2 µl of DTT and 1 µl of 10 mM dNTP mix (10 mM each dATP, dTTP, dCTP, dGTP diluted in DEPC-treated water; Amersham Pharmacia Biotech). The contents of the tube were mixed gently, centrifuged briefly and incubated for 2 minutes at 42°C. Finally, 1 µl of Superscript II (200 U/µL) was added and the reaction allowed to proceed at 42°C for 50 minutes before being terminated by heating to 70°C for 15 minutes. The cDNA products were stored at –20°C until further use.

2.7.4 Amplification of target sequences using PCR

PCR reactions were set up using Amplitaq Gold polymerase (Perkin Elmer Life Sciences, Boston, MA, USA) and the supplied buffer and $MgCl_2$. The following 25 µl reaction was set up for each template with each primer set: 1.25 µl of cDNA template was added to a 0.2 ml reaction tube and heat-denatured at 95°C for 10 minutes. The temperature was then reduced to 4°C and the following reagents added: 5 µl of each oligonucleotide primer at 5 pmol/µl, 2.5 µl of 10X reaction buffer, 1.25 µl of 25 mM $MgCl_2$, 0.5 µl of 10 mM dNTP mix (10 mM each dATP, dTTP, dCTP, dGTP diluted in sterile Milli-Q water; Perkin Elmer), 9.25 µl of sterile Milli-Q water and 0.25 µl of Amplitaq Gold polymerase (Perkin

Elmer). Reactions were cycled in a hot-bonnet thermal cycler as follows: (Step 1) 95°C 10 minutes; (Step 2) 95°C 30 seconds; (Step 3) 55°C 1 minute; (Step 4) 72°C 1 minute, with steps 2-4 repeated for the required number of cycles. After completion of cycling, an extension step of 5 minutes at 72°C was performed. All reactions were then held at 4°C until analysed.

2.7.5 Analysis of PCR products by agarose gel electrophoresis

Two percent (w/v) agarose gels were prepared by boiling agarose in TAE. Gels were run in TAE at ~100 mA in a horizontal gel apparatus. Following electrophoresis, gels were stained with SYBR-gold (diluted to 1X concentration in TAE; Molecular Probes) for 15-30 minutes and visualised/analysed using a Molecular Imager FX and Quantity One software package. The band volume values for each receptor were expressed as a ratio relative to band volume for the GAPDH PCR product amplified from the same template.

2.8 Statistical tests

Statistical tests were performed using GraphPad InStat software (San Diego, CA). Unless otherwise stated, the two-tailed, unpaired Student's t-test was used for statistical analysis. However, in some instances, the alternate one-tailed t-test was used. In analyses relating to EAE experiments, ANOVAs were performed in order to allow for the variability between the individual experiments. For all analyses, p values of less than 0.05 were considered significant.

Table 2.1 ***Synthetic chemokine peptides***. All synthetic chemokines used *in vivo* and *in vitro* are listed, along with their description and amino acid (a.a.) sequence. The first listed a.a. in the functional chemokine sequences corresponds to the first a.a. of the mature peptide. Synthesised chemokines were a kind gift from Pr Ian Clark-Lewis (Biomedical Research Centre, University of British Columbia, Vancouver, Canada).

Peptide	Description	Sequence (N → C Terminus)
huSDF-1 / CXCL12 (1-67)	Functional human CXCL12, residues 1-67 (mature peptide)	KPVSLSYRCPCRFFESHVARANVKHLKILNTRNCALQI VARLKNNNRQVCIDPKLKWIQEYLEKALN
mIP-10 / CXCL10 (1-77)	Functional murine CXCL10, residues 1-77 (mature peptide)	IPLARTVRCNCIHIDDGPVRMRAIGKLEIIPASLSCPR VEIIATMKKNDEQRCLNPESKTIKNLMKAFSQKRSKRA P
mI-TAC / CXCL11 (1-79)	Functional murine CXCL11, residues 1-79 (mature peptide)	FLMFKQPRCLCIGPGMKAVKMAEIEKASVIYPSNGCDK VEVIVTMKAHKRQRCLDPRSKQARLIMQAIEKKNFLRR QNM
mMIG / CXCL9 (1-104)	Functional murine CXCL9, residues 1-104 (mature peptide)	TLVIRNARCSCISTSRGTIHYKSLKDLKQFAPSPNCNK TEIIATLKNGDQTCLDPDSANVKKLMKEWEKKINQKKK QKRGKHQKNMKNRKPKTPQSRRRSRKTT
mRANTES / CCL5 (1-68)	Functional murine CCL5, residues 1-68 (mature peptide)	SPYGSDTTPCCFAYLSLALPRAHVKEYFYTSSKCSNLA VVFVTRRNRQVCANPEKKWVQEYINYLEMS
mMIP-1β / CCL4 (1-69)	Functional murine CCL4, residues 1-69 (mature peptide)	APMGSDPPTSCCFSYTSRQLHRSFVMDYYETSSLCSKP AVVFLTKRGRQICANPSEPWVTEYMSDLELN
mMCP-1 / CCL2 (1-125)	Functional murine CCL2, residues 1- 125 (mature peptide)	QPDAVNAPLTCCYSFTSKMIPMSRLESYKRITSSRCPK EAVVFVTKLKREVCADPKKEWVQTYIKNLDRNQMRSEP TTLFKTASALRSSAPLNVKLTRKSEANASTTFSTTTSS TSVGVTSVTVN
SDF-1 P2G	huCXCL12 substitution mutant	K**G**VSLSYRCPCRFFESHVARANVKHLKILNTRNCALQI VARLKNNNRQVCIDPKLKWIQEYLEKALN
I-TAC 3-79	mCXCL11 truncation mutant	--MFKQPRCLCIGPGMKAVKMAEIEKASVIYPSNGCDK VEVIVTMKAHKRQRCLDPRSKQARLIMQAIEKKNFLRR QNM
I-TAC 4-79	mCXCL11 truncation mutant	---FKQPRCLCIGPGMKAVKMAEIEKASVIYPSNGCDK VEVIVTMKAHKRQRCLDPRSKQARLIMQAIEKKNFLRR QNM
I-TAC 5-79	mCXCL11 truncation mutant	----KQPRCLCIGPGMKAVKMAEIEKASVIYPSNGCDK VEVIVTMKAHKRQRCLDPRSKQARLIMQAIEKKNFLRR QNM
RANTES 9-68	huCCL5 truncation mutanat	--------PCCFAYIARPLPRAHIKEYFYWSGKCSNPA VVFVTRKNRQVCANPEKKWVREYINSLEMS
MCP-ala	Control non-functional peptide of huCCL2	--------VT**AA**YNFTNRKISVQRLASYRRITSSK**A**PK EAVIFKTIVAKEI**A**ADPKQKWVQDSMDHLDKQTQTPKT

Table 2.2 ***Primary Antibodies***

Antigen	Clone	Isotype	Conjugate	Source
CD4	H129.19 GK1.5	Rat IgG2a Rat IgG2b	PE FITC	BD Parmingen (San Diego, CA, USA)
CD8α	53-6.7	Rat IgG2a	PE	BD Parmingen
CD11c	HL3	Ham IgG	PE	BD Parmingen
Mouse IgG (κ light chain)	R8-140	Rat IgG2a	FITC	BD Parmingen
F4/80	A3-1	Rat IgG2b	FITC	Caltag Laboratories (Burlingame, CA, USA)
CXCR4	Polyclonal	Goat IgG	-	Santa Cruz Biotechnology (Santa Cruz, CA, USA)
CXCR3	Polyclonal	Goat IgG	-	Santa Cruz Biotechnology
CCR5	Polyclonal	Goat IgG	-	Santa Cruz Biotechnology

Table 2.3 *Secondary Detection Reagents*

Reagent	Conjugate	Source
Streptavidin	FITC, PE, HRP	Rockland Immunochemicals (Gilbertsville, PA, USA)
Streptavidin	Tri-color conjugate	Caltag Laboratories
Anti-goat IgG (polyclonal)	Biotin	Rockland Immunochemicals
Anti-mouse IgG (polyclonal)	HRP	Rockland Immunochemicals
Anti-goat IgG (polyclonal)	Alexa 594	Molecular Probes (Eugene, OR, USA)

Table 2.4 *Enzymes used for DNA synthesis*

Enzyme	Description	Application	Source
Superscript II	Reverse Transcriptase	Single-stranded cDNA synthesis	Life Technologies (Gilbertsville, PA, USA)
RQ1 RNase-free DNase	DNase	DNase treatment of RNA samples	Promega (Madison, WI, USA)
AmpliTaq Gold	A-tailing DNA polymerase	Analytical PCR	Perkin Elmer Life Sciences (Boston, MA, USA)

Table 2.5 ***Oligos for analytical PCR***. Oligos are listed by name, with their sequence. The annealing temperature at which they used was 55°C (see section 2.7.4).

Primer Name	Sequence 5' → 3'
CCR1-F	GGC TAT TGT CCA TGC TGT GT
CCR1-R	CCA AGA GTC TCT GTT GCC TG
CCR2-F	ACC TCA GTT CAT CCA CGG CA
CCR2-R	TGA GCA GGA AGA GCA GGT CA
CCR3-F	CAG TCC TCG CTA TCC AGA AG
CCR3-R	CCG GAA CCT CTC ACC AAC AA
CCR4-F	TCA TTG GCT TCT CCT GCT GG
CCR4-R	TTG CAG TAC GTG TGG TTG TG
CCR5-F	GGC TAT TGT CCA TGC TGT GT
CCR5-R	CTG AGA GAT AAC TCC GGA AC
CCR8-F	CCA TCT TGT ACT GCG TCT TG
CCR8-R	CAG ATA CCT GTC CAC ACT CA
CXCR3-F	GTG CTA GAT GCC TCG GAC TT
CXCR3-R	GAG GCG CTG ATC GTA GTT GG
CXCR4-F	ACC ACG GCT GTA GAG CGA GT
CXCR4-R	GCT GAT GAA GGC CAG GAT GA
GAPDH-F	TCC TTG GAG GCC ATG TAG GCC AT
GAPDH-R	TGA TGA CAT CAA GAA GGT GGT GAA G

Chapter 3

Identification of chemokine receptors that are specifically regulated on antigen-activated $CD4^+$ T cells during the induction of an immune response *in vivo*

3.1 Introduction

Upon activation, naïve T cells alter their migratory patterns, acquiring the ability to move through peripheral tissues as well as the general lymphoid circulation. Although the mechanisms responsible for these alterations are not well understood, it has been postulated that changes in chemokine receptor expression play a critical role (78, 88, 191). Recently, the regulation chemokine receptor expression on newly-activated T cells has been the focus of a number of *in vitro* studies (65, 88, 89, 192), however, little work has been conducted *in vivo* examining the regulation of chemokine receptor expression on antigen-activated T cells (78, 193, 194), particularly during the priming phase of an immune response.

To date, very few EAE studies have been conducted at the level of immune priming (or sensitisation) within the lymph nodes (LNs). Several studies involving EAE have reported chemokine gene expression in the CNS and by neuroantigen-specific (encephalitogenic) cells, however, there are few studies examining chemokine receptor expression at the level of sensitisation (in peripheral LNs) (142). Of relevance, a role for the chemokine MIP-3α/CCL20 in the sensitisation of lymphocytes during EAE has been reported (43) and preliminary data suggests a similar role for its cognate receptor CCR6 (Liston *et al*, manuscript in preparation). Accordingly, the major goal of the series of experiments outlined in this chapter was to assess chemokine receptor levels on antigen-activated $CD4^+$ T cells in the draining LNs during an immune response *in vivo*.

In order to examine a role for chemokine receptor regulation on $CD4^+$ T cells during CNS inflammation, a suitable model was required. EAE was chosen as it has been extensively

characterised in the literature with respect to a range of immune parameters (reviewed in (36)). The model of murine EAE, induced by immunisation with the immunodominant peptide of proteolipid protein ($PLP_{139-151}$; a component of the myelin sheath) (195), elicits a $CD4^+$ Th1-mediated disease (196) that is highly reproducible. A further advantage of this model of EAE is that the immune response can be separated into the priming and effector phases. This is achieved by restimulating $PLP_{139-151}$-specific cells and adoptively transferring them into naïve recipients. The active EAE-inducing mouse spinal cord homogenate (MSCH) model of EAE had previously been implemented in the laboratory, however, the model was found to be limited in terms of restimulation of T cells, since MSCH was observed to be toxic to those cells *in vitro* (unpublished), thereby limiting the usefulness of this model in terms of assessment of T cell priming as well as adoptive transfer. Given that no such problems have been documented with the use of the PLP model, this model was selected for the current study. However, since $PLP_{139-151}$–induced EAE had not been implemented in the laboratory previously, there was a need to first establish the model.

3.2 Results

3.2.1 Establishing an induction protocol for EAE

EAE was induced in susceptible mice (SJL/J ($H\text{-}2^S$)) by injecting s.c. 50 µg $PLP_{139-151}$ in CFA into the hind flanks in a volume of 50 µl/flank. Control mice received s.c. an equivalent volume of PBS in CFA. In addition, an intravenous injection of pertussigen, a crude extract of *Bordatella pertussis*, was required for efficient induction of EAE. PLP_{139-}

$_{151}$-immunised mice that did not receive pertussigen treatment failed to develop clinical disease (data not shown). While the requirement for extracts of *Bordatella pertussis* in disease induction is not well understood, it may be necessary for appropriate immune stimulation, increased vascular permeability of the BBB, Th1/Th2 deviation (119, 197, 198), or a combination of these factors. Thus, both $PLP_{139-151}$- and PBS-immunised mice were treated with 5 μg of pertussigen in 250 μl on days 0 and 2 post-immunisation. All mice were then monitored for clinical signs of paralysis as described in section 2.2.3.

Following immunisation, PLP-immunised mice began to show signs of clinical disease, characterised by the appearance of ascending paralysis, between 9 and 11 days post-immunisation (Fig. 3.1). In this particular experiment, the mean day of onset of clinical disease was approximately day 10 post-immunisation (Table 3.1). The paralysis peaked around 12 days post-immunisation, with maximum disease scores similar to those in previous studies (199) (Table 3.1). Clinical disease had completely subsided by 20 days post-immunisation (disease remission). Control mice showed no signs of clinical disease (data not shown), indicating that the observed clinical disease symptoms were antigen ($PLP_{139-151}$)-dependent.

3.2.2 Characterisation of the immune response in the draining lymph nodes

3.2.2.1 Time-course of viable cell yield

The extent of the immune response occurring in the draining (inguinal) lymph nodes during sensitisation to the antigen was initially evaluated by enumerating the viable cells

recovered per lymph node (LN). EAE induction ($PLP_{139-151}$ in CFA) resulted in a significant increase in the mean number of viable cells recovered from the draining inguinal LN at day 6 post-immunisation, and remained significantly elevated for up to 21 days post-immunisation compared with that recovered from day 0 LNs (Fig 3.2 (A); $p < 0.05$). Following the initial 2.5-fold increase in cell number at day 6, the mean LN cell numbers appeared to plateau into the period of peak clinical disease (day 12), before increasing again by day 21 post-immunisation (disease remission). Immunisation with PBS in CFA also elicited an increase in viable cell numbers in the draining LNs, which followed a similar response to EAE induction, however, unlike the case with $PLP_{139-151}$ in CFA, these increases were not statistically significant until 21 days post-immunisation. Although the number of cells recovered from the EAE mice appeared to be slightly higher than those from the control immunised LNs at all time-points examined, these differences were not statistically significant, with exception to day 6 post-immunisation (Fig 3.2 (A); $p = 0.04$). In both cases, the increase in cellularity in the draining LNs was accompanied by an enlargement of the inguinal LNs (data not shown).

Flow cytometric analysis of the draining LNs removed at 9 days post-immunisation from PLP/CFA-immunised mice demonstrated that 55.4 ± 1.5% of the cells were $CD4^+$, 22.7 ± 0.8% of the cells were $CD8^+$, 10.6 ± 0.9% of the cells expressed surface immunoglobulin (Ig), and 1.2 ± 0.1% of the cells were positive for CD11c (Fig. 3.2 (B)).

3.2.2.2 Chemokine receptor expression in the draining LNs following immunisation

An initial screen examining the expression patterns of chemokine receptors in the peripheral LNs during EAE focused on the receptors CXCR4, CXCR3, CCR1, CCR2 and

CCR5. Examination of CXCR4, CXCR3 and CCR5 expression was pursued because expression of these receptors was shown to be modulated on $CD4^+$ T cells following allogeneic activation *in vitro* (88, 89). CCR1 and CCR2 expression was also examined in the draining LNs since roles for both of these receptors have been demonstrated for the induction of EAE (101, 146, 147). Comparative RT-PCR was chosen for the initial screen because antibodies were not available for all of the above receptors. Initially, preliminary studies were conducted for each set of primers at a range of cycle numbers, to ensure that the PCR reaction was in the linear range, and thus was comparative in nature (data not shown).

Following induction of EAE (PLP/CFA), or control-immunisation (PBS/CFA), groups of mice were sacrificed at time points corresponding to pre-clinical disease (Day 9 post-immunisation), acute disease (Day 12 post-immunisation) and remission (Day 21 post-immunisation), perfused to remove peripheral blood leukocytes (Section 2.3.5), and the draining lymph nodes (inguinal) were removed and processed for analysis of CXCR4, CXCR3, CCR1, CCR2 and CCR5 mRNA expression. The level of receptor expression in the LNs was compared between normal (Day 0) mice, $PLP_{139-151}$-immunised mice, and PBS-immunised mice. Because there are no introns in most chemokine receptor genes, samples without RT were performed to control for genomic contamination. These controls were always negative (data not shown). Analysis of the LNs collected at the above time points indicated a basal expression of all chemokine receptors tested relative to the house keeping gene glyceraldehyde-3-phosphate dehydrogenase (GAPDH) in normal LNs (Day 0), albeit to different extents (Fig. 3.3). Of all receptors analysed, CXCR4 had the highest basal expression and this level of expression remained unchanged by immunisation with PLP in CFA or PBS in CFA (Fig 3.3(A)). Immediately prior to onset

of clinical disease (Day 9), there was a statistically significant upregulation of CXCR3, CCR1 and CCR2 expression (Fig 3.3(B-D)) above basal levels, with CCR1 and CCR2 also exhibiting a significantly higher expression in the PLP-immunised LNs than in the control-immunised (PBS/CFA) LNs ($p < 0.05$). Throughout the course of disease and into remission, CXCR3 expression remained significantly higher than in normal LNs, however, the lack of difference between the PLP-immunised and the control-immunised was sustained throughout disease (Fig 3.3(B)). Of the time points examined, CCR1 mRNA levels were highest at disease onset and maintained at elevated levels. However, at time points corresponding to peak disease and remission, this observed increase lost its statistical significance (Fig 3.3(C)). Expression of CCR2, on the other hand, continued to persist at significantly higher levels during the course of disease and into remission (Fig 3.3(D)). In contrast to the above-mentioned receptors, while CCR5 expression levels did not increase significantly above basal levels until peak clinical disease in a two-tailed T test, the elevated expression observed at day 9 was statistically significant in a one-tailed T test (Fig 3.3(E); $p < 0.05$). As the animals entered remission, CCR5 mRNA expression remained significantly elevated ($p<0.05$). In contrast to the PLP-immunised mice, there was no alteration of CCR5 expression evident in the LNs of control-immunised animals (Fig 3.3(E)).

3.2.2.3 Evaluation of $CD4^+$ T cells undergoing division in the draining lymph nodes

Prior to the examination of chemokine receptor expression on $CD4^+$ T cells, an assay that enabled the identification of activated/divided $CD4^+$ T cells was required. The time-course analysis of cell yields discussed above (Section 3.2.2.1) revealed an ~2.5-fold increase in the total cell number of lymphocytes recovered from sensitised LNs compared

to day 0 LNs. In order to assess what proportion of this was due to proliferation in response to the antigen, proliferating cells were detected by means of 5-bromo-2-deoxyuridine (BrdU) incorporation. BrdU is a halogenated DNA precursor analogue which, when introduced into the circulation of an immunised animal, is incorporated into cells that are actively synthesising DNA. Proliferating cells can therefore subsequently be detected by means of an anti-BrdU antibody, followed by flow cytometric analysis (200, 201).

BrdU was administered continuously in the drinking water of immunised mice starting at day 6 post-immunisation. On days 9 and 12 post-immunisation, LNs were harvested and labelled with anti-BrdU as well as anti-CD4, and subjected to flow cytometric analysis. This approach of BrdU administration was chosen in order to detect all T cells that had proliferated in response to antigen in the previous 3-6 days as well as those that were in the process of proliferating at the time of harvesting.

The data presented in Figures 3.4 and 3.5 demonstrate the relative proportion of cells undergoing proliferation in the draining inguinal LNs. Nine days after immunisation with PLP in CFA, there was a significant increase in the percentage of BrdU-positive cells in the draining LNs compared to the control immunised mice (Fig 3.4 (A); $p < 0.05$). Representative density plots are shown in Fig 3.4 (B) illustrating the presence of readily detectable populations of $CD4^+$ T cells that had incorporated BrdU at day 9 in both control- and PLP-immunised animals. Analysis of these plots demonstrated that, of the $CD4^+$ T cells present in the inguinal LNs, ~15% had proliferated as a result of immunisation (Fig 3.4 (C)). There was no significant difference between the control- and PLP-immunised mice with respect to these values. By day 12 post-immunisation, there

appeared to be a change in the kinetics of cell turnover in the draining lymph nodes. An extra 3 days of antigenic stimulation in the LNs resulted in a 2-2.5-fold increase in the percentage of divided cells in the control-immunised LNs (Fig 3.5 (A)). A similar increase was not observed in the LNs of PLP-immunised mice. Analysis of the $CD4^+$ T cell population at day 12 post-immunisation (Fig 3.5 (B)) demonstrated that the percentage of $CD4^+$ T cells incorporating BrdU in the control-immunised LNs was ~2-fold greater than the percentage of $CD4^+$ T cells incorporating BrdU at day 9 post-immunisation in the control-immunised LNs. It is likely that this increase in the proportion of dividing $CD4^+$ T cells was responsible for the increase in dividing cells in the control-immunised LNs in Fig 3.5 (A). However, in contrast to that observed in the control-immunised LNs, $CD4^+$ T cell examination of PLP-immunised LNs demonstrated that the lack of change in the percentage of $BrdU^+$ cells between day 9 and day 12 post-immunisation was due to the stabilisation of $CD4^+$ T cell proliferation in these LNs (Fig 3.5 (C)). It may be possible that, upon cessation of proliferation, PLP-activated cells migrate out of the LN, some to the site of immunisation, while others migrate to the CNS, thereby explaining why the percentage of $BrdU^+$ cells in the PLP-immunised LNs did not increase to those levels observed in the control-immunised LNs 12 days post-immunisation.

3.2.3 Analysis of chemokine receptor expression on CD4$^+$ T cells following EAE induction

3.2.3.1 Chemokine receptor expression on CD4$^+$ T cells undergoing cell division in the draining LNs of PLP-immunised mice

It was demonstrated in Figure 3.3 that there were changes in the level of mRNA expression of the chemokine receptors CXCR3, CCR1, CCR2 and CCR5 in the sensitised LN. However, the RT-PCR analysis did not examine specifically the level of expression of these receptors on CD4$^+$ T cells. Based on the receptor expression profile in the sensitised LNs, and also on the fact that CD4$^+$ T cells constitute >50% of the cells in the sensitised LN, the following experiments were carried out to examine chemokine receptor regulation upon activation of CD4$^+$ T cells. The specific chemokine receptors chosen for examination were CXCR4, CXCR3 and CCR5. Both CXCR3 and CCR5 were chosen based on their expression profiles in the initial RT-PCR screen of the draining LNs, and CXCR4 was chosen potentially as a representative homeostatic receptor. Furthermore, receptor examination was based on the availability of antibodies for flow cytometry.

In order to directly study the regulation of chemokine receptor expression on antigen-activated CD4$^+$ T cells *in vivo*, it was necessary to analyse receptor expression on CD4$^+$ T cells that were undergoing, or had undergone, division. Accordingly, LN cells from mice that had been immunised with PLP in CFA and given BrdU were collected at Days 9 and 12 post-immunisation, labelled with antibodies specific for CD4, BrdU and the above chemokine receptors, and subsequently analysed by flow cytometry.

Figure 3.6 demonstrates that a greater percentage of the $CD4^+$ T cells that had undergone cell division in the draining LNs expressed CXCR4, CXCR3 and CCR5 compared with undivided cells. Thus, at day 9, within the population of $CD4^+$ T cells that had incorporated BrdU, CXCR3 and CCR5 were expressed on a significantly greater percentage of cells (~16% for both) compared to the population of $CD4^+$ T cells that did not incorporate BrdU ($p = 0.0008$ and $p = 0.0006$, respectively) (Fig 3.6 (A)). The expression of CXCR4 also differed between the dividing and non-dividing $CD4^+$ T cell populations, such that the percentage of divided $CD4^+$ T cells expressing this receptor ($18.2 \pm 1.9\%$) was significantly greater than the percentage of non-divided $CD4^+$ T cells expressing this receptor ($p = 0.0012$) (Fig 3.6 (A)). This expression pattern was sustained at day 12 post-immunisation with all three receptors being expressed in significantly higher percentages on $CD4^+$ T cells that had incorporated BrdU (Fig 3.6 (B)). However, the magnitude of CXCR4 upregulation on the divided population at day 12 was less striking than the extent of upregulation seen at day 9. Thus, at both days 9 and 12, the percentage of divided $CD4^+$ T cells expressing CXCR3 was 5-8 times greater than the percentage of non-divided $CD4^+$ T cells expressing this receptor, and the percentage of divided $CD4^+$ T cells expressing CCR5 was 6-9 times greater than the percentage of non-divided $CD4^+$ T cells expressing this receptor. In contrast to day 9, where the percentage of divided $CD4^+$ cells expressing CXCR4 was 10-fold above the percentage of non-dividing $CD4^+$ cells expressing this receptor, by day 12, this difference had reduced to only 2.3-fold ($p < 0.05$).

3.2.3.2 Chemokine receptor expression on divided CD4$^+$ T cells in the peripheral blood of PLP-immunised mice

It is well established that following antigen activation in the lymph nodes, activated T cells exit the nodes via the efferent lymphatics and enter the circulation (202). Thus, chemokine receptor expression on the activated CD4$^+$ T cells in the peripheral blood was monitored at various stages in the disease process to determine if the antigen-activated CD4$^+$ T cells maintained the elevated levels of receptor expression observed upon initial activation. Accordingly, subsequent to the induction of EAE and administration of BrdU, groups of mice were sacrificed at time points corresponding to pre-clinical disease (Day 9 post-immunisation), acute disease (Day 12 post-immunisation) and disease remission (Day 21 post-immunisation), and the peripheral blood was collected as described in section 2.3.7. Following removal of red blood cells by hypotonic lysis, the leukocytes were labelled with antibodies specific for CD4, BrdU and the chemokine receptors, and subsequently analysed by flow cytometry.

At all time-points examined, expression of CXCR4, CXCR3 and CCR5 was significantly greater on CD4$^+$ T cells that had divided in response to the antigen than on the undivided CD4$^+$ T cells in the peripheral blood (Fig 3.7 (A-C)). Furthermore, a greater percentage of these cells were expressing the receptors than those in the draining LNs. At day 9 post-immunisation, the percentage of divided CD4$^+$ T cells expressing CXCR4 was ~40%, which was 10-fold higher than the percentage of undivided CD4$^+$ T cells expressing this receptor (Fig 3.7 (A); $p < 0.01$) and 2-fold greater than the value obtained in the LNs at the same time point. Similarly, CXCR3 and CCR5 expression was significantly higher on the divided population of CD4$^+$ T cells (~30% and ~37%, respectively) at day 9 post-

immunisation (Fig 3.7 (A); $p < 0.0001$ and $p < 0.05$, respectively). By peak clinical disease (day 12), the percentage of divided $CD4^+$ T cells expressing CXCR4 and CXCR3 had reached a plateau, such that there were 10-fold (CXCR4) and 5-fold (CXCR3) more divided $CD4^+$ T cells expressing each receptor than the percentage of undivided cells expressing the corresponding receptor (Fig 3.7 (B)). Conversely, within the peripheral blood, at 12 days post-immunisation, the percentage of divided $CD4^+$ T cells expressing CCR5 had increased up to ~50% (Fig 3.7 (B)). Not only was this value 17.3-times greater than the undivided $CD4^+$ T cells at the same time point, but it represented a 1.5-fold increase over the percentage of divided $CD4^+$ T cells collected at day 9 post-immunisation ($p < 0.05$).

By the time the animals had entered the remission phase, the percentage of divided $CD4^+$ T cells expressing the chemokine receptors in the peripheral blood had significantly decreased (Fig 3.7 (C); $p < 0.05$; unmarked in figure), however, in concordance with results obtained at both day 9 and day 12 post-immunisation, the percentage of divided cells expressing the three receptors remained higher than the percentage of undivided cells expressing the receptors. Within the population of cells that had incorporated BrdU, CXCR4 was expressed on a significantly greater percentage of cells compared to the population of $CD4^+$ T cells that did not incorporate BrdU ($p < 0.05$), however, the fold-increase was reduced to 4.6-times such that ~18.7% of divided $CD4^+$ T cells were positive for CXCR4 (Fig 3.7 (C)). With regard to CXCR3, there was a slight, but significant, decrease in the percentage of divided $CD4^+$ T cells expressing CXCR3 during remission (unmarked in figure), however, the percentage of divided $CD4^+$ T cells expressing the receptor in the peripheral blood remained relatively constant throughout the course of disease (Fig 3.7 (C)). In contrast, the percentage of divided $CD4^+$ T cells in the peripheral

blood expressing CCR5 varied during EAE (Fig 3.7 (A-C)). By day 21 post-immunisation, the percentage of $CCR5^{+}BrdU^{+}$ $CD4^{+}$ T cells had reduced to ~31% such that the difference between the divided and non-divided cells decreased from 17.3-fold to 10-fold (Fig 3.7 (C)).

3.2.4 The BrdU technique allows the detection of T cell proliferation with high efficiency

It was observed that a small, but considerable, proportion of $CD4^{+}$ T cells in the sensitised LN and peripheral blood that expressed CCR5, CXCR3 and CXCR4, had not incorporated BrdU. However, it was important to confirm that the BrdU technique was enabling the detection of proliferating T cells with high efficiency, and therefore had not underestimated the proportion of $CD4^{+}$ T cells in the LN undergoing division. Accordingly, the incorporation of BrdU by thymocytes was assessed in parallel with each BrdU-labelling experiment, as thymocytes undergo rapid, continual turnover and therefore should incorporate BrdU with high efficiency (203).

As demonstrated in Figure 3.8, a large proportion of thymocytes incorporated BrdU in the 3-6 day period between the first injection of BrdU and the collection of thymus samples. In the experiment shown, 43% of thymocytes were $BrdU^{+}$, while the average from four experiments was ~50%. This proportion of thymocytes observed to stain positive for BrdU in the present study is comparable to the proportion of $BrdU^{+}$ thymocytes detected in previous studies after similar BrdU administration regimes (204-206). Thus, although only a relatively small proportion of cells from LNs were found to incorporate BrdU (Figs

3.4-3.6), the thymocyte data, showing high efficiency of incorporation of BrdU, suggest that this assay accurately reflects the level of division.

3.2.5 Effect of in vitro antigen restimulation on chemokine receptor expression on $CD4^+$ T cells

3.2.5.1 The effect of in vitro stimulation with $PLP_{139-151}$ on cells recovered from EAE lymph nodes

The results from figures 3.6 and 3.7 demonstrate that following $CD4^+$ T cell activation *in vivo,* the chemokine receptors CXCR4, CXCR3 and CCR5 were upregulated on $CD4^+$ T cells. However, because of the use of CFA in those experiments, it cannot be assumed that the divided $CD4^+$ T cells were $PLP_{139-151}$-specific, since similar proportions of $CD4^+$ T cells proliferated in both the presence and absence of $PLP_{139-151}$. Thus, restimulation experiments using defined antigen (in this case $PLP_{139-151}$) were performed in order to establish a population of PLP-specific cells. Furthermore, it was of interest to determine whether restimulation of the cells *in vitro* affected chemokine receptor expression on $CD4^+$ T cells, since encephalitogenic cells are subject to reactivation within the CNS tissue during EAE (140).

It has previously been demonstrated that EAE can be transferred into naïve recipients through the injection of neuroantigen-activated LN cells (defined as encephalitogenic cells) (123, 141). In those experiments, LN cells from $PLP_{139-151}$-immunised mice were restimulated *in vitro* over 4 days in the presence of 50 μg/ml $PLP_{139-151}$. Accordingly, in

the present study, cells from $PLP_{139-151}$- immunised LNs were restimulated for 4 days *in vitro* with different amounts of $PLP_{139-151}$ to establish a $PLP_{139-151}$-specific population of cells for further study.

In order to measure the proliferative response and to determine which subsets of lymphocytes were proliferating upon restimulation, cells were labelled with the fluorescent tracker dye CFSE prior to the initiation of culture. In this assay, cell division is associated with a reduction in CFSE fluorescence intensity, thus enabling divided and non-divided cells to be identified by flow cytometry, and the expression of cell surface molecules to be correlated with the division status of individual cells (189, 207).

The dot-plot (A) in Fig 3.9 is representative of the forward and side-scatter characteristics of the restimulated population of cells. Subsequently, all analyses were performed within the gated population of lymphocytes based on these observed characteristics. The histograms shown in Fig 3.9 (B) illustrate the CFSE fluorescence intensity of lymphocytes from the cultures. The "Cells Only" histogram represents the events occurring in the absence of $PLP_{139-151}$; since there was no antigen present, cells from these cultures were not expected to have divided. Accordingly, less than 8% of cells displayed a reduced level of CFSE fluorescence. As the concentration of $PLP_{139-151}$ increased in the cultures, the lymphocytes displayed a clearly bimodal distribution of CFSE fluorescence, indicating the presence of a population of divided cells containing reduced levels of the CFSE dye. Of the concentrations examined, 50 μg/ml $PLP_{139-151}$ elicited the greatest proliferation of lymphocytes (~37%) (Fig 3.9 (B)). A bar-chart representing 2 individual proliferation assays is presented in Fig 3.9 (C). The values obtained for the reduced fluorescent intensity from "Cells Only" cultures were subtracted from those values from the cultures

that proliferated in response to $PLP_{139-151}$. Furthermore, the well-documented mitogen, Concanavalin A, elicited a dramatic proliferative response in the lymphocyte cultures, indicating that the CFSE dye-dilution technique is suitable for measuring the proliferative response of cells *in vitro*. In addition, the results from these experiments indicate the suitability of a concentration of 50 μg/ml $PLP_{139-151}$ in EAE transfer experiments.

3.2.5.2 Restimulation with $PLP_{139-151}$ promotes $CD4^+$ T cell division

In order to determine the phenotype of the population of divided cells detected in the encephalitogenic cultures, CFSE-labelled cells were collected after 4 days of culture in the presence of 50 μg/ml $PLP_{139-151}$, stained with antibodies to CD3, CD4 or CD8 and analysed by dual-parameter flow cytometry (Fig 3.10). Staining with antibodies to CD4 and CD8 indicated that both populations underwent proliferation upon restimulation (Fig 3.10), however, the majority of the divided cells (78%-83%) stained positive for CD4. An average of only 18 ± 0.25% $CD8^+$ T cells underwent division upon restimulation. Furthermore, staining with antibodies to CD3 confirmed that ~90% of the CD4-stained cells were T cells (data not shown). Although not specifically examined, it is likely that the remainder of cells that divided in the cultures were B cells or macrophages. However, further analysis was not performed, as the primary intention of these studies was to study the T cell population. Representative density plots are shown in Fig 3.10 (B) illustrating the presence of readily detectable populations of $CD4^+$ T and $CD8^+$ T cells that had divided.

3.2.6 Analysis of chemokine receptor expression on divided CD4$^+$ T cells in vitro

3.2.6.1 Comparison of chemokine receptor expression on CD4$^+$ T cells that have divided upon restimulation in vitro

Having established a $PLP_{139-151}$-specific population *in vitro*, further studies were carried out to define chemokine receptor regulation on encephalitogenic CD4$^+$ T cells. Accordingly, those lymphocyte cultures restimulated with 50 μg/ml $PLP_{139-151}$, in the presence of CFSE, were harvested and the cells were labelled with antibodies to CD4 and the chemokine receptors, and subsequently analysed by flow cytometry.

As illustrated in Fig 3.11, CXCR3 and CCR5 were both expressed on a greater proportion of CD4$^+$ T cells that had further divided *in vitro* compared to CD4$^+$ T cells from the cultures that had not divided ($p < 0.001$ and $p < 0.01$, respectively). These results were similar to those involving BrdU incorporation *in vivo*. However, in contrast to the results obtained in the draining LNs and peripheral blood, no significant alteration in the expression of CXCR4 was observed on encephalitogenic CD4$^+$ T cells (Fig 3.11 (A)). The representative density plots in Fig 3.11 (C & D) illustrate the upregulation of CXCR3 and CCR5 observed in the encephalitogenic cultures, where the percentage of CD4$^+$ T cells that displayed diminished CFSE fluorescence expressed increased levels of CXCR3 and CCR5 (upper left quadrant; (C) & (D), respectively) compared to the undivided CD4$^+$ T cells that expressed the CXCR3 and CCR5 (upper right quadrant; (C) & (D), respectively). Figure 3.11 (B) demonstrates the lack of alteration to the expression of CXCR4 on divided versus undivided cells (upper left quadrant versus upper right quadrant).

3.2.6.2 A sub-population of CD4 high T cells divide in response to $PLP_{139-151}$ restimulation

During the analysis of the encephalitogenic cultures a population of T cells expressing elevated levels of CD4 became increasingly apparent ($CD4^{hi}$). A histogram (A) in Fig 3.12 demonstrates the bimodal peak of the CD4 population following 4 days restimulation with 50 μg/ml $PLP_{139-151}$. Further investigations, using the CFSE dye dilution technique, demonstrated that the vast majority of $CD4^{hi}$ T cells had undergone division during the 4 days of restimulation. In addition, flow cytometric analysis confirmed that >95% these $CD4^{hi}$ T cells co-expressed CD3, thereby verifying that the sub-population were in fact T cells (data not shown). Thus, the upregulation of CD4 on T cells is coupled to cell division.

3.2.6.3 Chemokine receptor expression on $CD4^{hi}$ versus $CD4^{normal}$ T cells

Having established that the majority of cells undergoing division in the encephalitogenic cultures were $CD4^{hi}$ T cells, it was of interest to determine whether it was these cells that were responsible for the alterations in chemokine receptor expression seen in Fig 3.11. A comparison of chemokine receptor expression on $CD4^{hi}$ T cells and $CD4^{normal}$ T cells in encephalitogenic cultures revealed that the upregulation of CXCR3, CCR5, and the maintenance of CXCR4, were events limited exclusively to the $CD4^{hi}$ T cell population (Fig 3.13). When the $CD4^{normal}$ and $CD4^{hi}$ populations from encephalitogenic cultures were compared, a statistically significant difference in the percentage of cells staining positive was observed for CXCR3 and CCR5 (CXCR3, $p < 0.01$; CCR5, $p < 0.05$). Conversely, there was no significant difference between the $CD4^{normal}$ and $CD4^{hi}$

populations with respect to CXCR4 expression. Of note, the $CD4^{normal}$ T cells expressed an almost identical pattern of chemokine receptor expression to that observed on non-divided $CD4^+$ T cells from encephalitogenic cultures ($p > 0.05$ for all). Thus, the $CD4^{hi}$ phenotype marks a population of activated T cells that displays a distinct repertoire of chemokine receptor expression compared to that observed on non-activated ($CD4^{normal}$) bystander cells in the same cultures.

3.2.7 Functional consequences of altered patterns of chemokine receptor expression

3.2.7.1 $PLP_{139-151}$ restimulation results in altered migration toward chemokine ligands for CXCR4, CXCR3 and CCR5

The most obvious reason for T cells to begin expressing alternative patterns of chemokine receptors following cellular activation is to allow them to migrate in response to a distinct range of chemokine ligands. Accordingly, based on the prior data, $PLP_{139-151}$-activated T cells would be expected to demonstrate enhanced chemotactic responsiveness toward CXCR3 and CCR5, and exhibit no differences in their ability to migrate toward CXCR4 ligands. To test this hypothesis, cells from LNs of Day 0 (naïve) mice, cells from LNs of PLP-immunised (sensitised) mice and encephalitogenic (restimulated) cells were compared in Transwell® chemotaxis assays for their ability to migrate toward representative ligands; SDF-1/CXCL12 (the only identified CXCR4 ligand), IP-10/CXCL10 and I-TAC/CXCL11 (CXCR3 ligands) and RANTES/CCL5 and MIP-1β/CCL4 (CCR5 ligands). Subsequently, the ability of cells to migrate toward an optimised concentration range of each chemokine was compared between naïve, sensitised

and restimulated cells. In order to correct for any differences in spontaneous migration between the three culture conditions, the data (cell migration) are expressed as a percentage of the total input cells.

As shown in Fig 3.14, cells from all groups migrated toward the CXCR4 ligand SDF-1/CXCL12, albeit to different extents. A greater proportion of naïve and sensitised cells migrated toward SDF-1/CXCL12 than did restimulated cells, however, this was observed at higher concentrations of the ligand. At the lower concentrations (3-30 ng/ml), a greater proportion of sensitised and restimulated cells migrated to the lower chambers, indicating that these cells were more sensitive to lower concentrations of SDF-1/CXCL12. The migratory pattern of all cells was bell-shaped. The similarity witnessed between the three curves is in keeping with the observed regulation of CXCR4 on T cells from the draining LNs and *in vitro* cultures.

Figure 3.15 illustrates that migration toward the CXCR3 ligands IP-10/CXCL10 and I-TAC/CXCL11 was virtually undetectable in naïve cells, but started to increase in sensitised cells, however, only at higher concentrations of the ligands. Migration towards CXCR3 ligands increased significantly following restimulation ($p < 0.05$-0.01), in keeping with the observed upregulation of CXCR3 expression in encephalitogenic cultures following restimulation with $PLP_{139-151}$. In contrast to the responses seen towards SDF-1/CXCL12, the migratory behaviour of the sensitised and restimulated cells persisted to increase with increasing concentrations of IP-10/CXCL10 and I-TAC/CXCL11 (Fig 3.15). Similarly, as may be expected given the upregulation of CCR5 expression following sensitisation and restimulation, the ability of cells from sensitised LNs and encephalitogenic cultures to migrate toward RANTES/CCL5 and MIP-1β/CCL4 was

significantly increased compared to naïve leukocytes ($p < 0.05$; towards RANTES $p < 0.05$ for restimulated cells only) (Fig 3.16 (A-B)). Of note, the percentage of cells migrating in response to the CCR5 ligands was considerably lower than that to the CXCR4 and CXCR3 ligands.

3.3 Summary

The aim of this series of experiments was to identify chemokine receptors that demonstrated altered levels of expression during the sensitisation phase of EAE. Based on the results of initial RT-PCR screens in the draining LNs, CXCR4, CXCR3 and CCR5 were chosen for further analysis. The observed kinetics of chemokine receptor expression in the draining LNs was co-incident with the recruitment and activation of $CD4^+$ and $CD8^+$ T cells, suggesting a functional role for these receptors in the regulation of T cell recruitment and/or activation in the draining LNs. Subsequent analyses revealed that within the $CD4^+$ T cell subset, antigenic activation was associated with an upregulation of CXCR4, CXCR3 and CCR5. A greater proportion of $CD4^+$ T cells that had undergone division in response to immunisation expressed each of the receptors, thus providing evidence for the upregulation of these receptors upon T cell activation during EAE. The observed upregulation was maintained as the activated T cells migrated from the site of activation to the peripheral blood. Within the peripheral blood compartment, the frequency of the divided $CD4^+$ T cell population expressing each receptor was greater than that observed in the draining LNs. This may reflect the changes in adhesion molecule

expression following T cell activation that impact on the ability of effector cells to enter the LNs via the HEVs (4, 208).

Upon restimulation *in vitro* with the immunising antigen, a population of $CD4^+$ T cells underwent further divisions. Based on the terminology of previous studies, these cells are referred to as encephalitogenic cells (35, 209). It has previously been demonstrated that encephalitogenic T cells express mRNA for MIP-1α/CCL3, MIP-1β/CCL4 and TCA-3/CCL1 (35). Kuchroo *et al.* (1993) also analysed stimulated $PLP_{139-151}$-specific T cell clones and found that MIP-1α/CCL3, MIP-1β/CCL4 and TCA-3/CCL1 mRNA expression correlated with the ability of the T cell clones to induce EAE (209). However, very few studies have attempted to identify the array of chemokine receptors expressed by these cells. Thus, through use of flow cytometry, this is one of the first studies to examine chemokine receptor protein expression on the surface of PLP-specific $CD4^+$ T cells. Findings from these experiments revealed that encephalitogenic cells, expressing increased levels of CD4, further upregulated expression of CXCR3 and CCR5, however, did not alter surface expression of CXCR4. This may indicate that further upregulation of CXCR4 is not required for encephalitogenicity.

Although chemokines have been proposed to play a number of roles in T cell biology, chemotaxis is still generally considered to be the primary function of the chemokine gene superfamily. Therefore, based on the observational studies, it was considered likely that sensistisation would result in enhanced migration toward CXCR4, CXCR3 and CCR5 ligands. In addition, restimulation was predicted to enhance the migration of cells toward CXCR3 and CCR5 ligands, but would not alter the capacity of the cells to migrate toward the CXCR4 ligand, SDF-1/CXCL12. Chemotaxis assays confirmed these predictions to a

certain extent, however, it appears that further restimulation *in vitro* is required for a functional response to the CXCR3 ligands, IP-10/CXCL10 and I-TAC/CXCL11. With respect to CXCR4-mediated migration, it appears that modulation of receptor expression has no effect on the potential mobility of the cells.

These results indicate that CXCR4, CXCR3 and CCR5 are involved in the sensitisation phase of EAE, although their precise roles are yet to be elucidated.

Table 3.1: Characteristics of clinical EAE following immunisation with $PLP_{139-151}$. As stated in the figure legend of Figure 3.1, SJL/J mice were induced with EAE and then treated with 5 μg pertussigen. Mice were monitored for neurological symptoms until Day 25 post-immunisation. Throughout the course of disease, various parameters were analysed. These data are representative of 4 others performed with similar results.

Parameter	Active EAE induction
No. Sick / Total	13/13
Mean day of onset [a]	9.84 ± 0.19
Mean day of recovery [a]	17.4 ± 0.98
Mean length of disease (days) [a]	6.87 ± 0.64
Mean maximum clinical score [a]	2.9 ± 0.23

[a] Mean ± SEM

Fig 3.1. *Development of clinical symptoms of EAE in response to immunisation with* $PLP_{139\text{-}151}$. SJL/J mice were injected s.c. with 50 μg $PLP_{139\text{-}151}$ in CFA. Two hours before and two days after the injection of $PLP_{139\text{-}151}$ emulsion, the mice received 5 μg of pertussigen (i.v.). Mice were monitored for disease symptoms (Section 2.2.3) over a period of 25 days post-immunisation. Data are presented as mean ± SEM (n = 8-12). The experiment depicted in this figure is representative of 4 others performed with similar results.

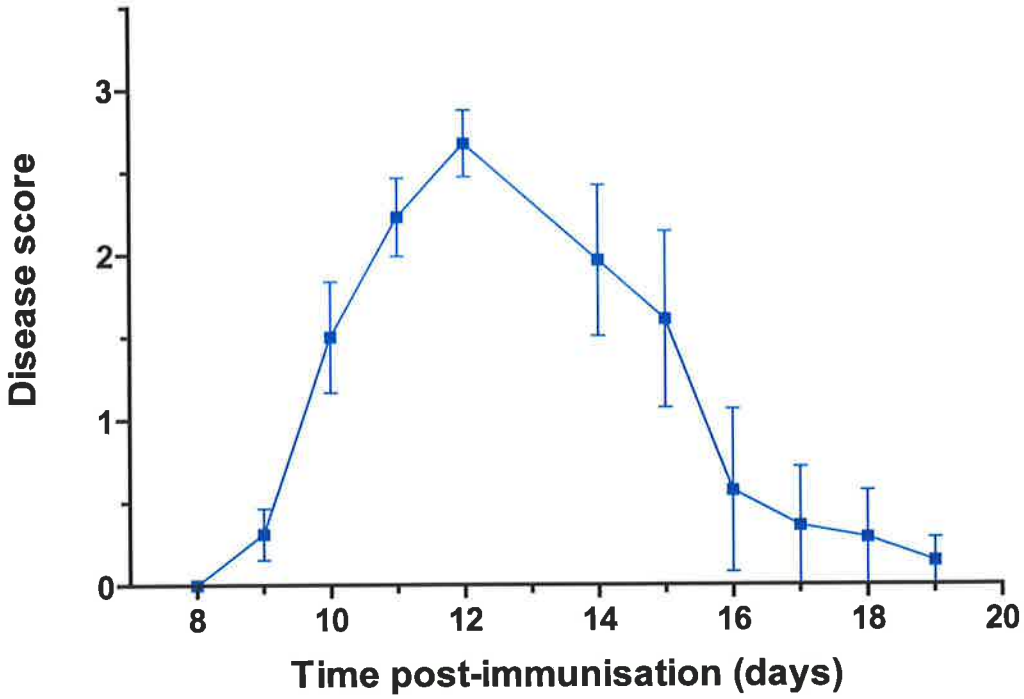
Disease score
0
1
2
3
8
10
12
14
16
18
20
Time post-immunisation (days)

Figure 3.2. *Time-course of total cell yields from the draining inguinal LNs following EAE induction.* EAE was induced in SJL/J mice as previously described (PLP/CFA) (Section 2.2.1). Control mice were subjected to CFA injection and pertussigen treatment, without the presence of PLP in the CFA emulsion (PBS/CFA). On days 0, 6, 9, 12 and 21 post-immunisation, the inguinal LNs were removed and single cell suspensions prepared. [A] The total number of viable cells recovered from each LN was then determined by counting on a haemocytometer after staining with trypan blue. *, Statistically significant from normal (Day 0) mice ($p < 0.05$). $^{\#}$, Statistically significant from PBS/CFA-immunised mice ($p < 0.05$). Data are presented as mean ± SEM ($n = 6$, from 2 independent experiments). [B] The cells recovered 9 days post-immunisation were labelled with either anti-CD4, anti-CD8, anti-surface immunoglobulin (sIg) or anti-CD11c and analysed by flow cytometry and the percentage of cells positive for CD4, CD8, sIg or CD11c was determined in comparison to staining with an isotype-matched control antibody. Data are presented as mean ± SEM ($n = 11$, from 2 independent experiments).

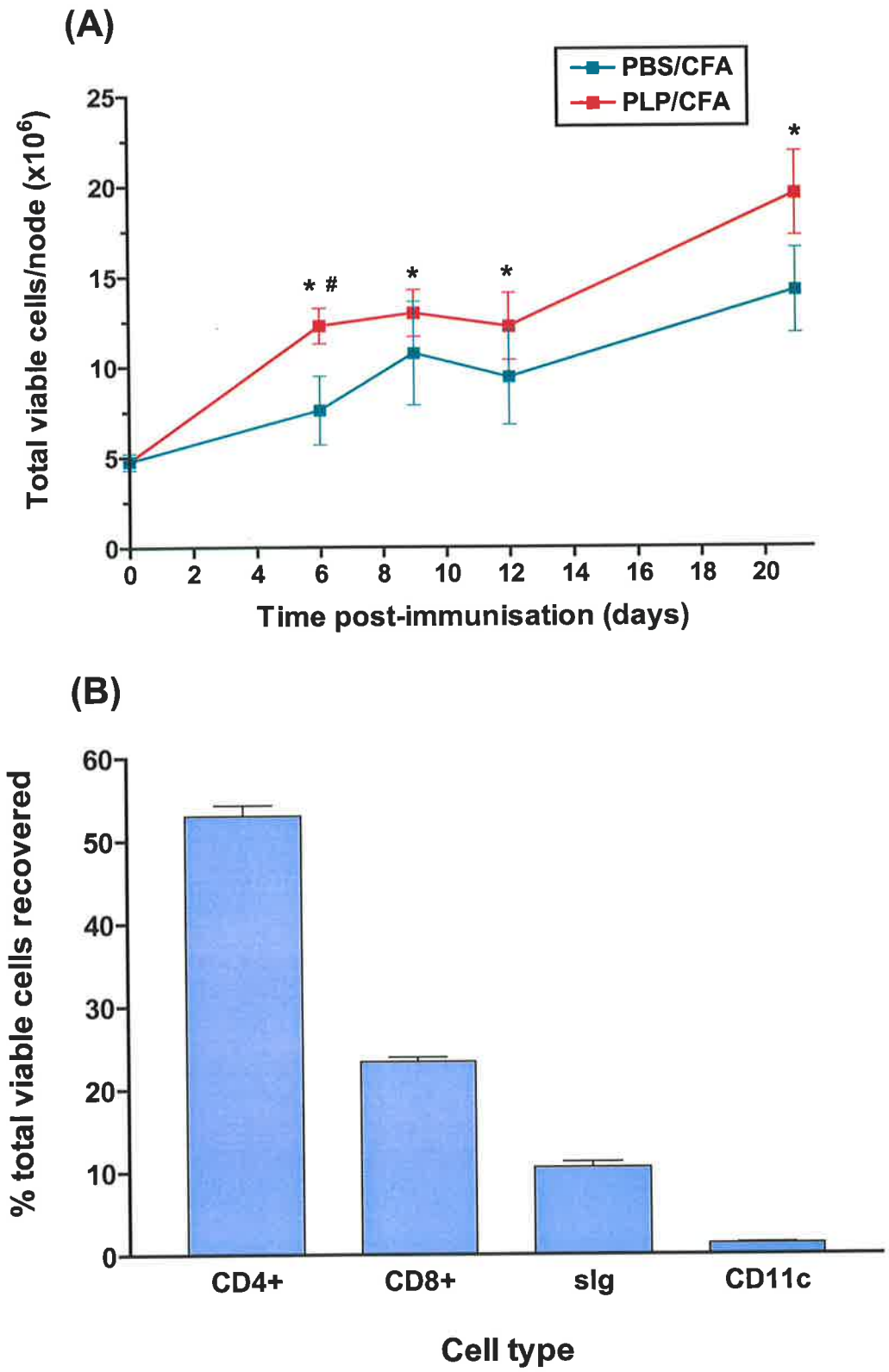
(A)
PBS/CFA
PLP/CFA
Total viable cells/node (x10^6)
25
20
15
10
5
0
0
2
4
6
8
10
12
14
16
18
20
Time post-immunisation (days)
* #
*
*
*
(B)
% total viable cells recovered
60
50
40
30
20
10
0
CD4+
CD8+
sIg
CD11c
Cell type

Figure 3.3. *Comparative PCR analysis of chemokine receptor mRNA levels in the draining LNs.* EAE was induced in SJL/J mice as previously described (PLP/CFA) (Section 2.2.1). Control mice were subjected to CFA injection and pertussigen treatment, without PLP in the CFA emulsion (PBS/CFA). On days 0, 9, 12 and 21 post-immunisation, draining LNs were removed and total RNA was extracted, DNase-treated and reverse-transcribed (Sections 2.7.1, 2.7.2 and 2.7.3, respectively). Specific oligonucleotide primers were then used to amplify CXCR4, CXCR3, CCR1, CCR2, CCR5 and GAPDH (Section 2.7.4). PCR-amplified products were analysed by 2.0% agarose gel electrophoresis followed by staining with Sybr Gold and the bands on the gel were quantified (Section 2.7.5.). The volume of each of the receptor bands was normalised to the GAPDH band volume for the same sample. Data shown are representative of 2 independent experiments. *, Significantly different from day 0 or the PBS/CFA value at the same time point ($p<0.05$). **, Significantly different from day 0 ($p<0.01$). ***, Significantly different from day 0 or the PBS/CFA value at the same time point ($p<0.001$). $^{\Psi}$, Significantly different from day 0 in a 1-way t test ($p < 0.05$). Data are presented as mean ± SEM ($n = 3$-6).

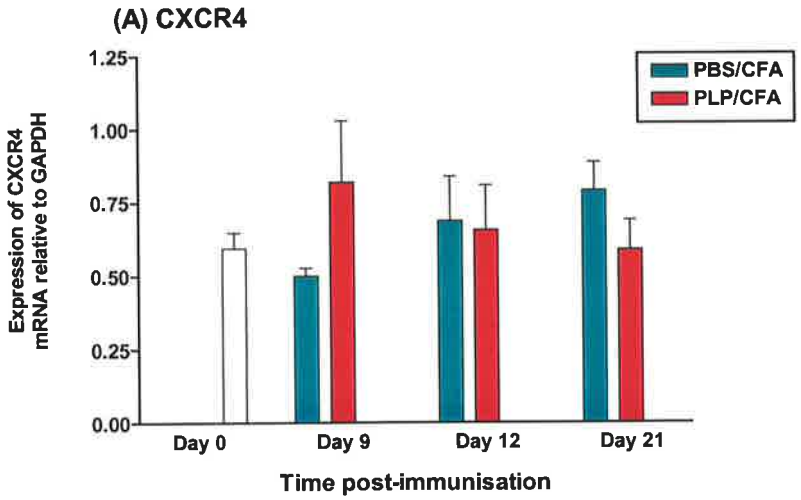
(A) CXCR4
PBS/CFA
PLP/CFA
Expression of CXCR4 mRNA relative to GAPDH
1.25
1.00
0.75
0.50
0.25
0.00
Day 0
Day 9
Day 12
Day 21
Time post-immunisation

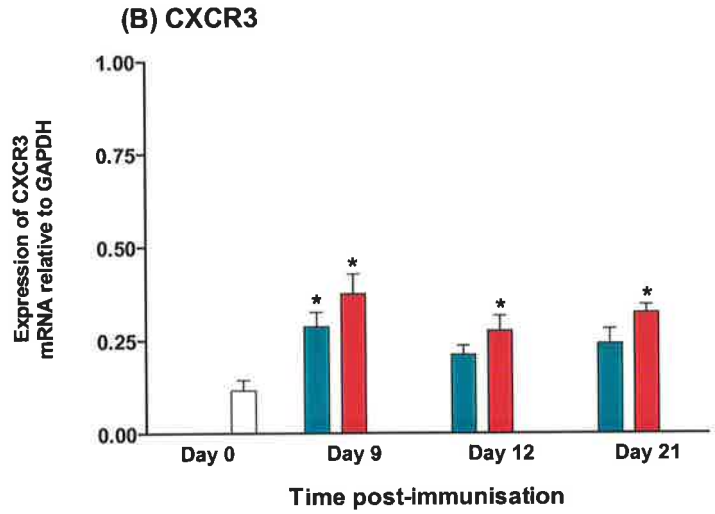
(B) CXCR3
Expression of CXCR3 mRNA relative to GAPDH
1.00
0.75
0.50
0.25
0.00
*
Day 0
Day 9
Day 12
Day 21
Time post-immunisation

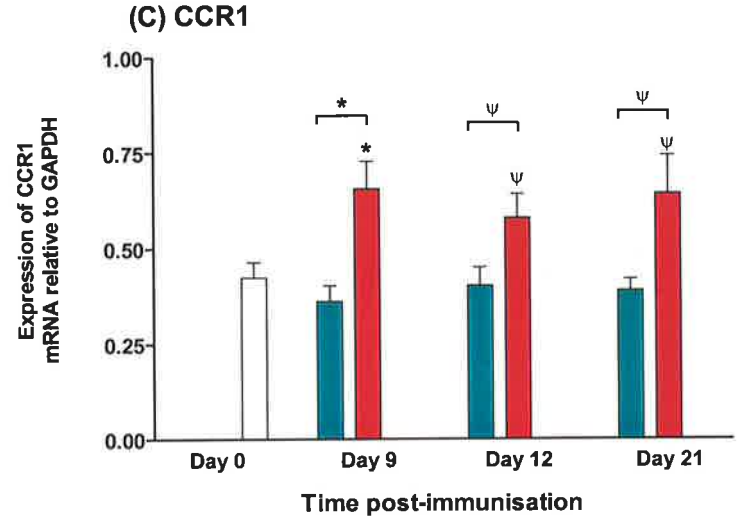
(C) CCR1
Expression of CCR1 mRNA relative to GAPDH
1.00
0.75
0.50
0.25
0.00
*
ψ
Day 0
Day 9
Day 12
Day 21
Time post-immunisation

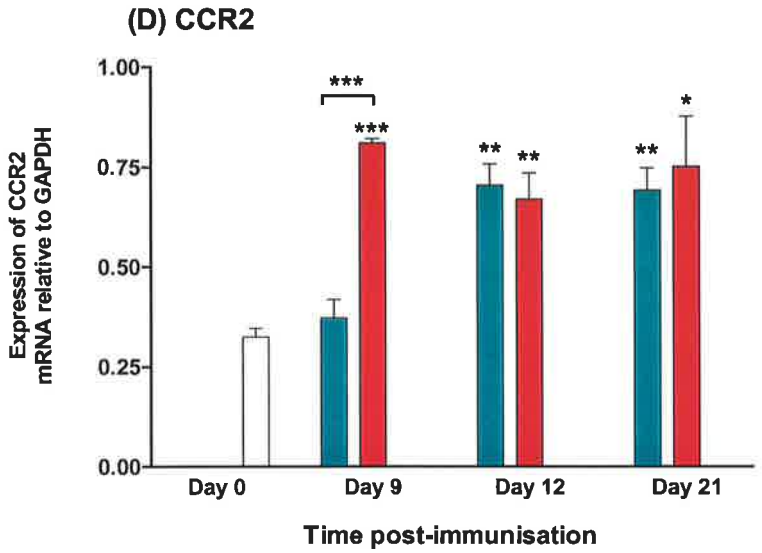
(D) CCR2
Expression of CCR2 mRNA relative to GAPDH
1.00
0.75
0.50
0.25
0.00
***
***
**
**
**
*
Day 0
Day 9
Day 12
Day 21
Time post-immunisation

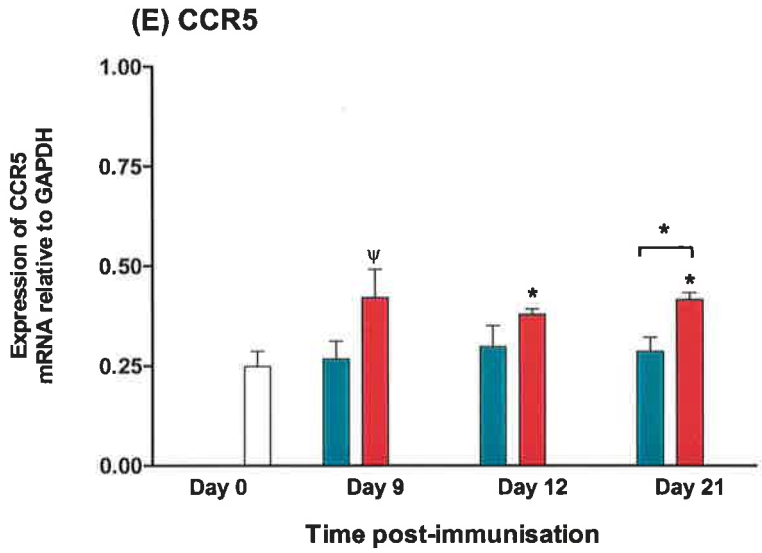
(E) CCR5
Expression of CCR5 mRNA relative to GAPDH
1.00
0.75
0.50
0.25
0.00
ψ
*
*
*
Day 0
Day 9
Day 12
Day 21
Time post-immunisation

Figure 3.4. *The percentage of total cells and $CD4^+$ T cells undergoing cell division in the inguinal lymph nodes from Day 9 control- and PLP-immunised mice.* EAE was induced in SJL/J mice as previously described (PLP/CFA) (Section 2.2.1). Control mice were subjected to CFA injection and pertussigen treatment, without PLP in the CFA emulsion (PBS/CFA). BrdU was administered as described (Section 2.2.6). Nine days later (just prior to disease onset), the inguinal LNs were removed and single cell suspensions prepared. Cells were labelled with anti-BrdU [A] or with anti-BrdU and anti-CD4 [B-C] and analysed by flow cytometry, gating on lymphocytes using forward and side scatter characteristics. A representative density plot of cells from PBS-immunised or PLP-immunised LNs stained with anti-BrdU and anti-CD4 is presented in [B]. The percentage of $CD4^+$ T cells that had incorporated BrdU at day 9 [C] was determined as a proportion of the total $CD4^+$ population. *, Significantly different from the PBS/CFA-immunised LNs ($p<0.05$). Data are presented as mean ± SEM (n = 5-6).

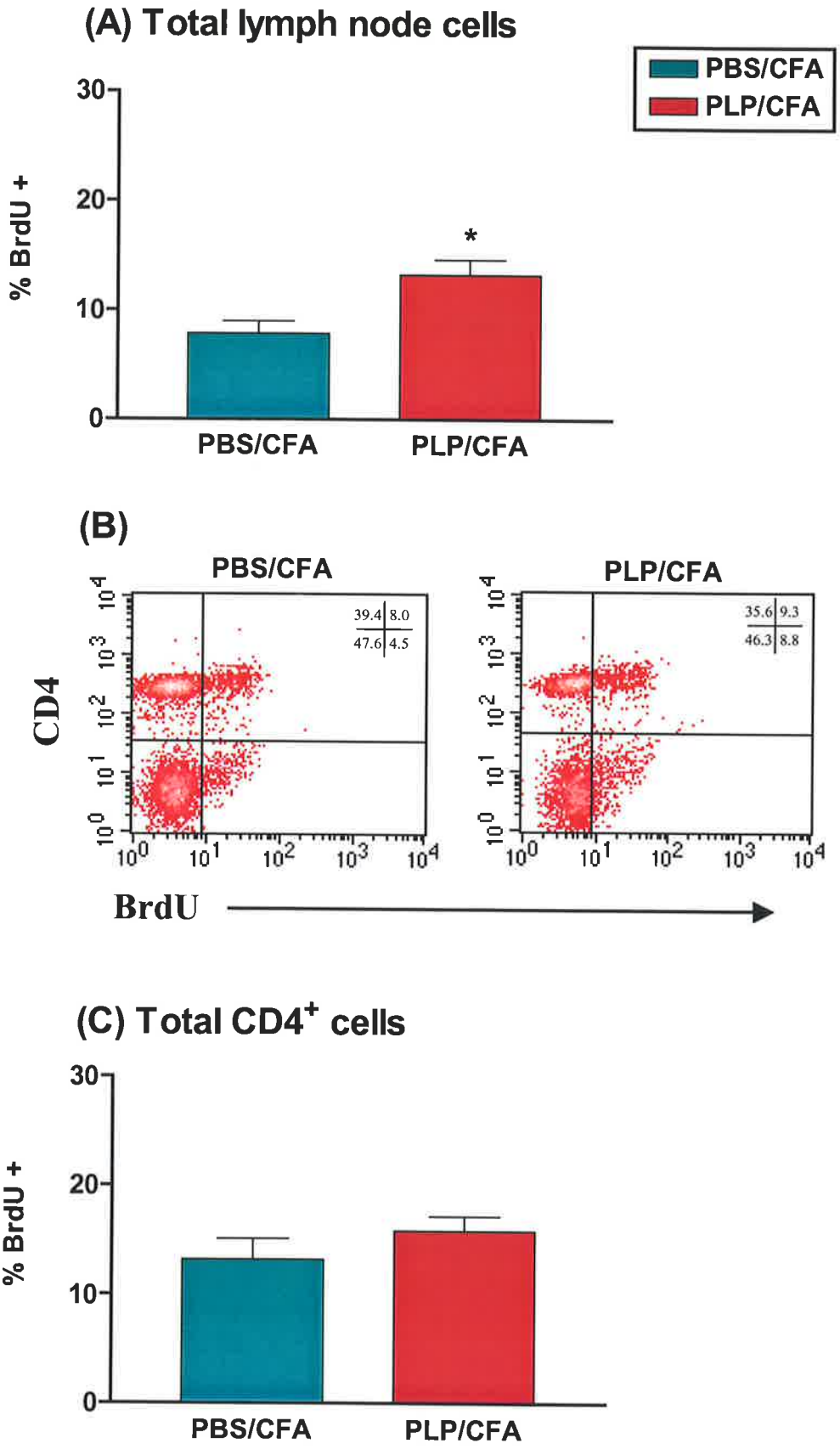
(A) Total lymph node cells
PBS/CFA
PLP/CFA
% BrdU +
30
20
10
0
*
PBS/CFA
PLP/CFA
(B)
PBS/CFA
PLP/CFA
39.4 8.0
47.6 4.5
35.6 9.3
46.3 8.8
CD4
BrdU
(C) Total CD4+ cells
% BrdU +
30
20
10
0
PBS/CFA
PLP/CFA

Figure 3.5. *The percentage of total cells and $CD4^+$ T cells undergoing cell division in the inguinal lymph nodes from Day 12 control- and PLP-immunised mice.* EAE was induced in SJL/J mice as previously described (PLP/CFA) (Section 2.2.1). Control mice were subjected to CFA injection and pertussigen treatment, without PLP in the CFA emulsion (PBS/CFA). BrdU was administered as described (Section 2.2.6). Twelve days later (peak disease), the inguinal LNs were removed and single cell suspensions prepared. Cells were labelled with anti-BrdU [A] or with anti-BrdU and anti-CD4 [B-C] and analysed by flow cytometry, gating on lymphocytes using forward and side scatter characteristics. A representative density plot of cells from PBS-immunised or PLP-immunised LNs stained with anti-BrdU and anti-CD4 is presented in [B]. The percentage of $CD4^+$ T cells that had incorporated BrdU at day 12 [C] was determined as a proportion of the total $CD4^+$ population. **, Statistically significant from the PBS-immunised LNs ($p < 0.005$). Data are presented as mean ± SEM (n = 8-14).

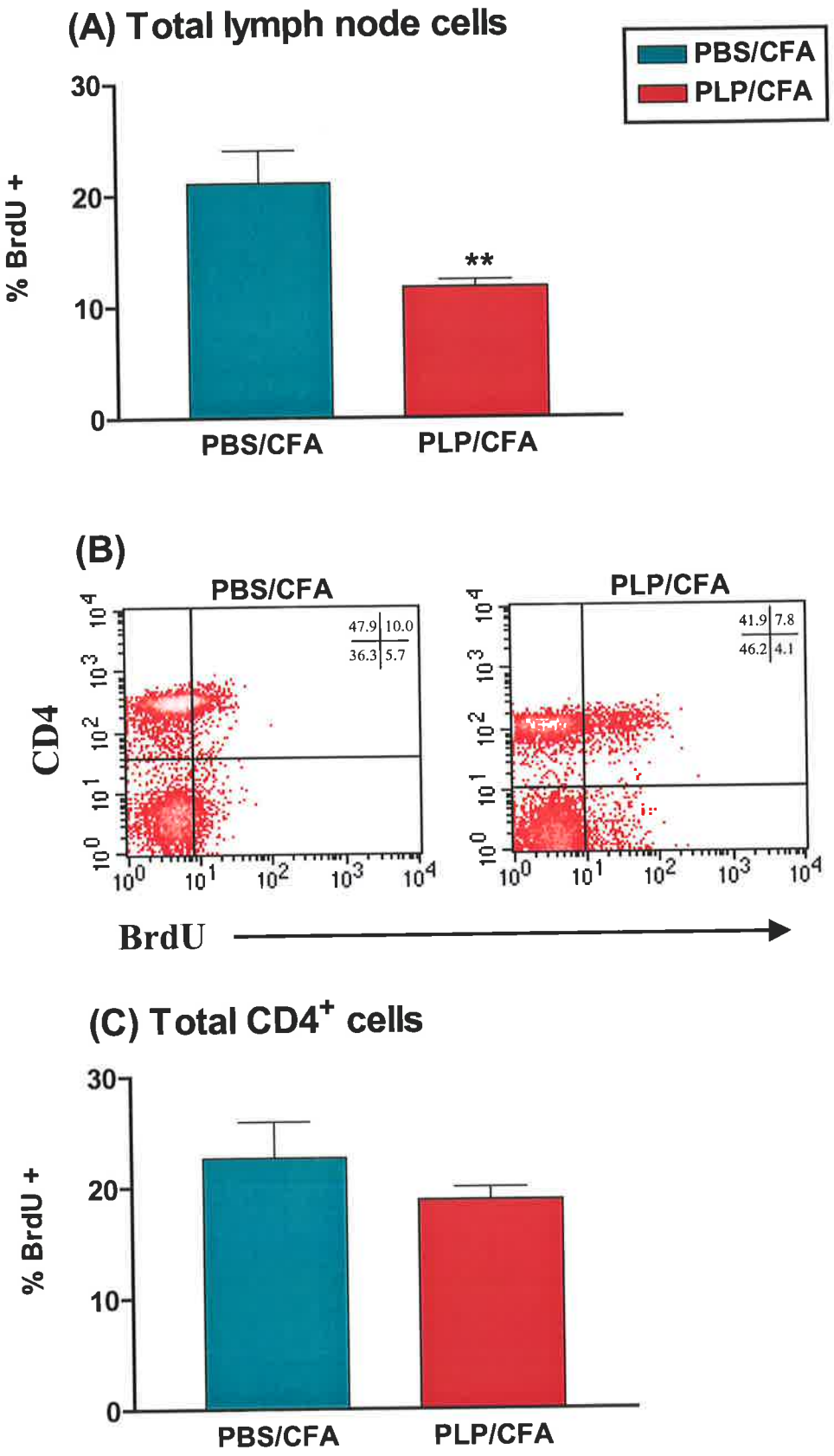
(A) Total lymph node cells
PBS/CFA
PLP/CFA
% BrdU +
30
20
10
0
**
PBS/CFA
PLP/CFA
(B)
PBS/CFA
PLP/CFA
47.9 10.0
36.3 5.7
41.9 7.8
46.2 4.1
CD4
BrdU
(C) Total CD4+ cells
% BrdU +
30
20
10
0
PBS/CFA
PLP/CFA

Figure 3.6. *Comparison of chemokine receptor expression on proliferating and non-proliferating $CD4^+$ T cells in draining lymph nodes from EAE mice.* EAE was induced in SJL/J mice as previously described (PLP/CFA) (Section 2.2.1). BrdU was administered as described (Section 2.2.6). Nine days (pre-clinical) [A] or 12 days (peak disease) [B] later, inguinal LNs were removed and single cell suspensions prepared. The cells were labelled with anti-BrdU, anti-CD4 and anti-chemokine receptor antibodies, and then analysed by flow cytometry, gating on lymphocytes using forward and side scatter characteristics. Within the $CD4^+$ T cell population, the percentage of $BrdU^+$ (divided) and $BrdU^-$ (non-divided) cells expressing each chemokine receptor was determined as a proportion of the total $BrdU^+$ or $BrdU^-$ population, respectively. **, Statistically significant from non-divided cells ($p < 0.005$). ***, Statistically significant from non-divided cells ($p < 0.001$). Data are presented as mean ± SEM (n = 6-9, from 2-3 independent experiments).

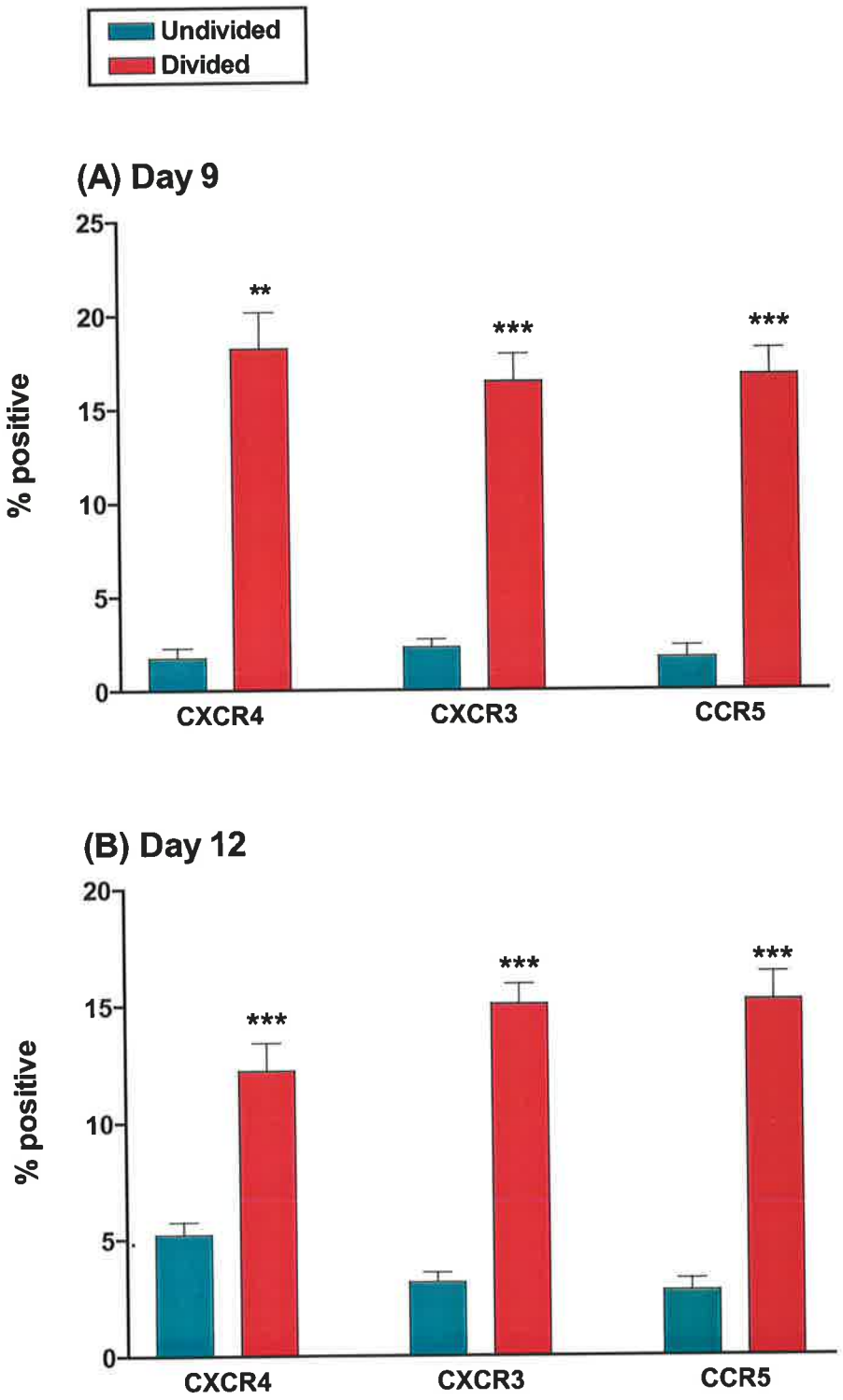
Undivided
Divided
(A) Day 9
% positive
25
20
15
10
5
0
**
***
***
CXCR4
CXCR3
CCR5
(B) Day 12
% positive
20
15
10
5
0
***
***
***
CXCR4
CXCR3
CCR5

Figure 3.7. *Comparison of chemokine receptor expression on proliferating and non-proliferating $CD4^+$ T cells in EAE peripheral blood.* EAE was induced in SJL/J mice as previously described (PLP/CFA) (Section 2.2.1). BrdU was administered as described (Section 2.2.6). Nine days (pre-clinical) [A], 12 days (peak disease) [B] or 21 days (remission) [C] later, peripheral blood was collected, red blood cells were lysed and single cell suspensions prepared (Section 2.3.7). The cells were labelled with anti-BrdU, anti-CD4 and anti-chemokine receptor antibodies, and then analysed by flow cytometry, gating on lymphocytes using forward and side scatter characteristics. Within the $CD4^+$ T cell population, the percentage of $BrdU^+$ (divided) and $BrdU^-$ (non-divided) cells expressing each chemokine receptor was determined as a proportion of the total $BrdU^+$ or $BrdU^-$ population, respectively. *, Statistically significant from non-divided cells ($p < 0.05$). **, Statistically significant from non-divided cells ($p < 0.005$). ***, Statistically significant from non-divided cells ($p < 0.001$). Data are presented as mean ± SEM ($n = 3$).

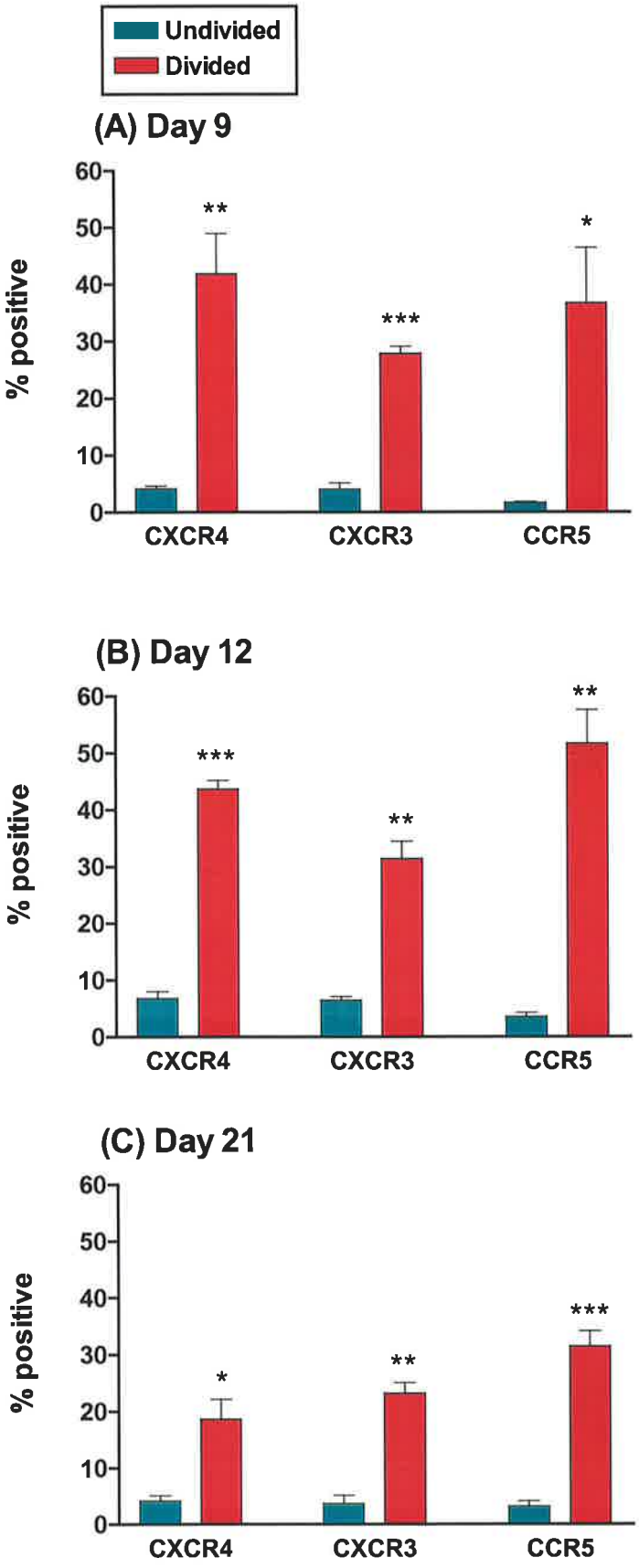
Undivided
Divided
(A) Day 9
% positive
60
50
40
30
20
10
0
**
***
*
CXCR4
CXCR3
CCR5
(B) Day 12
% positive
60
50
40
30
20
10
0
***
**
**
CXCR4
CXCR3
CCR5
(C) Day 21
% positive
60
50
40
30
20
10
0
*
**
***
CXCR4
CXCR3
CCR5

Figure 3.8. *Incorporation of BrdU by thymocytes.* BrdU was administered to SJL/J mice as described (Section 2.2.6), and 24 hours after the final water change, the thymus was removed and a single cell suspension was prepared. The cells were labelled with anti-BrdU and then analysed by flow cytometry, gating on lymphocytes using forward and side scatter characteristics. The percentage of cells that had incorporated BrdU was determined in comparison to staining with an isotype-matched negative control antibody. The data are representative of 4 independent experiments.

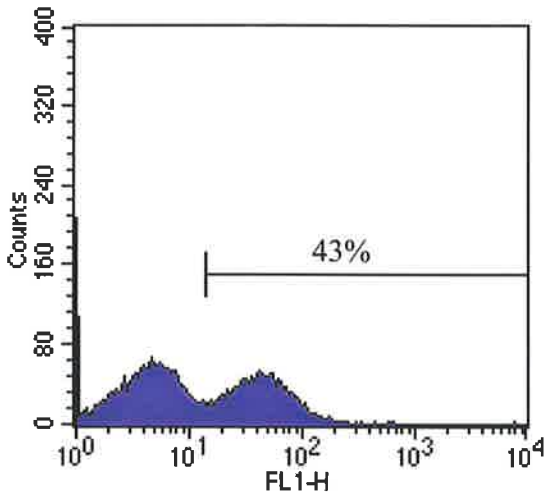
Counts
400
320
240
160
80
0
43%
10^0
10^1
10^2
10^3
10^4
FL1-H

Figure 3.9. *The effect of in vitro restimulation with $PLP_{139-151}$ on cells recovered from EAE lymph nodes.* SJL/J mice were immunised with 25 μg of $PLP_{139-151}$ peptide in CFA in a 120 μl volume (Section 2.2.2). Mice were killed on day 10 post-immunisation, the draining lymph nodes were collected, and single cell suspensions were prepared. These were stained with CFSE and cultured for 4 days in the presence of various concentrations of $PLP_{139-151}$. A representative dot plot is presented in [A] displaying the forward and side scatter characteristics of the restimulated population. Histograms show the effect of increasing concentrations of $PLP_{139-151}$, or Con A, on the CFSE fluorescent intensity of the gated population [B]. Shown in [C] is a bar-chart of the data obtained from 2 independent experiments, where the values obtained for the reduced fluorescent intensity from the cells in the absence of $PLP_{139-151}$ (Cells Only) has been subtracted from those values from the cultures that proliferated as a result of $PLP_{139-151}$-, or Con A-, stimulation. Data in [C] are presented as mean ± SD (n = 3). Data shown in [C] are representative of 2 independent experiments performed with similar results.

(A)

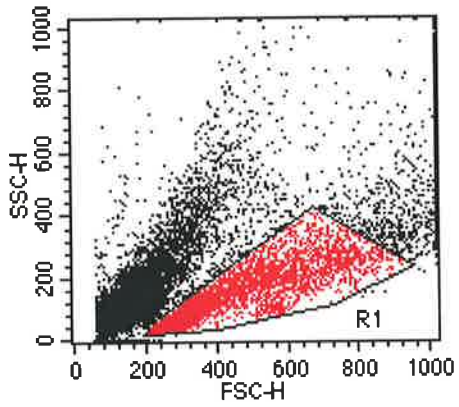
SSC-H
FSC-H
R1
0
200
400
600
800
1000

(B)

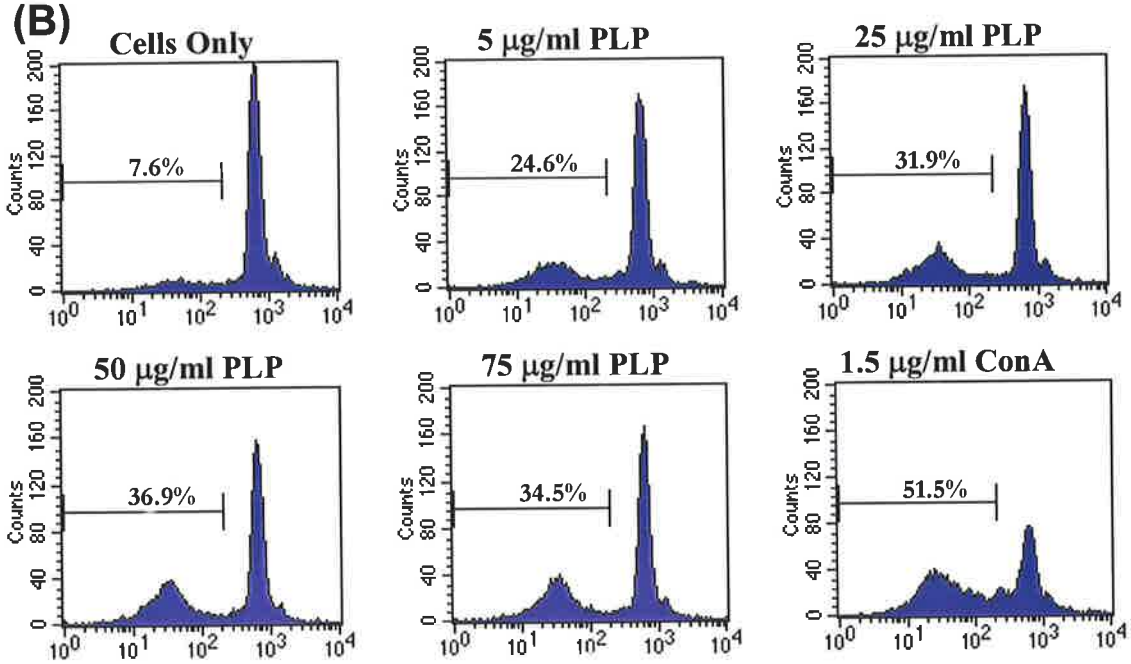
Cells Only
7.6%
5 µg/ml PLP
24.6%
25 µg/ml PLP
31.9%
50 µg/ml PLP
36.9%
75 µg/ml PLP
34.5%
1.5 µg/ml ConA
51.5%
Counts

(C)

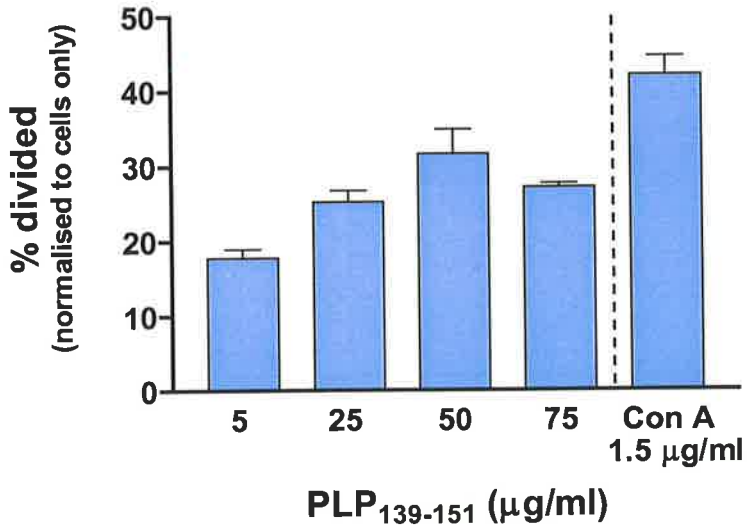
% divided
(normalised to cells only)
0
10
20
30
40
50
5
25
50
75
Con A
1.5 µg/ml
PLP139-151 (µg/ml)

Figure 3.10. *Restimulation with $PLP_{139-151}$ promotes $CD4^+$ T cell division.*

SJL/J mice were immunised with 25 μg of $PLP_{139-151}$ peptide in CFA in a 120 μl volume (Section 2.2.2). Mice were killed on day 10 post-immunisation, the draining lymph nodes were collected, and single cell suspensions were prepared. These were stained with CFSE and cultured for 4 days in the presence of 50 μg/ml of $PLP_{139-151}$. Following 4 days of culture, the cells were harvested, labelled with anti-CD4 or anti-CD8, and then analysed by flow cytometry, gating on lymphocytes using forward and side scatter characteristics. Within the population of cells demonstrating reduced fluorescence intensity in the CFSE channel (divided cells), the percentage of CD4 and CD8 expressing cells was determined as a proportion of the total divided population. Data are presented as mean ± SEM (n = 8). Representative density plots of divided and non-divided cell populations expressing CD4 and CD8 are shown in [B].

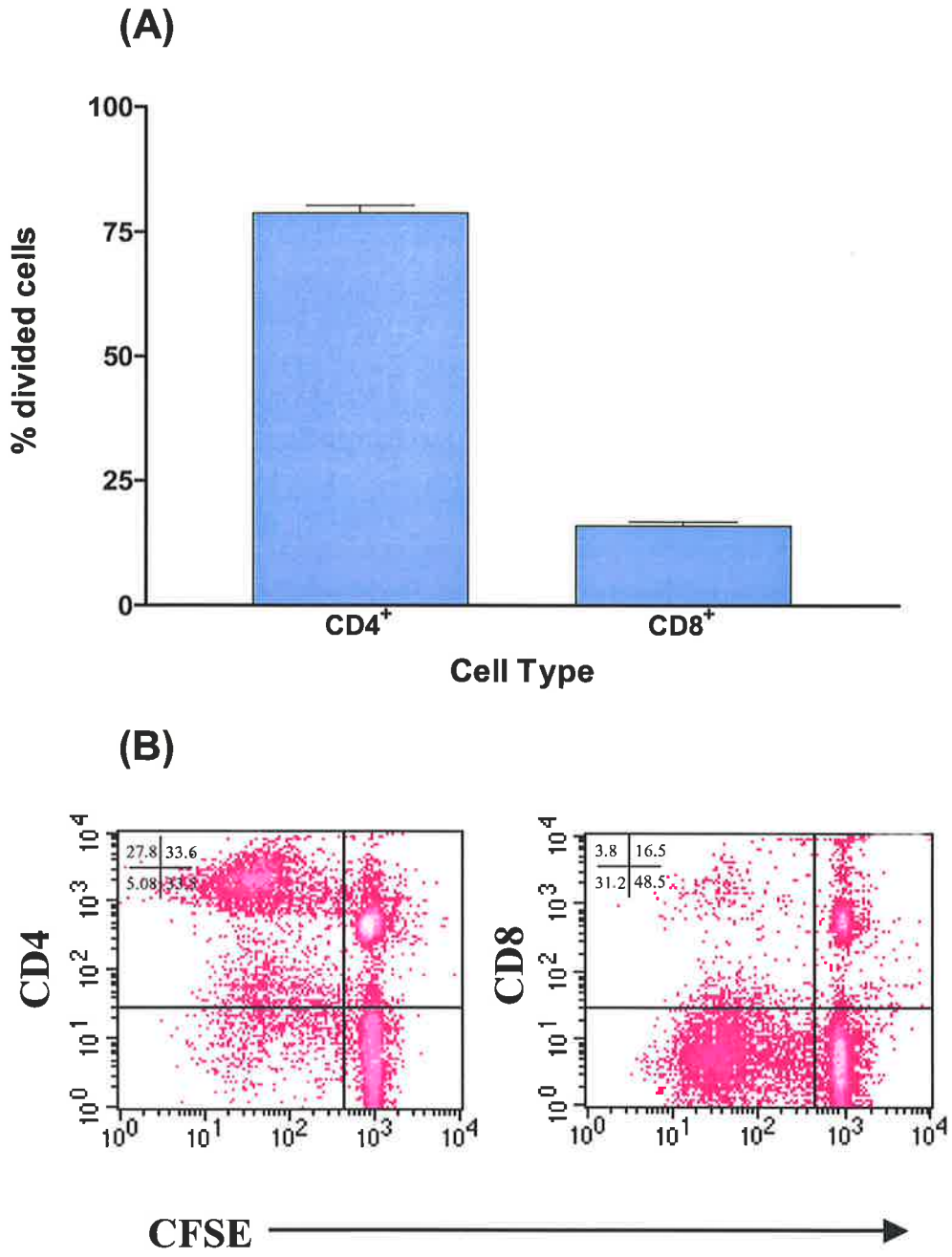
(A)
100
75
50
25
0
% divided cells
CD4+
CD8+
Cell Type
(B)
CD4
27.8
33.6
5.08
CD8
3.8
16.5
31.2
48.5
CFSE

Figure 3.11. *Comparison of chemokine receptor expression on $CD4^+$ T cells that have divided upon restimulation* in vitro. SJL/J mice were immunised with 25 μg of $PLP_{139-151}$ peptide in CFA in a 120 μl volume (Section 2.2.2). Mice were killed on day 10 post-immunisation, the draining lymph nodes were collected, and single cell suspensions were prepared. These were stained with CFSE and cultured for 4 days in the presence of 50 μg/ml of $PLP_{139-151}$. Following 4 days of culture, the cells were harvested, labelled with anti-CD4 and anti-chemokine receptor antibodies, and then analysed by flow cytometry, gating on lymphocytes using forward and side scatter characteristics. Within the $CD4^+$ T cell population, the percentage of cells demonstrating reduced fluorescence intensity in the CFSE channel (divided cells) and the percentage of cells demonstrating high fluorescence intensity in the CFSE channel (non-divided) expressing each chemokine receptor was determined as a proportion of the total divided or non-divided population, respectively [A]. **, Statistically significant from non-divided cells ($p < 0.005$). ***, Statistically significant from non-divided cells ($p < 0.001$). Data are presented as mean ± SEM ($n = 3$). Representative density plots of divided and non-divided $CD4^+$ T cell populations expressing CXCR4, CXCR3 and CCR5 are shown in [B-D], respectively.

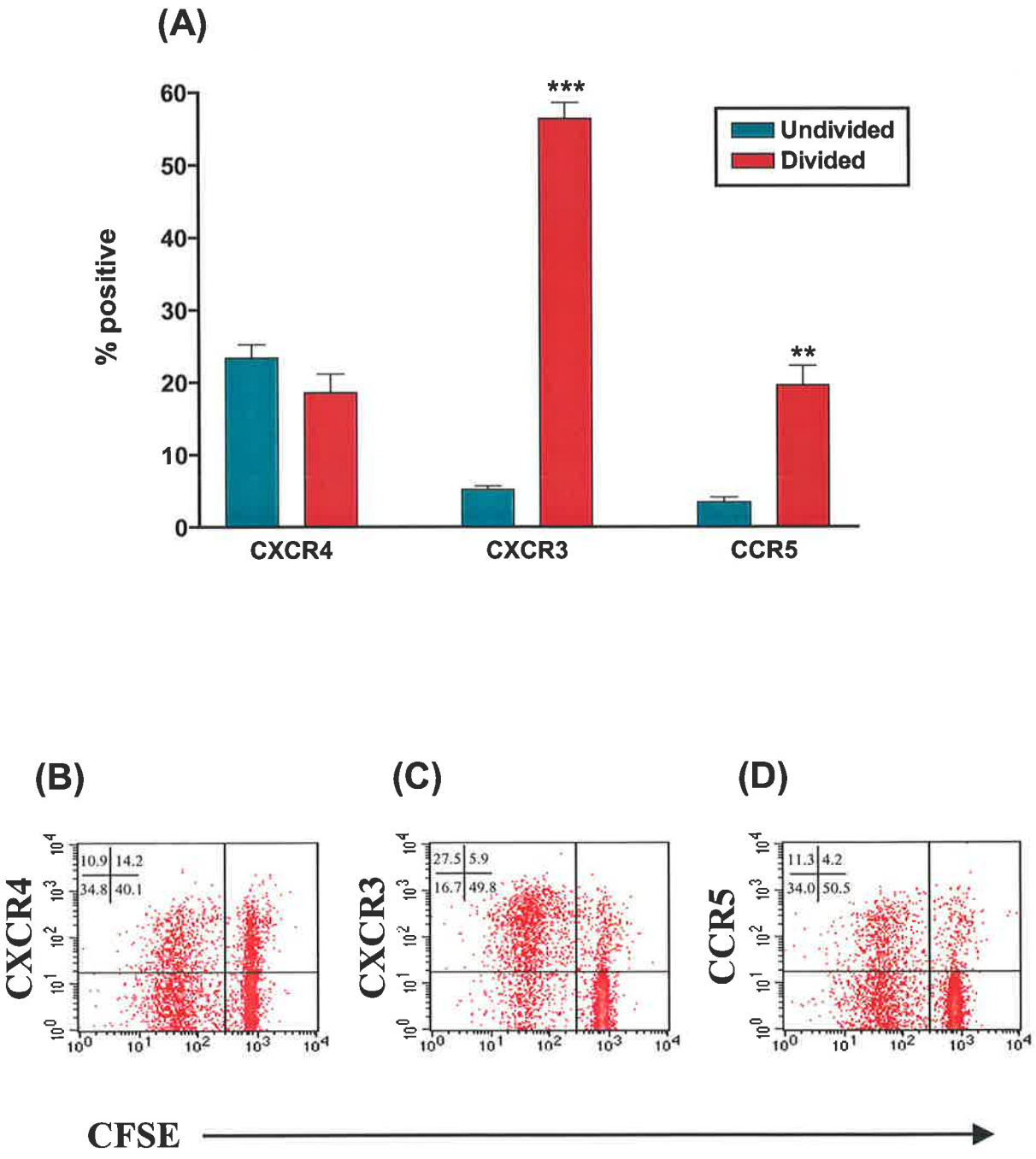
(A)
% positive
60
50
40
30
20
10
0
***
**
Undivided
Divided
CXCR4
CXCR3
CCR5
(B)
(C)
(D)
CXCR4
CXCR3
CCR5
10.9
14.2
34.8
40.1
27.5
5.9
16.7
49.8
11.3
4.2
34.0
50.5
CFSE

Figure 3.12. *A sub-population of CD4 high T cells divide in response to $PLP_{139-151}$ restimulation.* SJL/J mice were immunised with 25 μg of $PLP_{139-151}$ peptide in CFA in a 120 μl volume (Section 2.2.2). Mice were killed on day 10 post-immunisation, the draining lymph nodes were collected, and single cell suspensions were prepared. These were stained with CFSE and cultured for 4 days in the presence of 50 μg/ml of $PLP_{139-151}$. Following 4 days of culture, the cells were harvested, labelled with anti-CD4 antibodies and analysed by flow cytometry, gating on lymphocytes using forward and side scatter characteristics. Shown in [A] is a fluorescence histogram demonstrating the presence of the $CD4^{high}$ population in the restimulated culture. Within the population of cells demonstrating reduced fluorescence intensity in the CFSE channel (divided cells), the percentage of lymphocytes with normal ($CD4^{normal}$) or elevated levels of CD4 ($CD4^{high}$) expression were determined as a proportion of the total divided population [B]. ***, Significantly different from the $CD4^{normal}$ value ($p<0.001$). Data are presented as mean ± SEM ($n = 6$).

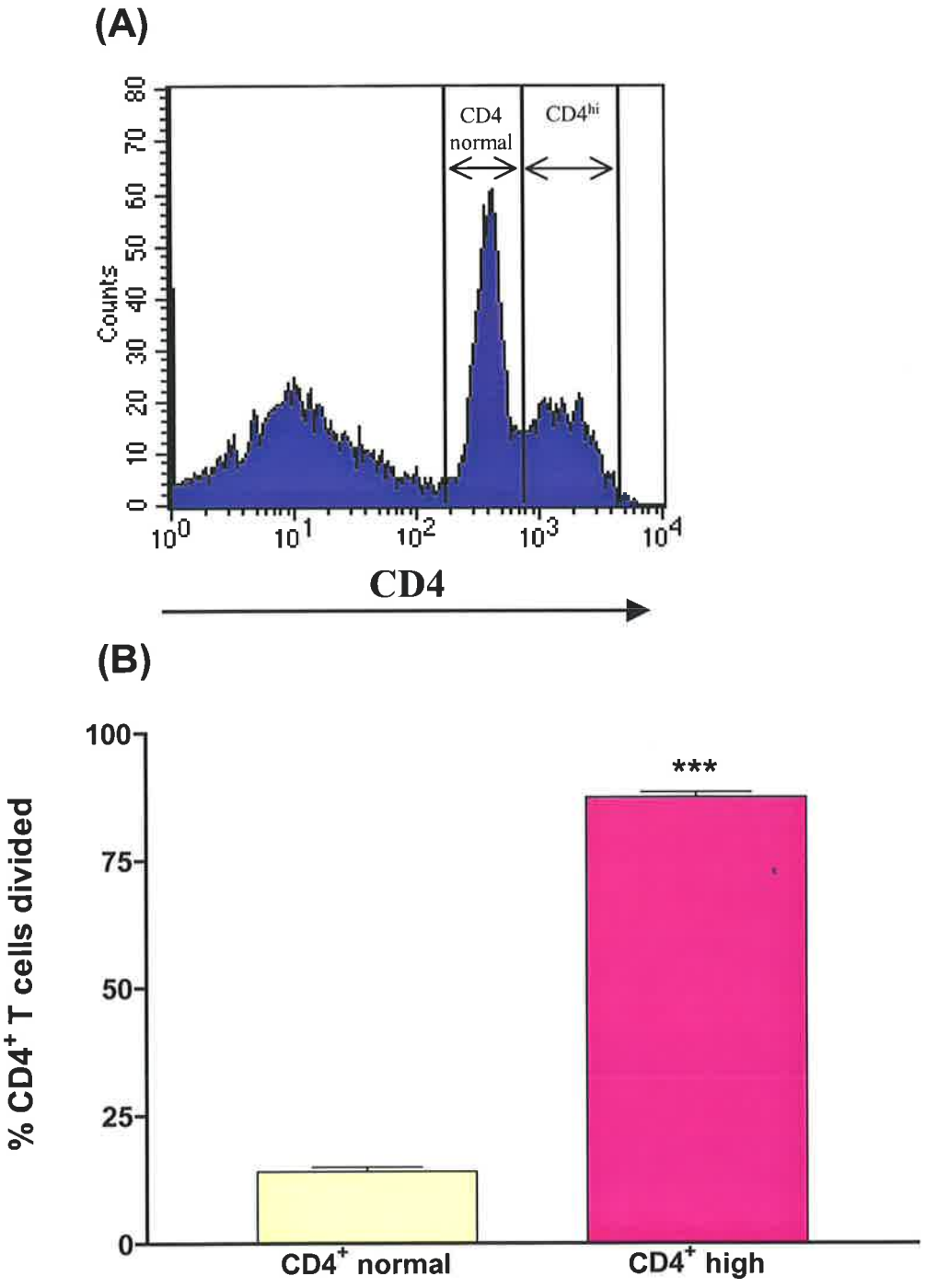
(A)
CD4 normal
CD4hi
Counts
0
10
20
30
40
50
60
70
80
10^0
10^1
10^2
10^3
10^4
CD4
(B)
% CD4+ T cells divided
100
75
50
25
0
***
CD4+ normal
CD4+ high

Figure 3.13. *Differential expression of chemokine receptors on $CD4^{normal}$ and $CD4^{high}$ T cell sub-populations.* SJL/J mice were immunised with 25 μg of $PLP_{139-151}$ peptide in CFA in a 120 μl volume (Section 2.2.2). Mice were killed on day 10 post-immunisation, the draining lymph nodes were collected, and single cell suspensions were prepared. These were stained with CFSE and cultured for 4 days in the presence of 50 μg/ml of $PLP_{139-151}$. Following 4 days of culture, the cells were harvested, labelled with anti-CD4 and antibodies to chemokine receptors and analysed by flow cytometry, gating on lymphocytes using forward and side scatter characteristics. Sub-populations of $CD4^{normal}$ and $CD4^{high}$ T cells were electronically gated, and the percentage of cells expressing the relevant chemokine receptor was determined for each population. *, Significantly different from the $CD4^{normal}$ ($p<0.05$). **, Significantly different from the $CD4^{normal}$ ($p<0.01$). Data are presented as mean ± SEM (n = 3). Representative density plots of divided and non-divided $CD4^{hi}$ T cell populations expressing CXCR4, CXCR3 and CCR5 are shown in [B-D], respectively.

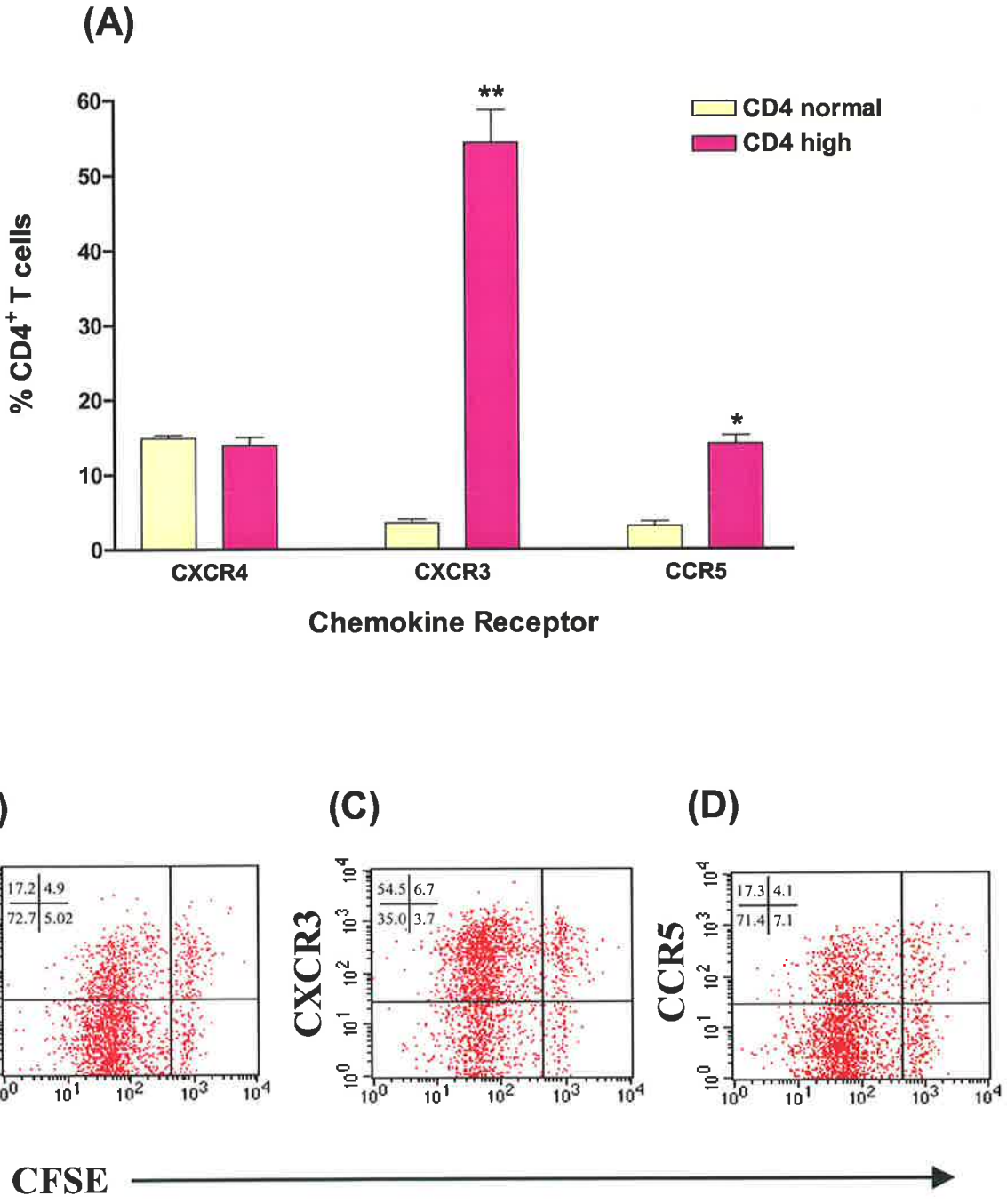
(A)
% CD4+ T cells
60
50
40
30
20
10
0
**
*
CD4 normal
CD4 high
CXCR4
CXCR3
CCR5
Chemokine Receptor
(B)
(C)
(D)
CXCR4
CXCR3
CCR5
17.2 4.9
72.7 5.02
54.5 6.7
35.0 3.7
17.3 4.1
71.4 7.1
CFSE

Figure 3.14. *Dose-response of naïve, activated and restimulated cell migration towards the CXCR4 ligand, SDF-1/CXCL12*. Lymph nodes were removed from non-immunised SJL/J mice (naïve) and PLP/CFA-immunised mice (sensitised), and single cell suspensions prepared. In addition, cells from PLP/CFA-immunised lymph nodes were cultured for 4 days in the presence of $PLP_{139-151}$ (restimulated). All cells were loaded with calcein fluorophore. One million cells (in 100 µl) were loaded into the upper compartment of Transwell® chambers, and 600 µl of media containing various concentrations of SDF-1/CCL12 were added to the lower chamber. Assays were conducted at 37°C for 3 hours, after which the level of fluorescence in the lower chambers was determined (Section 2.5.4). Data points represent the mean value ± SEM (n = 2-4).

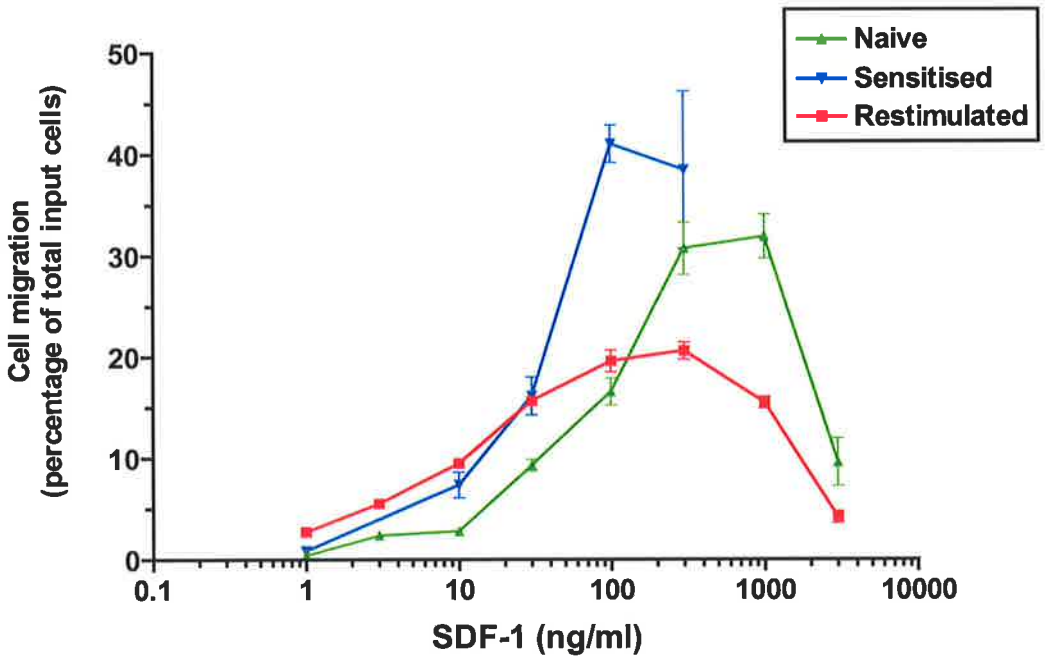
Naive
Sensitised
Restimulated
Cell migration
(percentage of total input cells)
50
40
30
20
10
0
0.1
1
10
100
1000
10000
SDF-1 (ng/ml)

Figure 3.15. *Dose-response of naïve, activated and restimulated cell migration towards CXCR3 ligands, IP-10/CXCL10 and I-TAC/CXCL11.* Lymph nodes were removed from non-immunised SJL/J mice (naïve) and PLP/CFA-immunised mice (sensitised), and single cell suspensions prepared. In addition, cells from PLP/CFA-immunised lymph nodes were cultured for 4 days in the presence of $PLP_{139-151}$ (restimulated). All cells were loaded with calcein fluorophore. One million cells (in 100 µl) were loaded into the upper compartment of Transwell® chambers, and 600 µl of media containing various concentrations of muIP-10/CXCL10 [A] or muI-TAC/CXCL11 [B] were added to the lower chamber. Assays were conducted at 37°C for 3 hours, after which the level of fluorescence in the lower chambers was determined (Section 2.5.4). Data points represent the mean value ± SEM (n = 2-4).

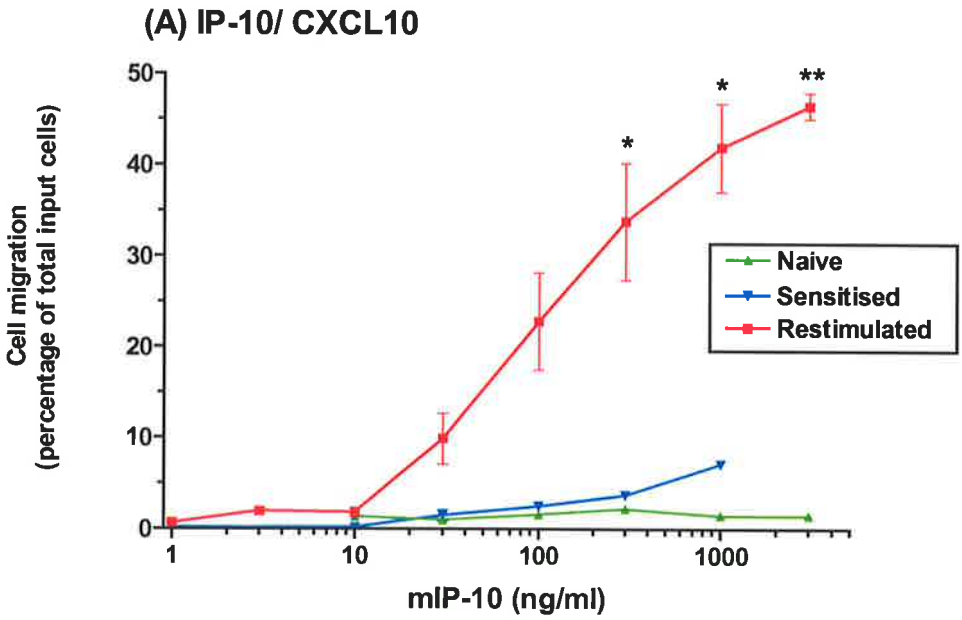
(A) IP-10/ CXCL10
Cell migration
(percentage of total input cells)
50
40
30
20
10
0
1
10
100
1000
mIP-10 (ng/ml)
*
*
**
Naive
Sensitised
Restimulated

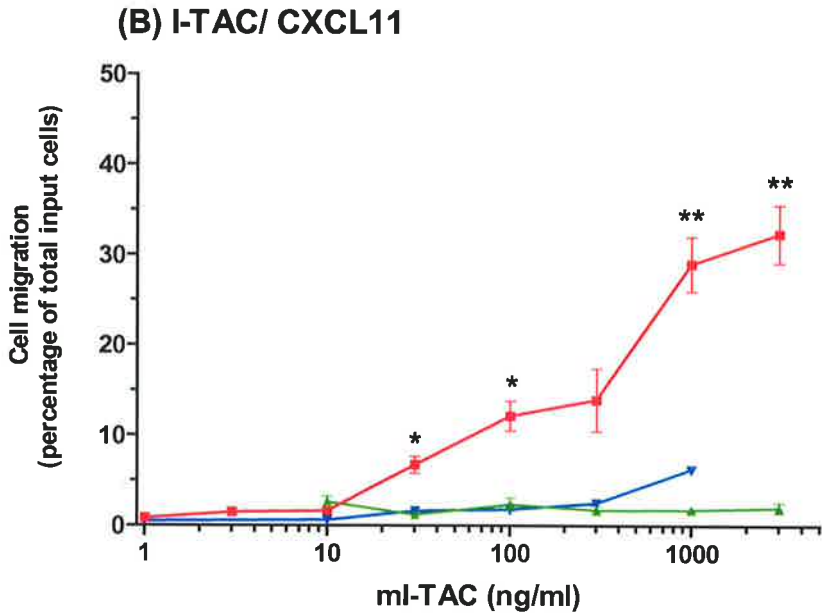
(B) I-TAC/ CXCL11
Cell migration
(percentage of total input cells)
50
40
30
20
10
0
1
10
100
1000
mI-TAC (ng/ml)
*
*
**
**

Figure 3.16. *Dose-response of naïve, activated and restimulated cell migration towards CCR5 ligands, RANTES/CCL5 and MIP-1β/CCL4.* Lymph nodes were removed from non-immunised SJL/J mice (naïve) and PLP/CFA-immunised mice (sensitised), and single cell suspensions prepared. In addition, cells from PLP/CFA-immunised lymph nodes were cultured for 4 days in the presence of $PLP_{139-151}$ (restimulated). All cells were loaded with calcein fluorophore. One million cells (in 100 µl) were loaded into the upper compartment of Transwell® chambers, and 600 µl of media containing various concentrations of RANTES/CCL5 [A] or MIP-1β/CCL4 [B] were added to the lower chamber. Assays were conducted at 37°C for 3 hours, after which the level of fluorescence in the lower chambers was determined (Section 2.5.4). *, Significantly different from the naïve value ($p<0.05$). **, Significantly different from the naïve value ($p<0.01$). Data points represent the mean value ± SEM ($n = 2$).

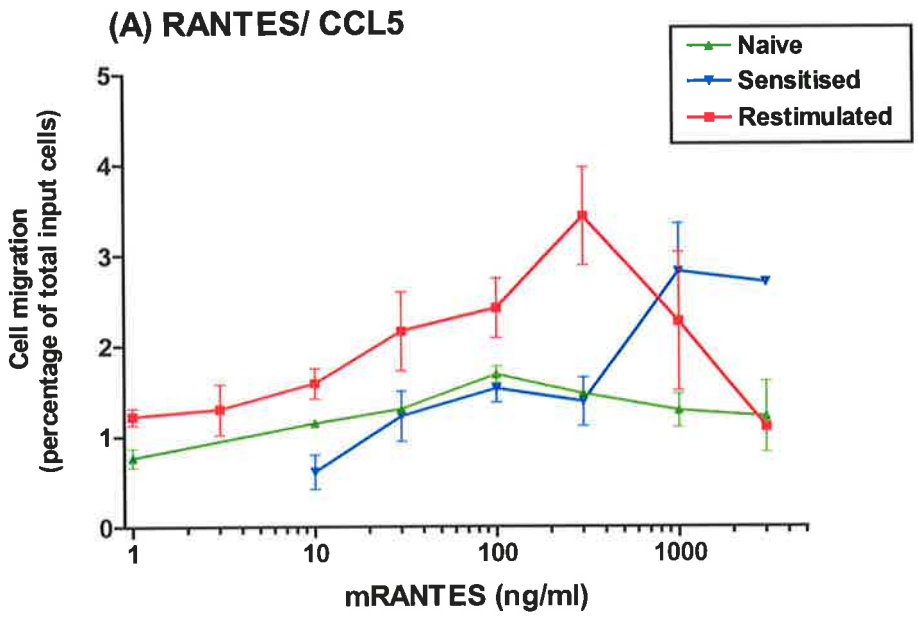
(A) RANTES/ CCL5
Naive
Sensitised
Restimulated
Cell migration
(percentage of total input cells)
0
1
2
3
4
5
1
10
100
1000
mRANTES (ng/ml)

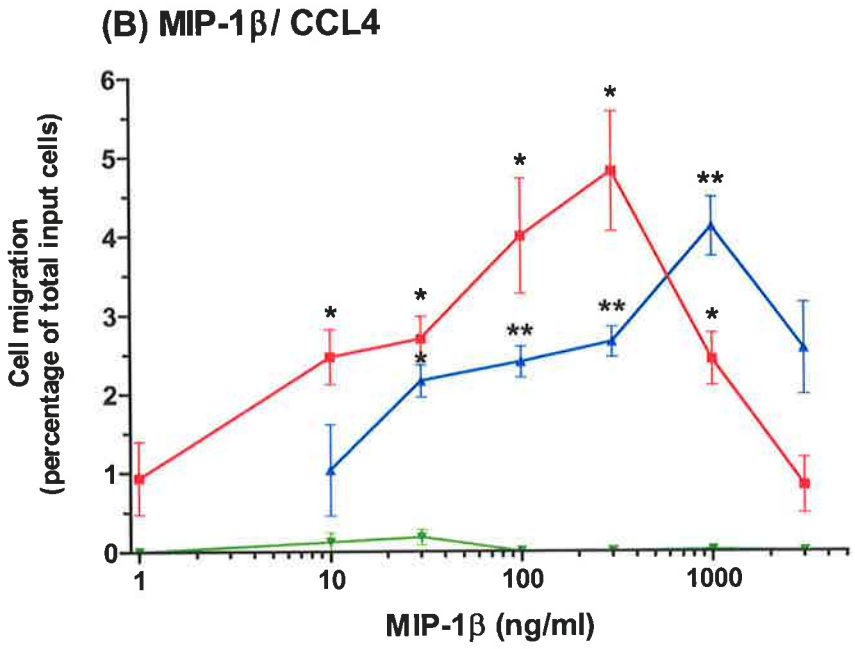
(B) MIP-1β/ CCL4
Cell migration
(percentage of total input cells)
0
1
2
3
4
5
6
1
10
100
1000
MIP-1β (ng/ml)

Chapter 4

Detailed characterisation of CXCR4, CXCR3 and CCR5 expression on encephalitogenic $CD4^+$ T cells accumulating in the CNS during EAE

4.1 Introduction

The aim of the experiments presented in Chapter 3 was to monitor the expression patterns of chemokine receptors on $CD4^+$ T cells following initial activation in the periphery. The results from those experiments demonstrated that there were significant alterations in the expression of CXCR4, CXCR3 and CCR5 following T cell activation. However, from the results obtained *in vivo*, it was difficult to identify neuroantigen-specific $CD4^+$ T cells since the *Mycobacterium tuberculosis* in the CFA also elicited a $CD4^+$ T cell-mediated immune response. Therefore, *in vitro* restimulation studies were performed in order to ascertain alterations in the receptor profiles on the $CD4^+$ T cells. In context of an immune response, it is also important to analyse receptor expression on a population of activated/proliferating neuroantigen-specific $CD4^+$ T cells at the site of antigen expression. Accordingly, all further experimentation will be focused on monitoring chemokine receptor expression in the CNS, in particular on $CD4^+$ T cells present in the CNS following EAE induction.

The aim of the experiments presented in this chapter is to test the hypothesis that '**the chemokine receptors CXCR4, CXCR3 and CCR5 are upregulated on neuroantigen-specific $CD4^+$ T cells in the CNS.**'

4.2 Results

4.2.1 Chemokine Receptor expression in the CNS during EAE

To determine whether there was a relationship between chemokine receptor expression in the CNS and development of EAE, organ specific mRNA expression was examined by comparative RT-PCR. Thus, following induction of EAE with PLP in CFA or control immunisation (PBS in CFA), groups of mice were sacrificed at time points corresponding to pre-clinical disease (Day 9 post-immunisation), acute disease (Day 12 post-immunisation) and remission (Day 21 post-immunisation), perfused as described in Section 2.3.5, and the spinal cords were removed and processed for analysis of CXCR4, CXCR3, CCR1, CCR2, CCR3, CCR4, CCR5 and CCR8 mRNA expression. Spinal cords from normal (Day 0) mice were also removed and analysed for basal expression of chemokine receptors. As stated in Chapter 3, comparative RT-PCR was chosen for the initial screen because antibodies were not available for all of the above receptors. The primers selected for CXCR4, CXCR3, CCR1, CCR2 and CCR5 mRNA amplification were the same as those used in Chapter 3. With regard to CCR3, CCR4 and CCR8, preliminary studies were conducted for each set of primers at a range of cycle numbers, to ensure that the PCR reaction was in the linear range (data not shown). Because there are no introns in most chemokine receptor genes, samples without RT were performed to control for genomic contamination. These controls were always negative (data not shown). As demonstrated in Figure 4.1 (A-H), expression of the receptors CXCR4, CXCR3, CCR1, CCR2 and CCR5 increased with disease severity, whilst there was little or no detectable expression the receptors CCR3, CCR4 and CCR8.

With regard to the CXC receptors, analysis of the spinal cords collected from normal SJL/J mice (Day 0) revealed a low level of basal expression of CXCR4 and CXCR3 (Fig 4.1 (A and B)). Immediately prior to the onset of clinical disease in the PLP-immunised cohort, there was an increase in expression of CXCR4; however, the observed upregulation was not significantly higher than basal levels until mice were exhibiting signs of severe paralysis (Day 12) ($p < 0.01$). At day 12 post-immunisation, levels of CXCR4 mRNA were 7.5-fold higher than the control-immunised mice at the same time point (Fig 4.1 (A)). As the animals entered remission, CXCR4 expression in the CNS remained elevated, although the fold-increase over expression in control animals had decreased to 3.5-fold ($p < 0.05$). In contrast, expression of CXCR3 in the CNS did not increase until day 12 post-immunisation, where expression was 6-fold above that in the control cohort (Fig 4.1 (B); $p < 0.001$). Furthermore, expression of CXCR3 persisted at high levels until day 21 post-immunisation with levels remaining 6-fold above the control-immunised animals ($p < 0.001$).

Both CCR1 and CCR2 mRNA expression was dependent upon EAE induction. There was minimal expression of these two receptors in normal CNS tissue, however, by day 9 post-immunisation, there was a strong upregulation, with peak expression of both CCR1 and CCR2 correlating with the peak of clinical disease (Fig 4.1 (C and D); $p < 0.01$ for both). Levels of CCR1 and CCR2 expression continued to be significantly elevated above those in the control mice as the animals entered remission (Fig 4.1 (C and D)). With regard to CCR3 and CCR4, EAE induction had no effect on the levels of expression in the CNS (Fig 4.1 (E and F)). There was no basal expression of CCR3 or CCR4 mRNA in the spinal cords of normal mice. As illustrated in Fig 4.1 (F), there may have been a minor

upregulation of CCR4 at day 12 post-immunisation, however, this increase was not statistically significant.

Conversely, the kinetics of CCR5 expression was similar to those of the other inflammatory Th1 receptors (Fig 4.1 (G)). There was no evidence of expression in the normal spinal cord; however, as the animals began to display signs of clinical disease, expression of CCR5 was strongly upregulated. Levels started to increase prior to the onset of clinical disease (day 9), as did the levels in the control-immunised mice. By the peak of clinical disease, however, CCR5 expression in the spinal cord of the PLP-inmmunised mice was 7-fold above that in the control cohort ($p < 0.001$). Like CXCR4 and CCR1, CCR5 expression levels decreased as the mice entered remission, although they remained significantly elevated above the control mice at the same time-point ($p < 0.01$).

With regard to CCR8 expression in the CNS, there was a slight upregulation that was dependent upon EAE induction (Fig 4.1 (H)). Expression of CCR8 started to increase at peak clinical disease and remained slightly elevated as the mice entered remission. It is important to note that expression of mRNA for this receptor was not upregulated to the same degree as the inflammatory Th1-associated receptors.

In contrast to receptor expression levels observed in the LNs following disease induction (Fig 3.3), there were no alterations evident in the spinal cords of control-immunised (PBS/CFA) animals (Fig 4.1 (A-H)).

The results illustrated above, along with those obtained in Chapter 3, provide the rationale to pursue examination of CXCR4, CXCR3 and CCR5 expression on $CD4^+$ T cells

infiltrating the CNS during EAE. Expression of CCR1 and CCR2 was examined in the PCR screen in order to verify that the model of EAE implemented in the present study was neurologically in concordance with those used in previous research, which have demonstrated upregulation of these two receptors in the CNS during EAE (210, 211). CCR1 and CCR2 will not be studied in further detail since they have already been the focus of extensive studies involving EAE (101, 146, 147). Since mRNA expression of the Th2-associated receptors was negligible following EAE induction, no further examination into their expression on $CD4^+$ T cells will be conducted in the present study.

4.2.2 Characteristics of cellular infiltration into the CNS following induction of EAE with $PLP_{139-151}$.

4.2.2.1 Time course of viable cell yield

One of the hallmarks of the immunopathogenesis of EAE is the migration of both antigen-specific and non-specific T cells as well as monocytes/macrophages to the CNS (212, 213). In order to assess the time-frame over which the cellular infiltration into the spinal cord developed, the number of viable cells recovered per spinal cord was determined on days 0, 6, 9, 12 and 22, post-induction of EAE (Fig 4.2 (A)). In normal mice (Day 0), there was a low level of cells in the spinal cord. Following immunisation, there was no significant change in the number of cells recovered from spinal cords collected at Day 6 post-immunisation, in comparison to the number recovered at the same time-point following control immunisation (PBS in CFA). However, by Day 9, the mean number of cells recovered from EAE spinal cords increased such that there were more cells than that

recovered following control immunisation. However, this increase was not statistically significant. At Day 12 post-immunisation, the number of viable cells recovered peaked at ~28 x 10^4, such that peak infiltration correlated with peak clinical disease. The value obtained was 5.6-fold above the control value for the same time-point ($p < 0.01$). By 22 days post-immunisation, the number of viable cells recovered from the spinal cord started to decline, but remained significantly elevated above control values ($p < 0.05$). The $CD4^+$ T cell population in the spinal cord was examined by flow cytometry (Figure 4.2 (B)). In general, the kinetics of $CD4^+$ T cell infiltration was similar to that of cellular infiltration described above. The number of $CD4^+$ T cells infiltrating the spinal cords of the control-immunised mice remained minimal at ~1 x 10^3 cells per cord, with no discernable fluctuation throughout the course of disease. In contrast, the number of $CD4^+$ T cells infiltrating the spinal cords of those mice with EAE increased over time, such that by 9 days post-immunisation, the number of $CD4^+$ T cells was significantly greater than the number recovered from the control-immunised mice ($p < 0.05$). The maximum number of $CD4^+$ T cells recovered was at day 12 post-immunisation where there were 50-fold more than the control value for the same time-point ($p < 0.01$). The total number of $CD4^+$ T cells in the spinal cords had decreased by the time the mice had entered remission, but remained significantly elevated ($p < 0.01$).

4.2.2.2 Composition of cells recovered from the spinal cords following EAE induction

The time-course analysis of the cell yield discussed above revealed that there was a significant increase in the number of viable cells recovered from the spinal cords following EAE induction, and that peak infiltration correlated with peak clinical disease. Furthermore, it was demonstrated that there was a significant increase in the number of

$CD4^+$ T cells infiltrating the spinal cord. However, as seen in Figure 4.3, it is apparent that the $CD4^+$ T cells were not the only cells responsible for the increase in total cell number. Accordingly, at 12 days post-immunisation, following spinal cord removal and Percoll separation (section 2.3.2), the recovered cells were labelled with antibodies to CD4, CD8 or F4/80, and subsequently analysed by flow cytometry.

Figure 4.3 demonstrates that, at peak clinical disease, there was a significantly greater percentage of $CD4^+$ T cells recovered from the spinal cords of PLP-immunised mice than from control-immunised mice ($p < 0.001$). Approximately 27% of the recovered cells were $CD4^+$, which was ~10 fold greater than that recovered from the control-immunised mice. In addition, a small, but measurable, $CD8^+$ T cell population was identified in the spinal cords of PLP-immunised mice. Approximately 4% of the cells recovered from those spinal cords stained positive for CD8, which was a ~3-fold increase over the percentage of $CD8^+$ T cells recovered from control-immunised mice ($p < 0.05$). There were also a significantly greater proportion of cells staining positive for F4/80, a marker for monocytes/macrophages and also microglia, in the spinal cord recovered from mice displaying clinical signs of EAE ($p < 0.05$). With regard to the cells recovered from control-immunised spinal cords, the percentage of cells staining positive for F4/80 was greater than the percentage of cells staining positive for CD4 and CD8 (PBS/CFA; Fig 4.3). This may be representative of the population of resident microglia. The percentages total less than 100%, thus suggesting that the Percoll separation recovers cells other than mononuclear cells. Although not specifically examined, it was observed during staining of cytospins of the recovered cells that there were a significant proportion of polymorphonuclear cells present (data not shown). Since there is no specific marker for neutrophils, flow cytometric analysis did not identify this population. Furthermore, it is

possible that some astrocytes were isolated during the centrifugation process. Flow cytometric staining for glial fibrillary acidic protein (GFAP) would confirm this hypothesis.

4.2.3 Analysis of chemokine receptor expression on CD4$^+$ T cells in the CNS following EAE induction

4.2.3.1 Detection of CD4$^+$ T cells expressing CXCR4, CXCR3 and CCR5 in the spinal cords of mice displaying clinical signs of EAE

In order to determine if the infiltrating CD4$^+$ T cells were in any part responsible for the observed alterations in chemokine receptor expression in the CNS following EAE induction, samples of spinal cord tissue were collected from mice displaying clinical signs of disease. Cryostat sections of the tissue samples were labelled with antibodies to CD4 and the chemokine receptors CXCR4, CXCR3 or CCR5, and subsequently examined by fluorescence microscopy. In Figure 4.4, both single and 2-colour analysis is presented. In each section, the upper panel represents the staining obtained with anti-CD4 (green), while the staining obtained with anti-chemokine receptor antibodies is represented in the middle panel (red). In the lower panel of each section, a 2-colour analysis is presented, in which the staining patterns obtained from the upper and middle panels, are overlayed. Where the two colours overlap, a yellow colour is obtained.

Presented in (A) are photomicrographs of 4 samples of spinal cord tissue, stained with the two negative control antibodies. The upper panel represents the staining obtained with the

control monoclonal antibody for anti-CD4 (green), where as the lower panel represents the staining obtained with the control goat IgG, a negative control for the anti-chemokine receptor antibodies (red). In general there was very little background staining with either control antibody, although in a couple of photomicrographs, a small number of fluorescent cells were evident, which must be taken into account when analysing the samples stained with specific antibodies (presented in Fig 4.4 (B-D)). Also, in most samples, regions of tissue appeared moderately bright in the red channel, this is probably a result of high levels of autofluorescence emitted by the lipid filled tissue when viewed through this filter. Also, in both channels, the outer edges of the tissue have stained relatively brightly, most likely due to the non-specific trapping of antibody along the tissue edges.

When lumbar spinal cord samples were stained with anti-CD4 and anti-CXCR4 (Fig 4.4 (B)), $CD4^+$ T cells could be detected both in discreet clusters in the perivascular space and also scattered throughout the meninges and parenchyma. However, the pattern of staining for CXCR4 (red), was more wide-spread. When analysing the overlayed images, some of the $CXCR4^+$ cells also stained with the anti-CD4 antibody (yellow), suggesting the presence of $CXCR4^+$ $CD4^+$ T cells. Nevertheless, the majority of CXCR4-stained cells remained red following the image overlay procedure, thus suggesting the presence of cells in the CNS capable of expressing CXCR4. These cells would most likely be astrocytes and endothelial cells, and will be discussed in more detail in Chapter 7.

With regard to CXCR3 staining, both CD4- and CXCR3-expressing cells could be detected in the diseased spinal cords (Fig 4.4 (C)). The pattern of CD4-staining was similar to that observed in (B). In contrast to that observed for CXCR4 expressing cells, there appeared to be fewer $CXCR3^+$ cells in the spinal cord of mice with EAE. When

analysing the overlayed images, it became evident that a number of the $CXCR3^+$ cells co-stained with the anti-CD4 antibody (yellow), suggesting the presence of $CXCR3^+$ $CD4^+$ T cells in EAE spinal cord at the peak of clinical disease. However, similarly to that observed with CXCR4, there was a significant proportion of $CXCR3^+$ cells that were not $CD4^+$. Likewise, there was a significant proportion of $CD4^+$ cells that were not $CXCR3^+$.

When analysing the spinal cord sections for the presence of CCR5 expressing $CD4^+$ T cells, it was noted that the CD4 staining co-localised with the CCR5 staining (Fig 4.4 (D)), albeit to a lesser extent than that observed for both CXCR4 and CXCR3. In both the middle left and right panels, fewer $CCR5^+$ cells were detected compared with CXCR4 and CXCR3. Furthermore, it is interesting to note that there were numerous cells staining positive for CD4 that did not stain positive for CCR5. This was also observed in the cases of CXCR4 and CXCR3, however, it was considerably more evident with CCR5.

4.2.3.2 Time-course of chemokine receptor expression on $CD4^+$ T cells in the spinal cord

Using RT-PCR it was shown that CXCR4, CXCR3 and CCR5 were expressed in the CNS following EAE induction, and immunofluorescence further illustrated that a percentage of infiltrating $CD4^+$ T cells were expressing these chemokine receptors in the diseased spinal cord. Therefore, the following experiments were conducted in order to analyse the expression of CXCR4, CXCR3 and CCR5 on $CD4^+$ T cells infiltrating the spinal cord during the course of EAE. Accordingly, chemokine receptor expression was assessed on Days 6, 9, 12 and 22 post-immunisation using flow cytometry. Analysis was not performed on $CD4^+$ T cells in the spinal cords of normal mice (Day 0), because it was difficult to isolate sufficient cells at this time-point. As seen in Figure 4.5, the expression

of CXCR4 on $CD4^+$ T cells did not vary significantly between any time-point. At all time-points tested, ~50% of the $CD4^+$ T cells expressed CXCR4. As seen in the density plot analysis of representative day 12 data (Fig 4.5 (B-C)), there was an equal proportion of $CD4^+$ T cells that did not stain positively for CXCR4.

The pattern of CXCR3 expression on $CD4^+$ T cells observed following EAE induction illustrates that on day 6 post-immunisation, only 8% of $CD4^+$ T cells expressed CXCR3 (Fig 4.6 (A)). By day 9, the percentage positive for this receptor increased to ~28%, which was significantly higher than data observed at day 6 ($p < 0.05$). At day 12 post-immunisation, however, the extent of CXCR3 upregulation was considerably more pronounced compared with that observed on day 6, with ~50% of the $CD4^+$ T cells expressing CXCR3. On those $CD4^+$ T cells infiltrating the CNS, CXCR3 expression remained near maximum levels until day 21 post-immunisation. Thus, EAE induction resulted in a statistically significant increase in the proportion of $CD4^+$ T cells in the CNS expressing CXCR3 ($p < 0.05$). CXCR3 expression on $CD4^+$ T cells in the spinal cord is further illustrated in Figure 4.6 (B-C), in which typical flow cytometric profiles are compared for isotype-matched control staining and CXCR3 staining at day 12 post-immunisation. These plots also demonstrate the expression of CXCR3 on the $CD4^-$ population (which is likely to consist of $CD8^+$ T cells). However, this issue was not specifically investigated, as the primary intention of these studies was to study the $CD4^+$ T cell population.

The pattern of CCR5 expression on $CD4^+$ T cells observed following immunisation with $PLP_{139-151}$ was similar to that observed for CXCR3. The percentage of $CD4^+$ T cells expressing CCR5 on day 6 post-immunisation was ~6%, and this significantly increased

by day 9 (Fig 4.7; $p< 0.01$). Again, at the height of clinical disease, the percentage of $CD4^+$ $CCR5^+$ T cells in the CNS peaked at ~55%, and this was significantly greater than those values for either day 6 or 9 post-immunisation ($p< 0.01$). As the mice entered remission, there was a significant decrease in the percentage of $CD4^+$ T cells expressing CCR5, such that the proportion expressing this receptor was ~25%, equivalent to that at day 9 post-immunisation ($p< 0.01$). It is interesting to note that, at all time-points, the percentage of $CD4^+$ T cells expressing CCR5 was quite similar to the percentage expressing CXCR3 (~6% at day 6, ~28% at day 9, ~50-55% at day 12). In contrast, the density plots illustrated in Figure 4.7 (B-C) demonstrate that the expression of CCR5 on non-$CD4^+$ lymphocytes was far less extensive than the expression of CXCR3. A final piece of interesting information obtained from these density plots is the observation that, as observed in restimulation cultures *in vitro*, the upregulation of CCR5 expression appeared to be associated with sub-population of T cells expressing elevated levels of CD4. This phenomenon was not observed on the density plots for CXCR4 or CXCR3.

In the context of a dynamic system such as the CNS, percentage values can sometimes be misleading, as changes in an unrelated population can profoundly affect the relative proportions of the population under investigation. To address this concern, in Figure 4.8, the percentage of $CD4^+$ T cells expressing each chemokine receptor has been combined with total cell count values, such that the absolute number of $CD4^+$ T cells expressing each chemokine receptor can be estimated. With regard to CXCR4, at the time-points tested greater than day 9, there was a significant increase in the absolute number of $CXCR4^+$ $CD4^+$ T cells present in spinal cords compared with day 6 post-immunisation ($p < 0.05$ and $p < 0.01$ for Days 12 and 21, respectively; Fig 4.8 (A)). This is in contrast to the results presented in Figure 4.6, which demonstrated that there was no change to the

relative proportion of $CXCR4^+$ $CD4^+$ T cells present in the CNS in response to EAE induction. Thus, consistent with the fact that a large proportion of $CD4^+$ T cells express CXCR4, the increase in CNS cellularity that occurred upon $PLP_{139-151}$-immunisation resulted in an increase in the number of CXCR4-expressing $CD4^+$ T cells, but the relative proportion of $CXCR4^+$ $CD4^+$ T cells present was not altered throughout the course of disease.

The number of $CXCR3^+$ $CD4^+$ T cells present in CNS that had been immunised with PLP in CFA increased significantly throughout the course of clinical disease (Fig 4.8 (B)). On day 6 post-immunisation, the number of $CXCR3^+$ $CD4^+$ T cells were low. However, the number of these cells started to increase by day 9 post-immunisation. A marked increase was not observed until day 12 post-immunisation, where the number of $CD4^+$ T cells expressing CXCR3 was ~9-fold greater than 3 days previously. The number of $CXCR3^+$ $CD4^+$ T cells present in the CNS started to decline as the mice entered remission, however, remained significantly higher than the numbers present on day 6 post immunisation ($p < 0.05$). Similarly, the number of $CCR5^+$ $CD4^+$ T cells also increased significantly as EAE progressed ($p < 0.05$ for Days 9 and 12, and $p < 0.01$ for Day 21; Fig 4.8 (C)). These trends are in accordance with the observed increase in the relative proportions of CXCR3-expressing and CCR5-expressing $CD4^+$ T cells. However, the changes observed here take into account the large increase in CNS cellularity that occurred following immunisation. Essentially, the data presented in Figure 4.8 mimic that seen in Fig 4.2 (B), in that there was a large influx of $CD4^+$ T cells into the CNS following immunisation, and that the changes to the relative proportion of chemokine receptor expressing $CD4^+$ T cells had little effect on this infiltration.

4.2.4 Analysis of divided cells in CNS following EAE induction

4.2.4.1 The percentage of $CD4^+$ T cells undergoing division in the CNS following EAE induction

As was demonstrated in Figure 4.2, by day 12 post-immunisation, there was a 5.6-fold increase in the total cell number, and a 50-fold increase in the number of $CD4^+$ T cells infiltrating the EAE spinal cord compared with control-immunised spinal cords. In order to assess what proportion of this increase was due to neuroantigen-specific cells, and what proportion was due to the non-specific influx of lymphocytes in response to inflammatory stimuli, the $CD4^+$ T cells that had divided (neuroantigen-specific) were detected by means of BrdU incorporation.

BrdU was administered continuously in the drinking water of immunised mice starting at day 6 post-immunisation (Section 2.2.6). At the time-point corresponding to peak clinical disease, Day 12 post-immunisation, mice were sacrificed, perfused with PBS and the leukocytes were harvested following Percoll centrifugation (Section 2.3.2). Subsequently the cells were labelled with anti-BrdU (Section 2.6.3.2) as well as anti-CD4 and analysed by flow cytometry.

In cells recovered from the spinal cords of non-immunised mice, no detectable incorporation of BrdU was observed (data not shown). However, immunisation with PLP in CFA, and control-immunisation (PBS in CFA), resulted in a detectable population of divided cells in the spinal cords 12 days post-immunisation (Fig 4.9 (A)). There was a

significantly greater percentage of divided cells in the EAE spinal cords compared to the control-immunised cords, with ~11% of the total cells present having undergone division ($p < 0.001$). Representative density plots are shown in Fig 4.9 (B) illustrating the presence of a readily detectable population of $CD4^+$ T cells that had incorporated BrdU at Day 12 in PLP-immunised mice, and to a lesser extent in control-immunised spinal cords. Analysis of these plots demonstrated that, in contrast to observations in the draining LNs (Figs 3.4 and 3.5), ~50% of the $CD4^+$ T cells present in the CNS had divided following induction of EAE using PLP in CFA (Fig 4.9 (C)). This was 10-fold above the percentage of $CD4^+$ T cells that had divided in the CNS of control-immunised animals ($p< 0.001$).

4.2.4.2 Absolute numbers of divided and non-divided $CD4^+$ T cells in the spinal cord of diseased mice

The data presented in Figure 4.9 demonstrate that the relative proportions of divided $CD4^+$ T cells in the CNS was significantly increased following EAE induction. In Figure 4.10, the percentage BrdU data have been combined with total cell count data, similar to the analysis of chemokine receptor expressing $CD4^+$ T cell data presented in Figure 4.8. This has allowed the absolute numbers of divided and undivided $CD4^+$ T cells in the spinal cord to be calculated. This analysis demonstrates that the extent of the T cell proliferative response was greater in terms of absolute numbers than that suggested by the percentage values. Based on these calculations, at peak clinical disease, there were 18.7 times as many proliferating $CD4^+$ T cells in EAE spinal cords compared with controls ($p = 0.001$; Fig 4.10).

Thus, upon EAE induction, there was a large increase in proliferation of $CD4^+$ T cells and in the number of these cells in the CNS. When compared with the number of T cells

present in the CNS that were $BrdU^-$ (Fig 4.10), it is clear that some of the increase in spinal cord cellularity observed following immunisation was due to the influx of undivided cells. There was a 3-fold increase in the number of non-dividing $CD4^+$ T cells in the EAE spinal cords compared with control-immunised spinal cords ($p < 0.05$; Fig 4.10). Thus, Figure 4.10 illustrates that, in addition to the influx of divided/proliferating cells into the spinal cord following immunisation, there was also an influx of undivided lymphocytes. However, it also demonstrates that there were significantly more divided lymphocytes infiltrating the CNS than undivided lymphocytes following immunisation with $PLP_{139-151}$ in CFA ($p < 0.01$). Therefore, although a number of non-specific cells were recruited into the CNS following EAE induction, the majority of the increased cellularity observed in the EAE spinal cord was due to the recruitment of antigen-primed lymphocytes.

4.2.4.3 Co-ordination of chemokine receptor up-regulation with cell division in the CNS

Using the BrdU technique, it was demonstrated in Fig 4.10 that the large increase in cellularity observed within the spinal cord following immunisation was due mostly to the influx of antigen-primed lymphocytes. However, there was also a significant proportion of non-specific cells that had accumulated in the EAE spinal cord. Thus, in order to study the regulation of chemokine receptor expression on CNS-infiltrating neuroantigen-specific $CD4^+$ T cells, receptor expression was analysed on the $CD4^+$ T cells that were undergoing, or had undergone, division. Consequently, cells were isolated from the spinal cords of mice at the height of clinical disease (as previously described), labelled with antibodies to CD4, BrdU and CXCR4, CXCR3 or CCR5, and subsequently analysed by flow cytometry.

Similarly to expression patterns observed in the draining LNs and peripheral blood (Figs 3.6 and 3.7, respectively), the divided population of $CD4^+$ T cells in the spinal cord at peak clinical disease expressed significantly higher levels of CXCR4, CXCR3 and CCR5 compared with the population of cells that had not divided (Fig 4.11). The percentage of divided $CD4^+$ T cells expressing CXCR4 was ~29%, which was 3.2-fold above the percentage of undivided $CD4^+$ cells expressing this receptor ($p < 0.01$). Furthermore, within the population of $CD4^+$ T cells that had incorporated BrdU, both CXCR3 and CCR5 were expressed on a significantly greater percentage of cells compared with the population of $CD4^+$ T cells that did not incorporate BrdU ($p < 0.01$ for both). The data relating to these receptors demonstrated that the percentage of divided cells expressing CXCR3 and CCR5 were 4.0 and 4.6-fold greater, respectively, than the percentage of non-divided cells expressing these receptors.

4.3 Summary

In this series of experiments, chemokine receptor expression was monitored in the CNS by comparative RT-PCR and on $CD4^+$ T cells infiltrating the CNS over the course of EAE. Initial analyses revealed that there was a strong upregulation of mRNA for the inflammatory chemokine receptors CXCR3, CCR1, CCR2, and CCR5, as well as CXCR4. This apparent upregulation was associated with an influx of both antigen-specific and non-specific $CD4^+$ T cells as well as other cells into the CNS tissue, the positioning of which revealed that in addition to forming discrete clusters in the perivascular space, there was

further penetration into the surrounding parenchyma. The observed influx resulted in a large increase in the absolute numbers of $CXCR4^+$, $CXCR3^+$ and $CCR5^+$ $CD4^+$ T cells, as determined by immunofluorescence and flow cytometry. Additionally, immunofluorescent photomicrographs demonstrated that there was a significant population of $CD4^+$ T cells present in the CNS that did not co-express the chemokine receptor protein. This observation was supported by flow cytometric experiments. In these experiments, analysis of the relative proportions of $CD4^+$ T cell populations suggested that the accumulation of the $CD4^+$ T cells expressing CXCR3 or CCR5 in the CNS was more efficient than the accumulation of CXCR4-expressing cells. BrdU labelling experiments confirmed the presence of non-specific $CD4^+$ T cells in the CNS as well as antigen-activated $CD4^+$ T cells, as has previously been suggested (32, 118, 212, 213). Analysis of the $BrdU^+$ population revealed that, similarly to activated $CD4^+$ T cells in the draining LNs, divided antigen-specific $CD4^+$ T cells that had accumulated in the CNS displayed increased surface expression levels of CXCR4, CXCR3 and CCR5 compared with their non-specific counterparts. The results from this chapter reveal that antigen specificity is associated with the upregulation of CXCR4, CXCR3 and CCR5, thereby providing direct evidence for the upregulation of these receptors on neuroantigen-specific $CD4^+$ T cells infiltrating the CNS during EAE. Furthermore, when combined with the results from Chapter 3, the findings from the results presented in this chapter indicate that, following sensitisation, these inflammatory chemokine receptors are upregulated upon activation $CD4^+$ T cells and remain elevated, such that the cells can perform their effector function at the site of antigen expression.

Figure 4.1. *Comparative PCR analysis of chemokine receptor mRNA levels in the CNS.* EAE was induced in SJL/J mice as previously described (PLP/CFA) (Section 2.2.1). Control mice were subjected to CFA injection and pertussigen treatment, without PLP in the CFA emulsion (PBS/CFA). On days 0, 9, 12 and 21 post-immunisation, spinal cords were removed and total RNA was extracted, DNase-treated and reverse-transcribed (Sections 2.7.1, 2.7.2 and 2.7.3, respectively). Specific oligonucleotide primers were then used to amplify CXCR4, CXCR3, CCR1, CCR2, CCR3, CCR4, CCR5, CCR8 and GAPDH (Section 2.7.4). PCR-amplified products were analysed by 2.0% agarose gel electrophoresis followed by staining with Sybr Gold and the bands on the gel quantified (Section 2.7.5). The volume of the receptor bands was normalised according to GAPDH band volume for the same sample. *, Statistically significant different from day 0 or the PBS/CFA value at the same time point ($p<0.05$). **, Statistically significant different from day 0 or the PBS/CFA value at the same time point ($p<0.01$). ***, Statistically significant different from day 0 or the PBS/CFA-immunised value at the same time point ($p<0.001$). Data are presented as mean ± SEM ($n = 3$-6, from 2 independent experiments).

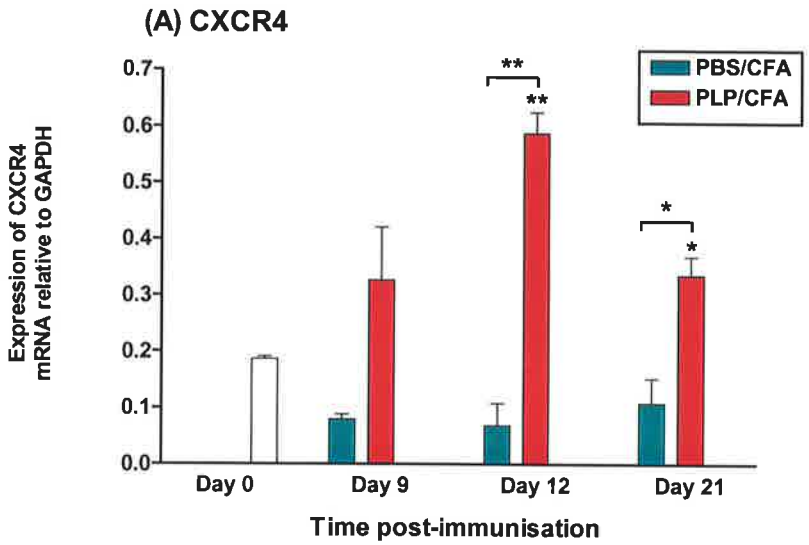
(A) CXCR4
Expression of CXCR4 mRNA relative to GAPDH
0.7
0.6
0.5
0.4
0.3
0.2
0.1
0.0
**
**
*
*
PBS/CFA
PLP/CFA
Day 0
Day 9
Day 12
Day 21
Time post-immunisation

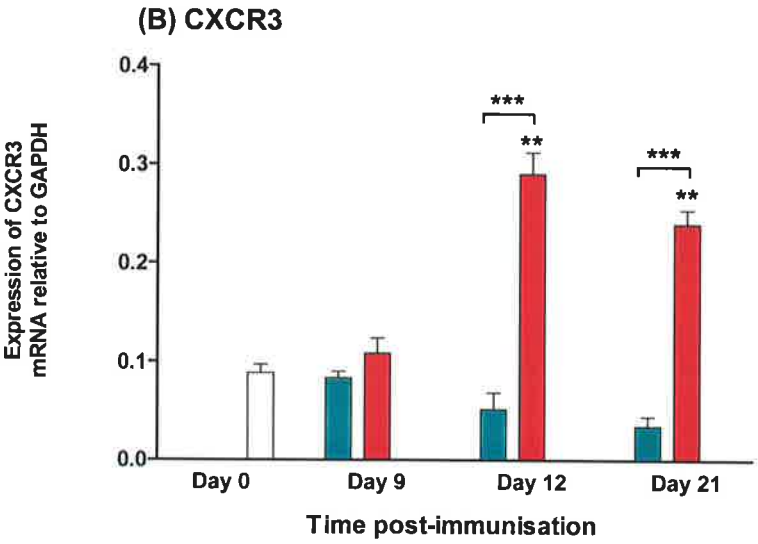
(B) CXCR3
Expression of CXCR3 mRNA relative to GAPDH
0.4
0.3
0.2
0.1
0.0
***
**
***
**
Day 0
Day 9
Day 12
Day 21
Time post-immunisation

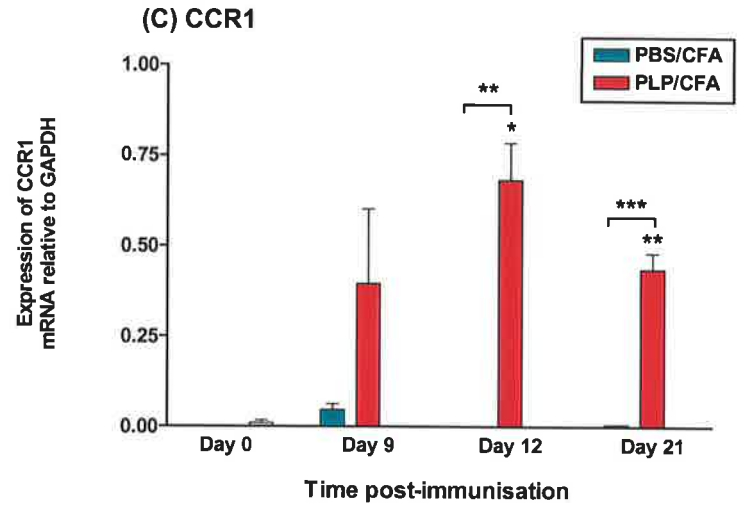
(C) CCR1
PBS/CFA
PLP/CFA
Expression of CCR1 mRNA relative to GAPDH
1.00
0.75
0.50
0.25
0.00
**
*
***
**
Day 0
Day 9
Day 12
Day 21
Time post-immunisation

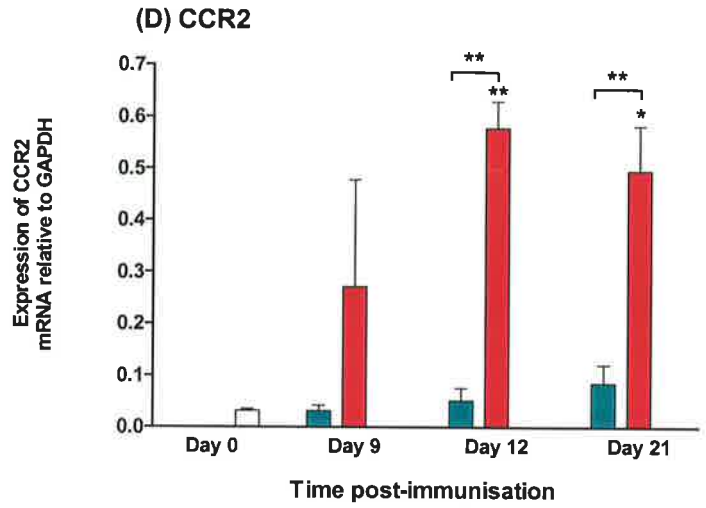
(D) CCR2
Expression of CCR2 mRNA relative to GAPDH
0.7
0.6
0.5
0.4
0.3
0.2
0.1
0.0
**
**
**
*
Day 0
Day 9
Day 12
Day 21
Time post-immunisation

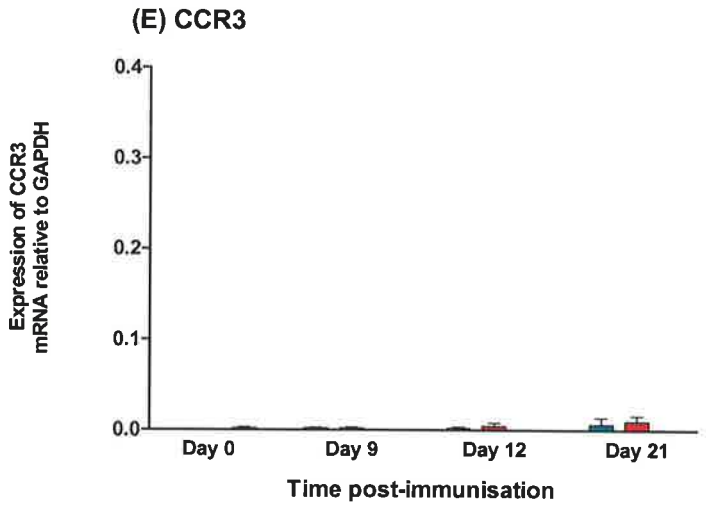
(E) CCR3
Expression of CCR3 mRNA relative to GAPDH
0.4
0.3
0.2
0.1
0.0
Day 0
Day 9
Day 12
Day 21
Time post-immunisation

(F) CCR4

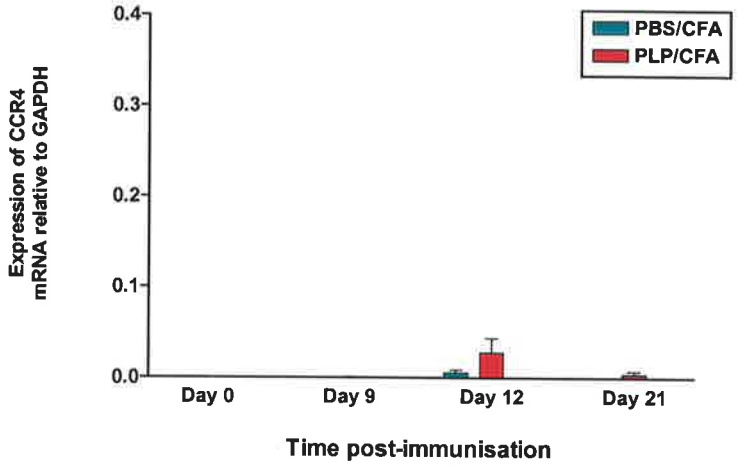

(G) CCR5

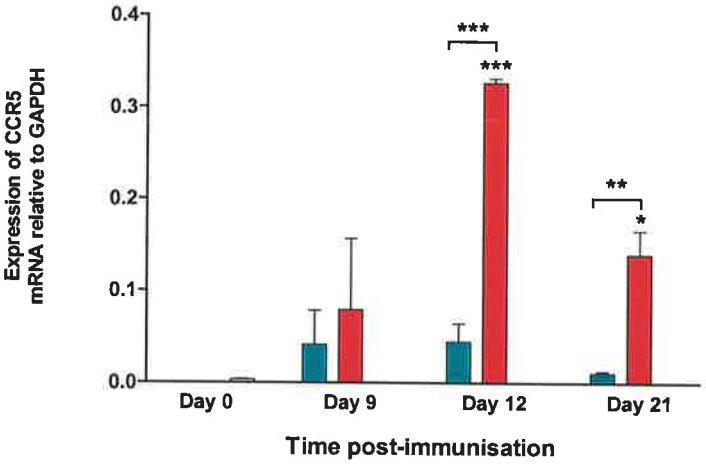

(H) CCR8

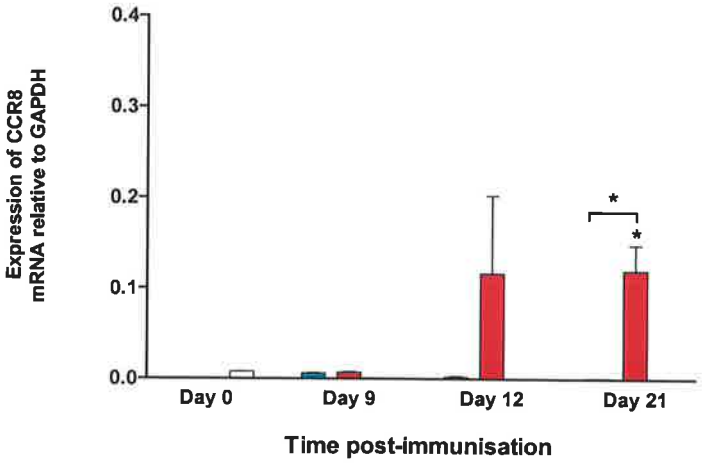

Figure 4.2. *Time-course of cell yields from spinal cords following EAE induction.* EAE was induced in SJL/J mice as previously described (PLP/CFA) (Section 2.2.1). Control mice were subjected to CFA injection and pertussigen treatment, without PLP in the CFA emulsion (PBS/CFA). On days 0, 6, 9, 12 and 22 post-immunisation, spinal cords were removed and single cell suspensions prepared. The total number of viable cells recovered from each spinal cord was then determined by counting on a haemocytometer after staining with trypan blue [A]. Cells were labelled with anti-CD4 and analysed by flow cytometry, gating on lymphocytes using forward and side scatter characteristics. The percentage of CD4-positive cells was multiplied by the total cell count value for the same time-point, such that the absolute number of $CD4^+$ cells could be determined [B]. *, Statistically significant different from the PBS/CFA value at the same time point ($p<0.05$). **, Statistically significant different from day 0 or the PBS/CFA value at the same time point ($p<0.01$). Data are presented as mean ± SEM ($n = 4$).

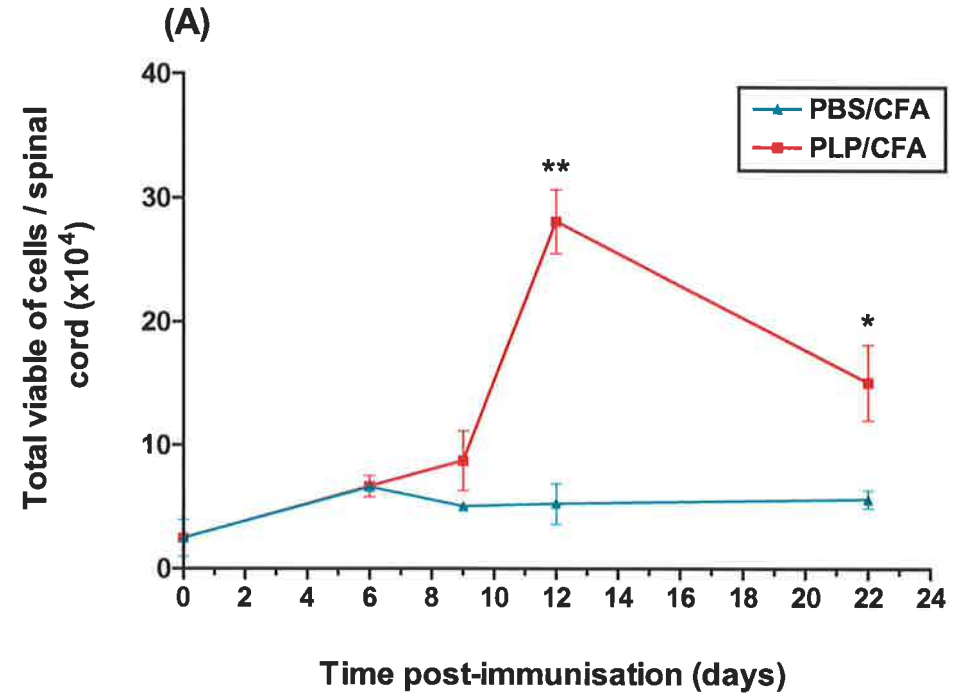
(A)
Total viable of cells / spinal cord (x10^4)
PBS/CFA
PLP/CFA
**
*
Time post-immunisation (days)

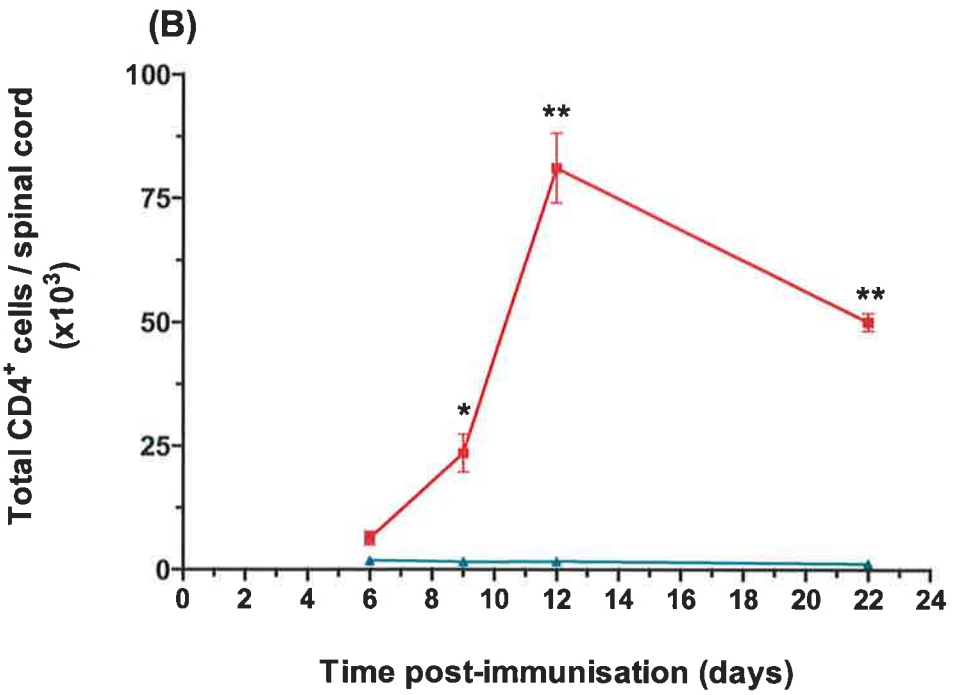
(B)
Total CD4+ cells / spinal cord (x10^3)
**
*
**
Time post-immunisation (days)

Figure 4.3. *The percentage of $CD4^+$, $CD8^+$ and $F4/80^+$ cells recovered from Day 12 control- and PLP-immunised spinal cords.* EAE was induced in SJL/J mice as previously described (PLP/CFA) (Section 2.2.1). Control mice were subjected to CFA injection and pertussigen treatment, without PLP in the CFA emulsion (PBS/CFA). Twelve days later (peak disease), spinal cords were removed, separated on a Percoll gradient (Section 2.3.2) and single cell suspensions were prepared. Cells were labelled with either anti-CD4, anti-CD8 or anti-F4/80 and analysed by flow cytometry. The percentage of cells positive for CD4, CD8 or F4/80 was determined in comparison to staining with an isotype-matched control antibody. A statistically significant difference between PBS/CFA- and PLP/CFA-immunised mice is indicated by an asterisk. *, Statistically significant from PLP/CFA-immunised values ($p < 0.05$). ***, Statistically significant from PLP/CFA-immunised values ($p < 0.001$). Data are presented as mean ± SEM (n = 3-4).

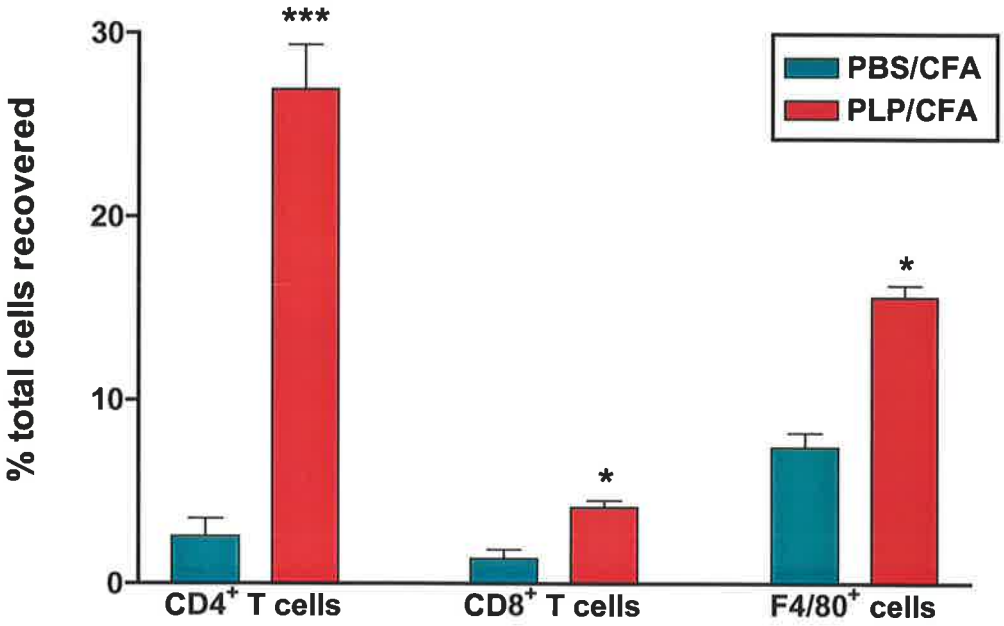
% total cells recovered
30
20
10
0
***
*
*
PBS/CFA
PLP/CFA
CD4+ T cells
CD8+ T cells
F4/80+ cells

Figure 4.4. *Expression of CXCR4, CXCR3 and CCR5 by $CD4^+$ T cells within EAE spinal cords.* EAE was induced in SJL/J mice as previously described (PLP/CFA) (Section 2.2.1). Twelve days later, the mice were sacrificed, perfused to remove circulating leukocytes (Section 2.6.1), the spinal cord was removed, frozen in OCT and 6 μm cryostat sections were prepared. The sections were fixed and then stained with one of the following combinations of antibodies: negative control monoclonal antibody and control goat IgG [A; upper and lower panel, respectively], anti-CD4 and anti-CXCR4 [B], anti-CD4 and anti-CXCR3 [C] or anti-CD4 and anti-CCR5 [D]. The sections were analysed by fluorescence microscopy, two images were collected from each sample using different filters (upper and middle panels), and the images overlayed (lower panels). Cells stained with anti-CD4 only appear green (upper panel), and cells stained with anti-chemokine receptor only appear red (middle panel). Where staining with the two antibodies coincides, cells appear yellow (lower panel). Shown are 3 representative images of each condition, captured using the 10X objective or the 20X objective, as displayed on image.

(A)

Control monoclonal rat IgG

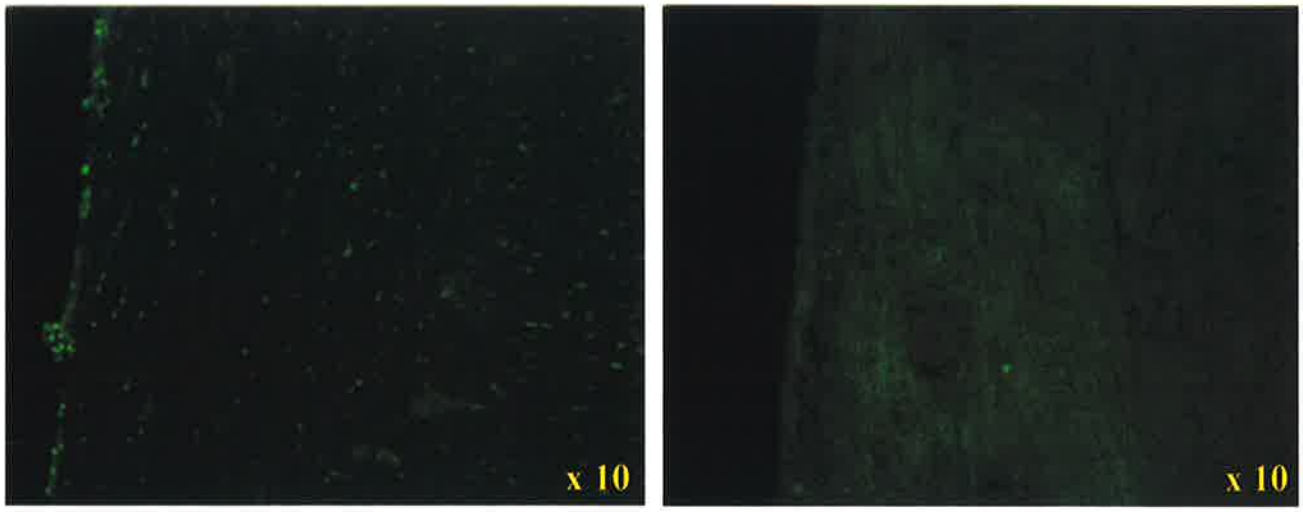

Control goat IgG

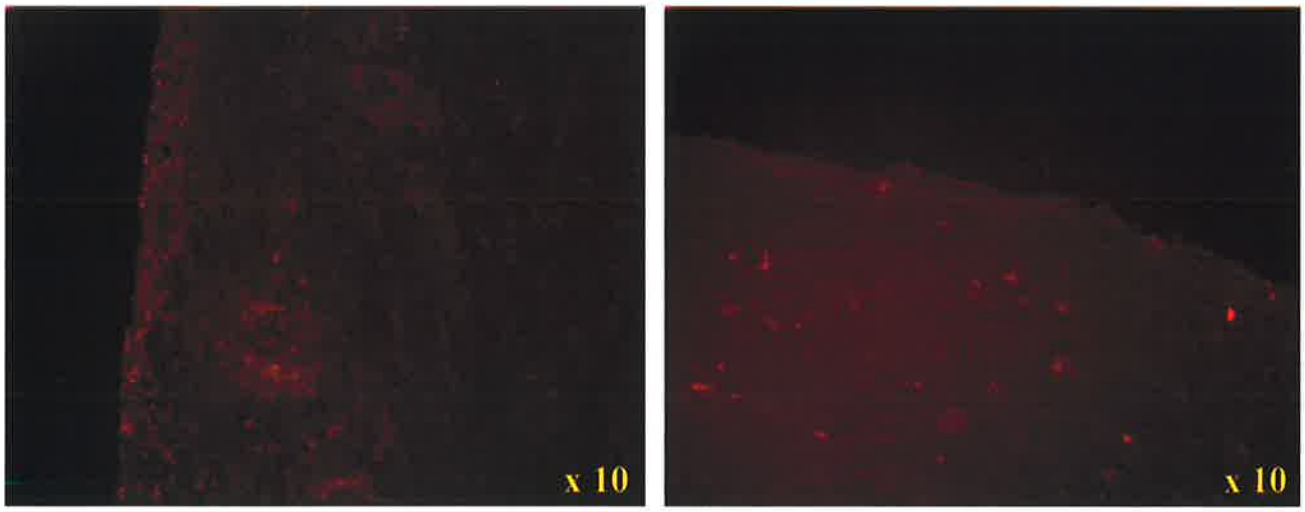

(B)

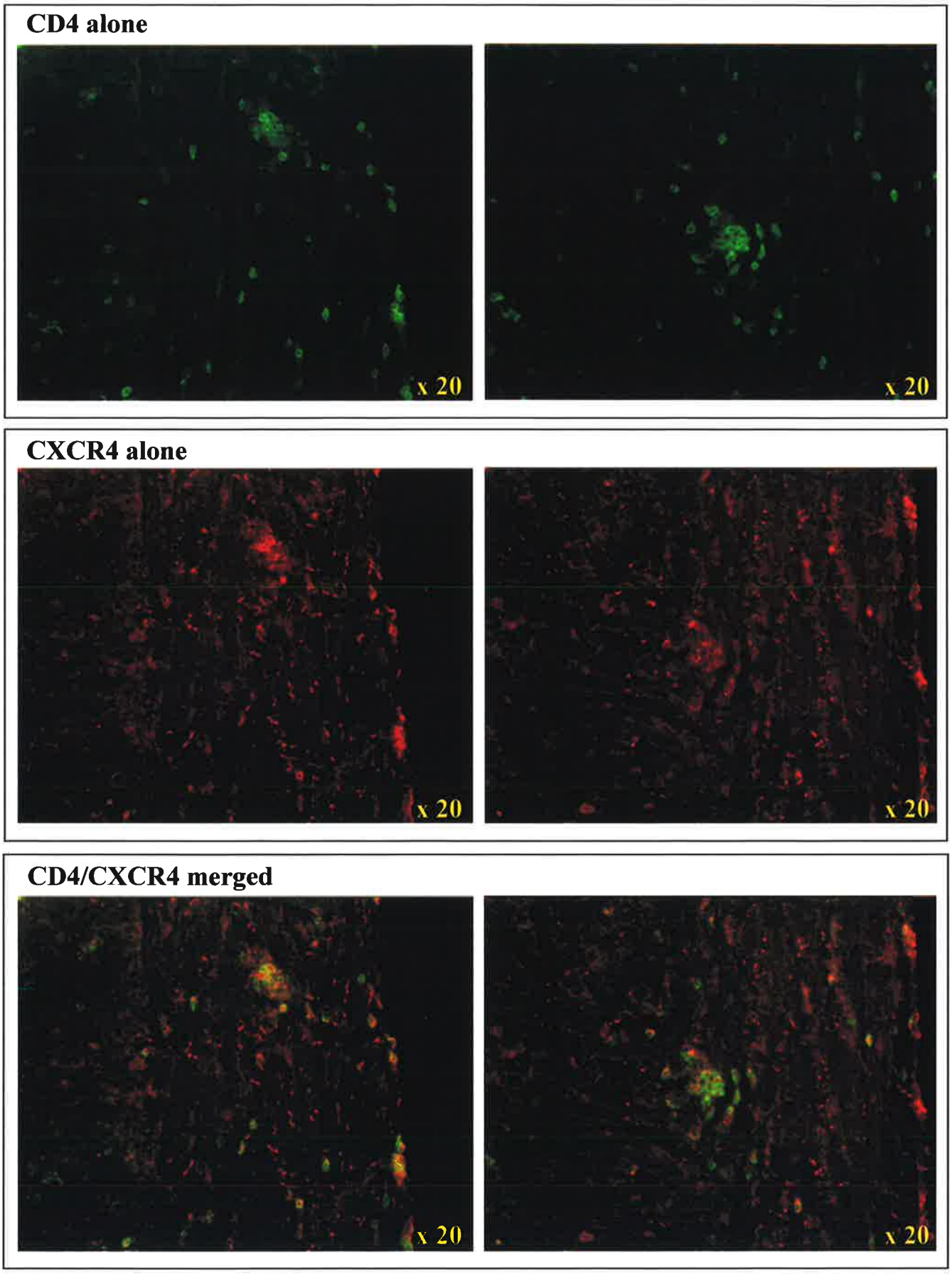
CD4 alone
x 20
x 20
CXCR4 alone
x 20
x 20
CD4/CXCR4 merged
x 20
x 20

(C)

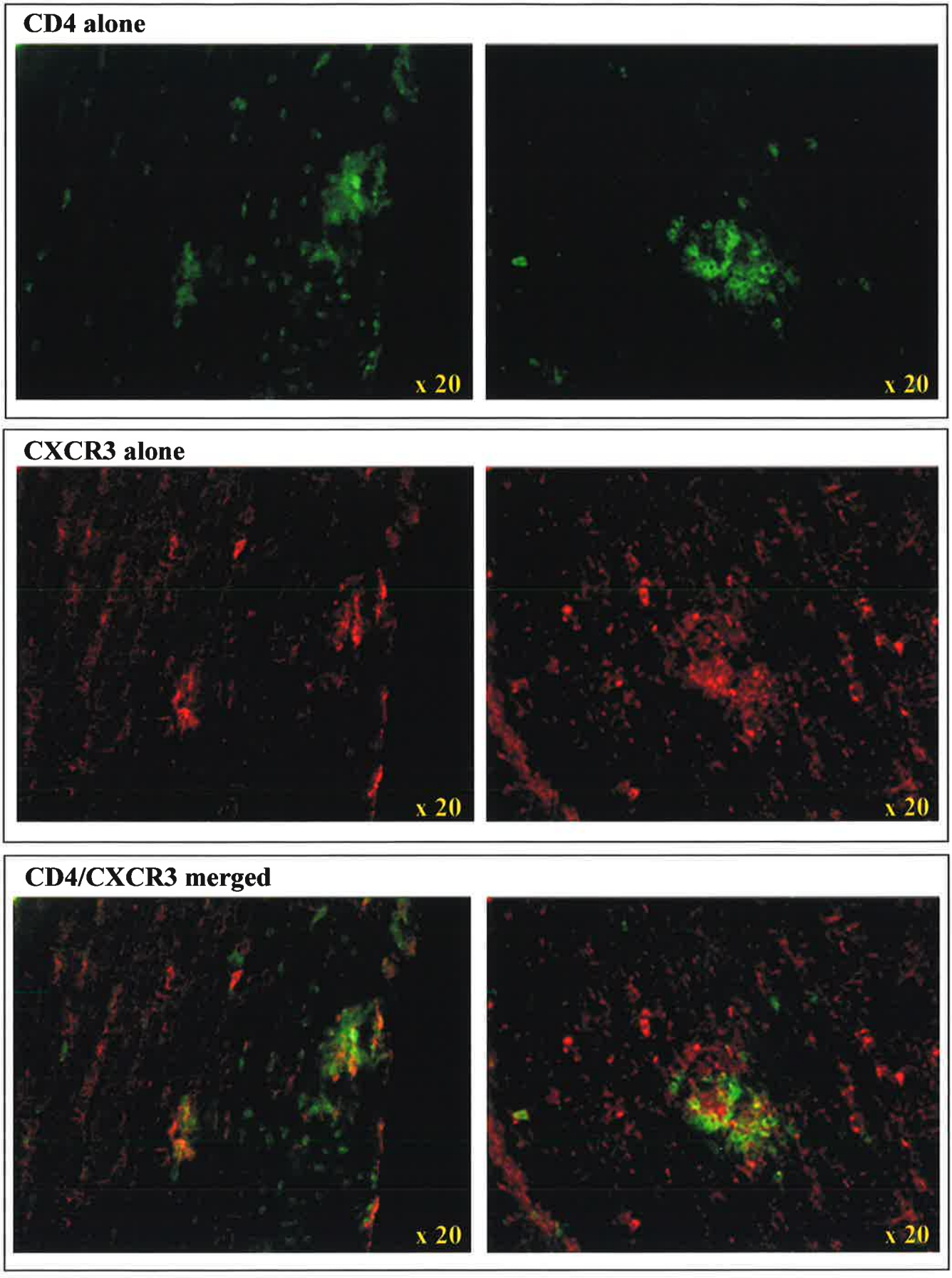
CD4 alone
x 20
x 20
CXCR3 alone
x 20
x 20
CD4/CXCR3 merged
x 20
x 20

(D)

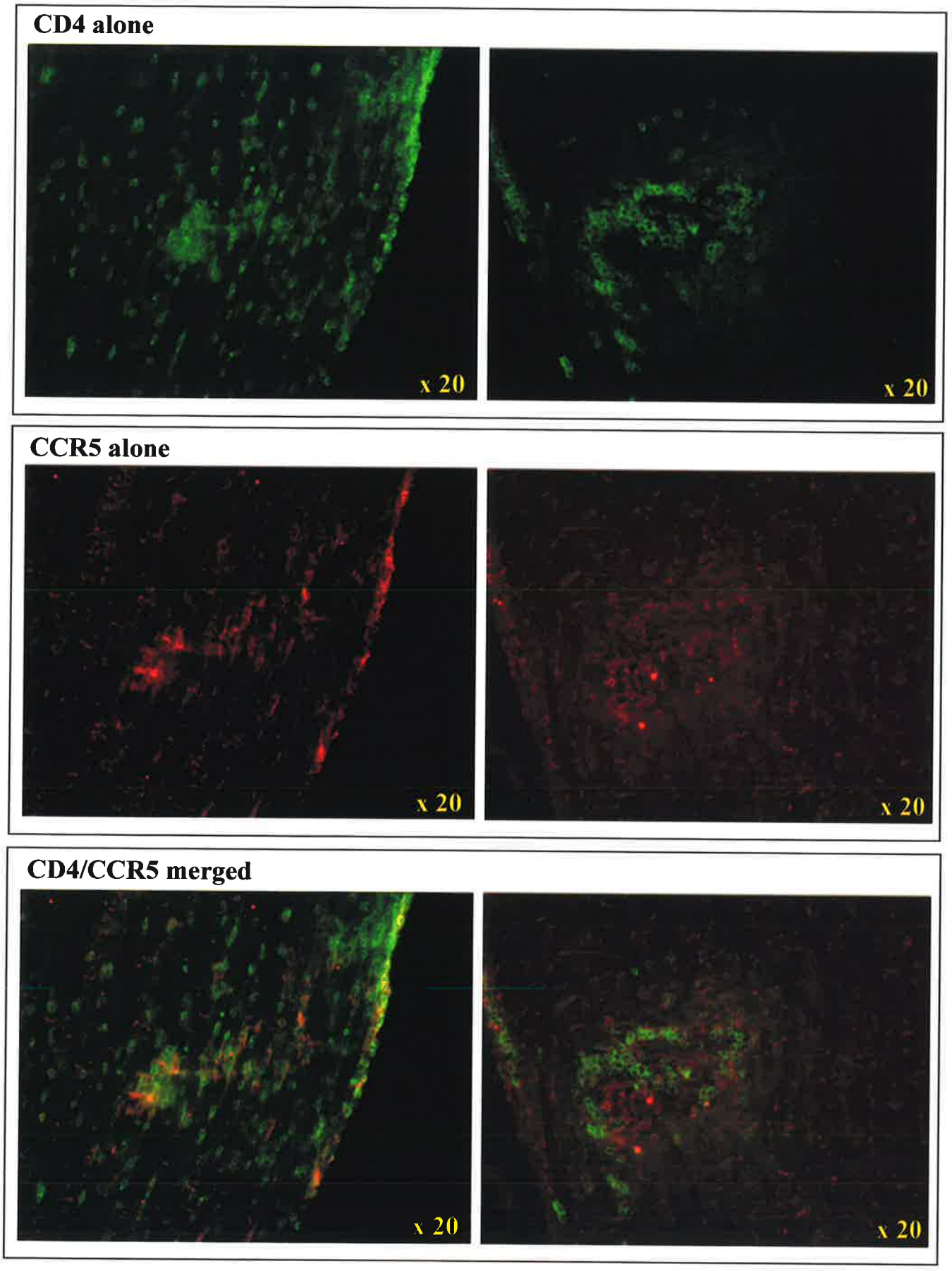

Figure 4.5. *Time-course of CXCR4 expression on $CD4^+$ T cells in EAE spinal cords.* EAE was induced in SJL/J mice as previously described (PLP/CFA) (Section 2.2.1). After the indicated period of time, spinal cords were removed, separated on a Percoll gradient (Section 2.3.2) and single cell suspensions were prepared. Cells were labelled with antibodies against CD4 and CXCR4 and analysed by flow cytometry, gating on lymphocytes using forward and side scatter characteristics. In [A], the percentage of cells positive for CXCR4 was determined in comparison to staining with control goat IgG. The percentage of $CD4^+$ T cells that expressed detectable levels of CXCR4 was then calculated as a proportion of total $CD4^+$ T cells. Data are presented as mean ± SEM (n = 6-9, from 3 independent experiments). Representative density plots of day 12 spinal cord cells stained with control goat IgG and anti-CD4 [B], and anti-CXCR4 and anti-CD4 [C] are also shown.

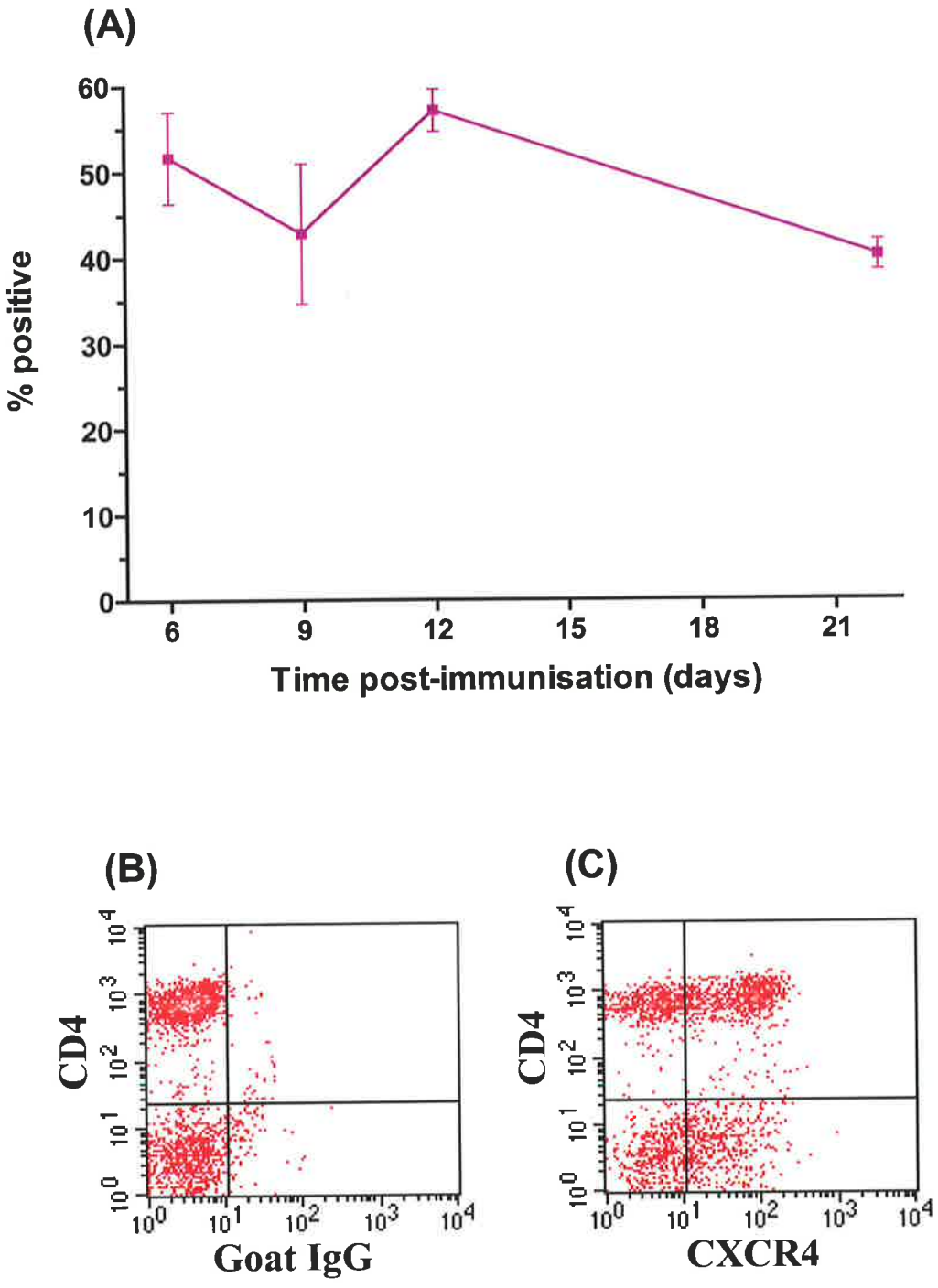
(A)
% positive
60
50
40
30
20
10
0
6
9
12
15
18
21
Time post-immunisation (days)
(B)
CD4
Goat IgG
(C)
CD4
CXCR4

Figure 4.6. *Time-course of CXCR3 expression on $CD4^+$ T cells in EAE spinal cords.* EAE was induced in SJL/J mice as previously described (PLP/CFA) (Section 2.2.1). After the indicated period of time, spinal cords were removed, separated on a Percoll gradient (Section 2.3.2) and single cell suspensions were prepared. Cells were labelled with antibodies against CD4 and CXCR3 and analysed by flow cytometry, gating on lymphocytes using forward and side scatter characteristics. In [A], the percentage of cells positive for CXCR3 was determined in comparison to staining with control goat IgG. The percentage of $CD4^+$ T cells that expressed detectable levels of CXCR3 was then calculated as a proportion of total $CD4^+$ T cells. Data are presented as mean ± SEM (n = 6-9, from 3 independent experiments). *, Statistically significant from day 6 values ($p < 0.05$). **, Statistically significant from day 6 values ($p < 0.01$). Representative density plots of day 12 spinal cord cells stained with control goat IgG and anti-CD4 [B], and anti-CXCR3 and anti-CD4 [C] are also shown.

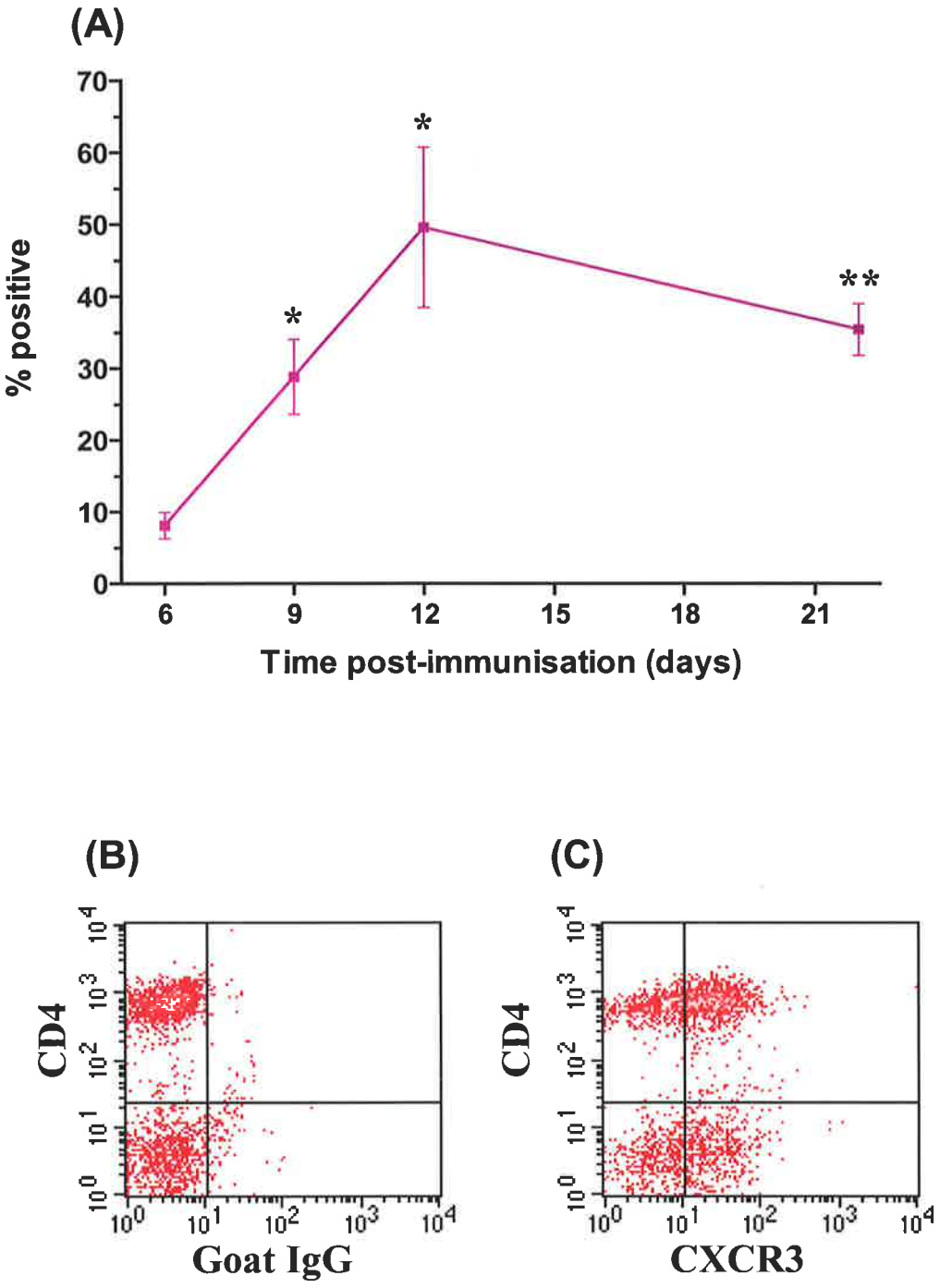
(A)
% positive
70
60
50
40
30
20
10
0
6
9
12
15
18
21
Time post-immunisation (days)
*
*
**
(B)
CD4
Goat IgG
(C)
CD4
CXCR3

Figure 4.7. *Time-course of CCR5 expression on $CD4^+$ T cells in EAE spinal cords.* EAE was induced in SJL/J mice as previously described (PLP/CFA) (Section 2.2.1). After the indicated period of time, spinal cords were removed, separated on a Percoll gradient (Section 2.3.2) and single cell suspensions were prepared. Cells were labelled with antibodies against CD4 and CCR5 and analysed by flow cytometry, gating on lymphocytes using forward and side scatter characteristics. In [A], the percentage of cells positive for CCR5 was determined in comparison to staining with control goat IgG. The percentage of $CD4^+$ T cells that expressed detectable levels of CCR5 was then calculated as a proportion of total $CD4^+$ T cells. Data are presented as mean ± SEM (n = 6-9, from 3 independent experiments). **, Statistically significant from day 6 values ($p < 0.01$). Representative density plots of day 12 spinal cord cells stained with control goat IgG and anti-CD4 [B], and anti-CCR5 and anti-CD4 [C] are also shown.

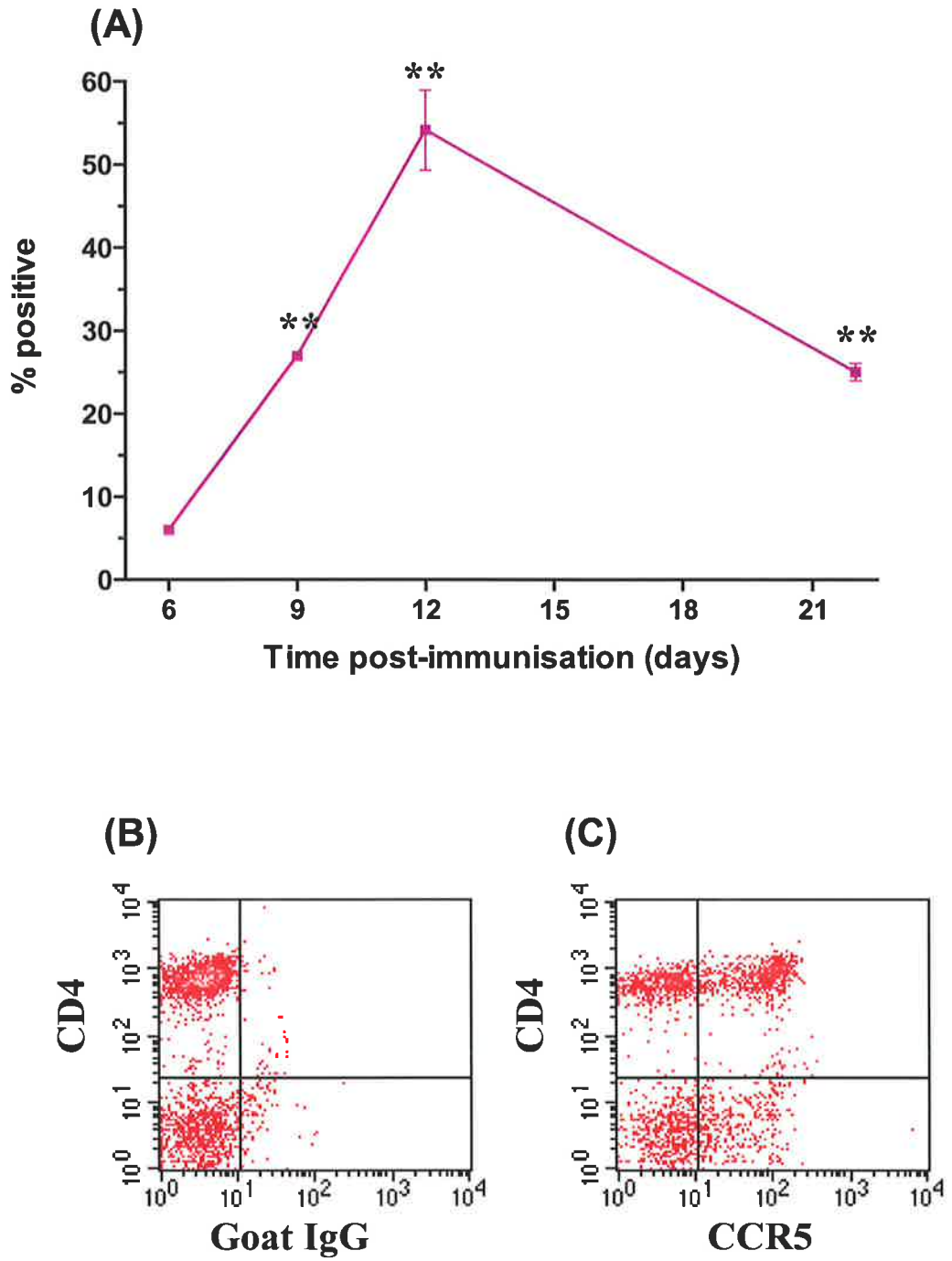
(A)
% positive
60
50
40
30
20
10
0
**
**
**
6
9
12
15
18
21
Time post-immunisation (days)
(B)
CD4
Goat IgG
(C)
CD4
CCR5

Figure 4.8. *Absolute number of $CD4^+$ T cells expressing CCR5, CXCR3 and CXCR4 in control and EAE spinal cords.* EAE was induced in SJL/J mice as previously described (PLP/CFA) (Section 2.2.1). After the indicated period of time, spinal cords were removed and single cell suspensions prepared. Cells were labelled with antibodies against CD4 and either CXCR4 [A], CXCR3 [B] or CCR5 [C], and analysed by flow cytometry, gating on lymphocytes using forward and side scatter characteristics. The percentage of $CD4^+$ T cells expressing the relevant chemokine receptor was determined as a proportion of total lymphocytes, and this value multiplied by the total cell count value for the same time-point, such that the absolute number of cells of each phenotype could be determined. *, Statistically significant from day 6 values ($p < 0.05$). **, Statistically significant from day 6 values ($p < 0.01$). Data are presented as mean ± SEM ($n = 4$).

(A) CXCR4

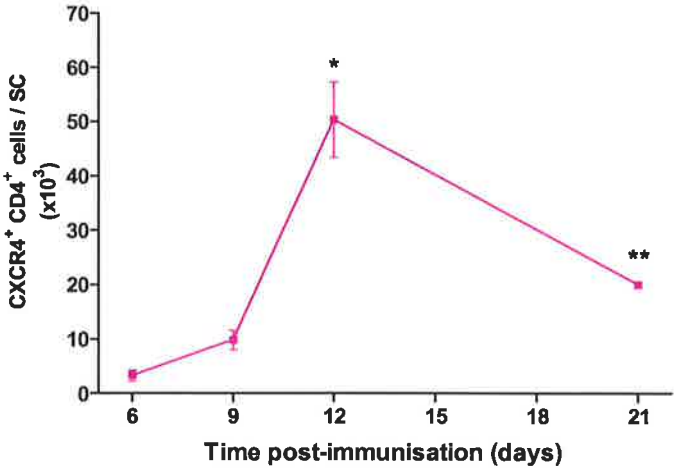

(B) CXCR3

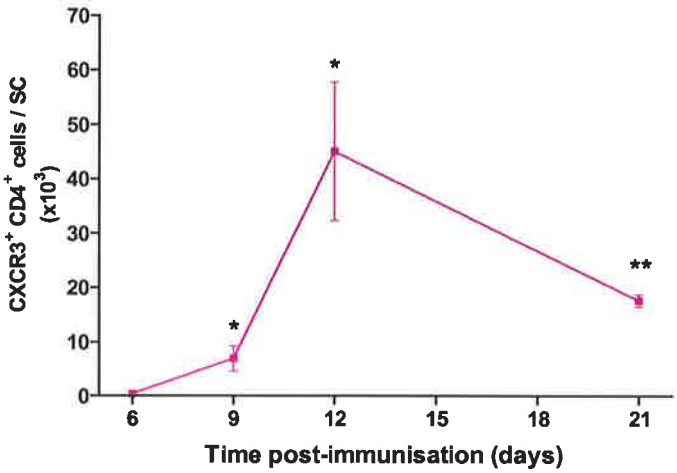

(C) CCR5

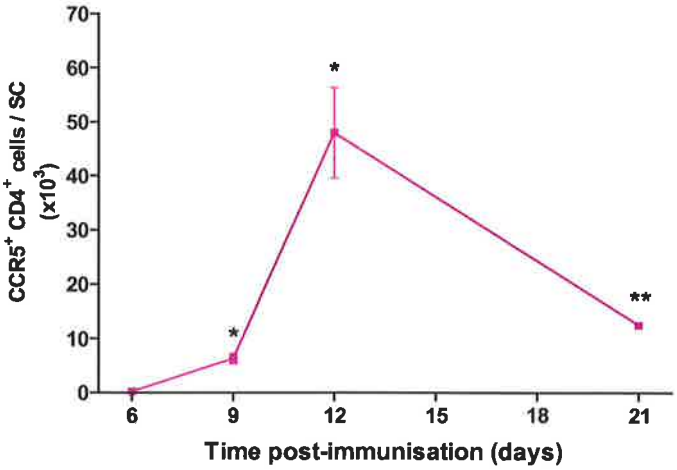

Figure 4.9. *The percentage of total cells and $CD4^+$ T cells undergoing cell division in Day 12 control and PLP-immunised spinal cords.* EAE was induced in SJL/J mice as previously described (PLP/CFA) (Section 2.2.1). Control mice were subjected to CFA injection and pertussigen treatment, without PLP in the CFA emulsion (PBS/CFA). BrdU was administered as described (Section 2.2.6). Twelve days later (peak disease), spinal cords were removed, separated on a Percoll gradient (Section 2.3.2) and single cell suspensions were prepared. Cells were labelled with anti-BrdU [A] or with anti-BrdU and anti-CD4 [B-C] and analysed by flow cytometry, gating on lymphocytes using forward and side scatter characteristics. A representative density plot of cells from PBS-immunised or PLP-immunised spinal cords stained with anti-BrdU and anti-CD4 is presented in [B]. The percentage of $CD4^+$ T cells that had incorporated BrdU at day 12 [C] was determined as a proportion of the total $CD4^+$ population. ***, Statistically significant from the PBS-immunised spinal cords ($p < 0.001$). Data are presented as mean ± SEM (n = 4 (PBS-immunised) and n = 14 (PLP-immunised)).

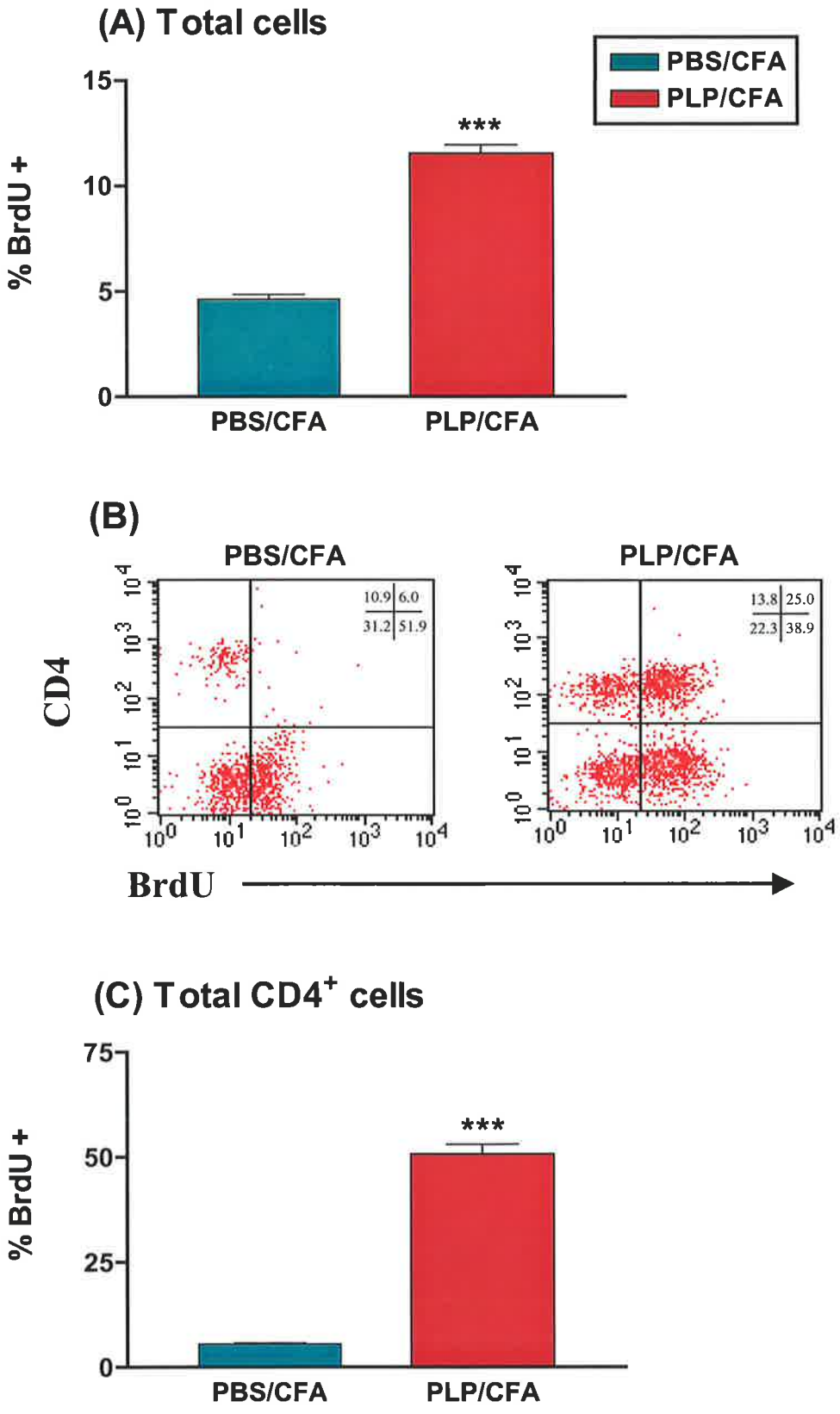
(A) Total cells
PBS/CFA
PLP/CFA
% BrdU +
15
10
5
0
***
PBS/CFA
PLP/CFA
(B)
PBS/CFA
PLP/CFA
CD4
10.9 6.0
31.2 51.9
13.8 25.0
22.3 38.9
BrdU
(C) Total CD4+ cells
% BrdU +
75
50
25
0
***
PBS/CFA
PLP/CFA

Figure 4.10. *The absolute numbers of divided and non-divided $CD4^+$ T cells in control and PLP-immunised spinal cords.* EAE was induced in SJL/J mice as previously described (PLP/CFA) (Section 2.2.1). Control mice were subjected to CFA injection and pertussigen treatment, without PLP in the CFA emulsion (PBS/CFA). BrdU was administered as described (Section 2.2.6). Twelve days later (peak disease), spinal cords were removed, separated on a Percoll gradient (Section 2.3.2) and single cell suspensions were prepared. Cells were labelled with anti-BrdU and anti-CD4 and analysed by flow cytometry, gating on lymphocytes using forward and side scatter characteristics. The percentage of double positive ($CD4^+$ and $BrdU^+$), and the percentage of single positive ($CD4^+$ and $BrdU^-$) cells was multiplied by the total cell count value for the same time-point, such that the absolute number of cells of each phenotype could be determined. *, Statistically significant from PLP/CFA-immunised values ($p < 0.05$). **, Statistically significant from PLP/CFA-immunised values ($p < 0.01$). A statistically significant difference between the number of divided and undivided cells in the PLP-immunised spinal cords is indicated by two asterisks above a bar. Data are presented as mean ± SEM (n = 4 (PBS-immunised) and n = 14 (PLP-immunised)).

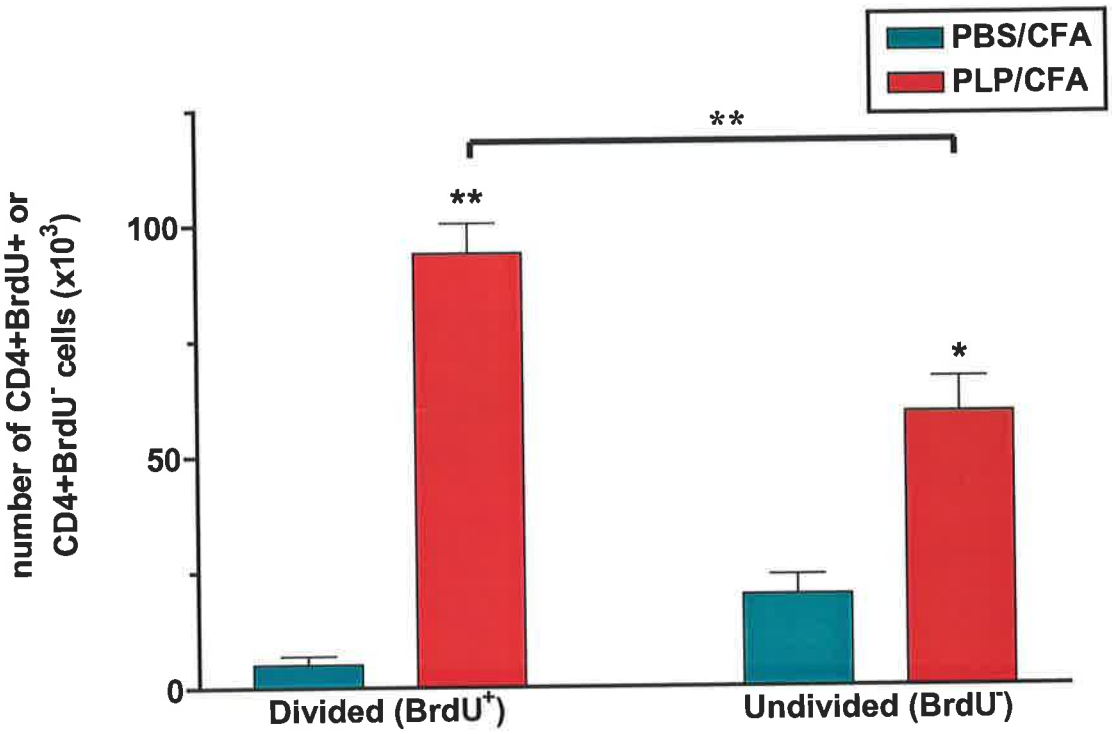
PBS/CFA
PLP/CFA
**
**
*
100
50
0
number of CD4+BrdU+ or CD4+BrdU- cells (x10^3)
Divided (BrdU+)
Undivided (BrdU-)

Figure 4.11. *Comparison of chemokine receptor expression on proliferating and non-proliferating CD4$^+$ T cells in EAE spinal cords.* EAE was induced in SJL/J mice as previously described (PLP/CFA) (Section 2.2.1). BrdU was administered as described (Section 2.2.6). Twelve days later (peak disease), spinal cords were removed, separated on a Percoll gradient (Section 2.3.2) and single cell suspensions were prepared. The cells were labelled with anti-BrdU, anti-CD4 and anti-chemokine receptor antibodies, and then analysed by flow cytometry, gating on lymphocytes using forward and side scatter characteristics. Within the CD4$^+$ T cell population, the percentage of BrdU$^+$ (divided) and BrdU$^-$ (non-divided) cells expressing each chemokine receptor was determined as a proportion of the total BrdU$^+$ or BrdU$^-$ population, accordingly. **, Statistically significant from undivided values ($p < 0.01$). Data are presented as mean ± SEM (n = 8, from 3 independent experiments).

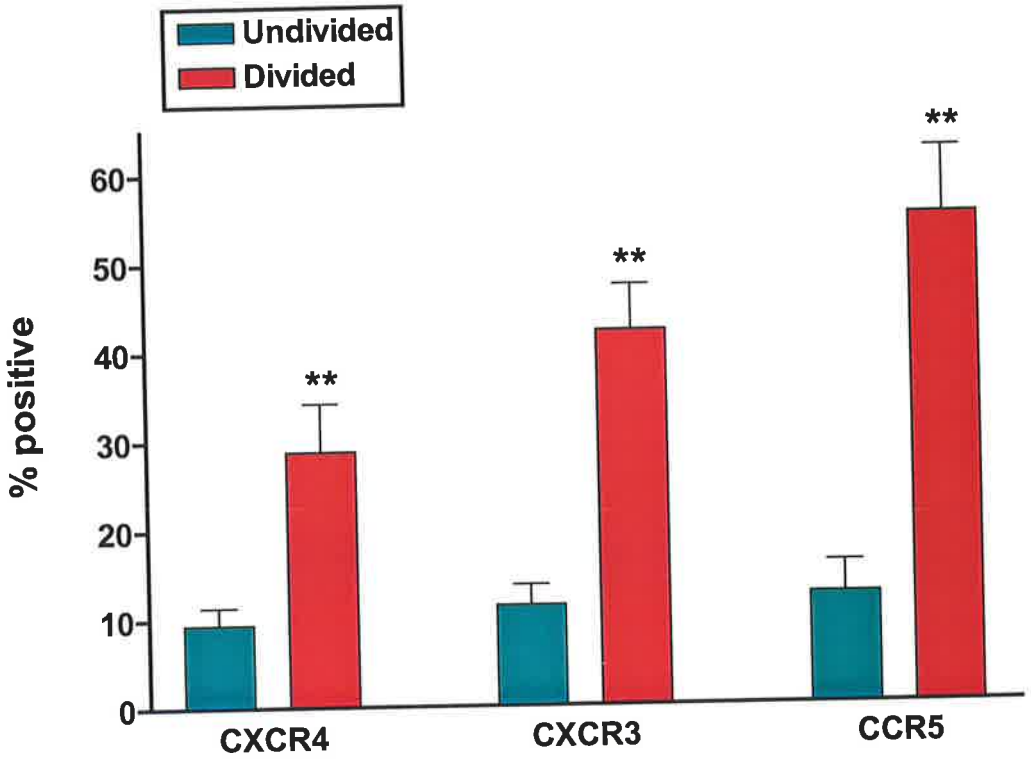
Undivided
Divided
% positive
60
50
40
30
20
10
0
**
**
**
CXCR4
CXCR3
CCR5

Chapter 5

The functional consequences of CXCR4, CXCR3 and CCR5 upregulation during EAE

5.1 Introduction

The experiments outlined in this chapter involve determining the functional consequences of the observed receptor upregulation in the CNS during EAE. Thus, the hypothesis to be tested is, '**Synthetic chemokine antagonists that interfere with ligand/receptor binding will alter the course of $PLP_{139-151}$-induced EAE in SJL/J mice (by retarding cellular infiltration/accumulation into the CNS)**'. In order to test this hypothesis, experiments involving receptor antagonism using N-terminal substitution or truncation mutants of SDF-1, mI-TAC and RANTES were undertaken, with the aim to inhibit receptor function during the pathogenesis of EAE. However, prior to their use *in vivo*, *in vitro* characterisation of the mutants was required. Initially the reagents were generated and assessed for the ability to inhibit migration of $PLP_{139-151}$-specific cells towards functional chemokine ligands *in vitro*, using an established chemotaxis assay. Those found to inhibit migration towards ligands of CXCR4, CXCR3 and CCR5 were subsequently tested for their ability to modulate the pathogenesis of active EAE. Further experiments were then conducted in order to determine the mechanisms by which the antagonists were modulating EAE. These experiments included: analysing the effect of the antagonists on histopathology in the spinal cords of mice exhibiting clinical signs of EAE, examining the effect of antagonist treatment on the accumulation/infiltration of leukocytes into CNS during EAE, and determining whether a humoral immune response was mounted against the antagonists, and if so, whether it affected the outcome of EAE.

5.2 Results

5.2.1 Characterisation of synthetic N-terminal mutants

Modified chemokine peptides have emerged as useful and convenient tools for examining effects of inhibiting ligand/receptor interactions. A brief description of the mutants used in the present study and their sequences are shown in Fig 5.1. The SDF-1 mutant (SDF-1 P2G) consisted of the full amino acid (a.a.) sequence of functional human SDF-1 (1-67), however, the proline in position two was substituted to glycine (Fig 5.1 (A)). Binding studies showed that this modification resulted in no loss of binding capacity to CXCR4, however, it prevented the subsequent activation of CXCR4 (160). All other mutants were N-terminal truncation mutants where the first few amino acids were removed with the intention to bind to the receptor but block signal transduction cascades. The a.a. sequence of the RANTES mutant (Fig 5.1 (B)) was identical to that of the 68 a.a. human wild-type sequence, however, the first eight amino acids had been removed. This mutant was subsequently referred to as RANTES 9-68. RANTES 9-68 has previously been shown to compete with binding of its parent chemokine to RANTES binding sites on human monocytic cells and prevent RANTES-induced migration of these cells (214). In the context of CXCR3 ligands, no synthetic antagonist had previously been made or characterised. Therefore, for the purpose of the present study, three potential murine (m) I-TAC truncation mutants were synthesised and tested for the ability to antagonise activation of mCXCR3. These mutants were I-TAC 3-79, I-TAC 4-79 and I-TAC 5-79, where the first two, three or four amino acids were removed, respectively (Fig 5.1 (C)). The rationale behind the choice for an I-TAC mutant will be discussed in more detail in

Chapter 7. In order to analyse the specific *in vitro* or *in vivo* effects of the above-mentioned antagonists, however, a similar sized peptide was required that would serve as an appropriate negative control for all experiments. Hence, MCP-ala was used. MCP-ala is a truncated and non-functional peptide of MCP-1 with cysteine to alanine substitutions disrupting the structure that allowed the functional analogue to bind chemokine receptors (Fig 5.1 (D)). MCP-ala has previously been used *in vivo* as a negative control for the synthetic antagonist MCP-1 9-76 (165).

5.2.1.1 SDF-1 P2G and RANTES 9-68 are poorly chemotactic

Although an antagonistic role for RANTES 9-68 in a murine model for arthritic inflammation has previously been suggested (165), its capacity to act as an antagonist in the laboratory in which the present study was being performed remained to be defined. Furthermore, *in vitro* characterisation of SDF-1 P2G and the series of I-TAC mutants was required before they could be used as antagonists *in vivo*. Therefore, the mutants were tested to determine whether they exerted any direct chemotactic effect on antigen-activated cells and if not, whether they antagonised the chemotactic effect of the wild-type ligands. To test for direct effects, chemotaxis assays on cells restimulated with $PLP_{139-151}$ (SDF-1 P2G and RANTES 9-68) or lymphocytes stimulated with the mitogen Con A (I-TAC mutants) were performed, where increasing concentrations of the relevant mutant was added to the lower chamber of the transwell plate, and 10^6 cells were added to the upper chamber. SDF-1 P2G was poorly chemotactic (Fig 5.2 (A)). The maximum level of migration of $PLP_{139-151}$-specific cells in response to SDF-1 P2G was negligible with only ~2.4% of total input cells migrating to the lower chamber. Similarly, RANTES 9-68 induced negligible migration of $PLP_{139-151}$-specific cells with only ~1.9% of the cells that

were initially added to the upper chamber migrating to the lower chamber of the transwell (Fig 5.2 (B)). All values calculated were normalised to the random movement of cells in the absence of a gradient (chemokinesis). Thus, both SDF-1 P2G and RANTES 9-68 were demonstrated to have negligible agonistic effects on $PLP_{139-151}$-specific cells.

5.2.1.2 Determination of I-TAC 4-79 as an effective I-TAC antagonist

Similarly to the experiments performed above, synthetic I-TAC mutants were initially tested for any potential agonistic properties. In these experiments, Con A-stimulated lymphocytes were added to the upper chambers of transwell plates and various concentrations of the mutants were added to the lower chambers. Con A was used to stimulate cells since limited stocks of $PLP_{139-151}$ were available. As seen in Figure 5.3 (A), I-TAC 3-79 exhibited chemotactic activity with 1 μg/ml of the mutant inducing migration of ~15% of the cells added to the upper chamber of the transwell. I-TAC 4-79 also displayed modest chemotactic capacity such that ~6.5% of the cells migrated to the lower chamber (Fig 5.3 (A)). In contrast, I-TAC 5-79 was shown to be poorly chemotactic for the ConA-stimulated cells, where only ~2% of the cells responded to the mutant in the chemotaxis assays. Inhibition assays were performed next in order to ascertain the mutant most efficient at inhibiting the migration of Con A-stimulated lymphocytes in response to a sub-optimal concentration of the wild-type I-TAC. The results from these experiments demonstrate that although I-TAC 5-79 had the least agonistic properties, it also lacked the ability to inhibit the migration in response to I-TAC until very high concentrations were added (Fig 5.3 (B)). In contrast, the I-TAC 4-79 mutant dose-dependently inhibited the migration of the cells to the wild-type ligand

beginning at concentrations of 10 μg/ml or higher ($p < 0.05$). In addition, I-TAC 3-79 significantly inhibited migration at concentrations of 3, 10, 30, 100 and 300 μg/ml ($p < 0.01$). Complete inhibition was observed with 300 μg/ml I-TAC 3-79 (Fig 5.3 (B)). Despite I-TAC 3-79 exhibiting the most efficient antagonistic capacities, I-TAC 4-79 was chosen for use in subsequent research since it demonstrated limited direct chemotactic activity when compared with the former.

5.2.1.3 Verification of chemokine receptor antagonism by the synthetic antagonists in vitro

The most effective doses of SDF-1 P2G, I-TAC 4-79 and RANTES 9-68 needed to be determined for the purpose of the present study. The ability of the mutants to prevent migration to CXCR4, CXCR3 and CCR5 ligands was tested by analysing their effects on the migration of antigen-activated cells during *in vitro* chemotaxis assays (Section 2.5.4). Based on the dose-response data of the cells observed in Chapter 3 (Figs 3.14-3.16), the ability of the mutant or the negative control peptide, MCP-ala, to neutralise chemotaxis was tested using a sub-optimal dose of each ligand. In each assay, the agonist and mutant were combined in the lower chamber of the transwell, while 1 x 10^6 cells were added to the upper chamber. Figure 5.4 demonstrates the inhibition of migration of $PLP_{139-151}$-specific cells towards SDF-1 with increasing concentrations of SDF-1 P2G. In this figure, MCP-ala had a negligible effect on SDF-1-induced chemotaxis. In contrast, SDF-1 P2G significantly inhibited SDF-1-induced migration at concentrations of 10, 30, 100, and 300 μg/ml. Complete inhibition was observed with 300 μg/ml SDF-1 P2G. The effect of I-TAC 4-79 on the chemotaxis of $PLP_{139-151}$-specific cells to the CXCR3 ligands mI-

TAC/CXCL11, mIP-10/CXCL10 and mMig/CXCL9 was also examined and the results are demonstrated in Figure 5.5. In these experiments MCP-ala failed to inhibit migration in response to all three ligands. In fact, in the case of mI-TAC, MCP-ala was shown to moderately enhance the migration of $PLP_{139-151}$-restimulated cells (Fig 5.5 (A)). In contrast, I-TAC 4-79 dose-dependently inhibited the migration of the $PLP_{139-151}$-restimulated cells in response to all three wild-type ligands (Fig 5.5 (A-C)). Statistically significant inhibition of migration was not observed, however, until the concentration of the antagonist exceeded 30 μg/ml. In the cases of mIP-10/CXCL10 and mMig/CXCL9, complete inhibition was not observed, even with the highest concentration of antagonist used.

With regard to RANTES 9-68, many inhibition assays were performed using PLP-reactive lymphocytes, however, the level of migration of the cells to the wild-type ligand was too inconsistent for reliable conclusions to be drawn. Therefore, an alternative migration assay involving T cells isolated from the peritoneum of *Salmonella enteritidis*-immunised mice purified on nylon wool columns (Sections 2.3.3 and 2.3.4) was used to investigate the ability of RANTES 9-68 to inhibit RANTES- and MIP-1β-mediated chemotaxis. The results from these experiments are demonstrated in Figure 5.6. In the absence of RANTES 9-68, 50 ng/ml of RANTES/CCL5 and MIP-1β/CCL4 induced migration in 8% and 12% of the cells, respectively (data not shown). Increasing concentrations of MCP-ala appeared to have negligible effects on the observed migration. In contrast, RANTES 9-68 dose-dependently inhibited the migration of the T cells to both of the CCR5 ligands, with significant inhibition at concentrations of 10, 30, 100, 300 and 1000 ng/ml (Fig 5.6). Complete inhibition to either ligand was not observed. Thus, RANTES 9-68 successfully inhibited CCR5-mediated migration, as demonstrated by its ability to prevent MIP-1β-

induced T cells chemotaxis. These experiments do not, however, demonstrate the specificity of RANTES 9-68. RANTES/CCL5 is a promiscuous chemokine, binding to several receptors including CCR1, CCR3 and CCR5. This will be discussed in more detail in Chapter 7.

5.2.2 The effect of receptor inhibition on the development of clinical EAE

5.2.2.1 Dosing regimen for chemokine antagonist treatment of mice

The chemokine antagonists were administered every second day by intraperitoneal injection using a maximal dose of 100-250 mg/mouse (~2-5 mg/kg/2 days), based on previous studies involving *in vivo* administration of other modified chemokine peptide antagonists that demonstrated maximal effects at a dose 2mg/kg/day (165). The concentration of I-TAC 4-79 administered to the mice was 2.5-fold greater than both SDF-1 P2G and RANTES 9-68, since higher concentrations were required to inhibit migration of antigen-activated cells in *in vitro* chemotaxis assays (Section 5.2.1.3). Spatial distribution of the modified peptides could not be determined due to their susceptibility to proteolytic cleavage. Therefore, data involving the use of neutralising antibodies *in vivo* was analysed. These data revealed detectable levels of antibodies in the CNS of mice in which EAE had been induced (data not shown). This indicates that smaller chemokine peptides may also be capable of crossing the BBB. In addition, results from experiments comparing intravenous versus intraperitoneal administration of antibodies revealed no apparent difference between the two routes of administration (data not shown). Therefore

intraperitoneal injections were subsequently used for antagonist treatment in the present study.

5.2.2.2 SDF-1/CXCL12 antagonism during EAE alters the course of clinical disease

Passive immunisation of mice with 100 μg SDF-1 P2G every second day starting 1 day post-immunisation with $PLP_{139-151}$ in CFA (Fig 5.7 (A-C)) significantly inhibited the development of EAE in three independent experiments. The results from these experiments have been combined and are presented in Figure 5.7 (n = 25). It is important to note, however, that the manifestations of disease varied slightly between the individual experiments. Accordingly, the results from each experiment will be discussed separately. In experiment one (Table 5.1), mice in the SDF-1 P2G-treated group exhibited a significantly lower maximal disease score and displayed a statistically significant reduction in the number of days in which the mice showed neurological signs of EAE when compared with mice in the control group. Furthermore, in contrast to the control cohort, not all mice developed neurological signs of disease. Results from the second experiment (Table 5.1) showed lower disease scores (significantly lower on days 10, 13, 14, 17 and 18) for the SDF-1 P2G-treated mice compared with the MCP-ala-treated mice. In addition, SDF-1 P2G treatment caused a significant reduction in the mean length of disease, and gave a trend towards delayed onset (Table 5.1). Seventy five percent of the SDF-1 P2G-treated mice developed neurological signs of EAE, while all of the MCP-ala-treated mice were affected. In experiment three (Table 5.1) disease scores were always lower than in the control group (statistically significant on days 10-13 post-immunisation), with the SDF-1 P2G-treated group exhibiting a significantly delayed disease onset and significantly lower maximal disease scores than the control group. However, the two

treatment groups eventually followed the same disease course. Furthermore, there was a significant reduction in the number of days that SDF-1 P2G-treated mice displayed neurological disease (Table 5.1). In experiment three, all mice from both cohorts developed clinical symptoms of EAE.

5.2.2.3 I-TAC 4-79 treatment decreases disease severity during EAE

Treatment of mice with I-TAC 4-79 was shown to alleviate the course of EAE in three separate experiments. EAE was induced in SJL/J mice followed by treatment every second day until day 15 with 250 μg I-TAC 4-79 or the inactive control peptide MCP-ala (Section 2.2.4). The results from all three experiments combined (n = 26) indicate that I-TAC 4-79 significantly reduces the severity of EAE, although not to the same extent as SDF-1 P2G (Fig 5.8). The results from the first experiment (Table 5.1) illustrate that I-TAC 4-79-treated mice took significantly longer to develop neurological signs of EAE and displayed lower disease scores throughout the course of clinical disease (significantly lower on days 10, 11, 13 and 14 post-immunisation). The second experiment using I-TAC 4-79 in EAE showed similar results to experiment one (Table 5.1). Mice in the I-TAC 4-79-treated cohort took significantly longer to develop clinical signs of EAE and had lower clinical scores than the MCP-ala-treated group. As well as displaying neurological symptoms for a significantly shorter period of time, mice from the I-TAC 4-79-treated cohort recovered significantly more rapidly than the control group (Table 5.1). In experiment three, the mean day that the mice in the I-TAC 4-79-treatment group began to display signs of clinical disease was ~2 days after, and significantly later, than mice in the control-treated group (Table 5.1). Collectively, I-TAC 4-79-treated mice consistently exhibited significantly lower disease scores (until day 16 post-immunisation) than the

MCP-ala-treated mice, which translated into a significantly reduced maximal clinical disease score. This treatment also resulted in a significantly shorter disease course (Fig 5.8, Table 5.1). In all three experiments, all MCP-ala-treated mice and all (except one in experiment 3) I-TAC 4-79-treated mice developed neurological symptoms associated with EAE.

5.2.2.4 RANTES 9-68 ameliorates clinical symptoms of EAE

Intraperitoneal injections of 100 μg RANTES 9-68 every second day following EAE induction were demonstrated to alleviate the course of EAE in three independent experiments, the combined results for which are shown in Figure 5.9 (n = 23). In experiment one (Fig 5.9, Table 5.1), treatment with RANTES 9-68 resulted in a significant reduction in the clinical disease score, beginning at 10 days post-immunisation, that lasted until day 16 post-immunisation ($p < 0.05$). During this time, mice treated with MCP-ala exhibited hind limb paralysis, whereas RANTES 9-68-treated mice displayed only incomplete tail paralysis. RANTES 9-68 treatment caused a significant delay in the onset of clinical disease and also significantly reduced the number of days during which mice showed neurological symptoms (Table 5.1). The difference in mean maximum clinical disease score of the RANTES 9-68-treated mice was ~1.3-fold lower than that of the control-treated cohort. The results from the second experiment also demonstrate disease reduction following RANTES 9-68 treatment (Fig 5.9, Table 5.1). A significant delay in the onset of clinical disease was observed in those animals treated with RANTES 9-68 compared with MCP-ala-treated animals. During onset and peak clinical disease, the mean clinical disease score was significantly lower in the RANTES 9-68-treated mice than the control group. However, as the mice began to recover, the two treatment groups

eventually followed the same disease course. In addition, the number of days on which the mice displayed clinical disease during EAE was significantly less in the RANTES 9-68-treated cohort compared with the control group (Table 5.1). The final experiment involving RANTES 9-68 treatment in active EAE resulted in a statistically significant reduction in the disease scores of the mice treated with RANTES 9-68 from days 10 to 15 post-immunisation ($p < 0.05$; Table 5.1). Animals in this treatment group never lost the ability to right themselves when placed on their backs. This is in contrast to that observed in the MCP-ala-treated group. Furthermore, the mice treated with RANTES 9-68 displayed delayed onset of clinical symptoms of the disease, a significantly lower maximum clinical disease score and reduced disease length (Table 5.1). In contrast to the MCP-ala-treated mice, not all of the RANTES 9-68-treated animals developed neurological signs of EAE across the three experiments.

5.2.3 Reduction of histopathology in the CNS by antagonist treatment

Mononuclear cell migration into the CNS precedes the development of disease symptoms (127). To determine whether antagonist treatment affected the infiltration of mononuclear inflammatory cells in the CNS, mice from the antagonist- or control-treated groups were killed for histological examination 12 days post-immunisation with $PLP_{139-151}$ emulsion. Mice that had received no treatment were also killed in order to provide background control tissue. Spinal cords from control- and antagonist-treated mice were removed from the mice after perfusion in the left ventricle with cold PBS to remove circulating leukocytes. Cryostat sections of the tissue samples were stained with haematoxylin/eosin (Section 2.6.5) and evaluated for the extent of mononuclear cell infiltration into the meninges, perivascular areas and parenchyma. Representative photomicrographs of

transverse sections of thoracic/lumbar regions of the spinal cord of normal SJL/J mice (Day 0), and MCP-ala- and antagonist-treated mice are shown in Figure 5.10 (A-E). It should be emphasised that, at the time of death, the mice from the MCP-ala-treated groups displayed clinical disease such that the mean disease scores were approximately 2.5-3.0 at the time of death, whereas mice from the SDF-1 P2G-, I-TAC 4-79- and RANTES 9-68-treatment groups had mean clinical disease scores of 1.66 ± 0.37, 1.93 ± 0.11 and 1.44 ± 0.33, respectively (Tables 5.10-5.13). Very few mononuclear cells were observed in the spinal cords of normal mice (Fig 5.10 (A)). Spinal cord sections from MCP-ala-treated mice in which EAE had been induced showed extensive meningeal and perivascular, and some parenchymal mononuclear cell infiltration (Fig 5.10 (B)). In contrast, spinal cord sections from SDF-1 P2G-treated mice showed little or no meningeal, perivascular, or parenchymal mononuclear cell infiltration (Fig 5.10 (C)). The sections representing spinal cords from the I-TAC 4-79-treated mice demonstrated a greater number of infiltrating cells than mice from the SDF-1 P2G-treated group, however, there were still fewer cells than in the MCP-ala-treated spinal cord sections (Figure 5.10 (D)). When analysing the sections from RANTES-9-68-treated animals, a few scattered cells could be seen in the lumbar spinal cord of these mice. However, in general, these spinal cords were consistent in appearance with those observed in normal (day 0) mice (Fig 5.10 (E)).

These histopathological data were quantified and are shown in Tables 5.2-5.4. Mice from each antagonist-treated group had significantly fewer lesions per section compared with the MCP-ala treated mice in the same experiment ($p < 0.0001$). Thus, in the spinal cords of antagonist-treated mice, the presence of infiltrating cells suggests that the antagonist treatment did not absolutely inhibit the entry of cells into the CNS, which is consistent with the lack of complete inhibition of neurological impairment in these mice.

5.2.4 Quantitation of cells recovered from the CNS of chemokine antagonist-treated mice during EAE

5.2.4.1 Effect of the synthetic antagonists on the accumulation of cells in the spinal cords of EAE mice

As suggested by the *in vitro* chemotaxis data and the histological analysis of spinal cord sections, one mechanism by which the antagonists might lessen the severity of EAE is by reducing leukocyte infiltration into the CNS. To address this hypothesis, mice were immunised with $PLP_{139-151}$ in CFA, treated with the relevant antagonist or control peptide every second day, then sacrificed at the peak of clinical disease (day 12) for quantitative analysis of inflammatory infiltrates in the CNS. The recovered viable cells were enumerated using a haemocytometer, labelled with antibodies against CD4, and subsequently analysed by flow cytometry. Haemocytometer counts revealed that antagonist treatment resulted in a significant decrease in the mean number of viable cells recovered from the spinal cords at the peak of clinical disease (Fig 5.11). There were ~1.6-fold less total viable cells recovered from the SDF-1 P2G-treated mice than from the MCP-ala treated mice, and ~2-fold fewer total viable cells recovered from the ITAC 4-79- and RANTES 9-68-treated mice compared with MCP-ala-treated mice. Flow cytometric analysis of the $CD4^+$ T cell population was performed, such that the absolute numbers of $CD4^+$ T cells in the CNS could be calculated (Fig 5.12). The data revealed that, in the case of all antagonists, significantly fewer $CD4^+$ T cells had accumulated in the CNS of the antagonist-treated animals compared with the MCP-ala-treated animals (Fig 5.12; $p < 0.05$). In fact, there were 3.25-fold fewer $CD4^+$ T cells recovered from the SDF-1 P2G-treated mice than from the MCP-ala-treated mice, and 2.3- and 2.7-fold less $CD4^+$ T cells

recovered from the I-TAC 4-79- and RANTES 9-68-treated mice, respectively, than from the MCP-ala-treated mice at the same time point.

5.2.4.2 Percentages of chemokine receptor expressing CD4$^+$ T cells in the CNS of chemokine antagonist-treated mice

Using the BrdU technique, it was demonstrated in the previous chapter that a greater percentage of divided CD4$^+$ T cells accumulated in the CNS following EAE induction expressed the chemokine receptors CXCR4, CXCR3, and CCR5 compared to their undivided counterparts. The aim of the following experiments was to determine whether antagonist treatment altered the percentage of chemokine receptor encephalitogenic CD4$^+$ T cells in the CNS, at peak clinical disease. Mice in each treatment group were fed BrdU continuously in drinking water from day 6 post-immunisation, before being sacrificed at the height of clinical disease (as previously described). The leukocytes were isolated from the spinal cords following Percoll separation (Section 2.3.2), labelled with antibodies to CD4, BrdU and CXCR4, CXCR3 or CCR5, and subsequently analysed by flow cytometry. As demonstrated in Figure 5.13 (A), there appeared to be a lower percentage of CXCR4$^+$CD4$^+$ T cells in the spinal cords of SDF-1 P2G-treated mice than in the negative control-treated mice at peak clinical disease, however, this trend was not statistically significant when either one- or two-tailed t tests were performed. Analysis of the BrdU$^+$ and BrdU$^-$ populations revealed SDF-1 P2G treatment had a negligible effect on the percentage of divided CD4$^+$ T cells expressing CXCR4 in the spinal cords of $PLP_{139-151}$-immunised mice (Fig 5.13 (B)). Approximately 35% of the divided CD4$^+$ T cells expressed CXCR4 in the CNS of SDF-1 P2G-treated mice, which was similar to the percentage of divided CD4$^+$ T cells expressing the receptor in the MCP-ala-treated mice.

In addition, there was no statistical difference between the percentage of undivided cells expressing CXCR4 in the SDF-1 P2G-treated mice and the percentage of undivided cells expressing this receptor in the MCP-ala-treated mice.

When analysing the percentage of CXCR3 expressing $CD4^+$ T cells in the spinal cords of I-TAC 4-79-treated mice (Fig 5.14 (A)), there appeared to be a lower percentage of $CXCR3^+CD4^+$ T cells compared with the MCP-ala-treated mice. Approximately 48% of the $CD4^+$ T cells in the CNS expressed CXCR3 in MCP-ala-treated mice, whereas the percentage of $CD4^+$ T cells positive for CXCR3 in the CNS of I-TAC 4-79-treated mice was ~37% (Fig 5.14 (A)). While the observed decrease was not significant in a two-tailed t test, the percentage of CXCR3-expressing $CD4^+$ T cells in the spinal cords of I-TAC 4-79-treated mice was statistically lower than the percentage of $CXCR3^+CD4^+$ T cells recovered from the spinal cords of MCP-ala-treated mice when a one-tailed t test was performed ($p = 0.02$). Similarly, a one-tailed t test revealed there to be a significantly lower percentage of divided ($BrdU^+$) $CD4^+$ T cells expressing CXCR3 in the CNS of I-TAC 4-79-treated mice than in the MCP-ala-treated cohort (Fig 5.14 (B); $p = 0.04$). These percentages were 37% and 46% in the I-TAC 4-79- and MCP-ala-treated mice, respectively. Analysis of the undivided population demonstrated that, of the undivided $CD4^+$ T cells present in the spinal cord, ~10% expressed CXCR3 (Fig 5.14 (B)). There was no significant difference between the MCP-ala- and I-TAC 4-79-treated mice with respect to these values.

With respect to the effect of RANTES 9-68 treatment on the percentage of CCR5 expressing $CD4^+$ T cells in the CNS following EAE induction, flow cytometric analysis of the cells recovered from the RANTES 9-68-treated spinal cords revealed there to be a

significantly lower percentage of CCR5 expressing $CD4^+$ T cells in those spinal cords than in the MCP-ala-treated CNS (Fig 5.15 (A); $p < 0.05$, two-tailed t test). This reduction may be reflective of a significantly smaller population of divided $CD4^+$ T cells expressing CCR5 in the RANTES 9-68-treated spinal cords than in the MCP-ala-treated spinal cords (Fig 5.15 (B); $p < 0.05$, two-tailed t test). Whilst over 57% of the $BrdU^+$ $CD4^+$ T cells in the CNS of MCP-ala-treated mice expressed CCR5, this percentage fell by 1.5-fold in the RANTES 9-68-treated mice, where only 40% of the divided $CD4^+$ T cells expressed this receptor. In contrast, the expression of CCR5 on undivided $CD4^+$ T cells did not vary significantly between the two treatment groups (Fig 5.15 (B)). In both the MCP-ala- and RANTES 9-68-treated spinal cords, ~10% of the $BrdU^-$ $CD4^+$ T cells expressed CCR5.

The data above suggest that a percentage of antigen-activated $CD4^+$ T cells bearing CXCR3 or CCR5 (or both) were specifically excluded from the CNS of I-TAC 4-79- or RANTES 9-68-treated mice, respectively, presumably because of a failure to cross the BBB, or a failure to accumulate in the CNS. However, with respect to the percentage of divided $CD4^+$ T cells expressing CXCR3 in I-TAC 4-79-treated spinal cords, further experiments are required to ensure the observed results are significant in a two-tailed t test.

5.2.5 Humoral immunity is not responsible for the amelioration of disease following antagonist treatment

It is possible that continuous injection of modified chemokines results in the formation of neutralising auto-antibodies against the endogenous wild-type (WT) chemokine and this could be involved in the amelioration of disease severity. To address this possibility, sera

from all mutant chemokine treated mice were collected at the end of each experiment. These sera were tested for the presence of antibodies against WT chemokines (ie, antibodies produced against the mutant that are cross-reactive towards the WT ligand) and against the antagonists themselves. Sera were also collected from untreated mice to provide background antibody levels. Overall, there was no humoral immunity observed in the antagonist-treated groups to which mitigation of disease could be accredited. Figure 5.16 illustrates the data obtained from a series of direct ELISAs (Section 2.5.5). In a direct ELISA against mMCP-1, MCP-ala- and antagonist-treated mice showed no increase in anti-MCP-1 antibody titres when compared to untreated mice (Fig 5.16 (A)). Serum samples were also tested for the presence of antibodies capable of binding MCP-ala. In contrast to that observed above, MCP-ala-treated mice showed a statistically significant increase in the level of anti-MCP-ala antibodies in the serum, compared with antagonist-treated mice and untreated mice. However, only low levels were present, since the highest recorded OD reading at 490 nm was 0.25 (Fig 5.16 (A)). In ELISAs directed against SDF-1 and SDF-1 P2G (B), there was no observed increase in the levels of anti-SDF-1 and anti-SDF-1 P2G from the serum collected from SDF-1 P2G-treated mice above that from the untreated mice and from mice treated with the other mutants. Serum samples were also tested for the presence of antibodies capable of binding endogenous WT mRANTES and RANTES 9-68. As demonstrated in (C), RANTES 9-68-treated mice showed a small, but statistically significant increase in anti-RANTES 9-68 antibodies, compared to mice treated with the other mutants or untreated mice. However, these antibodies were not cross-reactive to WT mRANTES, nor would they have any effect in terms of decreasing disease severity. Since the EAE experiments involving I-TAC 4-79 treatment were performed separately from the EAE experiments involving the other two antagonists, levels of antibodies against WT SDF-1, WT mRANTES and their respective

antagonists were not measured. In these ELISAs, ITAC 4-79-treated mice failed to produce antibodies to either muI-TAC or I-TAC 4-79 (D). Rather, levels of antibodies in the serum of I-TAC 4-79-treated mice towards the two molecules were comparable to levels seen in both the untreated mice and the MCP-ala-treated cohort.

5.3 Summary

The aim of this series of experiments was to determine the biological consequences of specific chemokine/receptor interactions during the immune response. A series of synthetic chemokine mutants were initially tested *in vitro* for their ability to act as antagonists in preventing the migration of antigen-activated lymphocytes to ligands of the receptors CXCR4, CXCR3 and CCR5. These analyses revealed that the synthetic mutants SDF-1 P2G, I-TAC 4-79 and RANTES 9-68 possessed potent antagonistic capacities, yet each lacked the ability to act as an agonist *in vitro*. Accordingly, the above mutants were selected for use in the PLP chronic relapsing-remitting model of EAE in the SJL/J mouse. Treatment every second day with the antagonists until day 15 resulted in a significant decrease in the severity of the neurological symptoms of EAE. Histological analyses demonstrated that the reduction in disease severity corresponded with a reduced number of inflammatory infiltrates in the spinal cords of antagonist-treated mice at peak clinical disease compared with control-treated mice. In addition, flow cytometric analysis revealed that the mechanism of inhibition of EAE might be directly related to a decrease in the number of $CD4^+$ T cells in the CNS of antagonist-treated mice, since there were significantly fewer $CD4^+$ T cells infiltrating the CNS in antagonist-treated mice compared

with control-treated mice. In order to determine whether chemokine receptor expressing $CD4^+$ T cells were being specifically excluded from entering the CNS tissue in the antagonist-treated mice, flow cytometry was performed on cells recovered from the CNS. Upon evaluating chemokine receptor expression on the antigen-activated $CD4^+$ T cells, it was discovered that I-TAC 4-79 and RANTES 9-68 treatment selectively prevented CNS entry and accumulation of CXCR3- and CCR5-bearing $CD4^+$ T cells, respectively. In contrast, similar proportions of CXCR4-expressing $CD4^+$ T cells entered the CNS in the SDF-1 P2G-treated mice, compared with those that entered the control-treated CNS tissue. Finally, experiments aimed at determining whether continuous injections of the antagonists resulted in the formation of neutralising auto-antibodies against the endogenous wild-type (WT) chemokine demonstrated that this was not the mechanism by which the antagonists were ameliorating disease.

The experiments described in Chapter 5, however, do not give any insight into the temporal and spatial effects of the antagonists. This will be the focus of the following chapter.

Figure 5.1: *Sequence alignments of synthetic mutants.* Shown are the sequences of wild type chemokines and the indicated analogs. SDF-1 and SDF-1 P2G [A], RANTES and RANTES 9-68 [B], murine I-TAC and I-TAC 3-79 to 5-79 [C], MCP-1 and MCP-ala [D].

(A)

```
SDF-1        KPVSLSYRCPCRFFESHVARANVKHLKILNTRNCALQIVARLKNNNRQVCIDPKLKWIQEYLEKALN
SDF-1 P2G    KGVSLSYRCPCRFFESHVARANVKHLKILNTRNCALQIVARLKNNNRQVCIDPKLKWIQEYLEKALN
```

(B)

```
RANTES       SPYSSDTTPCCFAYIARPLPRAHIKEYFYWSGKCSNPAVVFVTRKNRQVCANPEKKWVREYINSLEMS
RANTES 9-68  --------PCCFAYIARPLPRAHIKEYFYWSGKCSNPAVVFVTRKNRQVCANPEKKWVREYINSLEMS
```

(C)

```
mI-TAC       FLMFKQPRCLCIGPGMKAVKMAEIEKASVIYPSNGCDKVEVIVTMKAHKRQRCLDPRSKQARLIMQAIEKKNFLRRQNM
mI-TAC 3-79  --MFKQPRCLCIGPGMKAVKMAEIEKASVIYPSNGCDKVEVIVTMKAHKRQRCLDPRSKQARLIMQAIEKKNFLRRQNM
mI-TAC 4-79  ---FKQPRCLCIGPGMKAVKMAEIEKASVIYPSNGCDKVEVIVTMKAHKRQRCLDPRSKQARLIMQAIEKKNFLRRQNM
mI-TAC 5-79  ----KQPRCLCIGPGMKAVKMAEIEKASVIYPSNGCDKVEVIVTMKAHKRQRCLDPRSKQARLIMQAIEKKNFLRRQNM
```

(D)

```
MCP-1        QPDAINAPVTCCYNFTNRKISVQRLASYRRITSSKCPKEAVIFKTIVAKEICADPKQKWVQDSMDHLDKQTQTPKT
MCP-ala      --------VTAAYNFTNRKISVQRLASYRRITSSKAPKEAVIFKTIVAKEIAADPKQKWVQDSMDHLDKQTQTPKT
```

Figure 5.2: *SDF-1 P2G and RANTES 9-68 demonstrate negligible chemotactic activity.* Lymph nodes were removed from PLP/CFA-immunised mice and single cell suspensions were prepared. Cells were then cultured for 4 days in the presence of $PLP_{139-151}$. All cells were loaded with calcein fluorophore. RPMI-BSA (600 µl) containing various concentrations of SDF-1 P2G [A] or RANTES 9-68 [B] were added to the lower chamber of a Transwell® plate, and 1 x 10^6 cells (in 100 µl) were loaded into the upper chamber. Assays were conducted at 37°C for 3 hours, after which the level of fluorescence in the lower chambers was determined (Section 2.5.4). Chemokinesis (random cellular movement) was assessed in untreated cells. Data points represent the mean value ± SEM (n = 2).

(A) SDF-1 P2G

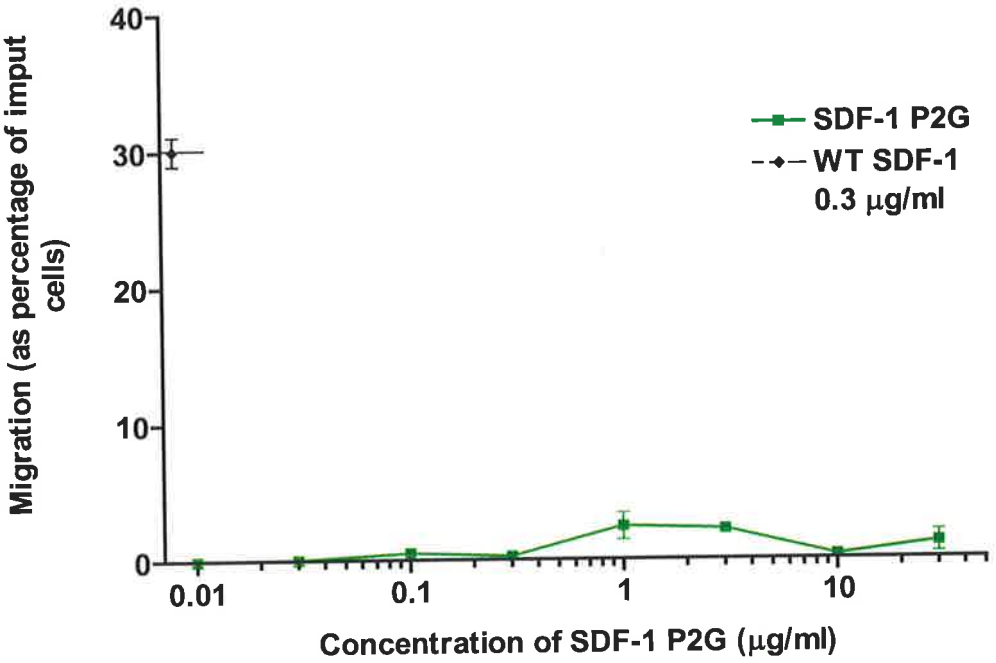

(B) RANTES 9-68

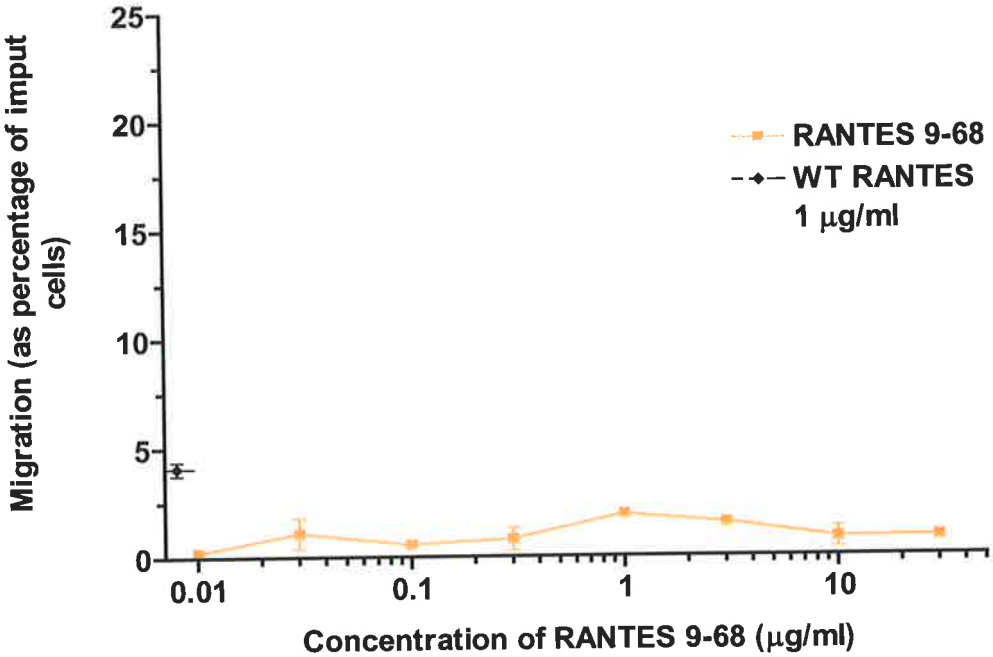

Figure 5.3: *Determination of an I-TAC antagonist.* Con A-stimulated SJL/J lymphocytes were loaded with calcein fluorophore. RPMI-BSA (600 µl) containing various concentrations of I-TAC 3-79, I-TAC 4-79 or I-TAC 5-79 [A] or containing 50 ng/ml wild-type murine I-TAC (WT mI-TAC) and varying concentrations of either I-TAC 3-79, I-TAC 4-79 or I-TAC 5-79 [B] were added to the lower chamber of a Transwell® plate, and 1 x 10^6 cells (in 100 µl) were loaded into the upper chamber. Assays were conducted at 37°C for 3 hours, after which the level of fluorescence in the lower chambers was determined (Section 2.5.4). In [B], total migration was then converted to a percentage of the level seen with 50 ng/ml WT mI-TAC alone. * indicates a statistically significant difference from that observed in the absence of the mutant at $p<0.05$. Data points represent the mean value ± SEM ($n = 2$ [A] and $n = 3$ [B]).

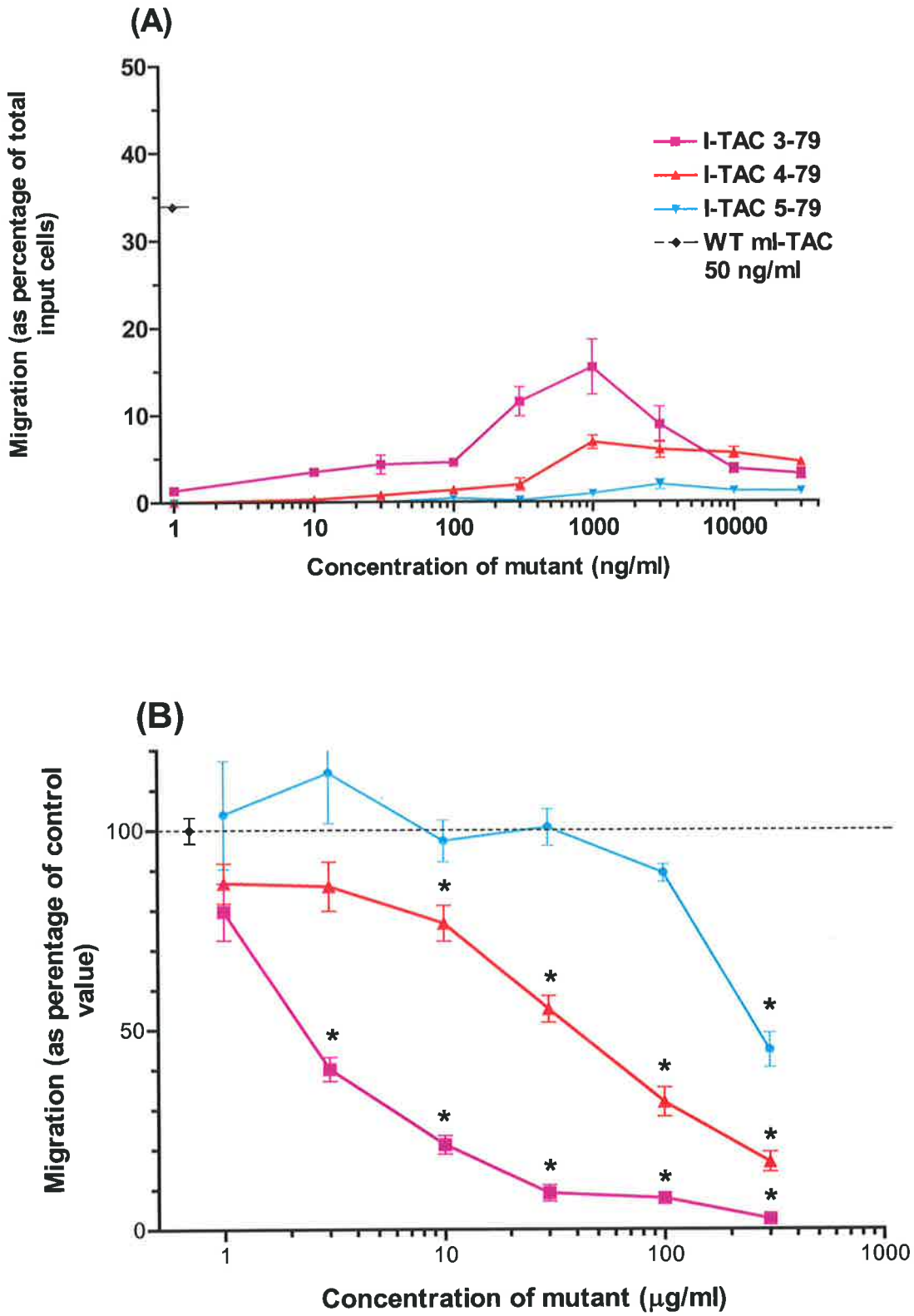
(A)
Migration (as percentage of total input cells)
50
40
30
20
10
0
1
10
100
1000
10000
Concentration of mutant (ng/ml)
I-TAC 3-79
I-TAC 4-79
I-TAC 5-79
WT mI-TAC 50 ng/ml
(B)
Migration (as perentage of control value)
100
50
0
1
10
100
1000
Concentration of mutant (μg/ml)
*

Figure 5.4: *SDF-1 P2G inhibits SDF-1/CXCL12-mediated migration of PLP-reactive lymphocytes.* Lymph nodes were removed from PLP/CFA-immunised mice and single cell suspensions were prepared. Cells were then cultured for 4 days in the presence of $PLP_{139-151}$. All cells were loaded with calcein fluorophore. RPMI-BSA (600 µl) containing 0.1 µg/ml SDF-1/CXCL12 and varying concentrations of either SDF-1 P2G or MCP-ala (control peptide) were added to the lower chamber of a Transwell® plate, and 1 x 10^6 cells (in 100 µl) were loaded into the upper chamber. Assays were conducted at 37°C for 3 hours, after which the level of fluorescence in the lower chambers was determined (Section 2.5.4). Total migration was then converted to a percentage of the level observed with 0.1µg/ml SDF-1/CXCL12 alone. * indicates a statistically significant difference from SDF-1/CXCL12 alone and the corresponding concentration of MCP-ala at $p<0.05$. Data points represent the mean value ± SEM (n = 4, from 4 independent experiments).

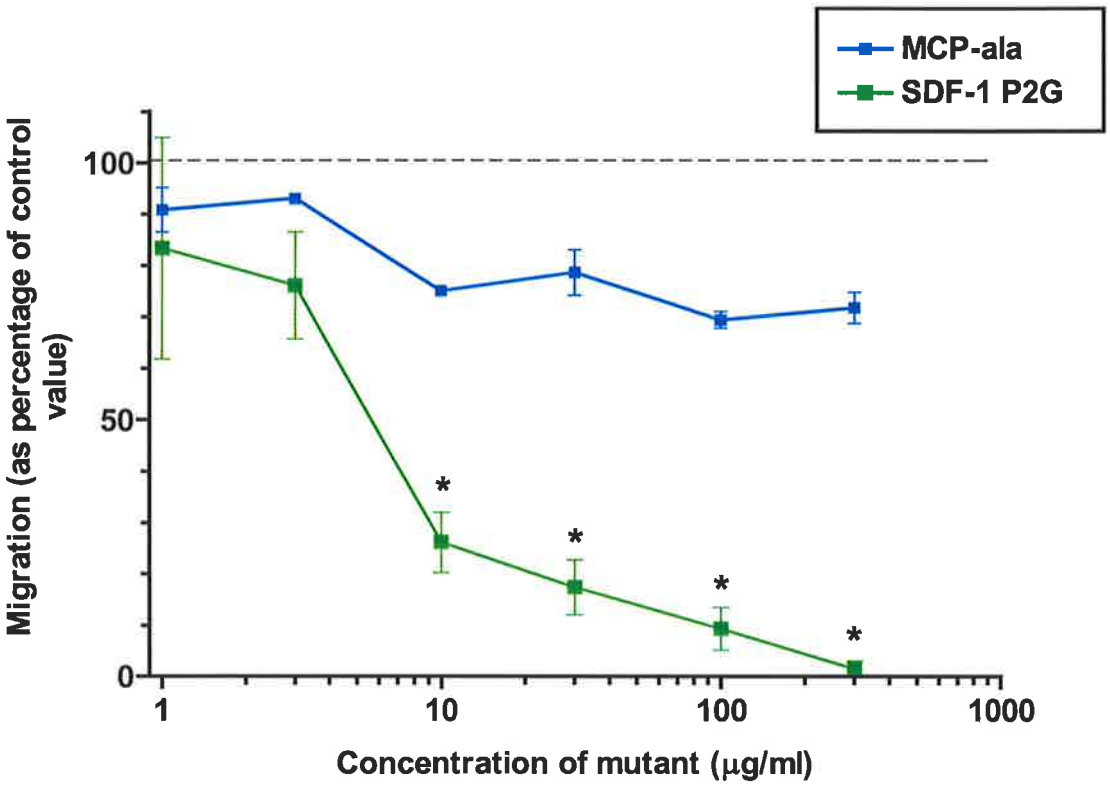
MCP-ala
SDF-1 P2G
Migration (as percentage of control value)
100
50
0
1
10
100
1000
Concentration of mutant (μg/ml)
*
*
*
*

Figure 5.5: *I-TAC 4-79 inhibits I-TAC/CXCL11-, IP-10/CXCL10- and Mig/CXCL9-mediated migration of PLP-reactive lymphocytes.* Lymph nodes were removed from PLP/CFA-immunised mice and single cell suspensions were prepared. Cells were then cultured for 4 days in the presence of $PLP_{139-151}$. All cells were loaded with calcein fluorophore. RPMI-BSA (600 µl) containing 50 ng/ml I-TAC/CXCL11 [A], 50 ng/ml IP-10/CXCL10 [B] or 100 ng/ml Mig/CXCL9 [C] and varying concentrations of either I-TAC 4-79 or MCP-ala (control peptide) were added to the lower chamber of a Transwell® plate, and 1 x 10^6 cells (in 100 µl) were loaded into the upper chamber. Assays were conducted at 37°C for 3 hours, after which the level of fluorescence in the lower chambers was determined (Section 2.5.4). Total migration was then converted to a percentage of the level observed with the agonist alone. * indicates a statistically significant difference from the agonist alone and the corresponding concentration of MCP-ala at $p<0.05$. Data points represent the mean value ± SEM (n = 4, from 4 independent experiments).

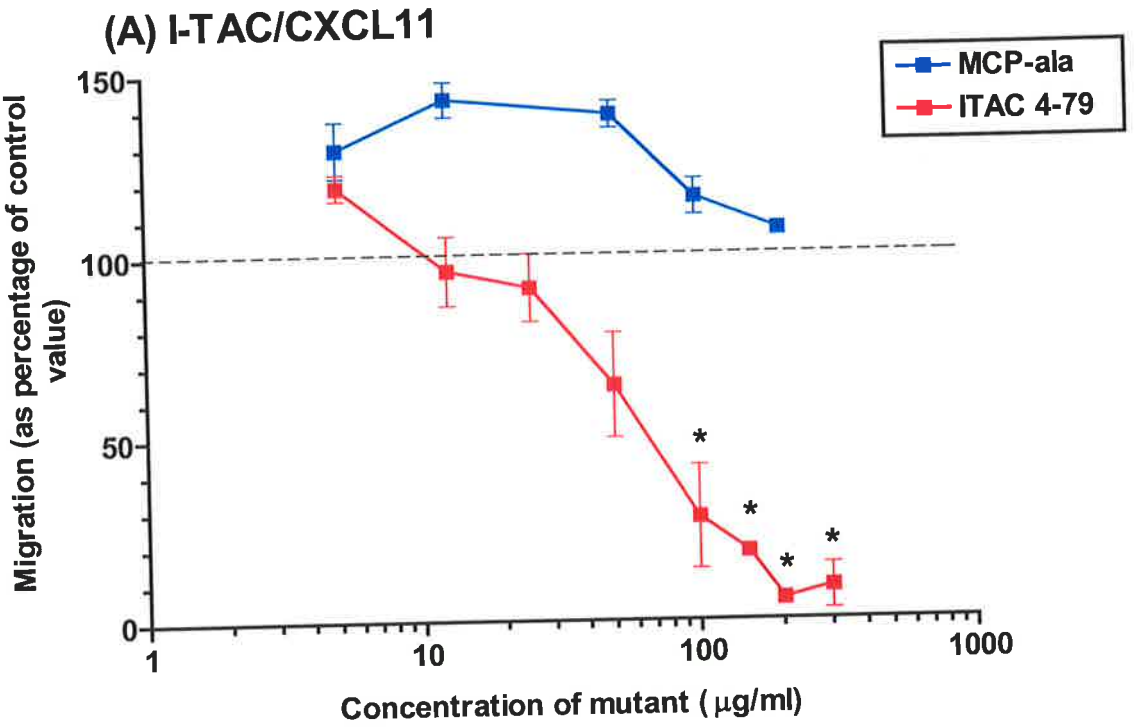
(A) I-TAC/CXCL11
MCP-ala
ITAC 4-79
Migration (as percentage of control value)
150
100
50
0
1
10
100
1000
Concentration of mutant (μg/ml)
*
*
*
*

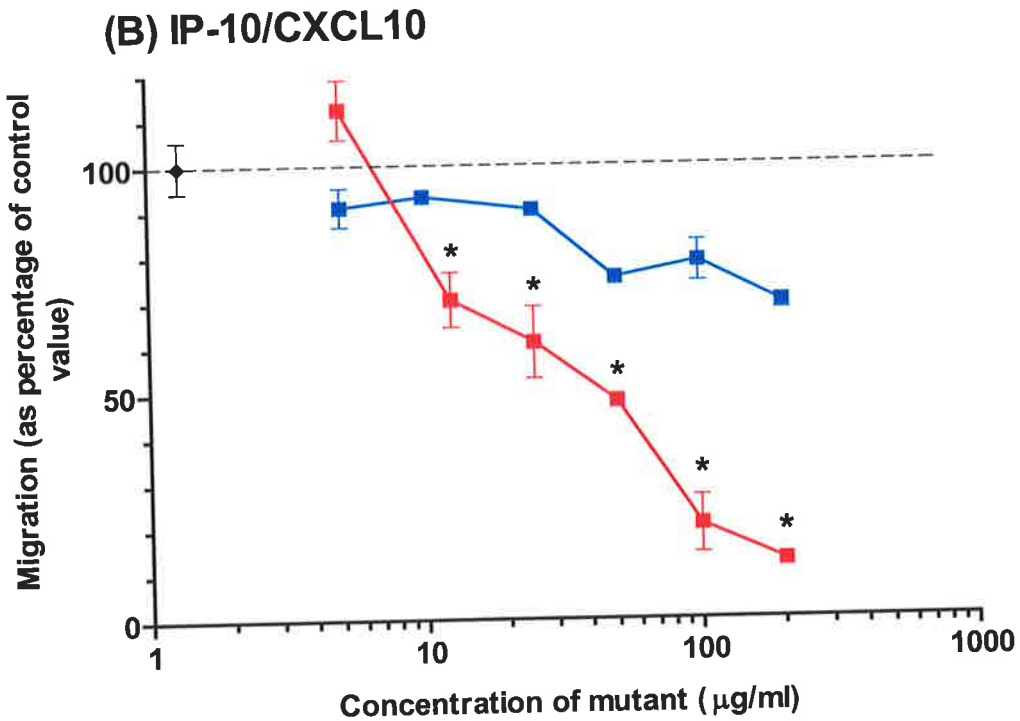
(B) IP-10/CXCL10
Migration (as percentage of control value)
100
50
0
1
10
100
1000
Concentration of mutant (μg/ml)
*
*
*
*
*

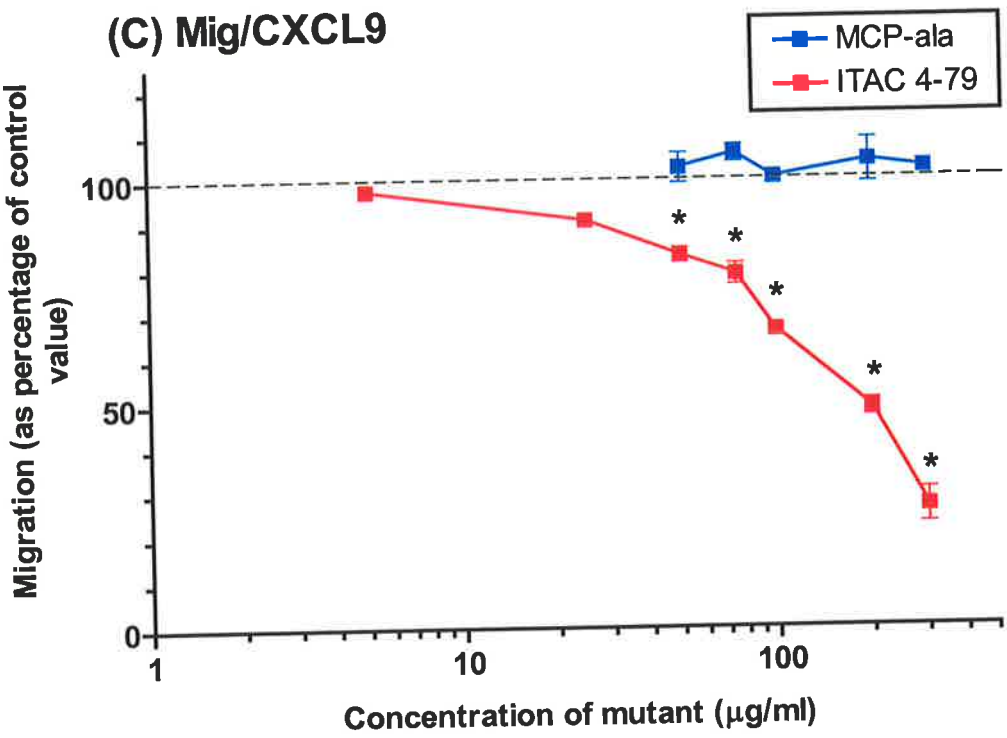
(C) Mig/CXCL9
MCP-ala
ITAC 4-79
Migration (as percentage of control value)
100
50
0
1
10
100
Concentration of mutant (μg/ml)
*
*
*
*
*

Figure 5.6: *RANTES 9-68 inhibits RANTES/CCL5 and MIP-1β/CCL4-mediated migration of Salmonella enteriditis-reactive T lymphocytes.* Balb/c mice were injected i.p. with 3 x 10^5 cfu *Salmonella enteriditis* (Section 2.2.5). Five days later, peritoneal washouts were performed and single cell suspensions were prepared (Section 2.3.3). Cells were then passed through nylon wool columns (Section 2.3.4) and the T lymphocytes were collected. All cells were loaded with calcein fluorophore. RPMI-BSA (600 µl) containing 50 ng/ml RANTES/CCL5 [A] or 50 ng/ml MIP-1β/CCL4 [B] and varying concentrations of either RANTES 9-68 or MCP-ala (control peptide) were added to the lower chamber of a Transwell® plate, and 3 x 10^5 cells (in 100 µl) were loaded into the upper chamber. Assays were conducted at 37°C for 3 hours, after which the level of fluorescence in the lower chambers was determined (Section 2.5.4). Total migration was then converted to a percentage of the level observed with the agonist alone. * indicates a statistically significant difference from the agonist alone and the corresponding concentration of MCP-ala at $p<0.05$. Data points represent the mean value ± SEM ($n = 2$).

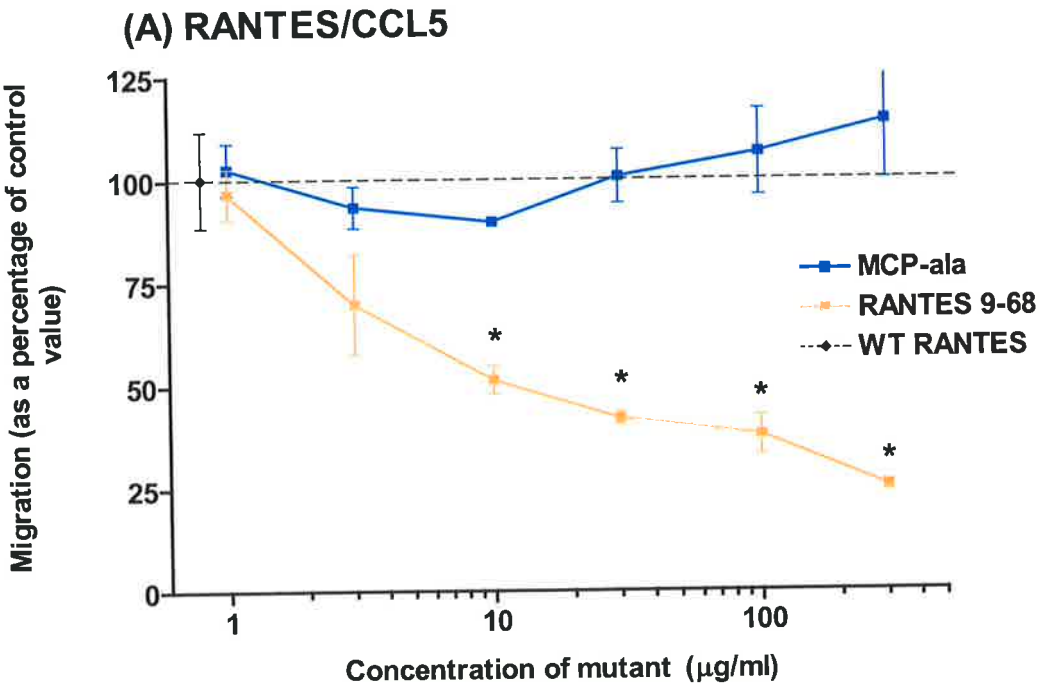
(A) RANTES/CCL5
Migration (as a percentage of control value)
125
100
75
50
25
0
1
10
100
Concentration of mutant (μg/ml)
MCP-ala
RANTES 9-68
WT RANTES
*
*
*
*

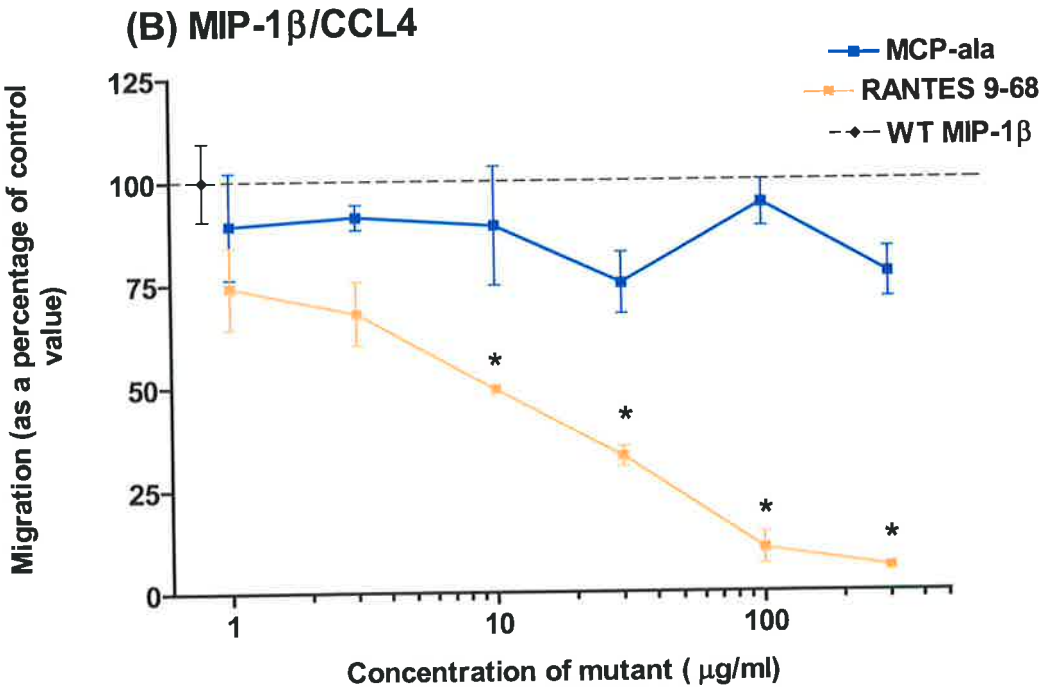
(B) MIP-1β/CCL4
Migration (as a percentage of control value)
125
100
75
50
25
0
1
10
100
Concentration of mutant (μg/ml)
MCP-ala
RANTES 9-68
WT MIP-1β
*
*
*
*

Table 5.1: The effect of antagonist treatment on the development of clinical EAE. EAE was induced in SJL/J mice. The mice were treated with either the relevant antagonist or MCP-ala, starting Day 1 post-immunisation for every second day until Day 15 post-immunisation. Throughout the course of clinical disease various parameters were analysed, and are presented below.

	Delay in disease onset[a]	**Difference in max clinical score [b]**	**Advance in disease recovery [a]**	**Reduction in disease length [b]**	**# days of significantly lower clinical score [b]**	**# mice sick**
SDF-1 P2G Experiment 1 (Section 5.2.2.1)	1 day	- 1.3 **	1 day	3 days **	5 days during peak disease	8/9
SDF-1 P2G Experiment 2 (Section 5.2.2.1)	1 day	- 1.2	None	3 days *	1 day at onset, 2 days during peak, 2 days of recovery	6/8
SDF-1 P2G Experiment 3 (Section 5.2.2.1)	2 ½ days **	- 0.7 *	None	> 2 ½ days**	4 days during onset	8/8
I-TAC 4-79 Experiment 1 (Section 5.2.2.2)	~ 1 day *	- 0.5	~ 1 day	> 1 ½ days *	3 days during onset, 1 day at peak disease	9/9
I-TAC 4-79 Experiment 2 (Section 5.2.2.2)	2 ½ days**	- 0.9	~ 1 day *	> 3 ½ days**	3 days during onset, 1 day of recovery	8/8
I-TAC 4-79 Experiment 3 (Section 5.2.2.2)	> 1 ½ days *	- 0.8 *	None	> 2 ½ days *	2 days during onset, 4 days during peak disease	9/10
RANTES 9-68 Experiment 1 (Section 5.2.2.3)	> 2 ½ days**	- 1.3 **	None	> 3 ½ days**	3 days during peak disease, 2 days of recovery	7/8
RANTES 9-68 Experiment 2 (Section 5.2.2.3)	2 days **	-0.9 *	None	> 2 days *	1 day at disease onset, 2 days during peak disease	8/8
RANTES 9-68 Experiment 3 (Section 5.2.2.3)	> 3 days *	-1.3 **	None	> 3 days *	2 days during disease onset, 4 days during peak disease	6/7

[a] Excluding non-responders (mice that never showed clinical manifestation of disease)
[b] Including non-responders (mice that never showed manifestation were classified as showing disease length of 0, and a maximum clinical score of 0)
* Statistically significant from the MCP-ala treatment group at $p < 0.05$
** Statistically significant from the MCP-ala treatment group at $p < 0.01$

Figure 5.7: *The effect of SDF-1 P2G treatment on the development of EAE.* SJL/J mice were injected s.c. with 50 μg of $PLP_{139-151}$ in CFA (Section 2.2.1). Two hours before and two days after the injection of emulsion, the mice received 5 μg of pertussigen (i.v.). On days 1, 3, 5, 7, 9, 11, 13 and 15 post-induction, the mice received an i.p. injection of 100 μg of SDF-1 P2G or 100 μg of MCP-ala (Section 2.2.4). Mice were scored for clinical manifestations of disease over a period of 25 days post-immunisation. The data presented were obtained from 3 independent experiments. Data are presented as mean clinical disease score ± SEM as a function of days after immunisation (n = 25). * indicates a significant difference from MCP-ala treatment at $p<0.05$ (ANOVA). ** indicates a significant difference from MCP-ala treatment at $p<0.005$ (ANOVA).

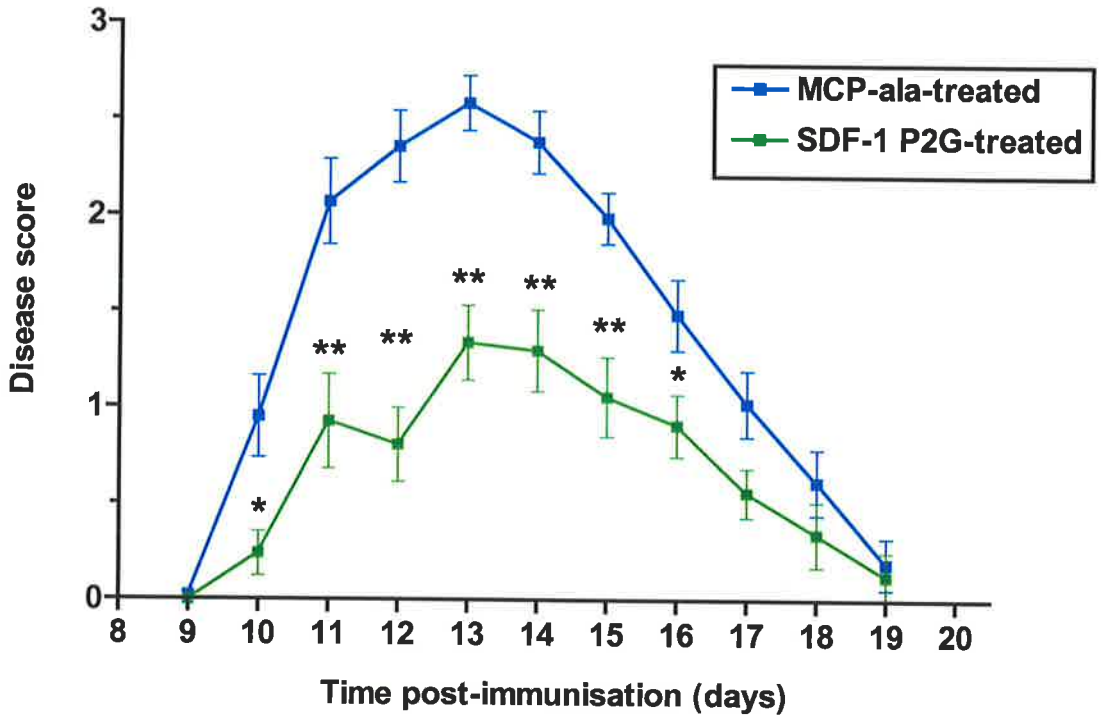
MCP-ala-treated
SDF-1 P2G-treated
Disease score
Time post-immunisation (days)
0
1
2
3
8
9
10
11
12
13
14
15
16
17
18
19
20
*
**
**
**
**
*

Figure 5.8: *The effect of I-TAC 4-79 treatment on the development of EAE.* SJL/J mice were injected s.c. with 50 μg of $PLP_{139-151}$ in CFA (Section 2.2.1). Two hours before and two days after the injection of emulsion, the mice received 5 μg of pertussigen (i.v.). On days 1, 3, 5, 7, 9, 11, 13 and 15 post-induction, the mice received an i.p. injection of 250 μg of I-TAC 4-79 or 250 μg of MCP-ala (Section 2.2.4). Mice were scored for clinical manifestations of disease over a period of 25 days post-immunisation. The data presented were obtained from 3 independent experiments. Data are presented as mean clinical disease score ± SEM as a function of days after immunisation (n = 26). * indicates a significant difference from MCP-ala treatment at $p<0.05$ (ANOVA). ** indicates a significant difference from MCP-ala treatment at $p<0.005$ (ANOVA).

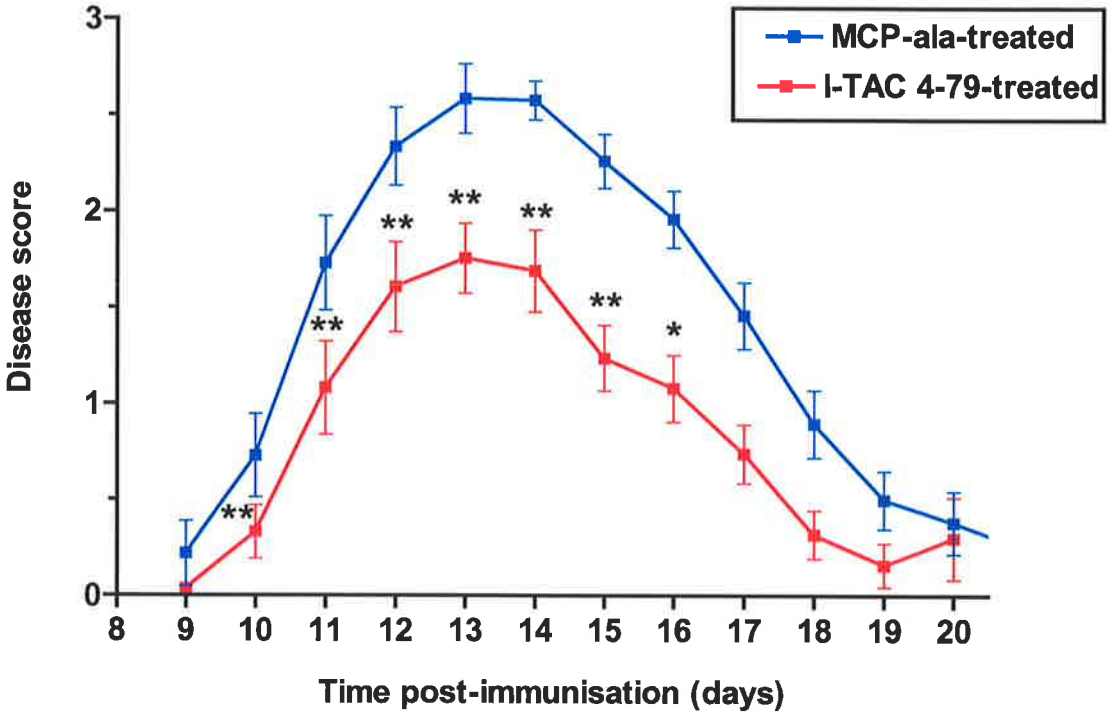
MCP-ala-treated
I-TAC 4-79-treated
Disease score
Time post-immunisation (days)
0
1
2
3
8
9
10
11
12
13
14
15
16
17
18
19
20
**
**
**
**
**
**
*

Figure 5.9: *The effect of RANTES 9-68 treatment on the development of EAE.* SJL/J mice were injected s.c. with 50 μg of $PLP_{139-151}$ in CFA (Section 2.2.1). Two hours before and two days after the injection of emulsion, the mice received 5 μg of pertussigen (i.v.). On days 1, 3, 5, 7, 9, 11, 13 and 15 post-induction, the mice received an i.p. injection of 100 μg of RANTES 9-68 or 100 μg of MCP-ala (Section 2.2.4). Mice were scored for clinical manifestations of disease over a period of 25 days post-immunisation. The data presented were obtained from 3 independent experiments. Data are presented as mean clinical disease score ± SEM as a function of days after immunisation (n = 23). ** indicates a significant difference from MCP-ala treatment at $p<0.005$ (ANOVA).

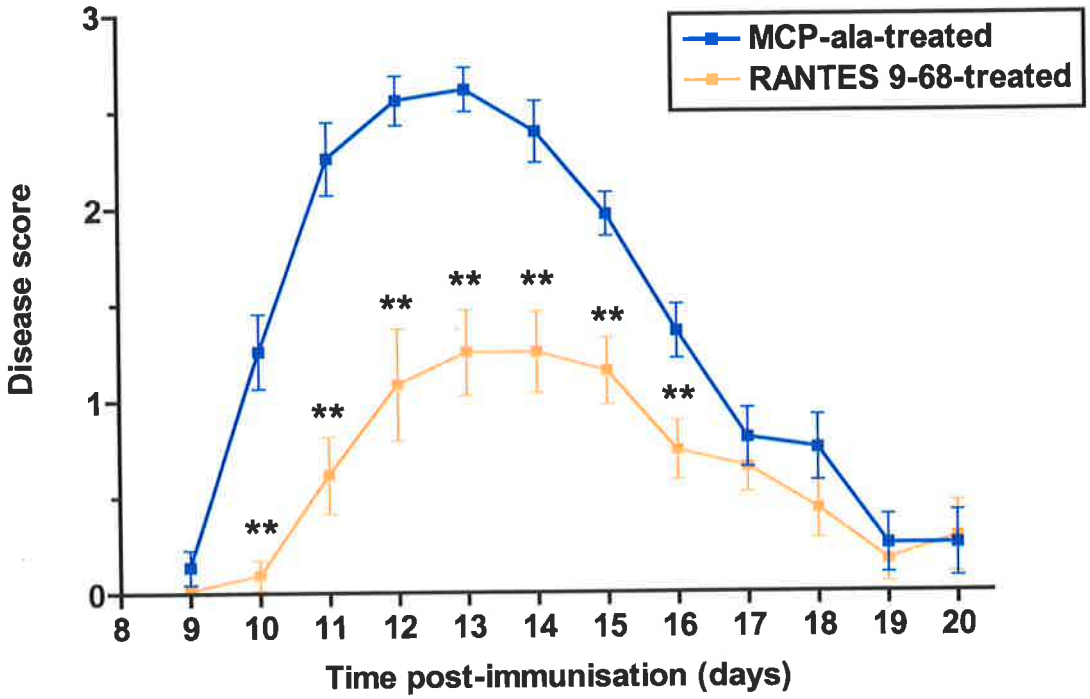
MCP-ala-treated
RANTES 9-68-treated
Disease score
Time post-immunisation (days)
0
1
2
3
8
9
10
11
12
13
14
15
16
17
18
19
20
**

Table 5.2: Decrease in the number of histopathological lesions in the CNS of SDF-1 P2G-treated mice.

Treatment group	Lesions/Transverse Section[a]
MCP-ala [b]	2.97 ± 0.14
SDF-1 P2G [b]	1.02 ± 0.11***

[a] data are the mean ± S.E.M. Total number of histopathological lesions enumerated from the thoracic lumbar region of the spinal cords from 3 representative animals from each treatment group. Thirty six 10 μm sections from each mouse were assessed for mononuclear cell infiltration in the meninges and white and grey matter following haematoxylin and eosin staining at 12 days post-induction of EAE.

[b]Treatment as follows: EAE was induced by immunisation with 50 μg $PLP_{139-151}$ and pertussigen, and on days 1, 3, 5, 7, 9 and 11 the mice were given 100 μg i.p. of SDF-1 P2G or control peptide (MCP-ala). At the time of sacrifice, disease scores (mean ± SEM) from the control mice versus the SDF-1 P2G-treated mice were 2.75 ± 0.32 and 1.66 ± 0.37, respectively.

***, Statistically significant from the control values at $p < 0.0001$.

Table 5.3: Decrease in the number of histopathological lesions in the CNS of I-TAC 4-79-treated mice.

Treatment group	Lesions/Transverse Section[a]
MCP-ala [b]	2.81 ± 0.10
I-TAC 4-79 [b]	2.02 ± 0.14***

[a] data are the mean ± S.E.M. Total number of histopathologcal lesions enumerated from the thoracic lumbar region of the spinal cords from 3 representative animals from each treatment group. Thirty six 10 μm sections from each mouse were assessed for mononuclear cell infiltration in the meninges and white and grey matter following haematoxylin and eosin staining at 12 days post-induction of EAE.

[b]Treatment as follows: EAE was induced by immunisation with 50 μg $PLP_{139-151}$ and pertussigen, and on days 1, 3, 5, 7, 9 and 11 the mice were given 250 μg i.p. of I-TAC 4-79 or control peptide (MCP-ala). At the time of sacrifice, disease scores (mean ± SEM) from the control mice versus the I-TAC 4-79-treated mice were 2.64 ± 0.26 and 1.93 ± 0.11, respectively.

***, Statistically significant from the control values at $p < 0.0001$.

Table 5.4: Decrease in the number of histopathological lesions in the CNS of RANTES 9-68-treated mice.

Treatment group	Lesions/Transverse Section[a]
MCP-ala [b]	2.97 ± 0.14
RANTES 9-68 [b]	0.88 ± 0.10***

[a] data are the mean ± S.E.M. Total number of histopathologlcal lesions enumerated from the thoracic lumbar region of the spinal cords from 3 representative animals from each treatment group. Thirty six 10 μm sections from each mouse were assessed for mononuclear cell infiltration in the meninges and white and grey matter following hAematoxylin and eosin staining at 12 days post-induction of EAE.

[b]Treatment as follows: EAE was induced by immunisation with 50 μg $PLP_{139-151}$ and pertussigen, and on days 1, 3, 5, 7, 9 and 11 the mice were given 100 μg i.p. of RANTES 9-68 or control peptide (MCP-ala). At the time of sacrifice, disease scores (mean ± SEM) from the control mice versus the RANTES 9-68-treated mice were 2.75 ± 0.32 and 1.44 ± 0.33, respectively.

***, Statistically significant from the control values at $p < 0.0001$.

Figure 5.10: *Effect of administration of chemokine antagonists on the histopathology of EAE in the CNS.* SJL/J mice were injected s.c. with 50 μg $PLP_{139-151}$ in CFA (Section 2.2.1). Two hours before and two days after the injection of emulsion, the mice received 5 μg of pertussigen (i.v.). On days 1, 3, 5, 7, 9, and 11 post-induction, the mice received an i.p. injection of the relevant antagonist or of MCP-ala (Section 2.2.4). Twelve days post-immunisation, the mice were sacrificed, perfused to remove circulating leukocytes (Section 2.6.1), the spinal cord was removed, frozen in OCT and 10 μm cryostat sections were prepared. Representative photomicrographs of haematoxylin/eosin-stained (Section 2.6.5) spinal cord sections from [A] Day 0 (normal) spinal cord tissue, [B] MCP-ala-treated mice, [C] SDF-1 P2G-treated mice, [D] I-TAC 4-79-treated mice or [E] RANTES 9-68-treated mice were assessed for mononuclear cell infiltration in the meninges and white and grey matter. These photomicrographs are representative of 36 sections from 3 mice per treatment group. At the time of sacrifice, the mean disease scores (mean ± SEM) from the MCP-ala-, SDF-1 P2G-, I-TAC 4-79-, and RANTES 9-68-treated mice were 2.75 ± 0.32, 1.66 ± 0.37, 1.93 ± 0.11, and 1.44 ± 0.33, respectively. Shown are 2 representative images of each condition, captured using the 4X objective.

(A) Day 0

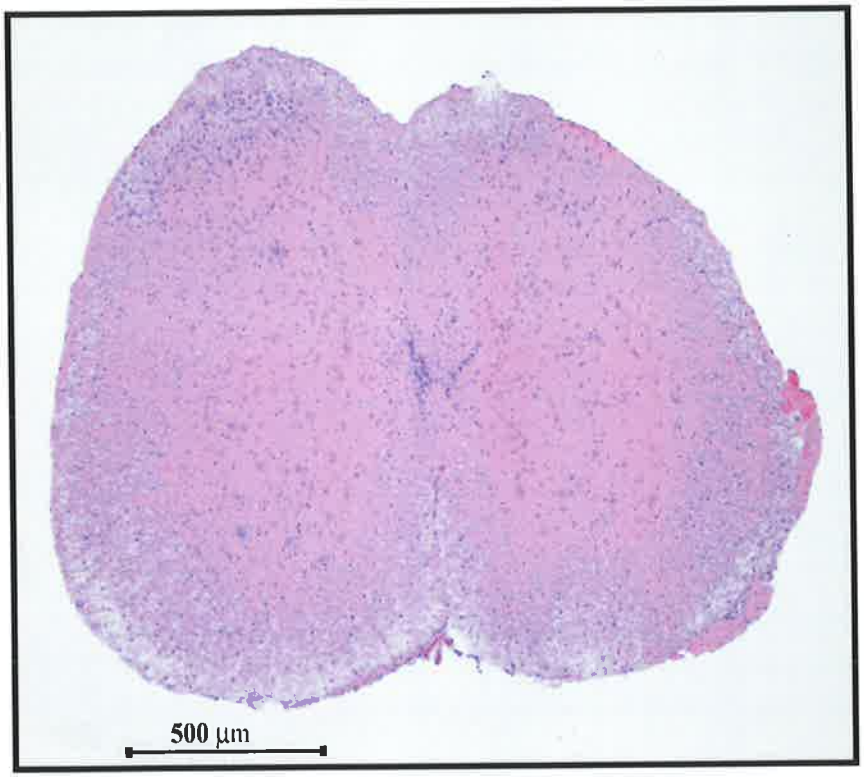

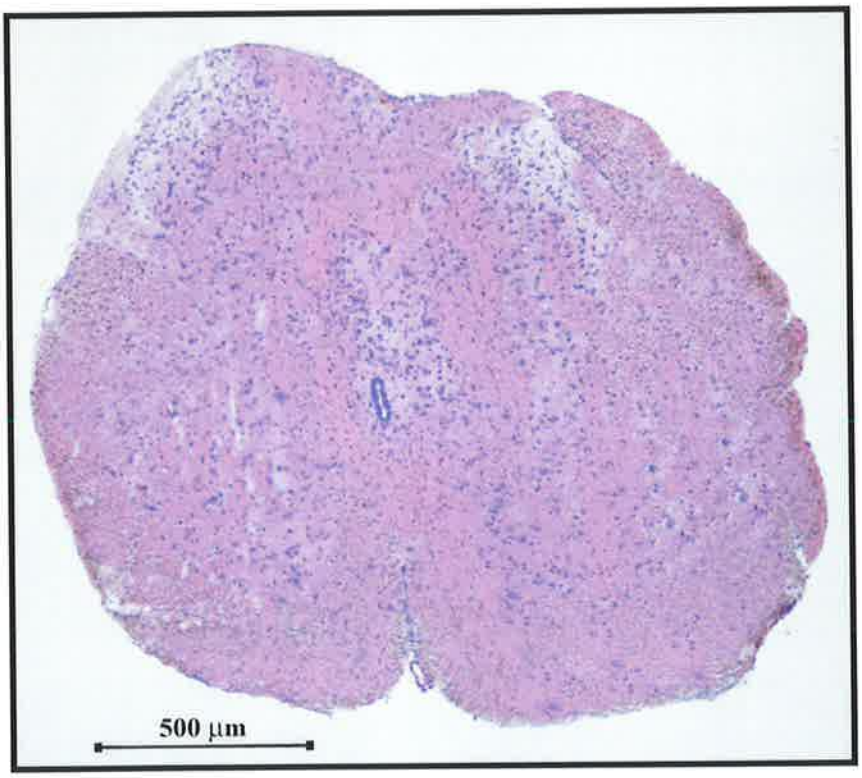

(B) MCP-ala-treated

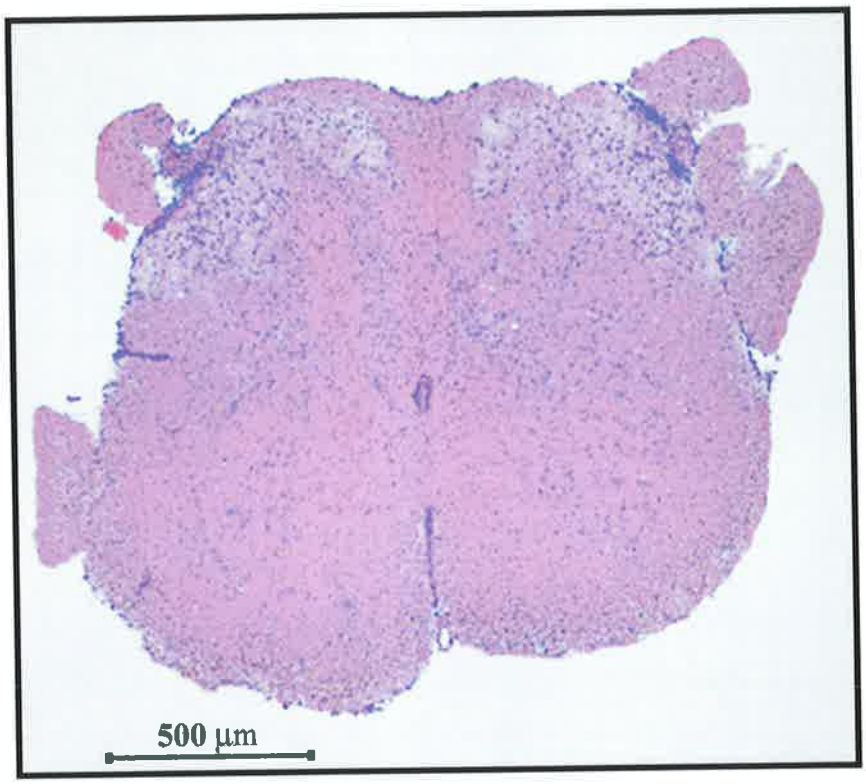

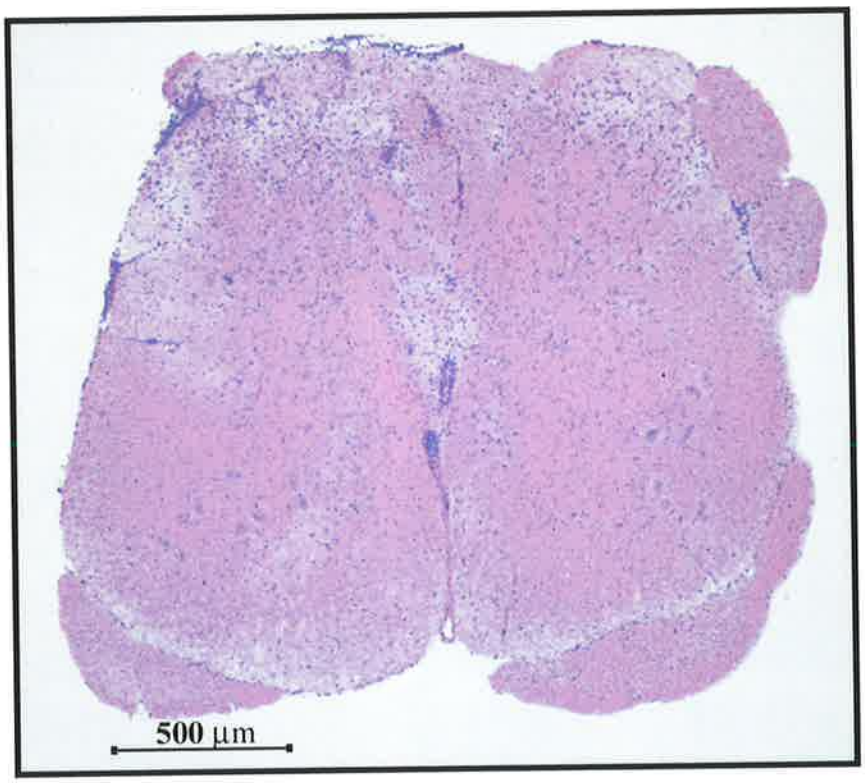

(C) SDF-1 P2G-treated

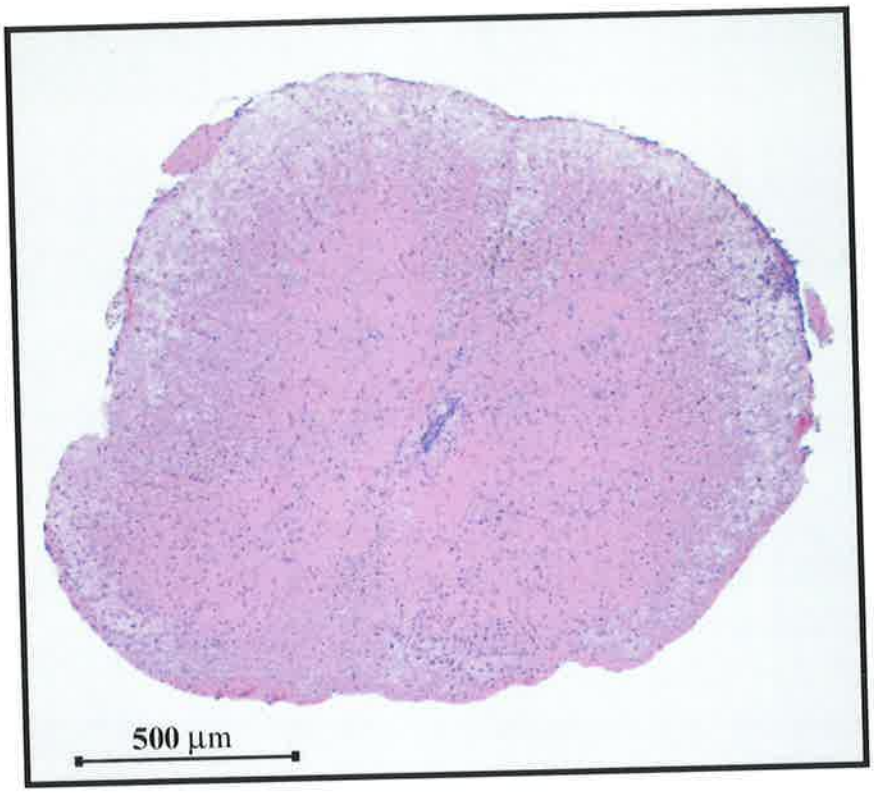

(D) I-TAC 4-79-treated

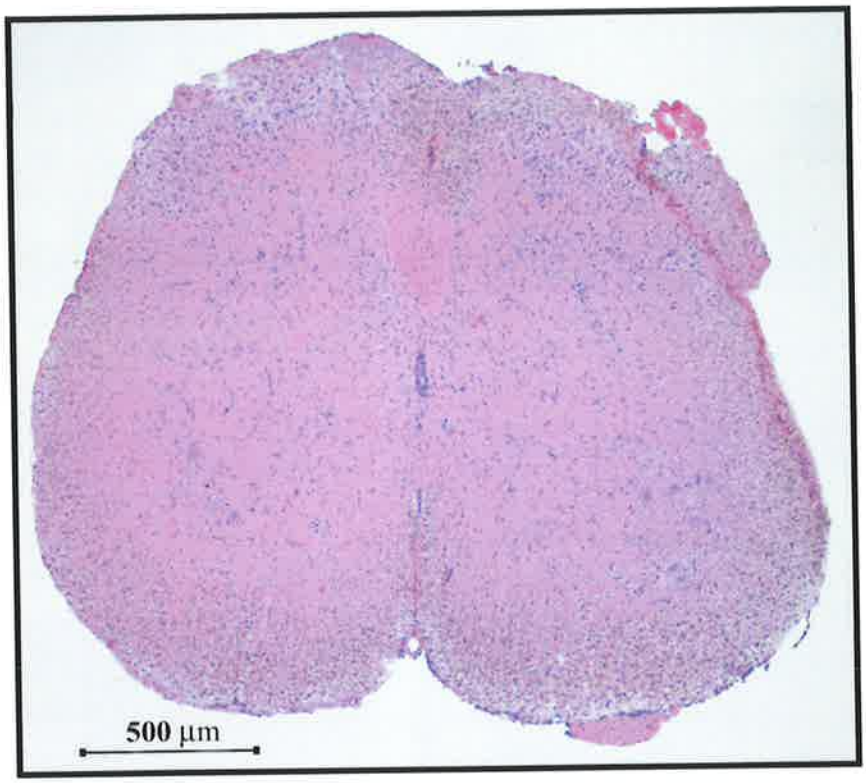

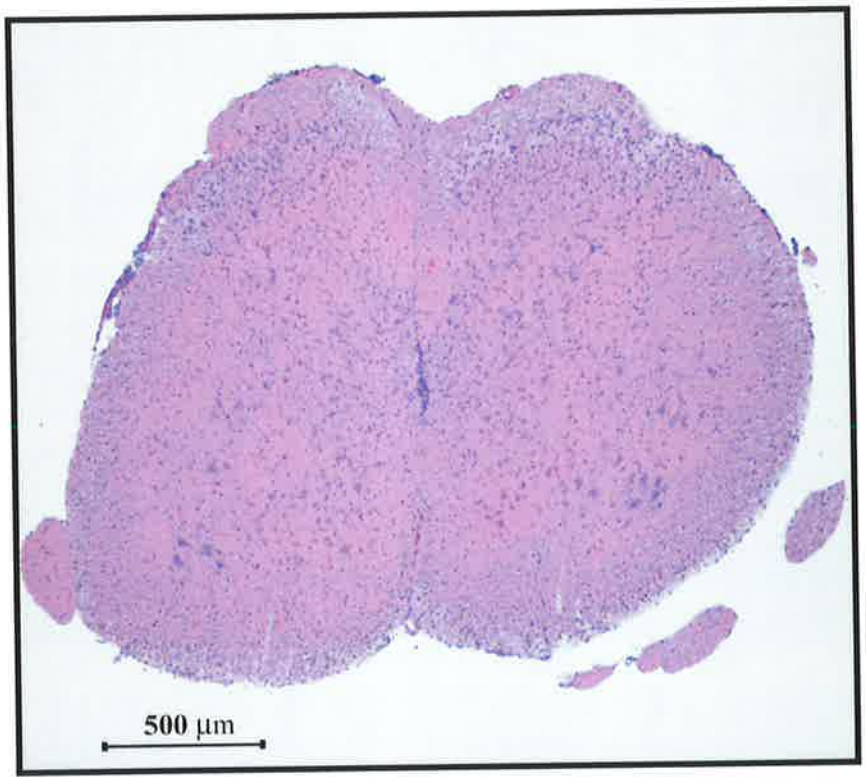

(E) RANTES 9-68-treated

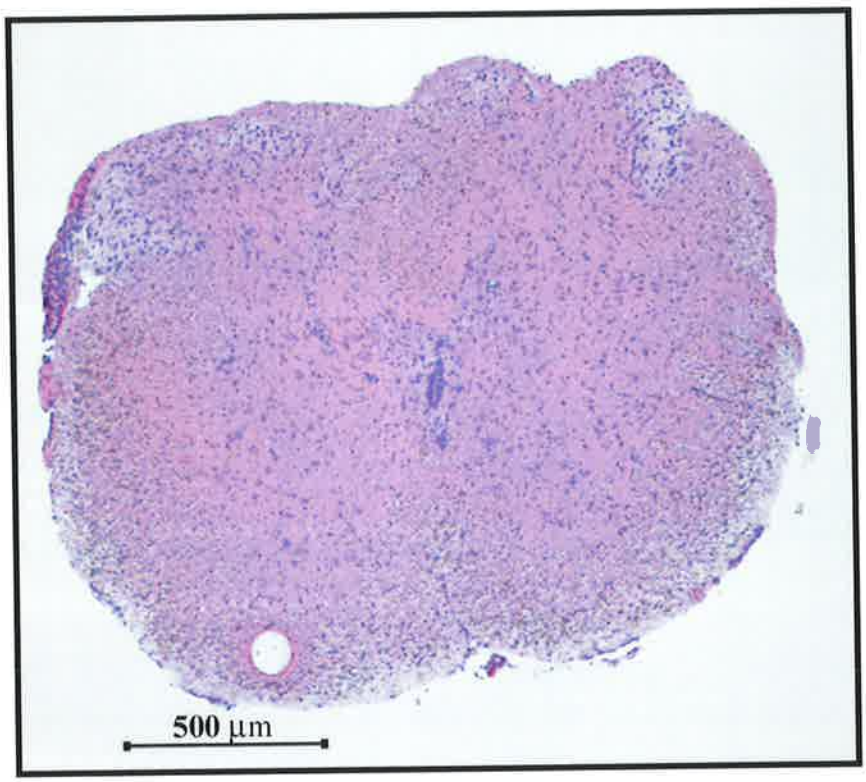

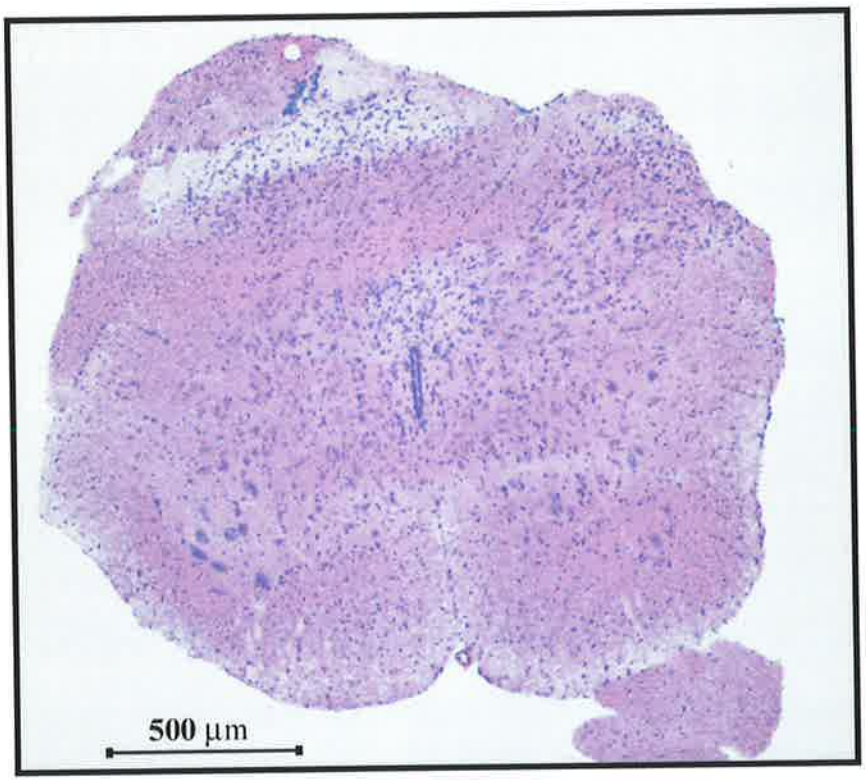

Figure 5.11. *The effect of antagonist treatment on the accumulation of cells in the spinal cords.* SJL/J mice were injected s.c. with 50 μg of $PLP_{139-151}$ in CFA (Section 2.2.1). Two hours before and two days after the injection of emulsion, the mice received 5 μg of pertussigen (i.v.). On days 1, 3, 5, 7, 9, and 11 post-immunisation, the mice received an i.p. injection of MCP-ala, SDF-1 P2G, I-TAC 4-79 or RANTES 9-68 (Section 2.2.4). Twelve days post-immunisation (peak disease), following whole animal perfusion, spinal cords were removed and single cell suspensions prepared (Section 2.3.2). The total number of viable cells recovered from each spinal cord was then determined by counting on a haemocytometer after staining with trypan blue. A statistically significant difference between antagonist-treated and MCP-ala-treated mice is indicated by an asterisk ($p < 0.05$). Data are presented as mean ± SEM ($n = 6$).

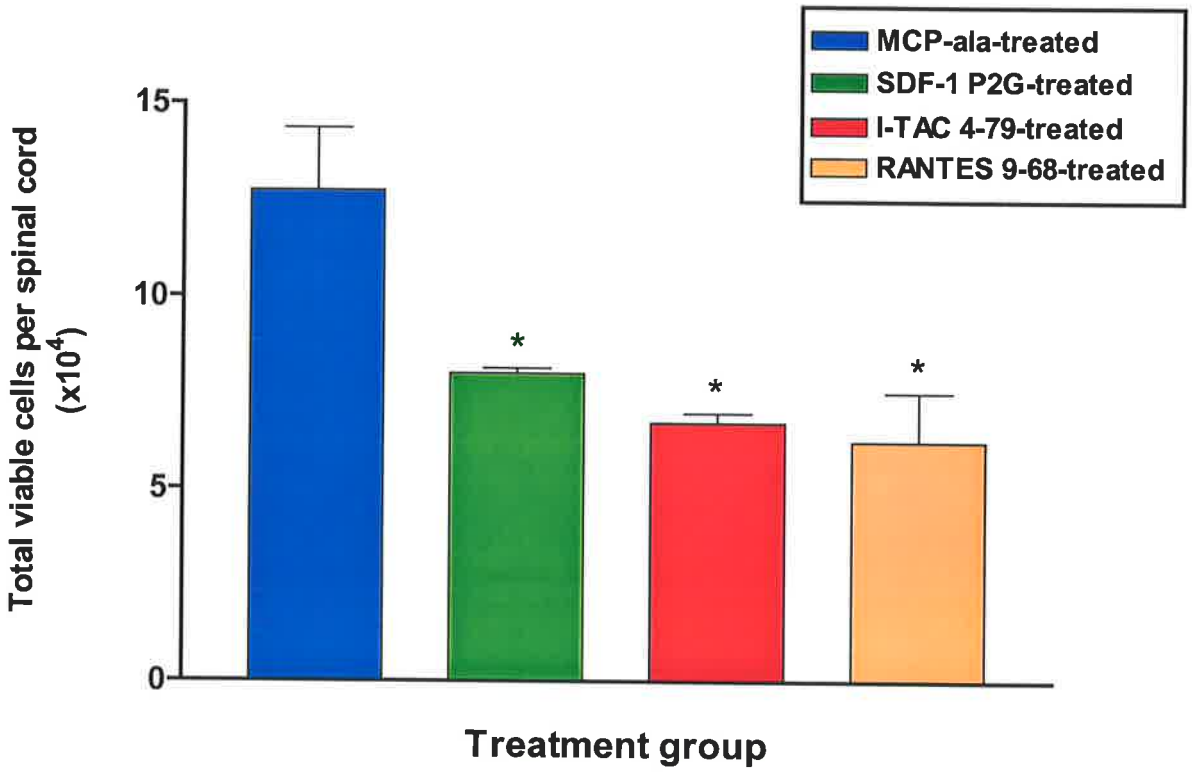
MCP-ala-treated
SDF-1 P2G-treated
I-TAC 4-79-treated
RANTES 9-68-treated
Total viable cells per spinal cord (x10^4)
15
10
5
0
*
*
*
Treatment group

Figure 5.12. *The effect of antagonist treatment on the accumulation of $CD4^+$ T cells in the spinal cords.* SJL/J mice were injected s.c. with 50 μg of $PLP_{139-151}$ in CFA (Section 2.2.1). Two hours before and two days after the injection of emulsion, the mice received 5 μg of pertussigen (i.v.). On days 1, 3, 5, 7, 9, and 11 post-immunisation, the mice received an i.p. injection of MCP-ala, SDF-1 P2G, I-TAC 4-79 or RANTES 9-68 (Section 2.2.4). Twelve days post-immunisation (peak disease), following whole animal perfusion, spinal cords were removed and single cell suspensions prepared (Section 2.3.2). The total number of viable cells recovered from each spinal cord was then determined by counting on a haemocytometer after staining with trypan blue. Cells were then labelled with anti-CD4 and analysed by flow cytometry, gating on lymphocytes using forward and side scatter characteristics. The percentage of CD4-positive cells was multiplied by the total cell count value, such that the absolute number of $CD4^+$ cells could be determined. A statistically significant difference between antagonist-treated and MCP-ala-treated mice is indicated by an asterisk ($p < 0.05$). Data are presented as mean ± SEM ($n = 6$).

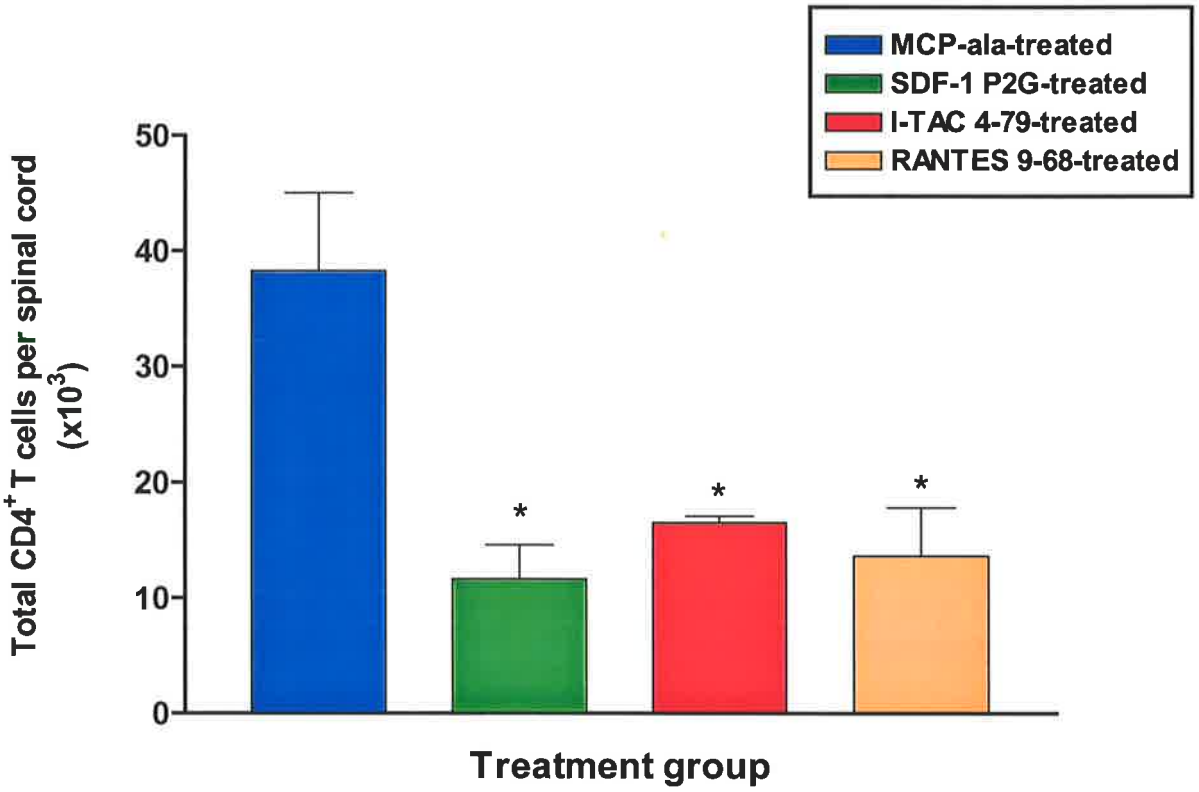
MCP-ala-treated
SDF-1 P2G-treated
I-TAC 4-79-treated
RANTES 9-68-treated
Total CD4+ T cells per spinal cord (x10^3)
50
40
30
20
10
0
*
*
*
Treatment group

Figure 5.13. *The effect of SDF-1 P2G treatment on the percentage of $CD4^+$ T cells expressing CXCR4 in the CNS.* SJL/J mice were injected s.c. with 50 μg of $PLP_{139-151}$ in CFA (Section 2.2.1). Two hours before and two days after the injection of emulsion, the mice received 5 μg of pertussigen (i.v.). On days 1, 3, 5, 7, 9 and 11 post-immunisation, the mice received an intraperitoneal injection of MCP-ala or SDF-1 P2G (Section 2.2.4). BrdU was administered as described (Section 2.2.6). At twelve days post-immunisation, following whole animal perfusion, spinal cords were removed and single cell suspensions prepared (Section 2.3.2). The cells were labelled with anti-BrdU, anti-CD4 and anti-CXCR4 antibodies, and then analysed by flow cytometry, gating on lymphocytes using forward and side scatter characteristics. [A] The percentage of $CXCR4^+$ cells was determined as a proportion of the total $CD4^+$ population in each treatment group. [B] Within the $CD4^+$ T cell population, the percentage of $BrdU^+$ (divided) and $BrdU^-$ (non-divided) cells expressing CXCR4 was determined as a proportion of the total $BrdU^+$ or $BrdU^-$ population, accordingly. Data are presented as mean ± SEM (n = 4).

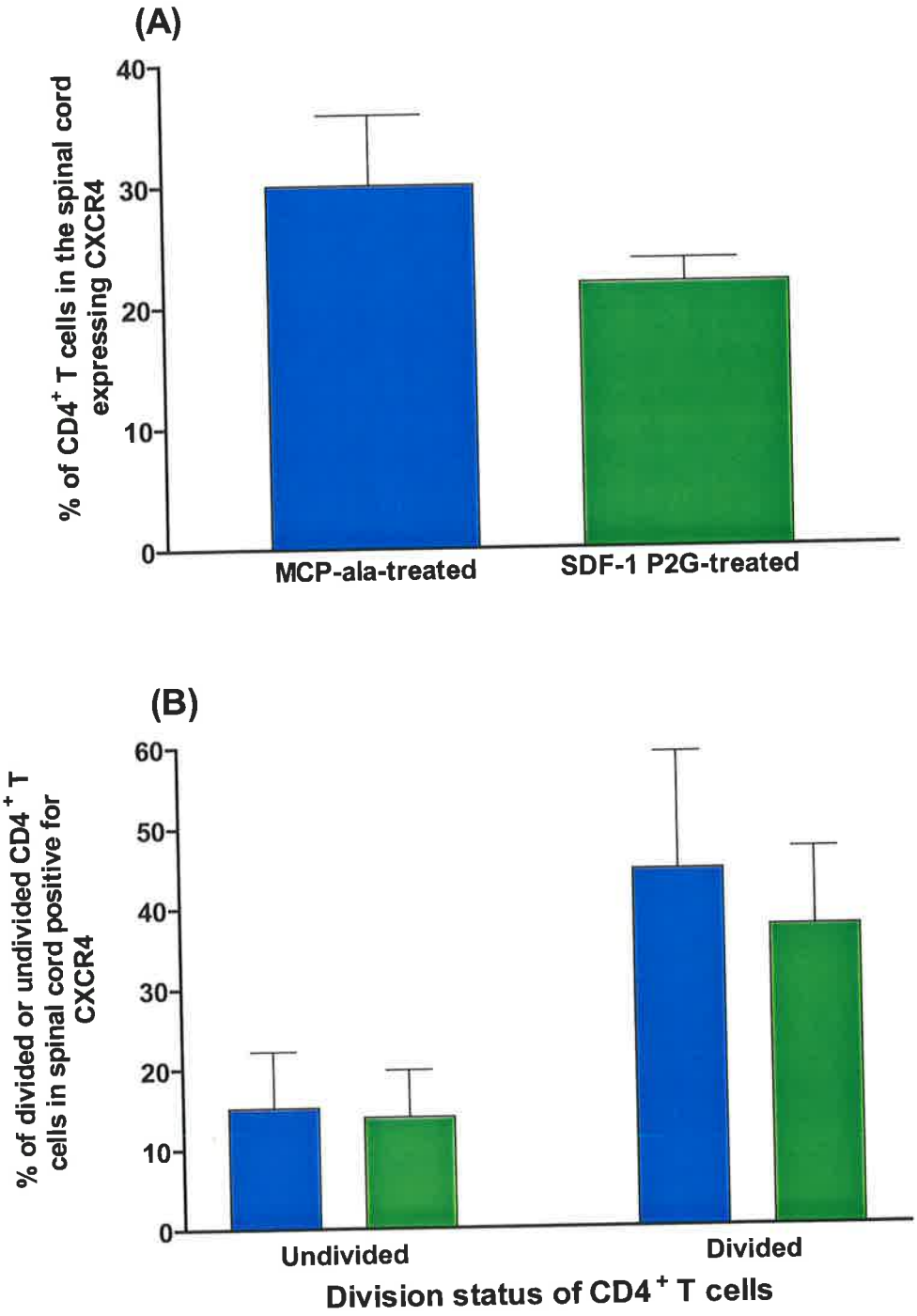
(A)
% of CD4+ T cells in the spinal cord expressing CXCR4
40
30
20
10
0
MCP-ala-treated
SDF-1 P2G-treated
(B)
% of divided or undivided CD4+ T cells in spinal cord positive for CXCR4
60
50
40
30
20
10
0
Undivided
Divided
Division status of CD4+ T cells

Figure 5.14. *The effect of I-TAC 4-79 treatment on the percentage of $CD4^+$ T cells expressing CXCR3 in the CNS.* SJL/J mice were injected s.c. with 50 μg of $PLP_{139-151}$ in CFA (Section 2.2.1). Two hours before and two days after the injection of emulsion, the mice received 5 μg of pertussigen (i.v.). On days 1, 3, 5, 7, 9 and 11 post-immunisation, the mice received an intraperitoneal injection of MCP-ala or I-TAC 4-79 (Section 2.2.4). BrdU was administered as described (Section 2.2.6). At twelve days post-immunisation, following whole animal perfusion, spinal cords were removed and single cell suspensions prepared (Section 2.3.2). The cells were labelled with anti-BrdU, anti-CD4 and anti-CXCR3 antibodies, and then analysed by flow cytometry, gating on lymphocytes using forward and side scatter characteristics. [A] The percentage of $CXCR3^+$ cells was determined as a proportion of the total $CD4^+$ population in each treatment group. [B] Within the $CD4^+$ T cell population, the percentage of $BrdU^+$ (divided) and $BrdU^-$ (non-divided) cells expressing CXCR3 was determined as a proportion of the total $BrdU^+$ or $BrdU^-$ population, accordingly. $^\Psi$, indicates a statistically significant difference between I-TAC 4-79-treated and MCP-ala-treated mice in one-tailed t-test ($p < 0.05$). Data are presented as mean ± SEM ($n = 3$).

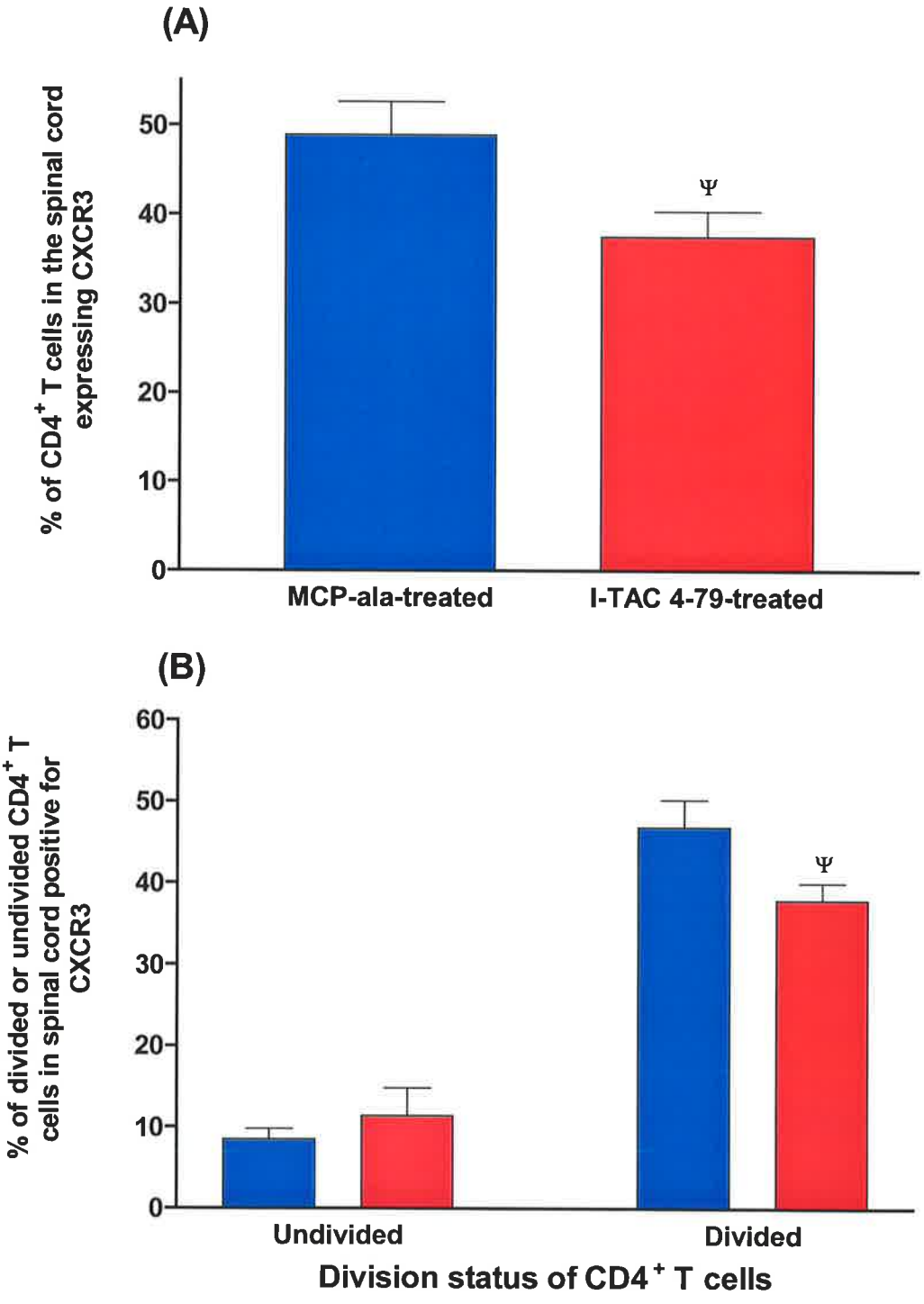
(A)
% of CD4+ T cells in the spinal cord expressing CXCR3
50
40
30
20
10
0
Ψ
MCP-ala-treated
I-TAC 4-79-treated
(B)
% of divided or undivided CD4+ T cells in spinal cord positive for CXCR3
60
50
40
30
20
10
0
Ψ
Undivided
Divided
Division status of CD4+ T cells

Figure 5.15. *The effect of RANTES 9-68 treatment on the percentage of $CD4^+$ T cells expressing CCR5 in the CNS.* SJL/J mice were injected s.c. with 50 μg of $PLP_{139-151}$ in CFA (Section 2.2.1). Two hours before and two days after the injection of emulsion, the mice received 5 μg of pertussigen (i.v.). On days 1, 3, 5, 7, 9 and 11 post-immunisation, the mice received an intraperitoneal injection of MCP-ala or RANTES 9-68 (Section 2.2.4). BrdU was administered as described (Section 2.2.6). At twelve days post-immunisation, following whole animal perfusion, spinal cords were removed and single cell suspensions prepared (Section 2.3.2). The cells were labelled with anti-BrdU, anti-CD4 and anti-CCR5 antibodies, and then analysed by flow cytometry, gating on lymphocytes using forward and side scatter characteristics. [A] The percentage of $CCR5^+$ cells was determined as a proportion of the total $CD4^+$ population in each treatment group. [B] Within the $CD4^+$ T cell population, the percentage of $BrdU^+$ (divided) and $BrdU^-$ (non-divided) cells expressing CCR5 was determined as a proportion of the total $BrdU^+$ or $BrdU^-$ population, accordingly. A statistically significant difference between RANTES 9-68-treated and MCP-ala-treated mice is indicated by an asterisk ($p < 0.05$). Data are presented as mean ± SEM ($n = 4$).

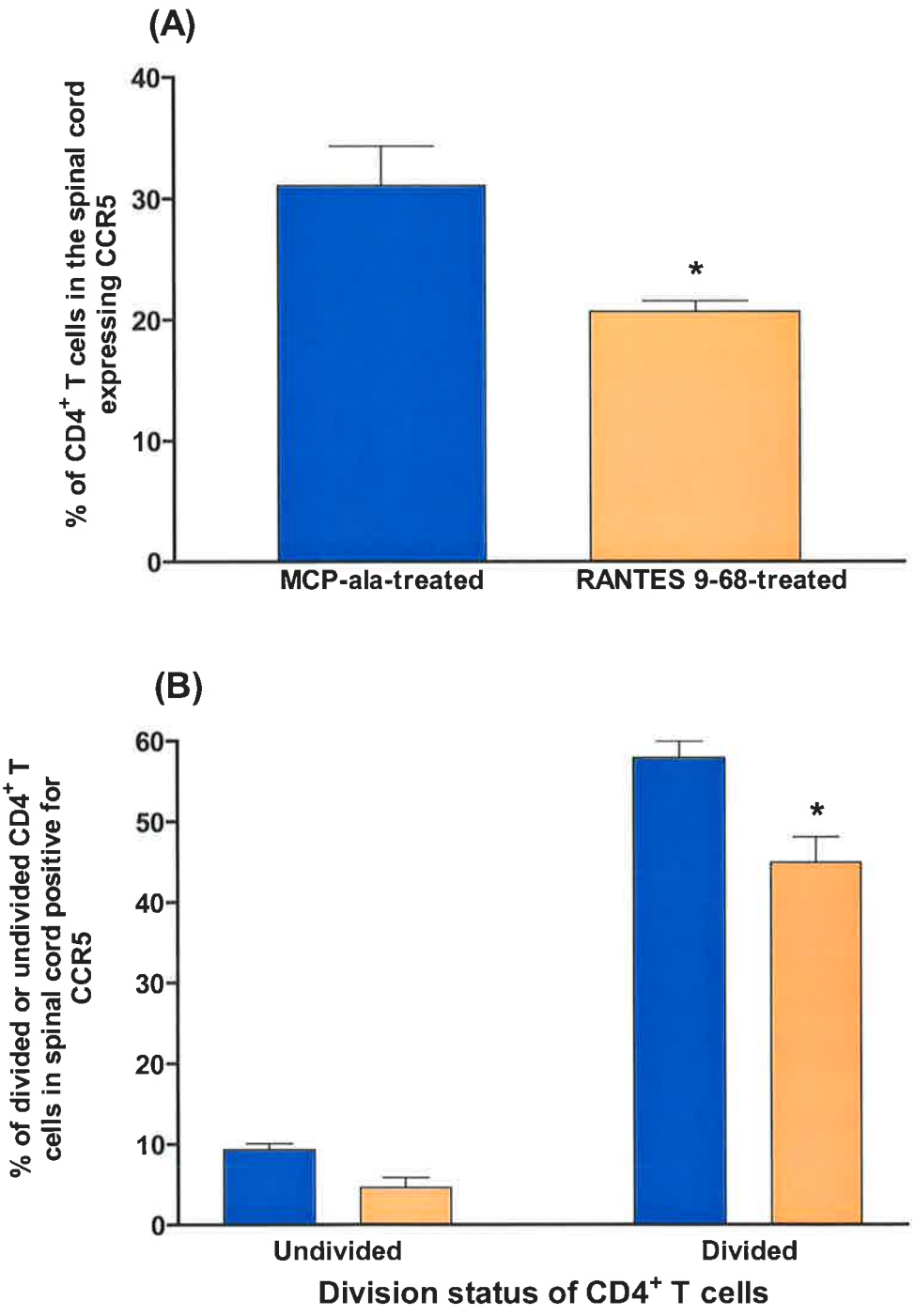
(A)
% of CD4+ T cells in the spinal cord expressing CCR5
40
30
20
10
0
*
MCP-ala-treated
RANTES 9-68-treated
(B)
% of divided or undivided CD4+ T cells in spinal cord positive for CCR5
60
50
40
30
20
10
0
*
Undivided
Divided
Division status of CD4+ T cells

Figure 5.16. *The effect of antagonist treatment on the production of anti-chemokine and anti-antagonist antibodies.* SJL/J mice were injected s.c. with 50 μg of $PLP_{139-151}$ in CFA (Section 2.2.1). Two hours before and two days after the injection of emulsion, the mice received 5 μg of pertussigen (i.v.). On days 1, 3, 5, 7, 9, 11, 13 and 15 post-immunisation, the mice received an intraperitoneal injection of MCP-ala, SDF-1 P2G, I-TAC 4-79 or RANTES 9-68 (Section 2.2.4). After all mice reached a clinical score of zero, mice were sacrificed and the serum was collected (Section 2.3.6). Serum was also collected from untreated mice. Serum was tested for the presence of anti-wild-type chemokine antibodies and anti-antagonist antibodies using a direct ELISA (Section 2.5.5). Serum samples were assessed in triplicate for each mouse at serum dilutions of 1 in 300. The triplicate readings from each mouse were then pooled per treatment group. [A] The levels of anti-mMCP-1 and anti-MCP-ala antibodies present in the serum of treated mice, [B] The levels of anti-SDF-1 and anti-SDF-1 P2G antibodies present in the serum of treated mice, [C] The levels of anti-RANTES and anti-RANTES 9-68 antibodies present in the serum of treated mice, and [D] The levels of anti-mI-TAC and anti-I-TAC 4-79 antibodies present in the serum of treated mice. ** indicates a significant difference from untreated (normal) mice at $p<0.01$. *** indicates a significant difference from untreated (normal) mice at $p<0.001$. Data points represent the mean OD_{490}nm (with the average background reading subtracted) ± SEM (n = 6, for each treatment group).

(A)

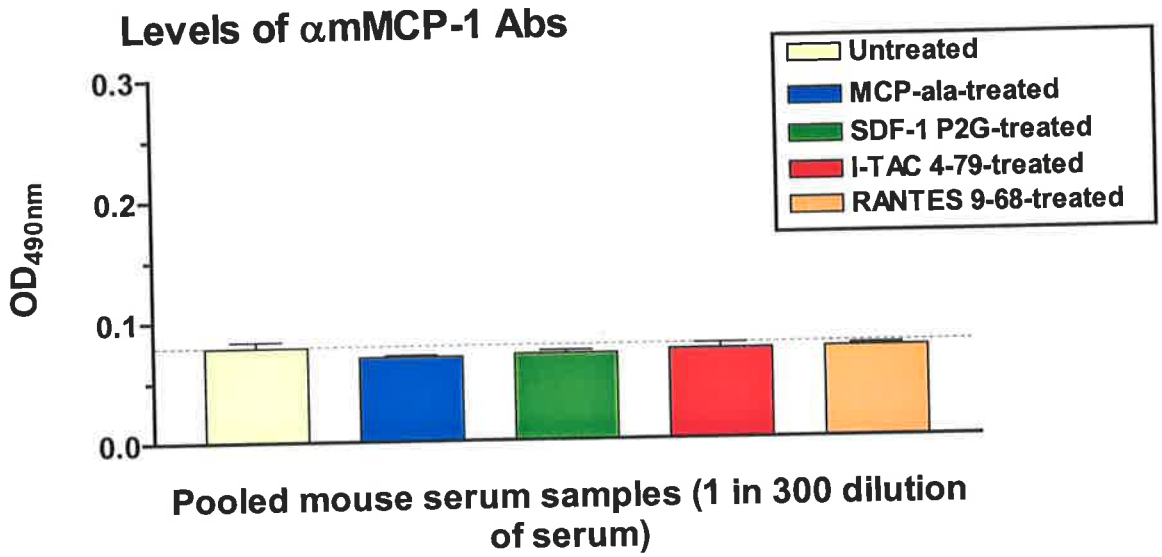
Levels of αmMCP-1 Abs
Untreated
MCP-ala-treated
SDF-1 P2G-treated
I-TAC 4-79-treated
RANTES 9-68-treated
OD490nm
0.3
0.2
0.1
0.0
Pooled mouse serum samples (1 in 300 dilution of serum)

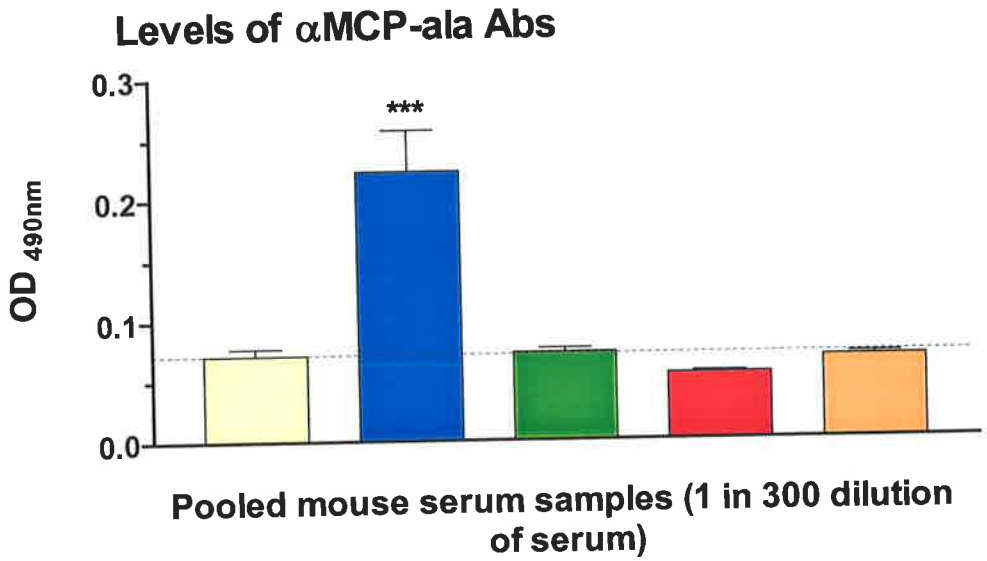
Levels of αMCP-ala Abs
OD 490nm
0.3
0.2
0.1
0.0
***
Pooled mouse serum samples (1 in 300 dilution of serum)

(B)

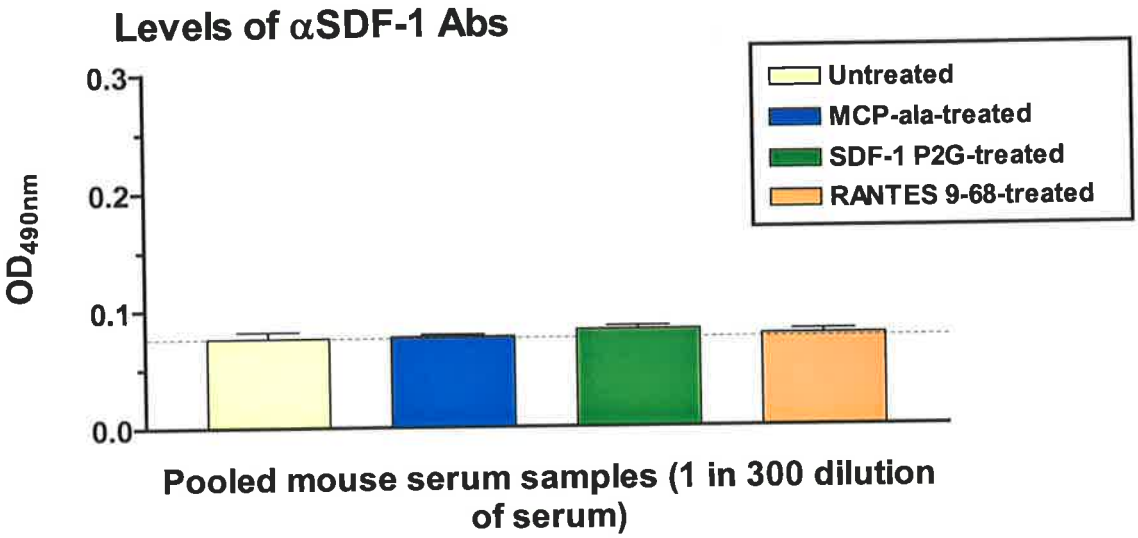
Levels of αSDF-1 Abs
Untreated
MCP-ala-treated
SDF-1 P2G-treated
RANTES 9-68-treated
OD490nm
0.3
0.2
0.1
0.0
Pooled mouse serum samples (1 in 300 dilution of serum)

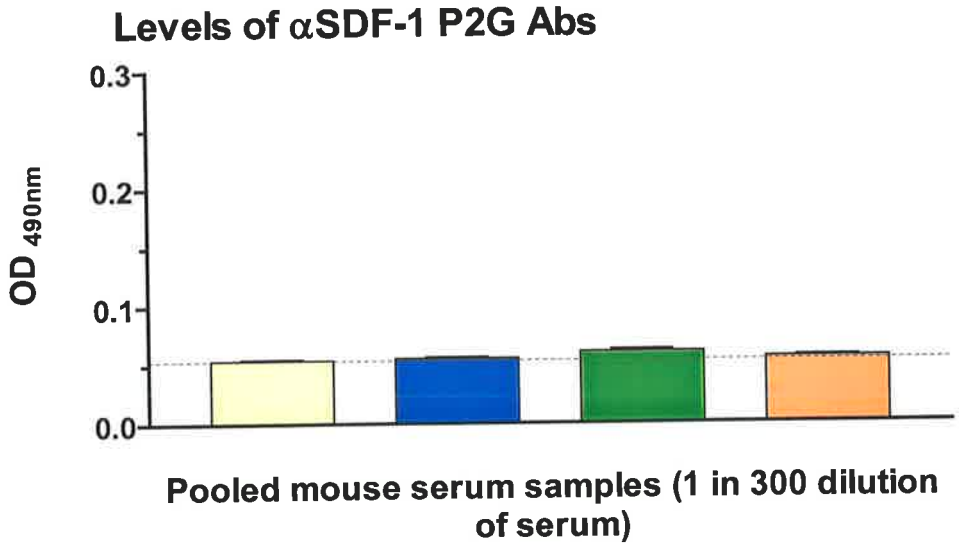
Levels of αSDF-1 P2G Abs
OD 490nm
0.3
0.2
0.1
0.0
Pooled mouse serum samples (1 in 300 dilution of serum)

(C)

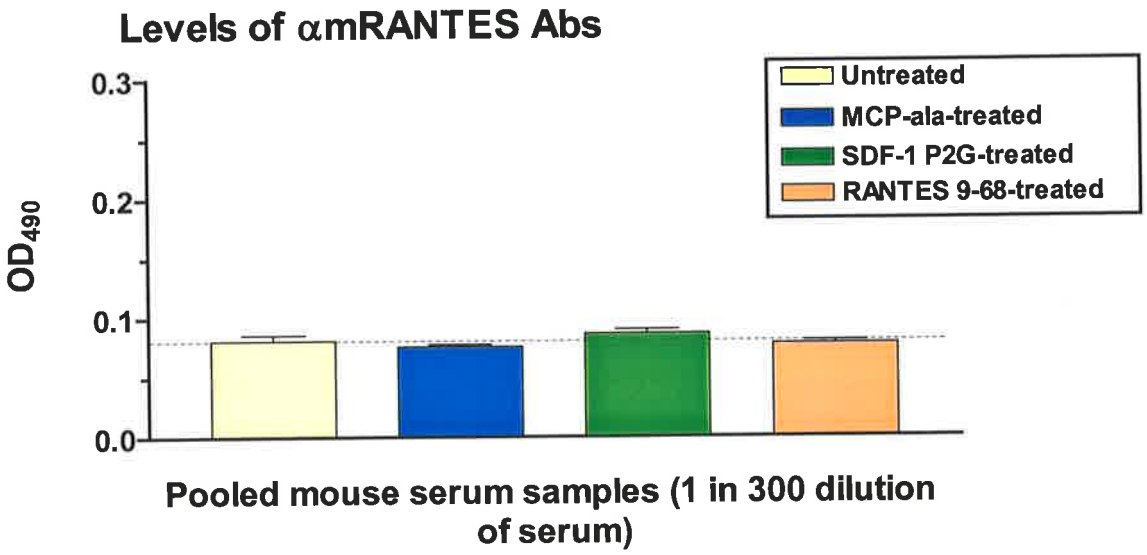
Levels of αmRANTES Abs
Untreated
MCP-ala-treated
SDF-1 P2G-treated
RANTES 9-68-treated
0.3
0.2
0.1
0.0
OD490
Pooled mouse serum samples (1 in 300 dilution of serum)

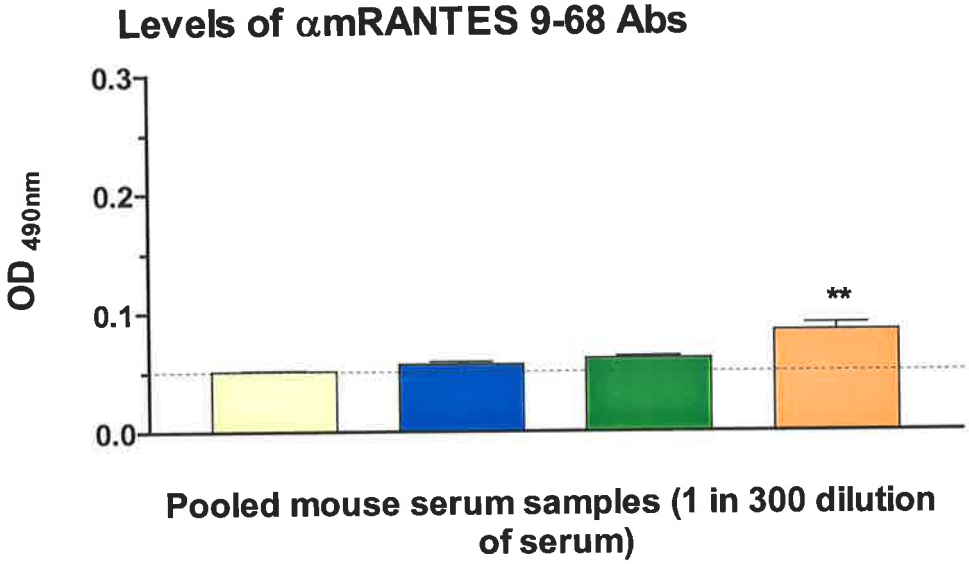
Levels of αmRANTES 9-68 Abs
0.3
0.2
0.1
0.0
OD 490nm
**
Pooled mouse serum samples (1 in 300 dilution of serum)

(D)

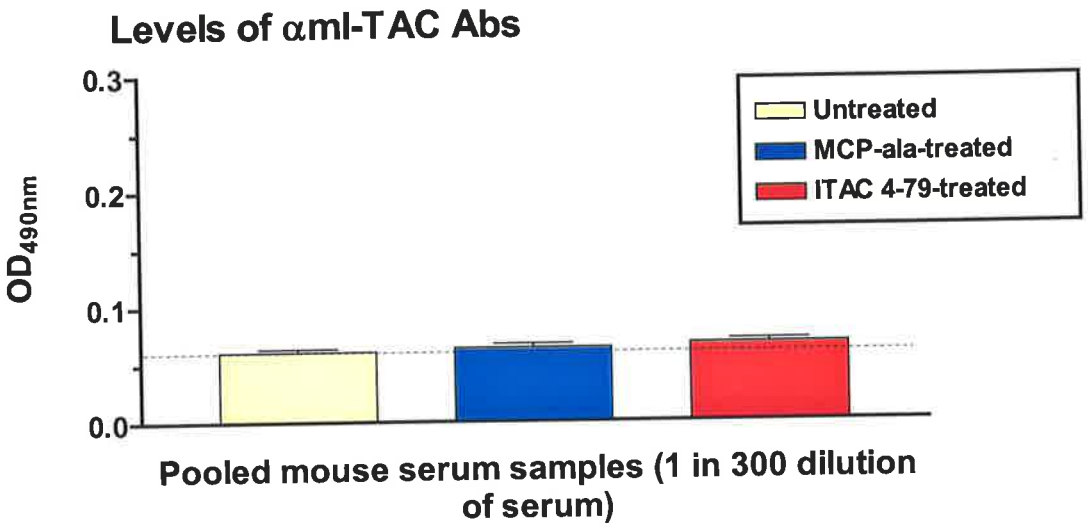
Levels of αml-TAC Abs
0.3
0.2
0.1
0.0
OD490nm
Untreated
MCP-ala-treated
ITAC 4-79-treated
Pooled mouse serum samples (1 in 300 dilution of serum)

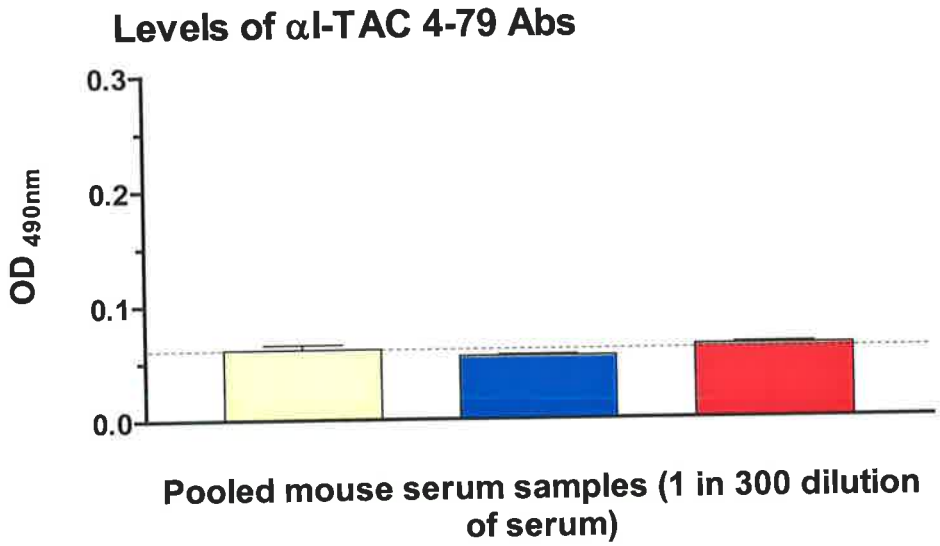
Levels of αl-TAC 4-79 Abs
0.3
0.2
0.1
0.0
OD 490nm
Pooled mouse serum samples (1 in 300 dilution of serum)

Chapter 6

Determination of the mechanisms by which changes in chemokine receptor expression influence the capacity of encephalitogenic cells to mediate disease

6.1 Introduction

Inhibition of EAE by blocking the interaction of specific chemokines with their receptors could occur by several mechanisms, including inhibition of the sensitisation and/or effector phases of EAE. The experiments outlined in this chapter were performed in order to identify the phase of the immune response at which amelioration of disease severity following treatment with the antagonists was occurring. Initially *in vitro* proliferation assays, similar to those conducted in Chapter 3, were performed using the CFSE dye dilution technique to evaluate the effect of the antagonists on the sensitisation phase of EAE. In order to determine whether the antagonists modulated the effector phase of the disease, adoptive transfer experiments were conducted. In these experiments, naive recipient mice were treated with the antagonists following the injection of PLP-specific cells and disease progression was monitored. The final experiments implemented in the present study involved combining antagonist treatment in order to ascertain whether the effects of blocking ligand/receptor interactions, involved in both the sensitisation and effector phases of the immune response, would have an enhanced inhibitory effect on the development of EAE. Spinal cords were removed from these mice for both histological and flow cytometric analysis with the aim of examining the effect of the combined antagonist treatment on the accumulation/infiltration of leukocytes into CNS during EAE.

6.2 Results

6.2.1 Effect of antagonists on the morphological features of the lymph nodes

In order to determine whether the previously observed inhibitory effects of chemokine antagonists were at the level of specific antigen priming, the draining LNs were removed from antagonist- or control-treated mice 9 days post-immunisation with $PLP_{139-151}$ in CFA. These LNs were weighed and the total number of viable cells present were enumerated. The results demonstrate that there was no significant difference between the weights of the LNs removed from the antagonist-treated mice and those removed from the MCP-ala-treated mice (Fig 6.1). In each of the MCP-ala-, SDF-1 P2G- and I-TAC 4-79-treated cohorts, the approximate mass of the draining LNs was ~50 mg. In contrast, the LNs removed from the RANTES 9-68-treated mice weighed ~65 mg, however, this increase was not statistically significant.

Enumeration of the viable cells recovered from the draining LNs revealed there to be slightly lower cell numbers in the LNs removed from SDF-1 P2G- and ITAC 4-79-treated mice than from the MCP-ala- and RANTES 9-68-treated mice (Fig 6.2). Statistical analysis revealed that, although there were ~ 1.5-fold and 1.25-fold less viable cells in the SDF-1 P2G- and I-TAC 4-79-treated mice than in the MCP-ala-treated mice, respectively, the observed reduction was not statistically significant.

6.2.2 Effect of antagonists on the sensitisation phase of EAE

Following removal of the lymph nodes and dissociation into single cell suspensions, the lymphocytes were restimulated with different amounts of $PLP_{139-151}$ for 4 days in the presence of CFSE (Section 2.5.3). Subsequently, the cultured cells were harvested, labelled with antibodies to CD4, and the proliferative response was assessed by flow cytometry using the CFSE dye dilution technique. In terms of percentage of cells, lymphocytes from SDF-1 P2G-treated mice exhibited a lower proliferative response than lymphocytes from MCP-ala mice when restimulated with the four concentrations of $PLP_{139-151}$ (Figure 6.3 (A)). This inhibitory action, however, was not statistically significant until the total number of divided $CD4^+$ T cells was calculated, which indicated that there were significantly fewer encephalitogenic $CD4^+$ T cells in the cultures prepared from the SDF-1 P2G-treated mice than those from the MCP-ala-treated mice ($p < 0.05$; Fig 6.3 (B)). Furthermore, the observed decrease in the proliferative potential and reduction of antigen-specific cells in the SDF-1 P2G-treated lymphocytes was specific, since no significant difference with respect to proliferation between $CD4^+$ lymphocytes from MCP-ala- or SDF-1 P2G-treated mice was observed in response to the mitogen Con A.

Antagonism of CXCR3 via I-TAC 4-79 had no effect on the capacity of lymphocytes to proliferate in response to $PLP_{139-151}$ (Fig 6.4). Equal percentages of lymphocytes from both MCP-ala- and I-TAC 4-79-treated mice responded to restimulation with 0.5, 5.0, 25, and 50 μg/ml $PLP_{139-151}$ (Fig 6.4 (A)). The total number of $CD4^+$ T cells that divided in response to restimulation with the antigen was also similar between the MCP-ala- and I-TAC-4-79-treated mice, such that ~2.5-3.5 x 10^6 $CD4^+$ T cells exhibited diminished

fluorescence intensity in the CFSE channel in both treatment groups (Fig 6.4 (B)). Once more, both the percentage of lymphocytes and the total number of $CD4^+$ T cells that responded to Con A from the I-TAC 4-79-treated mice were the same as those from the MCP-ala-treated mice.

The analysis of the proliferation assays involving lymphocytes recovered from RANTES 9-68-treated mice indicated that the receptors to which RANTES 9-68 bind are not involved in the sensitisation phase of EAE. The data presented in Figure 6.5 (A) demonstrate that there was no significant difference between the percentage of lymphocytes that divided in response to restimulation with $PLP_{139-151}$ from the RANTES 9-68-treated mice compared with the MCP-ala-treated mice. Analysis of the $CD4^+$ T cell populations revealed that equivalent numbers of $CD4^+$ T cells from the MCP-ala- and RANTES 9-68-treated mice proliferated in response to restimulation with different concentrations of $PLP_{139-151}$ *in vitro* (Fig 6.5 (B)).

6.2.3 Effect of antagonists on the effector phase of EAE

Given that the previous experiments revealed neither I-TAC 4-79 or RANTES 9-68 treatment effected the sensitisation phase of EAE, yet treatment resulted in a statistically significant reduction of both the clinical and histopathological features of the disease, it seemed likely that the I-TAC 4-79 and RANTES 9-68 antagonists were modulating the effector phase of EAE. In addition, it was possible that SDF-1 P2G was also influencing the effector phase of the disease. Therefore, to examine this possibility, adoptive transfer experiments were performed. However, prior to examination of antagonistic influences in the effector phase of the disease, it was necessary to establish the adoptive transfer model.

It has previously been shown that the adoptive transfer of activated $PLP_{139-151}$-specific T cells to SJL/J mice results in the induction of a form of EAE that is characterised by ascending hindlimb paralysis and accumulation of lymphocytes and macrophages in the white matter of the CNS (35, 123, 209). Based on the protocols outlined in these reports, naïve SJL/J mice received an intravenous injection of 5×10^7 lymphocytes from cultures restimulated with $PLP_{139-151}$ in a volume of 700 µl, and subsequently disease progression was monitored as described in section 2.2.3. A typical time-course of adoptively-transferred EAE is shown in Figure 6.6. In this experiment, recipient mice began to display neurological symptoms approximately 7 days post-transfer (Fig 6.6; Table 6.1). By day 10 post-transfer, the height of clinical disease was observed and the mice remained severely paralysed until approximately day 15, when recovery commenced. The mean maximum clinical disease scores were 3.25 ± 0.25, similar to that observed in other studies (123, 215). Although mice did show signs of recovery, clinical disease did not completely subside in all mice.

Recipient SJL/J mice were treated with the relevant antagonist or MCP-ala and injected with 5×10^7 $PLP_{139-151}$-reactive lymphocytes. As demonstrated in Figure 6.7, antagonism of CXCR4 had no effect on the effector phase of EAE, as no significant difference between the SDF-1 P2G- and MCP-ala-treated mice was observed with respect to any of the disease parameters measured (Table 6.2).

In contrast, treatment of recipient mice with I-TAC 4-79 alleviated the course of adoptively-transferred EAE in two separate experiments. The results from these experiments have been combined and are presented in Figure 6.8 ($n = 14$). Similarly to that observed during the active EAE experiments, the clinical manifestations of disease in

recipient mice varied slightly between each experiment. Accordingly, the results from each experiment will be discussed separately. In experiment one (Fig 6.8, Table 6.2), the mice treated with I-TAC 4-79 showed less severe symptoms of neurological disease with disease scores being significantly lower on days 7, 10, 12, and 15-20 post-transfer. Although the mean day of onset of clinical disease and the mean day of recovery in both groups did not significantly differ, I-TAC 4-79 treatment resulted in a significantly lower mean maximal clinical disease score than that observed with MCP-ala treatment ($p < 0.05$, Table 6.2). Similar results were observed in the second experiment. Mean clinical disease score was significantly lower in the I-TAC 4-79-treated mice on the first two days of neurological symptoms (Days 7 and 8 post-transfer) and while the mean clinical disease score in the I-TAC 4-79-treated cohort remained lower than in the control group, the two treatment groups eventually followed the same disease course (Fig 6.8; Table 6.2).

Treatment with RANTES 9-68 also inhibited the development of adoptively-transferred EAE. As illustrated in Figure 6.9, recipient mice treated with RANTES 9-68 displayed reduced paralysis compared with the control-treated mice in two independent experiments, from which the results have been combined. In the first experiment, RANTES 9-68-treated mice showed a significant delay in disease onset of greater than two days, and also showed significantly lower disease scores for over 50% of the days on which the mice displayed clinical disease (Table 6.2). Furthermore, the mean maximum clinical score of the RANTES 9-68-treated mice was significantly lower than that of the control-treated cohort ($p = 0.02$, Table 6.2). Disease progression appeared unmodified after day 14 post-transfer, with no significant difference in the mean day of recovery noted between the two treatment groups. In the second adoptive transfer experiment involving RANTES 9-68 (Table 6.2), the antagonist-treated cohort again showed a significant delay in disease onset

of more than 2 days, which also significantly reduced the number of days the mice were displaying neurological signs of disease ($p < 0.05$ and $p < 0.001$, respectively). In addition, the mice treated with RANTES 9-68 demonstrated a significantly lower mean maximal disease score compared with the MCP-ala-treated mice ($p = 0.0015$, Table 6.2). Mice from the RANTES 9-68-treated group began to recover 17 days post-transfer, whilst the control-treated mice began improving one day later at 18 days post-transfer. This expedited recovery was statistically significant ($p = 0.02$, Table 6.2).

6.2.4 Effect of combined antagonism of CXCR4 and CXCR3 on the development of EAE

6.2.4.1 Antagonism of both CXCR4 and CXCR3 enhances the inhibition of the neurological signs of EAE

The results obtained to date revealed a potential role for SDF-1 P2G in the sensitisation phase of the EAE, and a role for I-TAC 4-79 and RANTES 9-68 in the effector phase of EAE. Therefore, based on those findings, a group of experiments were planned in order to determine the effect of combined antagonist treatment on the development of EAE. The initial experiments focussed on co-administration of SDF-1 P2G and I-TAC 4-79. Accordingly, SJL/J mice were immunised with 50 µg $PLP_{139-151}$ in CFA and injected with 5 µg pertussigen on days 0 and 2 post-immunisation (Section 2.2.1). Starting on day 1 post-immunisation, the mice were injected i.p. with a combination of 100 µg SDF-1 P2G and 250 µg I-TAC 4-79, or 350 µg of MCP-ala, every second day up to day 11 post-

immunisation. Subsequently, the mice were monitored for signs of clinical disease for up to 25 days post-immunisation.

The findings from two separate experiments demonstrated that the combination of SDF-1 P2G and I-TAC 4-79 significantly inhibited clinical EAE and that disease incidence was markedly lower than that seen when mice were treated with single antagonists (Table 6.3). The combined results from the experiments are shown in Figure 6.10. In experiment one (Fig 6.10, Table 6.3), the combination antagonist treatment resulted in a significant reduction in clinical disease severity beginning at 10 days post-immunisation that lasted until day 16 post-immunisation ($p = 0.0001$-0.05). During this time, mice treated with MCP-ala exhibited complete tail paralysis and limited mobility, whereas the antagonist-treated mice possessed near perfect motor skills and no signs of paralysis. In addition to the fact that only five out of eight antagonist-treated mice developed mild neurological symptoms, there was a statistically significant delay in onset of these neurological signs, and the total number of days during which the mice were displaying evidence of disease was significantly reduced compared with the control-treated mice ($p = 0.01$ and $p = 0.003$, respectively). The mean maximum clinical score ascribed to the antagonist-treated group was 0.88 ± 0.36, which was 2.5-fold less than that given to the control-treated cohort.

The second experiment that involved the use of combined antagonist treatment yielded essentially the same results as the first (Fig 6.10, Table 6.3). In this experiment, there was a statistically significant delay of approximately two days in the manifestation of disease symptoms, which resulted in a significant reduction in the number of days on which the mice displayed clinical symptoms, compared with the MCP-ala-treated mice ($p < 0.05$, Table 6.3). Whilst mice from the MCP-ala-treated group consistently experienced

hindlimb paralysis from days 12 to 16 post-immunisation, mice from the combined antagonist treatment group only displayed signs of partial tail paralysis and agitated gaits (Fig 6.10). At all time points examined, except day 10 post-immunisation, the clinical scores of the mice from the antagonist-treated cohort were significantly lower than those from the control-treated group, until the mice entered remission ($p < 0.05$). Similar to that observed in experiment one, the mean maximum clinical disease score of the antagonist-treated cohort was significantly lower than that of the MCP-ala-treated cohort ($p < 0.01$, Table 6.3).

6.2.4.2 Decreased CNS histopathological lesions in SDF-1 P2G and I-TAC 4-79-treated mice

To determine whether combined antagonist treatment had any influence on the histopathology of EAE, mice from the SDF-1 P2G + I-TAC 4-79-, or MCP-ala-treated groups were sacrificed for histological examination at day 12 post-immunisation. Spinal cords from MCP-ala- and antagonist-treated mice were removed from the mice after perfusion in the left ventricle with cold PBS (Section 2.6.1). Cryostat sections of the tissue samples were stained with haematoxylin/eosin and evaluated for the extent of mononuclear cell infiltration into the meninges, perivascular areas and parenchyma. Representative photomicrographs of transverse sections of thoracic/lumbar regions of the spinal cord of MCP-ala- and SDF-1 P2G + I-TAC 4-79-treated mice are shown in Figure 6.11 (A & B). The sections from the MCP-ala treated mice illustrated inflammatory infiltrates in the perivascular spaces, meninges and parenchyma (Fig 6.11 (A)), whereas sections from the antagonist-treated mice contained fewer inflammatory lesions (Fig 6.11 (B)). At the time of death, the mice from the MCP-ala-treated group displayed severe

neurological impediments such that the mean disease score was 3.31 ± 0.2, while mice from the SDF-1 P2G- + I-TAC 4-79-treatment group had a mean clinical disease score of 1.75 ± 0.39 (Table 6.4). The number of inflammatory infiltrates per section were quantified. These analyses revealed that there were approximately 3.18 inflammatory lesions/section in the mice treated with MCP-ala, which was a significantly greater number that that present in the sections from SDF-1 P2G + I-TAC 4-79-treated mice ($p < 0.0001$). In the spinal cords removed from the antagonist-treated mice, there were approximately 2.10 inflammatory lesions/section (Table 6.4). These observations indicate that whilst the combined antagonist treatment significantly reduced the number of inflammatory lesions in the CNS compared to control-treated mice, it made no further improvement, in terms of lesion burden, to that seen in the CNS of mice treated with single antagonists (see Tables 5.2 and 5.3).

6.2.4.3 Treatment with SDF-1 P2G and I-TAC 4-79 reduces cellular infiltration into the CNS

The number of total viable cells, and the number of $CD4^+$ T cells that accumulating in the spinal cord at the height of clinical disease (Day 12) were compared in control and combined antagonist-treated mice (Figures 6.12 & 6.13, respectively). There were approximately 8×10^4 viable cells recovered from spinal cords of the SDF-1 P2G + I-TAC 4-79-treated mice, which was ~2-fold less that that recovered from the MCP-ala-treated CNS (Fig 6.12). Analysis of the $CD4^+$ T cell population revealed that there was also a statistically significant reduction in the number of $CD4^+$ T cells (~2.4-fold fewer) in the

spinal cords of mice treated with SDF-1 P2G + I-TAC 4-79 compared with MCP-ala-treated mice ($p < 0.05$; Fig 6.13).

6.3 Summary

The aim of this series of experiments was to identify the functional role of specific chemokine/receptor interactions during EAE. The ability to separate the disease process into two separate phases (sensitisation and effector) provided a means to investigate the temporal and spatial control that specific chemokine/receptor interactions exerted during the pathogenesis of EAE. Consequently, a series of *ex vivo* proliferation assays and adoptive transfer experiments were conducted. Initial analyses of lymph node weights and cell counts revealed no difference in the number of cells accumulating in the draining LNs of the antagonist-treated mice compared with the control-treated mice, indicating that antagonist-treatment had no general inhibitory effect on the ability of lymphocytes to migrate to the draining lymph nodes. However, through the use of *ex vivo* proliferation assays, a potential role for the SDF-1/CXCR4 interaction was identified in the sensistisation phase of the disease. In these experiments, lymphocytes from mice treated with SDF-1 P2G were unable to proliferate as efficiently as those from control-treated mice in response to restimulation with the immunising antigen. This indicates that SDF-1/CXCL12 and CXCR4 interactions not only play a role in homeostasis, but may also provide costimulatory signals to antigen-stimulated $CD4^+$ T cells. In contrast, neither I-TAC/CXCR3 nor RANTES/CCR5 interactions were demonstrated to be essential during the sensitisation phase of EAE.

Adoptive transfer experiments revealed roles for I-TAC/CXCR3 and RANTES/CCR5 interactions, but not SDF-1/CXCR4 interactions in the effector phase of EAE. Treatment of recipient mice with SDF-1 P2G failed to prevent the passive transfer of EAE, indicating that CXCR4 is not essential for the effector phase of this immune response. In contrast, prior treatment of recipients with I-TAC 4-79 and RANTES 9-68 significantly suppressed disease transfer, indicating that the receptors to which these antagonists bind are vital for the effector phase of EAE.

Combined SDF-1 P2G and I-TAC 4-79-treatment led to a dramatic reduction of clinical disease manifestations compared with the control-treated cohort, however, the extent of cellular infiltration into the CNS tissue did not differ significantly compared with mice treated with the antagonists individually. Further studies will be required to elucidate the mechanism of disease protection occurring following the combination therapy.

Figure 6.1. *The effect of antagonist treatment on the weight of the draining lymph nodes during EAE.* SJL/J mice were injected s.c. with 50 μg of $PLP_{139-151}$ in CFA (Section 2.2.1). Two hours before and two days after the injection of emulsion, the mice received 5 μg of pertussigen (i.v.). On days 1, 3, 5, and 7 post-immunisation, the mice received an intraperitoneal injection of MCP-ala, SDF-1 P2G, I-TAC 4-79 or RANTES 9-68 (Section 2.2.4). Mice from each treatment group were killed on day 9 post-immunisation, and the draining lymph nodes were collected and weighed. Data are presented as mean ± SEM (n = 4).

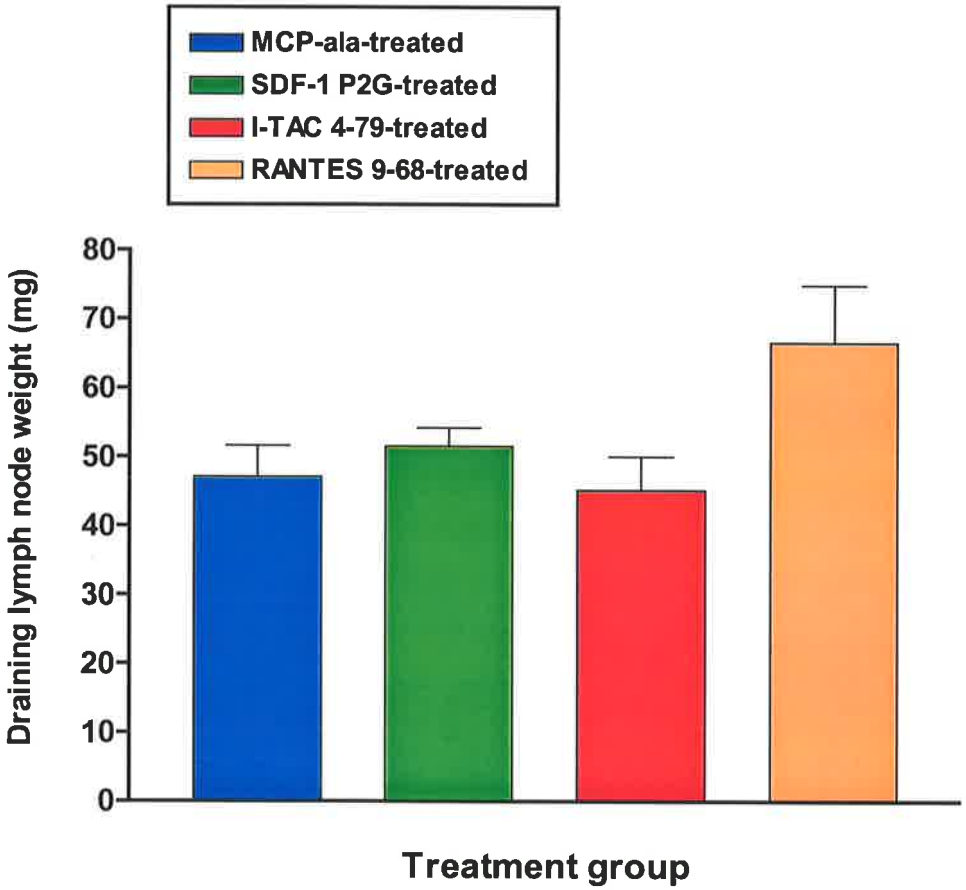
MCP-ala-treated
SDF-1 P2G-treated
I-TAC 4-79-treated
RANTES 9-68-treated
Draining lymph node weight (mg)
80
70
60
50
40
30
20
10
0
Treatment group

Figure 6.2. *The effect of antagonist treatment on the number of viable cells recovered from the draining lymph nodes during EAE.* SJL/J mice were injected s.c. with 50 μg of $PLP_{139-151}$ in CFA (Section 2.2.1). Two hours before and two days after the injection of emulsion, the mice received 5 μg of pertussigen (i.v.). On days 1, 3, 5, and 7 post-immunisation, the mice received an i.p. injection of MCP-ala, SDF-1 P2G, I-TAC 4-79 or RANTES 9-68 (Section 2.2.4). Mice from each treatment group were killed on day 9 post-immunisation, and the draining lymph nodes were collected and the viable cells were enumerated. Data are presented as mean ± SEM (n = 6-11).

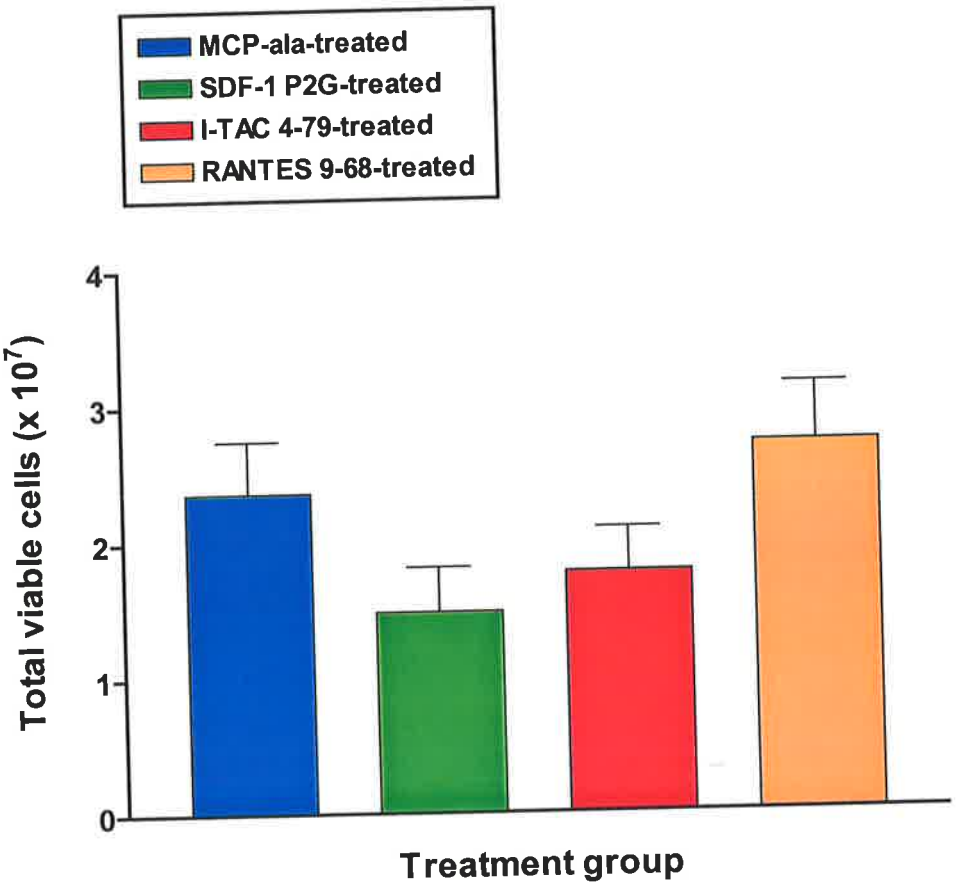
MCP-ala-treated
SDF-1 P2G-treated
I-TAC 4-79-treated
RANTES 9-68-treated
Total viable cells (x 10^7)
0
1
2
3
4
Treatment group

Figure 6.3. *The effect of SDF-1 P2G on the sensitisation of T cells to $PLP_{139-151}$.*

SJL/J mice were injected s.c. with 50 μg of $PLP_{139-151}$ in CFA (Section 2.2.1). Two hours before and two days after the injection of emulsion, the mice received 5 μg of pertussigen (i.v.). On days 1, 3, 5, and 7 post-immunisation, the mice received an i.p. injection of MCP-ala or SDF-1 P2G (Section 2.2.4). Mice from each treatment group were killed on day 9 post-immunisation, the draining lymph nodes were collected. Single cell suspensions were prepared, stained with CFSE and cultured for 4 days in the presence of various concentrations of $PLP_{139-151}$. Following 4 days of culture, the cells were harvested, labelled with anti-CD4 antibodies, and analysed by flow cytometry, gating on lymphocytes using forward and side scatter characteristics. The effect of treatment with SDF-1 P2G on lymphocyte division upon restimulation *in vitro* was determined as the percent of lymphocytes divided [A] and the total number of $CD4^+$ cells that had divided [B]. *, Significantly different from MCP-ala-treated group at $p<0.05$. Data are presented as mean ± SEM (n = 6, from 2 independent experiments).

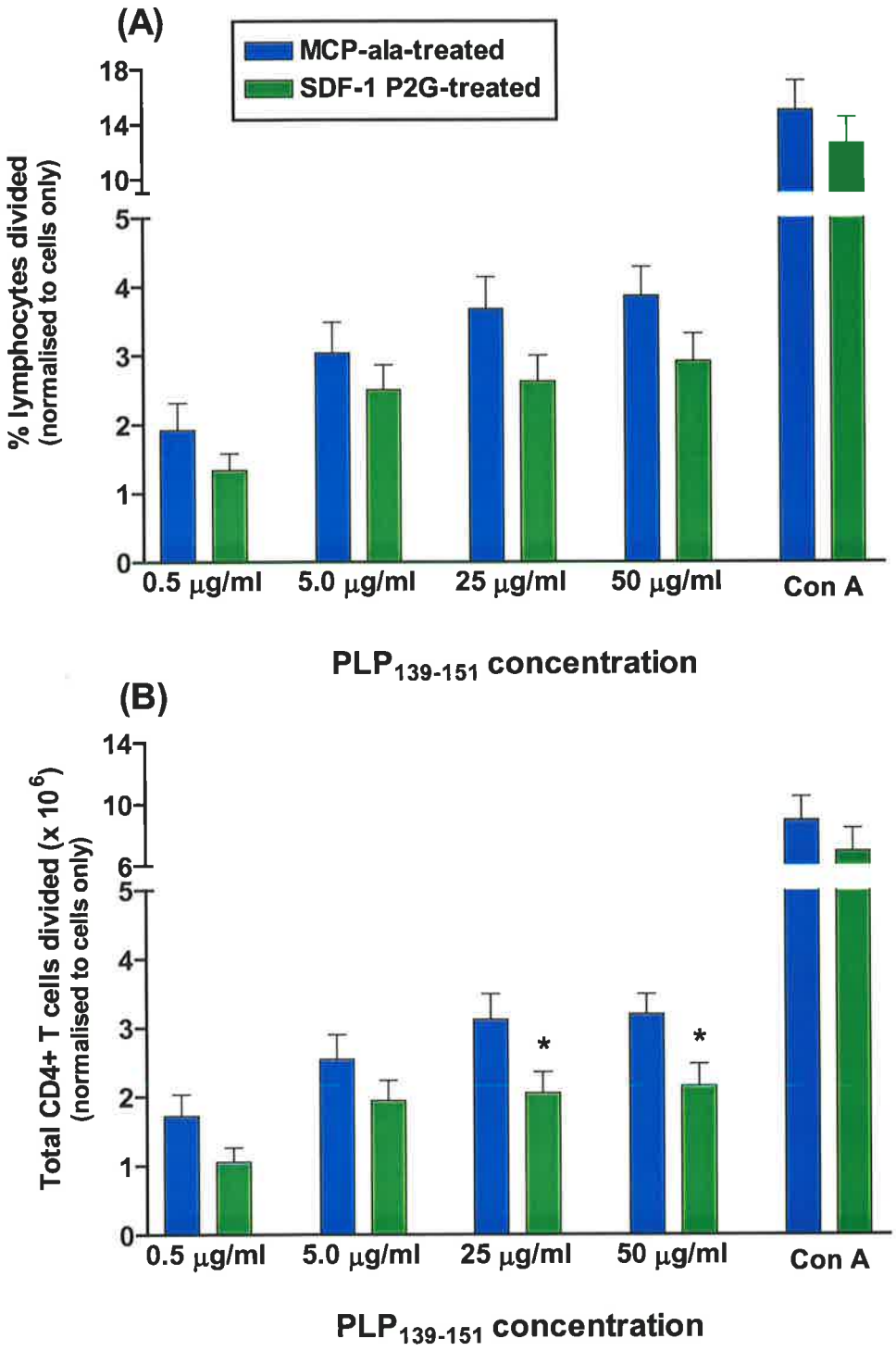
(A)
MCP-ala-treated
SDF-1 P2G-treated
% lymphocytes divided
(normalised to cells only)
18
14
10
5
4
3
2
1
0
0.5 μg/ml
5.0 μg/ml
25 μg/ml
50 μg/ml
Con A
PLP139-151 concentration
(B)
Total CD4+ T cells divided (x 10^6)
(normalised to cells only)
14
10
6
5
4
3
2
1
0
*
*
0.5 μg/ml
5.0 μg/ml
25 μg/ml
50 μg/ml
Con A
PLP139-151 concentration

Figure 6.4. *The effect of I-TAC 4-79 on the sensitisation of T cells to $PLP_{139-151}$.*

SJL/J mice were injected s.c. with 50 μg of $PLP_{139-151}$ in CFA (Section 2.2.1). Two hours before and two days after the injection of emulsion, the mice received 5 μg of pertussigen (i.v.). On days 1, 3, 5, and 7 post-immunisation, the mice received an i.p. injection of MCP-ala or I-TAC 4-79 (Section 2.2.4). Mice from each treatment group were killed on day 9 post-immunisation, the draining lymph nodes were collected. Single cell suspensions were prepared, stained with CFSE and cultured for 4 days in the presence of various concentrations of $PLP_{139-151}$. Following 4 days of culture, the cells were harvested, labelled with anti-CD4 antibodies, and analysed by flow cytometry, gating on lymphocytes using forward and side scatter characteristics. The effect of treatment with I-TAC 4-79 on lymphocyte division upon restimulation *in vitro* was determined as the percent of lymphocytes divided [A] and the total number of $CD4^+$ cells that had divided [B]. Data are presented as mean ± SEM (n = 4, from 2 independent experiments).

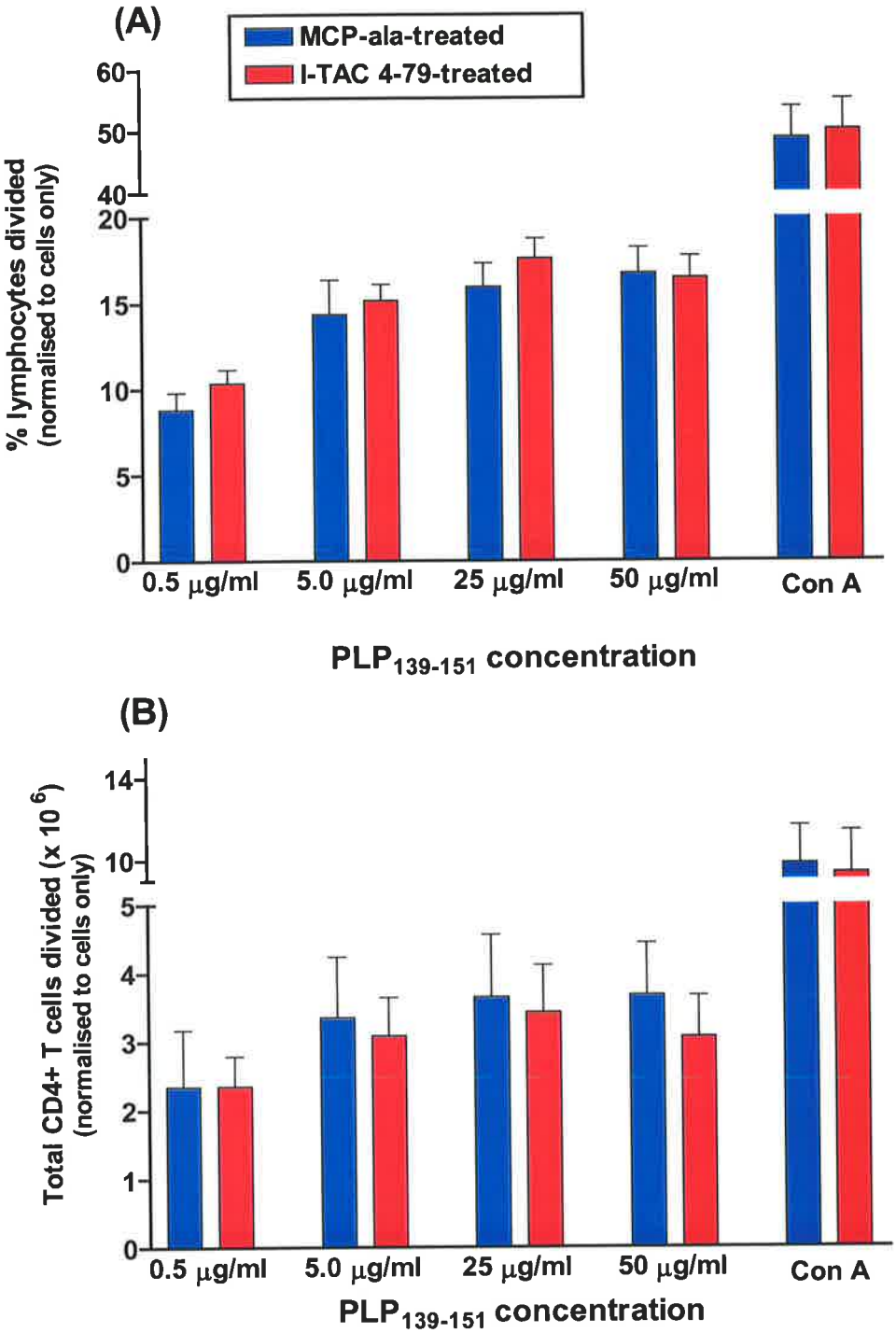
(A)
MCP-ala-treated
I-TAC 4-79-treated
% lymphocytes divided
(normalised to cells only)
60
50
40
20
15
10
5
0
0.5 μg/ml
5.0 μg/ml
25 μg/ml
50 μg/ml
Con A
PLP139-151 concentration
(B)
Total CD4+ T cells divided (x 10 6)
(normalised to cells only)
14
10
5
4
3
2
1
0
0.5 μg/ml
5.0 μg/ml
25 μg/ml
50 μg/ml
Con A
PLP139-151 concentration

Figure 6.5. *The effect of RANTES 9-68 on the sensitisation of T cells to $PLP_{139-151}$.* SJL/J mice were injected s.c. with 50 μg of $PLP_{139-151}$ in CFA (Section 2.2.1). Two hours before and two days after the injection of emulsion, the mice received 5 μg of pertussigen (i.v.). On days 1, 3, 5, and 7 post-immunisation, the mice received an i.p. injection of MCP-ala or RANTES 9-68 (Section 2.2.4). Mice from each treatment group were killed on day 9 post-immunisation, the draining lymph nodes were collected. Single cell suspensions were prepared, stained with CFSE and cultured for 4 days in the presence of various concentrations of $PLP_{139-151}$. Following 4 days of culture, the cells were harvested, labelled with anti-CD4 antibodies, and analysed by flow cytometry, gating on lymphocytes using forward and side scatter characteristics. The effect of treatment with RANTES 9-68 on lymphocyte division upon restimulation *in vitro* was determined as the percent of lymphocytes divided [A] and the total number of $CD4^+$ cells that had divided [B]. Data are presented as mean ± SEM (n = 6, from 2 independent experiments).

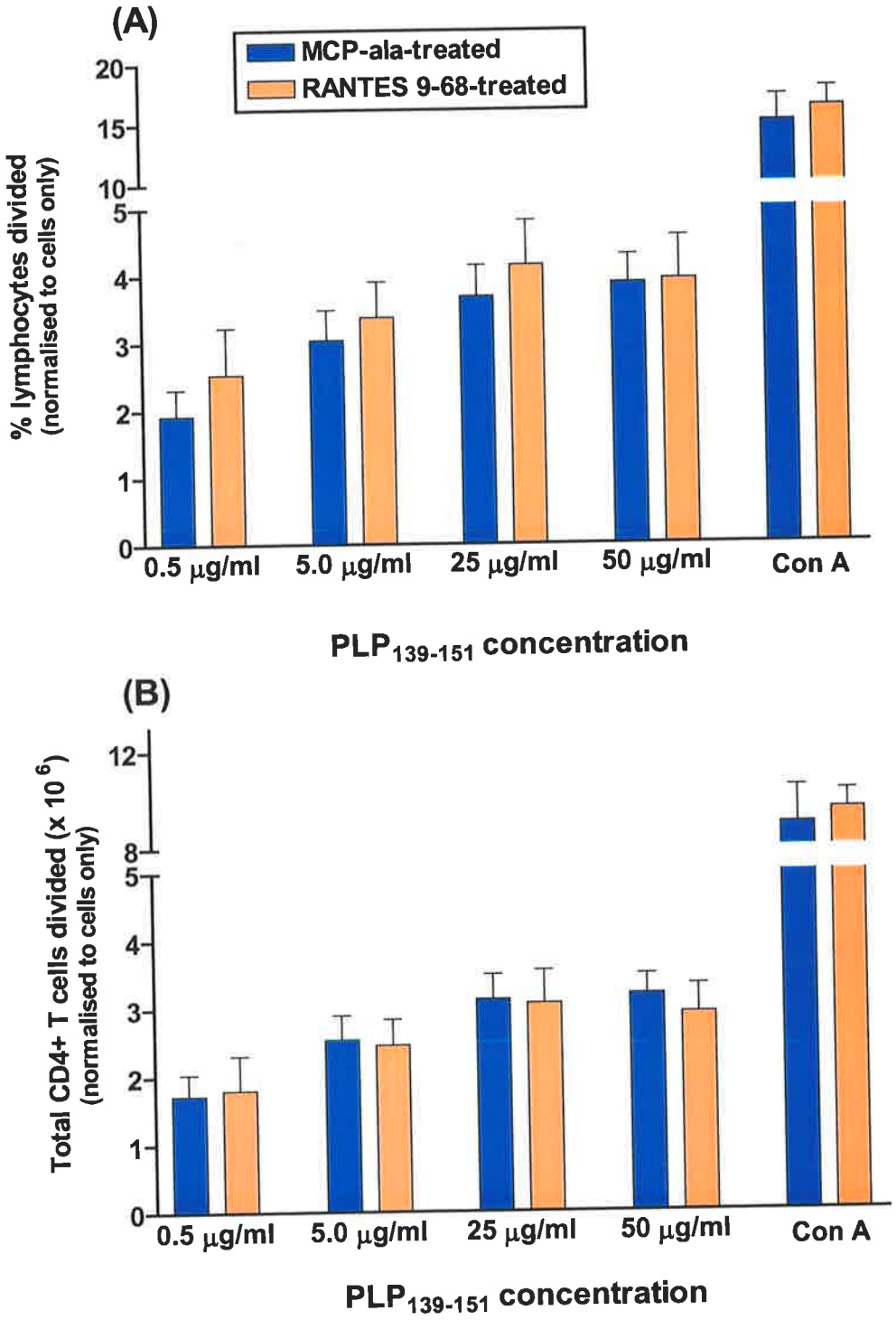
(A)
MCP-ala-treated
RANTES 9-68-treated
% lymphocytes divided
(normalised to cells only)
20
15
10
5
4
3
2
1
0
0.5 μg/ml
5.0 μg/ml
25 μg/ml
50 μg/ml
Con A
PLP139-151 concentration
(B)
Total CD4+ T cells divided (x 10^6)
(normalised to cells only)
12
8
5
4
3
2
1
0
0.5 μg/ml
5.0 μg/ml
25 μg/ml
50 μg/ml
Con A
PLP139-151 concentration

Table 6.1: Characteristics of clinical EAE following adoptive transfer of $PLP_{139-151}$-specific cells. Naïve SJL/J mice were intravenously injected with 5 x 10^7 $PLP_{139-151}$-restimulated cells. Mice were monitored for neurological symptoms until Day 25 post-transfer. Throughout the course of disease, various parameters were analysed. These data are representative of 2 others performed with similar results.

Parameter	Adoptively-transferred EAE
No. Sick / Total	4/4
Mean day of onset [a]	7.5 ± 0.29
Mean day of recovery [a]	22.0 ± 1.08
Mean length of disease (days) [a]	15.25 ± 1.55
Mean maximum clinical score [a]	3.25 ± 0.25

[a] Mean ± SEM

Fig 6.6. *Development of clinical symptoms of EAE in response to adoptive transfer of $PLP_{139-151}$-reactive lymphocytes.* Donor SJL/J mice were injected s.c. with 25 μg $PLP_{139-151}$ in CFA. Ten days post-immunisation, draining lymph node cells were harvested, stimulated for 4 days in the presence of 50 μg/ml of $PLP_{139-151}$, and 5 x 10^7 cells were transferred into naive recipients (Section 2.2.2). Recipient mice were monitored for disease symptoms (section 2.2.3) over a period of 25 days post-transfer. Data are presented as mean clinical disease score ± SEM, as a function of days after cell transfer (n = 6). The experiment depicted in this figure is representative of 2 others performed with similar results.

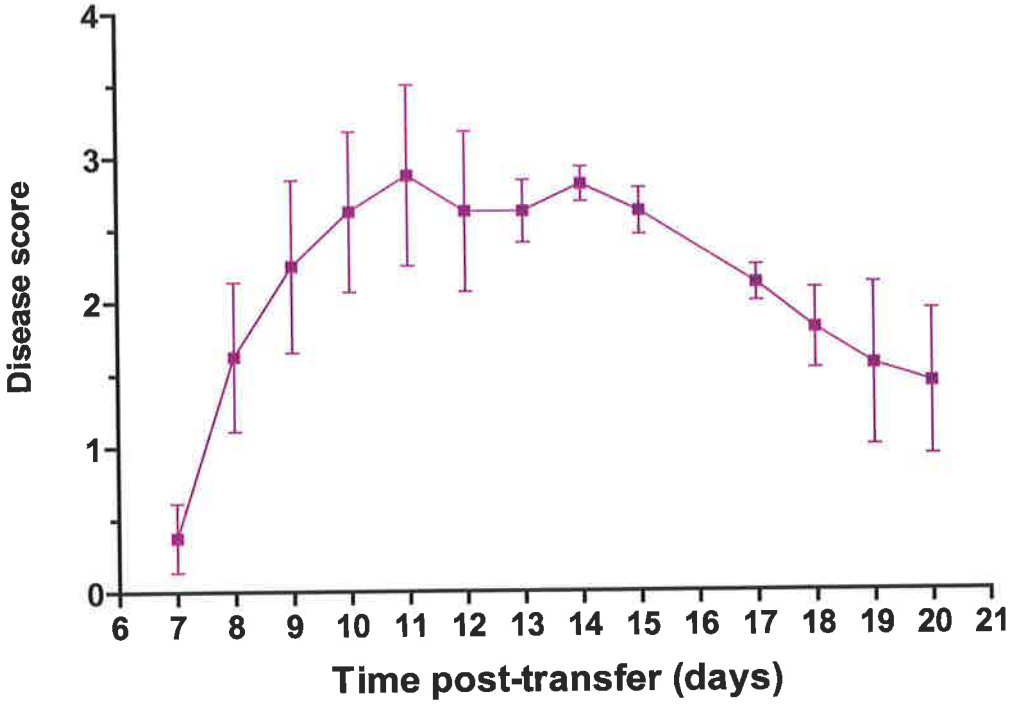
Disease score
0
1
2
3
4
6
7
8
9
10
11
12
13
14
15
16
17
18
19
20
21
Time post-transfer (days)

Table 6.2: The effect of antagonist treatment on the effector phase of EAE.
Naïve SJL/J mice were intravenously injected with 5 x 10^7 $PLP_{139-151}$-restimulated cells, then treated with either the relevant antagonist or MCP-ala every second day until Day 14 post-transfer. Mice were monitored for neurological symptoms until Day 25 post-transfer. Throughout the course of disease various parameters were analysed.

	Delay in disease onset	**Difference in max clinical score**	**Advance in disease recovery**	**Reduction in disease length**	**# days of significantly lower clinical score**	**# mice sick**
SDF-1 P2G Experiment 1 (Section 6.2.3)	~ 1 day	- 0.5	None	None	None	7/7
I-TAC 4-79 Experiment 1 (Section 6.2.3)	~ 1 day	- 0.55 *	ND	ND	1 day at onset. 2 days during peak disease, 6 days of recovery	6/6
I-TAC 4-79 Experiment 2 (Section 6.2.3)	~ 1 day **	- 0.9 *	None	~ 1 day	2 days during disease onset, 3 days during peak disease	7/7
RANTES 9-68 Experiment 1 (Section 6.2.3)	2 ½ days**	- 0.6 *	ND	ND	3 days during onset, 3 days during peak disease	7/7
RANTES 9-68 Experiment 2 (Section 6.2.3)	> 3 days *	-0.8 **	1 ½ days *	3 ½ days**	4 days during peak disease leading into recovery	6/6

* Statistically significant from the MCP-ala treatment group at $p < 0.05$
** Statistically significant different from the MCP-ala treatment group at $p < 0.01$
ND, not determined due to incomplete recovery

Figure 6.7. *Effect of SDF-1 P2G treatment on adoptive transfer of EAE.* Donor SJL/J mice were injected s.c. with 25 μg $PLP_{139-151}$ in CFA. Ten days post-immunisation, draining lymph node cells were harvested, stimulated for 4 days in the presence of 50 μg/ml of $PLP_{139-151}$, and 5 x 10^7 cells were transferred into naive recipients (Section 2.2.2). On the day of transfer and days 2, 4, 6, 8, 10, 12 and 14 post-transfer, the recipient mice received an i.p. injection of MCP-ala or SDF-1 P2G (Section 2.2.4). Mice were scored for clinical manifestations of disease over a period of 25 days post-transfer. Data are presented as mean clinical disease score ± SEM, as a function of days after transfer (n = 7).

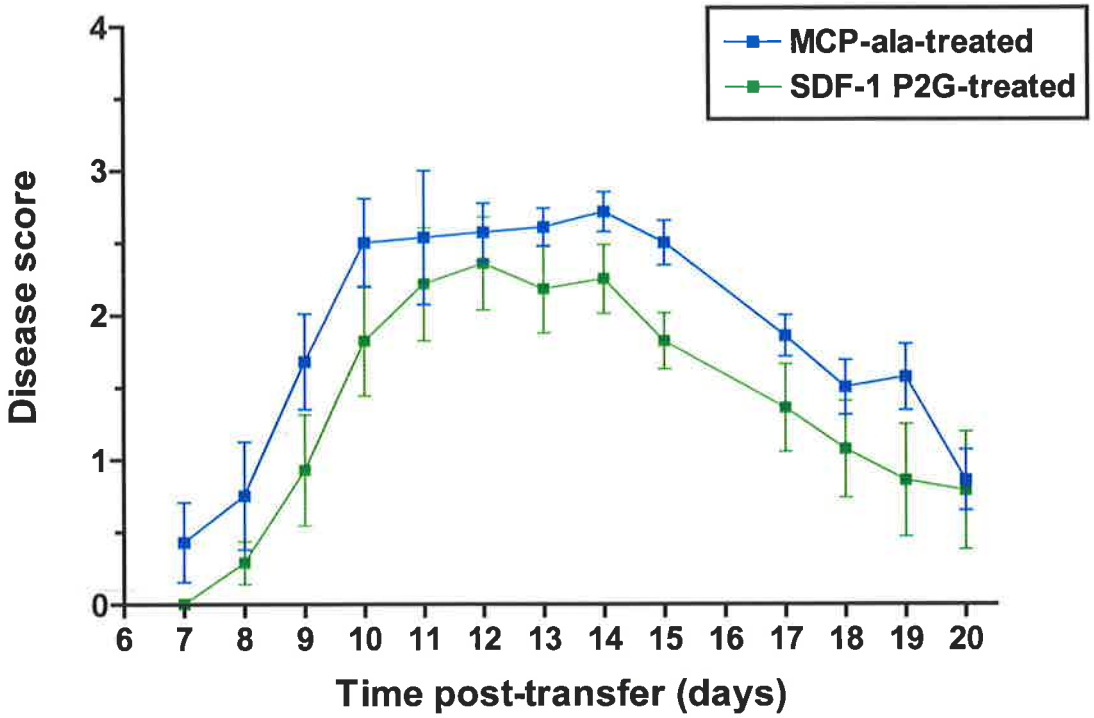
MCP-ala-treated
SDF-1 P2G-treated
Disease score
0
1
2
3
4
6
7
8
9
10
11
12
13
14
15
16
17
18
19
20
Time post-transfer (days)

Figure 6.8. *Effect of I-TAC 4-79 treatment on adoptive transfer of EAE.* Donor SJL/J mice were injected s.c. with 25 μg $PLP_{139-151}$ in CFA. Ten days post-immunisation, draining lymph node cells were harvested, stimulated for 4 days in the presence of 50 μg/ml of $PLP_{139-151}$, and 5 x 10^7 cells were transferred into naive recipients (Section 2.2.2). On the day of transfer and days 2, 4, 6, 8, 10, 12 and 14 post-transfer, the recipient mice received an i.p. injection of MCP-ala or I-TAC 4-79 (Section 2.2.4). Mice were scored for clinical manifestations of disease over a period of 25 days post-transfer. The data presented were obtained from 2 independent experiments. Data are presented as mean clinical disease score ± SEM, as a function of days after transfer (n = 14). * indicates a significant difference from MCP-ala treatment at $p<0.05$ (ANOVA). ** indicates a significant difference from MCP-ala treatment at $p<0.005$ (ANOVA).

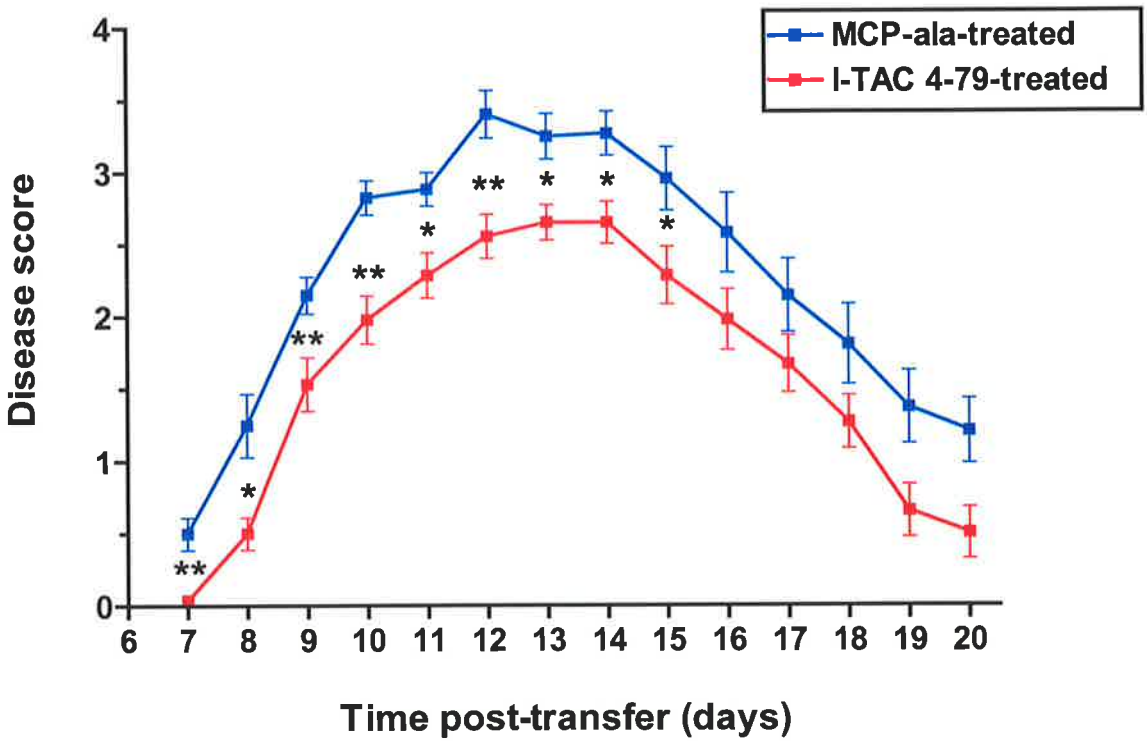
MCP-ala-treated
I-TAC 4-79-treated
Disease score
Time post-transfer (days)
0
1
2
3
4
6
7
8
9
10
11
12
13
14
15
16
17
18
19
20
**
*
**
**
*
**
*
*
*

Figure 6.9. *Effect of RANTES 9-68 treatment on adoptive transfer of EAE.* Donor SJL/J mice were injected s.c. with 25 μg $PLP_{139-151}$ in CFA. Ten days post-immunisation, draining lymph node cells were harvested, stimulated for 4 days in the presence of 50 μg/ml of $PLP_{139-151}$, and 5 x 10^7 cells were transferred into naive recipients (Section 2.2.2). On the day of transfer and days 2, 4, 6, 8, 10, 12 and 14 post-transfer, the recipient mice received an i.p. injection of MCP-ala or RANTES 9-68 (Section 2.2.4). Mice were scored for clinical manifestations of disease over a period of 25 days post-transfer. The data presented were obtained from 2 independent experiments. Data are presented as mean clinical disease score ± SEM, as a function of days after transfer (n = 13). * indicates a statistically significant difference from MCP-ala treatment at $p<0.05$ (ANOVA). ** indicates a statistically significant difference from MCP-ala treatment at $p<0.005$ (ANOVA).

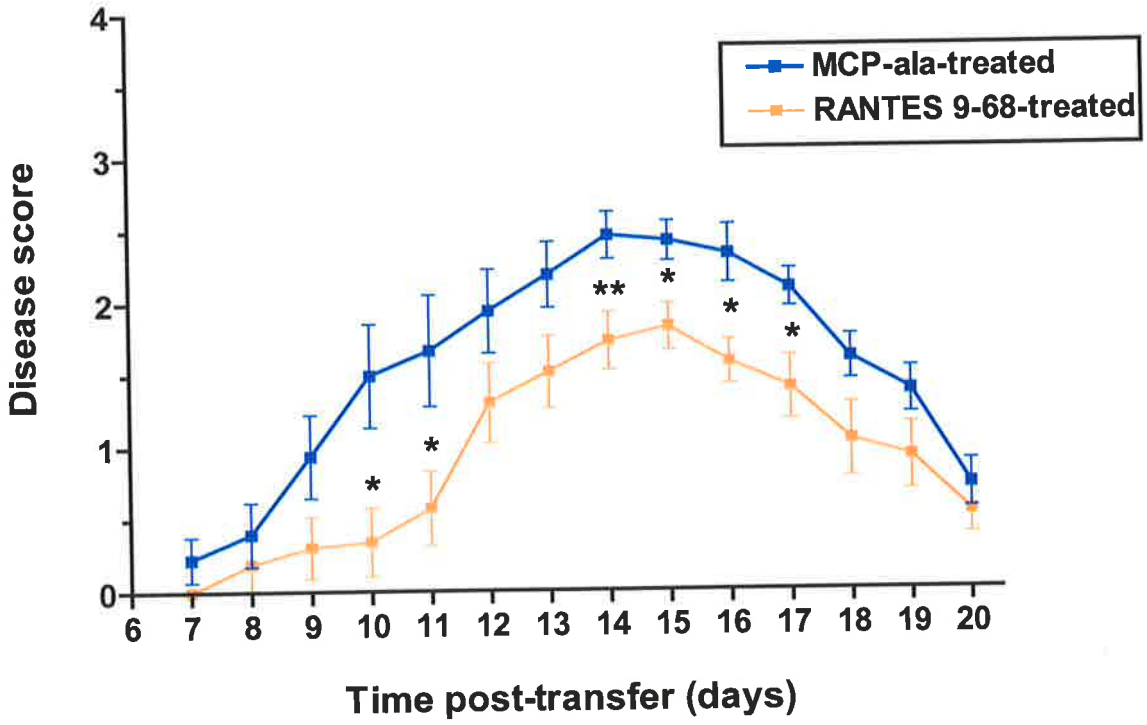
MCP-ala-treated
RANTES 9-68-treated
Disease score
Time post-transfer (days)
0
1
2
3
4
6
7
8
9
10
11
12
13
14
15
16
17
18
19
20
*
*
**
*
*
*

Table 6.3: The effect of combined antagonist treatment on the development of EAE. EAE was induced in SJL/J mice. The mice were treated with either SDF-1 P2G & I-TAC 4-79 or MCP-ala, starting Day 1 post-immunisation for every second day until Day 11 post-immunisation. Mice were monitored for neurological symptoms until Day 25 post-immunisation. Throughout the course of disease various parameters were analysed.

	Delay in disease onset [a]	**Difference in max clinical score** [b]	**Advance in disease recovery** [a]	**Reduction in disease length** [b]	**# days of significantly lower clinical score** [a]	**# mice sick**
SDF-1 P2G + I-TAC 4-79 Experiment 1 (Section 6.2.4)	~ 1 ½ days *	- 1.3 **	~ 1 day	4 ½ days**	7 days throughout disease	5/8
SDF-1 P2G + I-TAC 4-79 Experiment 2 (Section 6.2.4)	~ 2 days *	- 1.3 **	~ 1 ½ days	> 3 ½ days**	7 days throughout disease	7/8

[a] Excluding non-responders (mice that never showed clinical manifestation of disease)
[b] Including non-responders (mice that never showed manifestation were calssified as showing disease length of 0, and a maximum clinical score of 0)
* Statistically significant from control treatment group at $p < 0.05$
** Statistically significant from control treatment group at $p < 0.01$

Figure 6.10. *The effect of combined SDF-1 P2G and I-TAC 4-79 treatment on the development of EAE.* SJL/J mice were injected s.c. with 50 μg of $PLP_{139-151}$ in CFA (Section 2.2.1). Two hours before and two days after the injection of emulsion, the mice received 5 μg of pertussigen (i.v.). On days 1, 3, 5, 7, 9, and 11 post-induction, the mice received an i.p. injection of 100 μg of SDF-1 P2G + 250 μg of I-TAC 4-79 or 350 μg of MCP-ala (Section 2.2.4). Mice were scored for the clinical manifestation of disease over a period of 25 days post-immunisation. The data presented were obtained from 2 independent experiments. Data are presented as mean clinical disease score ± SEM as a function of days after immunisation (n = 16). * indicates a statistically significant difference from MCP-ala treatment at $p<0.05$ (ANOVA). ** indicates a statistically significant difference from MCP-ala treatment at $p<0.005$ (ANOVA).

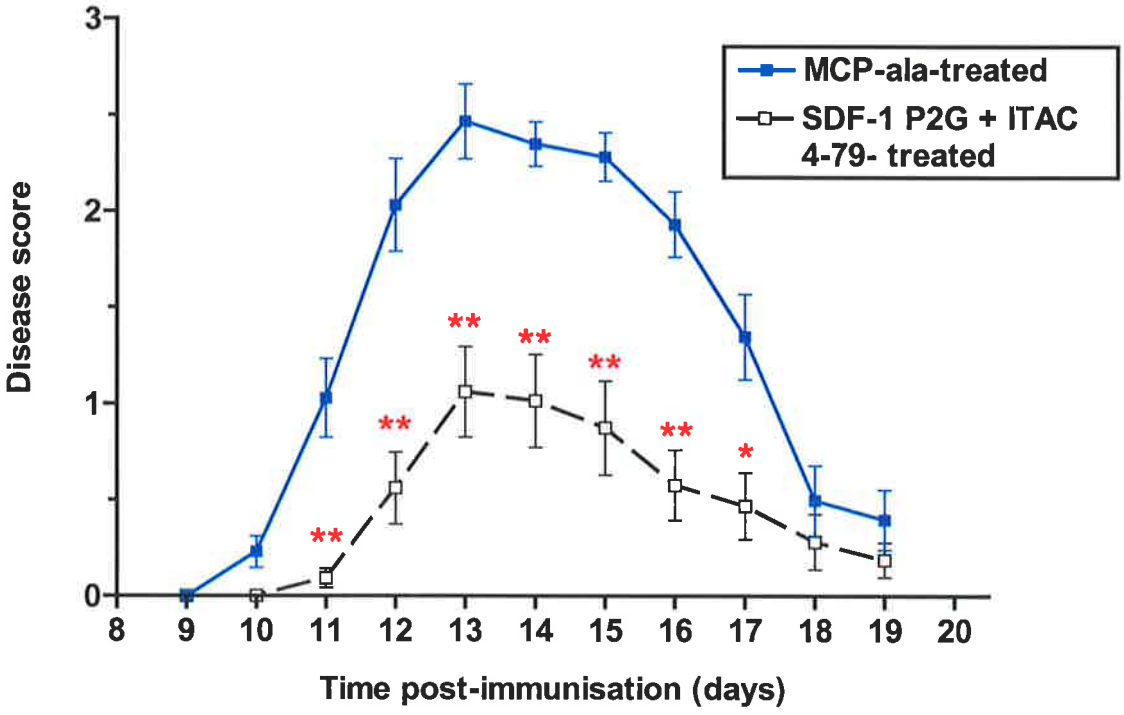
MCP-ala-treated
SDF-1 P2G + ITAC 4-79- treated
Disease score
Time post-immunisation (days)
0
1
2
3
8
9
10
11
12
13
14
15
16
17
18
19
20
**
**
**
**
**
**
*

Table 6.4: Decrease in the number of histopathological lesions in the CNS of SDF P2G- + I-TAC 4-79-treated mice.

Treatment group	Lesions/Transverse Section[a]
MCP-ala [b]	3.18 ± 0.13
SDF P2G- + I-TAC 4-79 [b]	2.10 ± 0.11***

[a] data are the mean ± S.E.M. Total number of histopathologcal lesions enumerated from the thoracic lumbar region of the spinal cords from 3 representative animals from each treatment group. Thirty six 10 μm sections from each mouse were assessed for mononuclear cell infiltration in the meninges and white and grey matter following haematoxylin and eosin staining at 12 days post-induction of EAE.

[b]Treatment as follows: EAE was induced by immunisation with 50 μg $PLP_{139-151}$ and pertussigen, and on days 1, 3, 5, 7, 9 and 11 the mice were given 100 μg of SDF P2G + 250 μg of ITAC 4-79 i.p. or 350 μg control peptide (MCP-ala). At the time of sacrifice, disease scores (mean ± SEM) from the control mice versus the SDF P2G- + I-TAC 4-79-treated mice were 3.31 ± 0.23 and 1.75 ± 0.39, respectively.

***, Statistically significant from the control values at $p < 0.0001$.

Figure 6.11. *Effect of administration of combined SDF-1 P2G and I-TAC 4-79 treatment on the histopathology of EAE in the CNS.* SJL/J mice were injected s.c. with 50 μg $PLP_{139-151}$ in CFA (Section 2.2.1). Two hours before and two days after the injection of emulsion, the mice received 5 μg of pertussigen (i.v.). On days 1, 3, 5, 7, 9, and 11 post-induction, the mice received an intraperitoneal injection of 100 μg of SDF-1 P2G + 250 μg of I-TAC 4-79 or 350 μg of MCP-ala (Section 2.2.4). Twelve days later, the mice were sacrificed, perfused to remove circulating leukocytes (Section 2.6.1), the spinal cord was removed, frozen in OCT and 10 μm cryostat sections were prepared. Representative photomicrographs of haematoxylin/eosin-stained (Section 2.6.5) spinal cord sections from [A] mice treated with MCP-ala or [B] mice treated with SDF-1 P2G + I-TAC 4-79 were assessed for mononuclear cell infiltration in the meninges and white and grey matter. These photomicrographs are representative of 36 sections from 3 mice per treatment group. At the time of sacrifice, mean disease scores (mean ± SEM) from the MCP-ala-treated mice and the SDF-1 P2G + I-TAC 4-79-treated mice were 3.18 ± 0.13 and 2.10 ± 0.11, respectively. Shown are 2 representative images of each condition, captured using the 4X objective.

(A) MCP-ala-treated

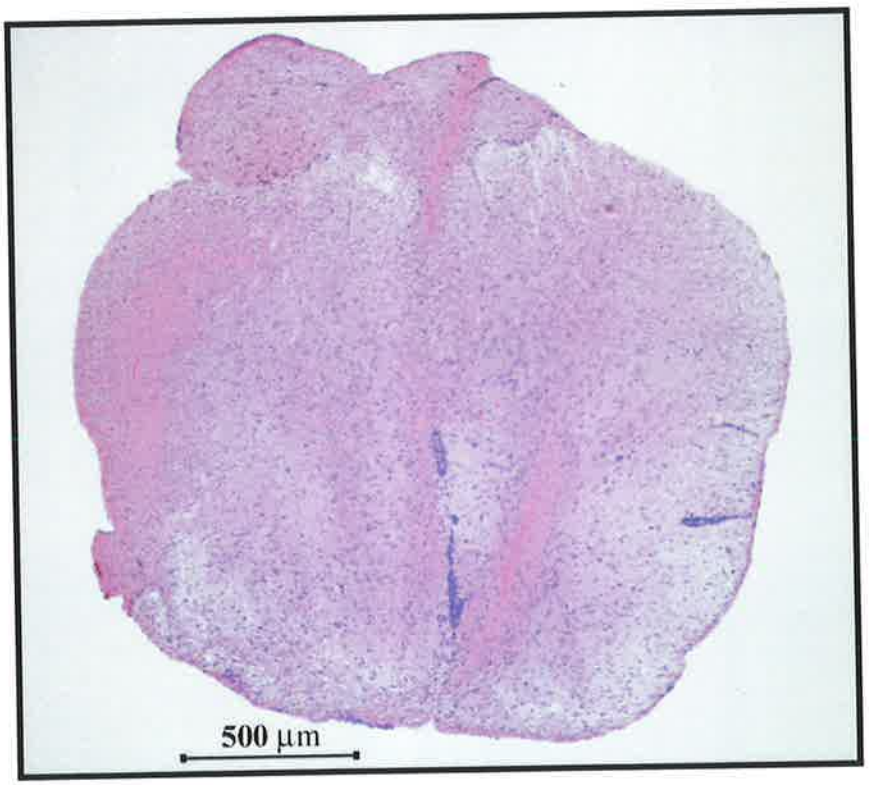

(B) SDF-1 P2G- + I-TAC 4-79-treated

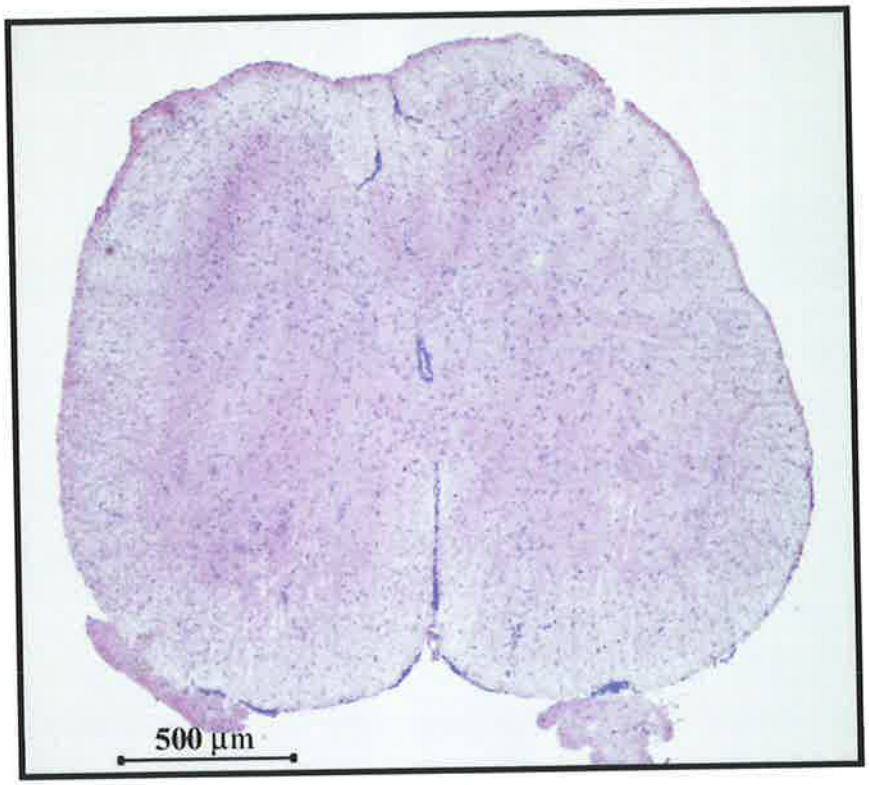

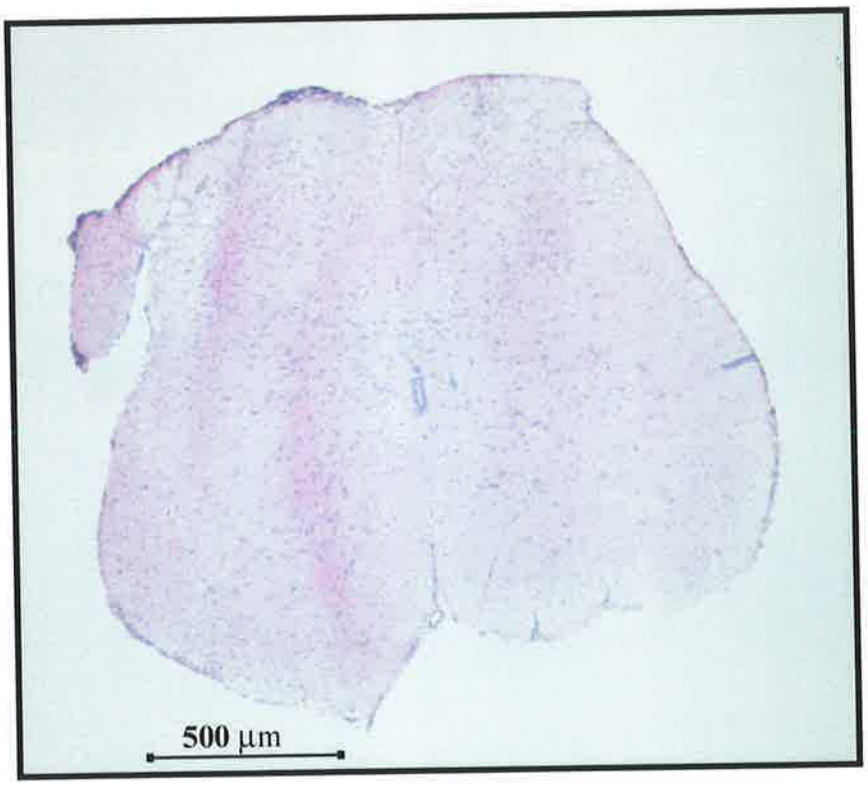

Figure 6.12. *The effect of combined SDF-1 P2G and I-TAC 4-79 treatment on the accumulation of cells in the spinal cords.* SJL/J mice were injected s.c. with 50 μg $PLP_{139-151}$ in CFA (Section 2.2.1). Two hours before and two days after the injection of emulsion, the mice received 5 μg of pertussigen (i.v.). On days 1, 3, 5, 7, 9 and 11 post-induction, the mice received an intraperitoneal injection of 100 μg of SDF-1 P2G + 250 μg of I-TAC 4-79 or 350 μg of MCP-ala (Section 2.2.4). Twelve days post-induction (peak disease), spinal cords were removed and single cell suspensions prepared. The total number of viable cells recovered from each spinal cord was then determined by counting on a haemocytometer after staining with trypan blue. A statistically significant difference between antagonist-treated and MCP-ala-treated mice is indicated by an asterisk ($p < 0.05$). Data are presented as mean ± SEM ($n = 4$).

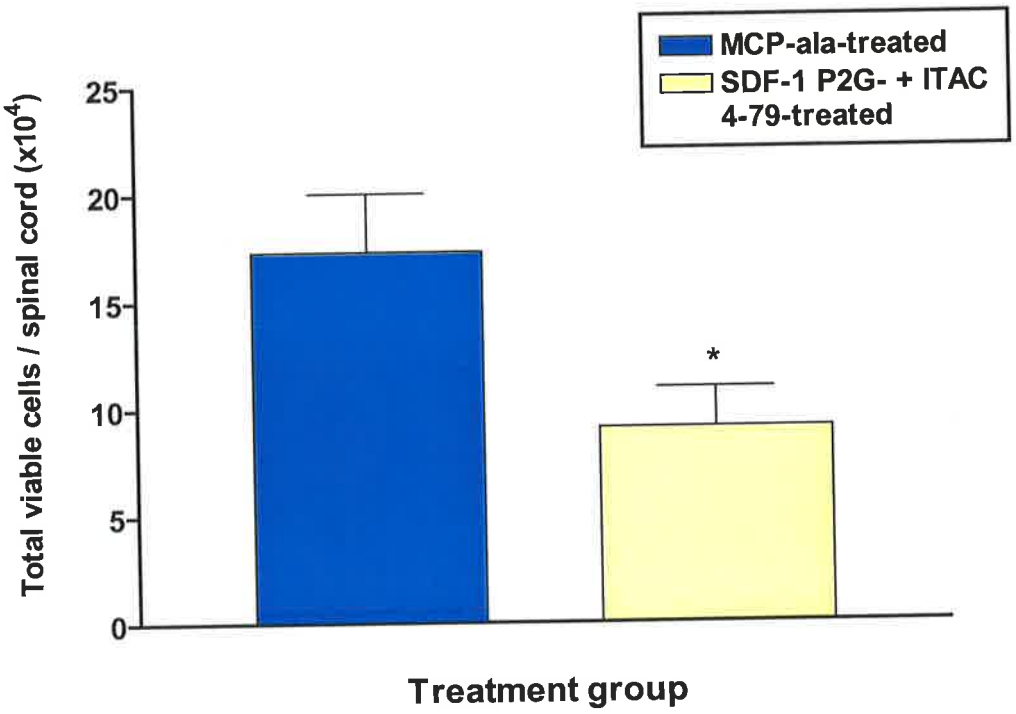
MCP-ala-treated
SDF-1 P2G- + ITAC 4-79-treated
Total viable cells / spinal cord (x10^4)
25
20
15
10
5
0
*
Treatment group

Figure 6.13. *The effect of combined SDF-1 P2G and I-TAC 4-79 treatment on the accumulation of $CD4^+$ T cells in the spinal cords.* SJL/J mice were injected s.c. with 50 μg $PLP_{139-151}$ in CFA (Section 2.2.1). Two hours before and two days after the injection of emulsion, the mice received 5 μg of pertussigen (i.v.). On days 1, 3, 5, 7, 9 and 11 post-induction, the mice received an intraperitoneal injection of 100 μg of SDF-1 P2G + 250 μg of I-TAC 4-79 or 350 μg of MCP-ala (Section 2.2.4). Twelve days post-induction (peak disease), spinal cords were removed and single cell suspensions prepared. The total number of viable cells recovered from each spinal cord was then determined by counting on a haemocytometer after staining with trypan blue. Cells were then labelled with anti-CD4 and analysed by flow cytometry, gating on lymphocytes using forward and side scatter characteristics. The percentage of CD4-positive cells was multiplied by the total cell count value, such that the absolute number of $CD4^+$ cells could be determined. A statistically significant difference between antagonist-treated and MCP-ala-treated mice is indicated by an asterisk ($p < 0.05$). Data are presented as mean ± SEM ($n = 6$).

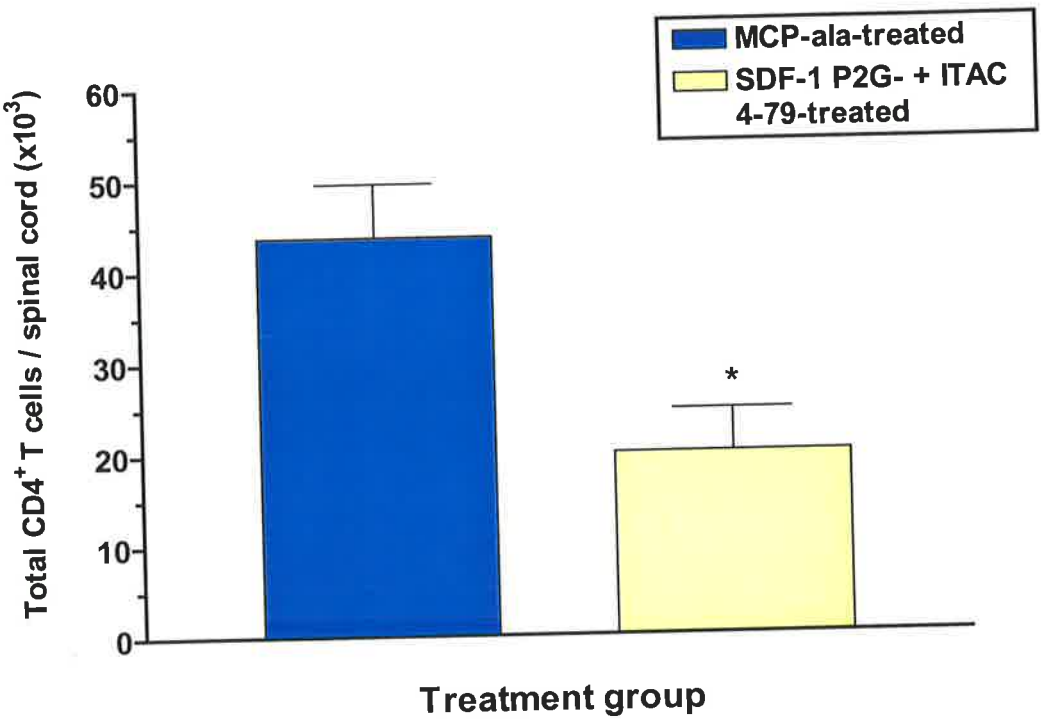
MCP-ala-treated
SDF-1 P2G- + ITAC 4-79-treated
Total CD4+ T cells / spinal cord (x10^3)
60
50
40
30
20
10
0
*
Treatment group

Chapter 7

General Discussion

7.1 Introduction

A considerable body of *in vitro* and *in vivo* data highlights the role of chemokines and their receptors in the regulation of leukocyte migration during both homeostasis and inflammation. Whilst homeostatic chemokines are thought to be responsible for immune system maintenance, inflammatory chemokines are believed to be responsible for the migration of leukocytes to peripheral tissues during inflammation. Like other leukocyte subpopulations, T lymphocytes appear to depend to a large degree on chemokine-regulated mechanisms for recruitment to, and accumulation at, sites of inflammation. However, with over 45 ligands and 19 receptors comprising the chemokine gene super family, the regulation and interplay of the chemokine network *in vivo* is extremely complex, and is thus far poorly understood. One of the major ways in which the chemokine system is likely to be regulated is at the level of receptor expression, for a potential target cell can clearly only respond to a chemokine if it expresses the cognate receptor(s). Accordingly, the aim of the research presented in this thesis was to investigate chemokine receptor regulation and function on $CD4^+$ T lymphocytes during T cell-mediated central nervous system (CNS) inflammation *in vivo*.

To achieve this aim, murine experimental autoimmune encephalomyelitis (EAE) (a model for multiple sclerosis (MS)) was used to study both the sensitisation and effector phases of a T cell-dependent immune response. In this model of inflammation, mice immunised with myelin-derived antigens (or injected with neuroantigen-specific T cells) develop severe neurological impairments as a result of mononuclear cell infiltration into the CNS tissue. Initially, comparative PCR screens of whole organ expression of specific chemokine receptors were performed in order to establish candidate receptors involved in

the sensitisation and effector phases of EAE. Subsequently, chemokine receptor regulation on neuroantigen-specific (encephalitogenic) $CD4^+$ T cells was examined in the draining lymph nodes (LNs), peripheral blood, as well as in the CNS. Finally, the biological relevance of chemokine receptor interactions with their ligands was investigated using chemokine receptor antagonists.

The results generated by this research provide several novel insights into the role of specific chemokines and their receptors in the immune response. They are also highly relevant in the context of MS because they provide evidence that CXCR4, CXCR3 and CCR5 may be useful targets in the control of this disease.

7.2 Pattern of chemokine receptor mRNA expression in the draining lymph nodes and CNS during EAE

As discussed in Chapter 1, naïve T cells are characterised by a distinctly different route of recirculation compared to effector and memory cells (2, 5, 216). Thus, naïve $CD4^+$ T cells recirculate primarily through the lymphatics, passing directly from the blood to the secondary lymphoid tissue through high endothelial venules (HEVs) and back to the blood again via the efferent lymphatic vessels and the thoracic duct. In contrast, effector and memory $CD4^+$ T cells are able to enter peripheral tissues, including the CNS (127, 140). Given the apparent importance of chemokines and their receptors in controlling leukocyte migration, it seemed likely that, upon activation, encephalitogenic $CD4^+$ T cells would be

subject to changes in the patterns of chemokine receptors expressed, and that these changes would contribute to the altered patterns of migration seen for naïve versus effector/memory cells.

The majority of previous studies examining chemokine/chemokine receptor gene expression during EAE have focussed on the spinal cord or the CNS (34, 35, 123, 126) with few specifically focussing on the LNs (142, 217). While data examining chemokine receptor expression in the draining LNs during immune activation are lacking, the expression of some inflammatory chemokines has been observed in conditions other than EAE. MIP-1α/CCL3 and MIP-1β/CCL4 were detected in the draining LNs following cutaneous administration of dinitrofluorobenzene (DNFB) (218), as well as in the LNs of a range of pathologies including HIV infection and granulomatous liver disease (78, 219, 220).

To expand upon the limited previous studies demonstrating chemokine receptor expression in the LNs and CNS during an immune response, an initial RT-PCR screen was conducted to analyse chemokine receptor expression in inguinal LN and spinal cord tissue samples at various time-points throughout EAE and control treatment. Since PLP-induced EAE is known to elicit a Th1-mediated immune response, mRNA expression of the Th1 chemokine receptors, CXCR3 and CCR5, as well as the homeostatic receptor CXCR4, and also CCR1 and CCR2, was analysed in the sensitised LN using RT-PCR. High levels of CXCR4 expression were observed in the LNs of non-immunised mice and expression of this receptor was not affected by EAE induction or mock immunisation, thereby reflecting a potential role for this receptor in the physiological maintenance of the secondary lymphoid organs (22, 221). In contrast, immunisation resulted in a time-dependent

increase in expression of the receptors CCR1, CCR2, CCR5 and CXCR3 in the draining LNs. Throughout the course of EAE, expression of these receptors remained significantly elevated and did not appear to decrease when the mice entered remission. This maintenance of elevated expression during remission may reflect continual cellular activation in the draining LNs due to the use of adjuvant. These results are similar to those obtained for CCR6 expression observed in the draining LNs following the induction of EAE (Liston and McColl, unpublished).

With regard to the CNS, there was specific upregulation of the chemokine receptors CXCR3, CCR1, and CCR5, as well as CXCR4 and CCR2 following EAE induction compared to control immunisation. In contrast, mRNA for the Th2-associated receptors, CCR3, CCR4 and CCR8, was not detected in either spinal cords from control mice or following immunisation, with exception to CCR8. It is important to note, however, that upregulation of CCR8 expression in the CNS was negligible when compared with the other receptors that demonstrated elevated levels of expression in the CNS during EAE. Of the receptors examined, CXCR4 demonstrated the highest level of expression in the normal spinal cord. This was expected since CXCR4 has previously been shown to be expressed by resident cells in the CNS including astrocytes, microglia and pyramidal neurons (210, 222-224). Experiments using wild-type and knock-out mice have revealed that CXCR4 plays a an important role in neuronal and cerebellar development (225). This may help explain the high expression levels of CXCR4 observed in the CNS in the present study. Despite prominent expression of CXCR4 in normal CNS tissue, the data from the present study revealed that CXCR4 mRNA was upregulated in the CNS following EAE induction, such that peak expression correlated with peak clinical disease. These results are similar to Jiang *et al.* (1998), who demonstrated that EAE in the rat was accompanied

by increased levels of CXCR4 mRNA in the lumbar spinal cords of diseased animals (210).

In accordance with previous findings, CXCR3 expression was also detected in the spinal cord in non-immunised animals. Initially, CXCR3 expression was thought to be limited to T cells, however, in the past 2 years, its expression has been observed in both human and murine astrocytes and microglia, and also in astrocytes during CNS inflammation including MS, HIV infection and ischaemic infarcts (226-228). In addition, one study demonstrated that the chemokine SLC/CCL21 initiated a Cl^- current and chemotaxis of microglia through activation of CXCR3, indicating that SLC/CXCR3 interactions may be required for the positioning of these cells in the CNS (53). While CXCR3 was expressed in normal CNS tissue, its expression was significantly upregulated following EAE induction, thus suggesting a role beyond that of maintenance and positioning of resident CNS cells.

Analysis of the PCR data revealed an increase in CCR1, CCR2 and CCR5 expression in the spinal cord over the course of EAE. Statistically significant elevation of these receptors was observed by peak clinical disease, indicating a close correlation between expression of these receptors in the spinal cord and disease symptoms. A significant upregulation of CCR5 mRNA levels was observed in the CNS following EAE induction with $PLP_{139-151}$in the present study. This is in agreement with previous data demonstrating an upregulation of CCR5 mRNA following PLP-induced EAE in SJL/J mice as well as in rat EAE (210, 229). CCR1 and CCR2 have been the focus of many previous studies concerning EAE and CNS injury, and the results yielded from the present study are in agreement with the previous data (210, 211). For example, elevated CCR1 and CCR2

expression has previously been documented in the CNS during EAE (see Table 1.6). Subsequent experiments aimed at determining the functional consequences of CCR1 and CCR2 upregulation involved the use of receptor-deficient mice (101, 146, 147). These experiments revealed that CCR1-deficient mice had decreased incidence of EAE and less severe clinical score (146), and that CCR2-deficient mice were almost completely protected from MOG-induced disease (101, 147). In addition, extensive *in vitro* restimulation assays and adoptive transfer experiments have also been performed using $CCR2^{-/-}$ cells in order to determine the mechanisms of CCR2 involvement in EAE (101, 147). Based on those previous studies, the examination of CCR1 and CCR2 expression in the EAE spinal cords served as a control to verify that the model of EAE implemented in the present study was similar to those used in the previous research. Since they were not the primary focus of the present study, and expression of CXCR4, CXCR3 and CCR5 was clearly modulated, expression of CCR1 and CCR2 was not assessed in further detail.

Previous *in vitro* studies have demonstrated that CCR3 is expressed in cultured human, mouse and rat microglia (226, 230). These studies also demonstrated that CCR3 expression was upregulated in the presence of the inflammatory mediator TNF-α (226, 230). Other studies have documented that CCR3 expression is elevated in the CNS during Alzheimer disease and SIV encephalomyelitis (231, 232). These findings are in contrast to those obtained in the present study, where CCR3 mRNA expression was not detected in the CNS of non-immunised animals, nor was it detected following EAE induction. CNS-specific upregulation of CCR3 has not been identified in other models of EAE.

Whilst comparative RT-PCR is a useful tool to screen for receptor expression, it is not quantitative, nor does it provide information relating to the cellular source of the receptor

expression without first isolating the cells. In addition, due to the readiness with which chemokine receptors are internalised, it is clear that the expression of receptor mRNA does not necessarily correspond to the expression of receptor protein on the cell surface, which is required for responsiveness to chemokine ligands (88). Furthermore, it is possible that subtle changes in the level of gene expression, or changes on only a minor subset of cells, would not be detected using whole organ RT-PCR. Nevertheless, the results obtained from the RT-PCR screen provided initial information relating to chemokine receptors that are upregulated during the pathogenesis of EAE in the SJL/J mouse. Subsequent experiments focussed on identifying changes in the expression and function of CXCR4, CXCR3 and CCR5 on the surface of $CD4^+$ T cells during EAE.

7.3 Spatial and temporal aspects of chemokine receptor regulation during EAE

Experiments aimed at examining receptor regulation on the surface of activated $CD4^+$ T cells during the initiation of EAE in the lymph node (the sensitisation phase) demonstrated that activation was associated with an upregulation of CXCR4, CXCR3 and CCR5. Although co-expression of the three receptors was not determined, many more $CD4^+$ T cells that had undergone division in response to antigenic challenge expressed each receptor, thereby providing evidence for the upregulation of CXCR4, CXCR3 and CCR5 upon T cell activation during EAE. The observed upregulation was maintained as the activated T cells moved from the site of activation to the peripheral blood. Within the blood compartment, the percentage of divided cells expressing the chemokine receptors

was significantly higher than that observed in the draining LNs. It is plausible that these activated $CD4^+$ T cells found in the blood had recently migrated from the LNs. It has previously been shown that effector $CD4^+$ T cells have a reduced capacity to enter the LN via the HEVs due to the modulation of surface adhesion molecule expression (4, 14). This may explain the observed increase in the frequency of divided $CD4^+$ T cells in the peripheral blood.

Flow cytometric analysis of spinal cord preparations revealed a significant increase in the absolute number, as well as the relative proportion, of $CD4^+$ T cells expressing CXCR4, CXCR3 or CCR5 in the CNS throughout the course of EAE. Considering the large influx of lymphocytes into the CNS following PLP-immunisation, it is not surprising that the number of $CCR5^+$, $CXCR3^+$ and $CXCR4^+$ $CD4^+$ T cells increased over the course of disease before declining in the remission phase. If an increase in any of these populations was not observed, this would suggest that cells bearing that receptor were specifically excluded from the CNS, presumably because of a failure to cross the BBB, or a failure to accumulate to detectable numbers in the CNS. This was clearly not the case. In fact, on the contrary, the increased proportion of $CD4^+$ T cells expressing CXCR3 and CCR5 in diseased spinal cord suggests that these cells were preferentially selected for entry and subsequent accumulation into the CNS, particularly at the peak of clinical disease. This was not, however, the case for CXCR4-expressing cells, as the proportion of $CXCR4^+$ $CD4^+$ T cells was not altered in CNS throughout the course of disease.

Thus, in order to specifically analyse regulation of CXCR4, CXCR3 and CCR5 on encephalitogenic $CD4^+$ T cells, the BrdU-positive population of $CD4^+$ T cells in the spinal cord at peak clinical disease was examined. This analysis revealed that antigen specificity

was associated with the upregulation of CXCR4, CXCR3 and CCR5, thereby providing direct evidence for the upregulation of these receptors on neuroantigen-specific $CD4^+$ T cells infiltrating the CNS during EAE. Furthermore, when combined with the results observed in the LN and peripheral blood, the findings from the present study indicate that during sensitisation, these chemokine receptors are upregulated upon activation of $CD4^+$ T cells and remain elevated, such that the cells can perform their effector function at the site of antigen expression. In addition, the results demonstrate that at least part of the increase in CXCR4-, CXCR3- and CCR5- expressing $CD4^+$ T cells in the CNS was due to the upregulation of these receptors on activated cells. The results from the present study are supported by the observation that the chemokine receptors CXCR4 and CCR5 were upregulated on the surface of MBP-specific T cells following transfer into naïve rats compared with cultured MBP-specific T cells (140). However, in contrast to the present study, there was no reported upregulation of CXCR3 on these cells. Thus, in at least two different EAE models, upregulation of specific, albeit different, chemokine receptors on encephalitogenic cells has been demonstrated.

The observed upregulation of CCR5 and CXCR3 on antigen-activated $CD4^+$ T cells during EAE is in keeping with previous studies demonstrating that the expression of these chemokine receptors is often associated with T cell-mediated inflammatory pathologies. For example, the rheumatoid synovium has been shown to be greatly enriched in T cells expressing CXCR3 and CCR5 (233, 234), and large numbers of CXCR3-expressing skin-homing $CD4^+$ T cells can be isolated from psoriatic epidermis (45). Further, in a murine model of bacteria-induced hepatic failure, liver-infiltrating $CD4^+$ T cells are predominantly $CCR5^+$ $CXCR3^+$ (157), and CXCR3 and CCR5 are upregulated on $CD4^+$ T cells in the draining LNs during an allogeneic immune response (204). Importantly,

however, with exception to Ebert *et al.* (2002), while these studies suggest that activated T cells expressing CCR5 and CXCR3 are associated with sites of immune activation, they do not provide evidence that these receptors are acquired during T cell activation. It is quite possible that T cells already expressing these receptors would be selected for localisation at inflammatory sites, in response to production of the cognate chemokine ligands.

With respect to CXCR4 levels on activated $CD4^+$ T cells, the literature is more confusing. CXCR4 expression seems to be dependent upon the nature of the activation signal and also on the species in which the regulation is taking place. However, the results from the present study indicate that CXCR4 is upregulated upon activation of $CD4^+$ T cells during sensitisation to myelin antigens.

Several studies have demonstrated that stimulation of human $CD4^+$ T cells *in vitro* with phytohemagglutinin (PHA) results in upregulation of CXCR4, however, upregulation was dependent upon several factors including cytokine environment, CD28 engagement and the presence of $CD14^+$ monocytes (235-237). In contrast, mitogenic stimulation using PHA resulted in CXCR4 down regulation on $CD4^+$ T cells in other studies (238, 239). Schabath *et al.* (1999) demonstrated that CXCR4 is expressed and regulated differently in human and mouse. Mitogenic activation *in vitro* resulted in an increase in the level of CXCR4 on murine T cells, whereas the receptor was strongly down regulated on human T cells (238). Furthermore, Schabath *et al.* (1999) demonstrated that there was no preferential expression of CXCR4 on naïve mouse T cells, which is contrary to that seen in the human system (23, 29, 65). Few *in vivo* studies examining CXCR4 regulation have been performed. Schabath *et al.* (1999) found that immunisation of mice with the T-

dependent antigen TNP-KLH did not result in any significant change to the percentage of $CD4^+$ T cells in the draining LNs expressing CXCR4, but did observe an increase in CXCR4 expression on $CD8^+$ T cells in the draining LNs. The results of the present study, which demonstrated an upregulation of CXCR4 on the divided $CD4^+$ T cell population, are supported by the observation that immunisation of mice with allogeneic DCs resulted in a significant upregulation of CXCR4 upon activated $CD4^+$ T cells (88). Thus, in at least two different *in vivo* experimental systems, upregulation of CXCR4 on $CD4^+$ T cells in the draining LNs has been demonstrated upon activation. However, as demonstrated, the regulation of CXCR4 expression on $CD4^+$ T cells may differ depending on the nature of the immune response generated.

Although little information has existed until now regarding the regulation of CXCR4, CXCR3 and CCR5 expression on $CD4^+$ T cells *in vivo*, the regulation of other chemokine receptors on $CD4^+$ and $CD8^+$ T cells has been investigated to some extent. Using an adoptive transfer/TCR-transgenic system, $CD8^+$ T cells have been shown to down-regulate expression of CCR7 following lymphocytic choriomeningitis virus (LCMV) infection, which was associated with a dramatically reduced ability to enter the splenic white pulp (240). Of interest, however, no change in the expression of CXCR3 was noted. In another study, ovalbumin-specific TCR-transgenic T cells were shown to upregulate expression of CXCR5 and responsiveness to the cognate ligand, BLC/CXCL13, following immunisation with ovalbumin in complete Freund's adjuvant (CFA), but not in the absence of adjuvant (241). Furthermore, activation of T cells in this system was also associated with reduced chemotactic responsiveness to MIP-3β/CCL19, SLC/CCL21 and SDF-1/CXCL12. While expression of the cognate receptors was not assessed, this observation nevertheless suggests that CCR7 and CXCR4 were down-regulated upon T

cell activation. Again, the conflicting data may indicate the possibility that regulation of chemokine receptors may vary depending on the nature of the immune response.

In summary, the data obtained in the present study provide clear evidence that CXCR4, CXCR3 and CCR5 are upregulated on encephalitogenic $CD4^+$ T cells *in vivo*. The ligands for CXCR3 and CCR5 are inflammatory chemokines, and as such, are produced in defined peripheral tissues, including the CNS, under conditions of inflammation. For example, as discussed in Chapter 1, EAE is associated with the increased production of ligands for CXCR3 and CCR5 in the CNS, including IP-10/CXCL10, I-TAC/CXCL11 (142, 217) and MIP-1α/CCL3, MIP-1β/CCL4 and RANTES/CCL5 (34, 123, 126), and a similar range of chemokines are found in the CNS of patients with MS (114, 115, 136). Ligands for CXCR3 are also readily detectable at sites of various skin pathologies in humans (47). In addition, RANTES/CCL5, MIP-1β/CCL4, as well as all three ligands for CXCR3, have been shown to be expressed at elevated levels following allogeneic transplantation (1). Whilst the ligand for CXCR4 is not considered an inflammatory chemokine, it too is produced at specific sites of inflammation. These include the CNS during EAE, and also the inflamed joints in a model of arthritis (140, 242).

Thus, considering that CXCR4, CXCR3 and CCR5 were upregulated on encephalitogenic $CD4^+$ T cells, and that the ligands for these receptors are known to be produced during CNS inflammation, it seems likely that the observed changes in chemokine receptor expression may contribute to the ability of these cells to migrate to, and accumulate at, the site of inflammation. In support of this hypothesis, the upregulation of CXCR3 and CCR5 on encephalitogenic cells resulted in a significant increase in the migration of these cells toward the relevant chemokine ligands, I-TAC/CXCL11 and MIP-1β/CCL4 *in vitro*. In

contrast, upregulation of CXCR4 did not enhance the migratory capacities of the encephalitogenic cells towards SDF-1, suggesting that CXCR4 upregulation may serve an alternate purpose.

7.4 Chemokine receptor expression is modulated on dividing $CD4^+$ T cells *in vitro*

7.4.1 Comparison of chemokine receptor expression on $CD4^+$ T cells that have divided upon re-stimulation in vitro

Although the $CD4^+$ T cells examined in draining LNs were antigen activated, neuroantigen specificity could not be guaranteed due to the use of CFA in those experiments. Thus, re-stimulation experiments using a defined neuroantigen ($PLP_{139-151}$) were performed in order to establish a population of PLP-specific cells for analysis of receptor expression, and also for use in subsequent adoptive transfer experiments. Furthermore, based on the findings that MBP-specific effector cells are reactivated within the CNS parenchyma following adoptive transfer (140), it was of interest to examine whether cellular reactivation resulted in further modulation of chemokine receptor expression on the surface of $CD4^+$ T cells.

The results from these experiments revealed that re-stimulation with $PLP_{139-151}$ resulted in an increase in the percentage of divided (PLP-specific) $CD4^+$ T cells expressing CXCR3 and CCR5, an observation that supports that observed during $CD4^+$ T cell activation in the

draining LN *in vivo*. In addition, these findings are consistent with other *in vitro* studies demonstrating upregulation of these receptors during allogeneic activation (88, 89) and increased mRNA expression in other neuroantigen-activated $CD4^+$ T cells (243).

Interestingly, the results from *in vitro* chemotaxis assays in the present study indicated that restimulation was required for a functional change in CXCR3 expression. This was demonstrated by the ability of PLP-restimulated cells to migrate in response to low concentrations of CXCR3 ligands, whereas higher concentrations of the ligands were necessary for the movement of PLP-sensitised cells. Therefore, it is postulated that PLP-sensitised T cells upregulate CXCR3 expression, however, require further stimulation in order to migrate in response to CXCR3 ligands. In contrast to that observed for CXCR3-mediated migration, the initial upregulation of CCR5 on PLP-sensitised cells is sufficient for functional migration of these cells towards CCR5 ligands, although the migratory responses to the CCR5 ligands was lower than those towards the CXCR3 ligands.

In contrast to that observed for CXCR3 and CCR5, the percentage of divided cells expressing CXCR4 was similar to the percentage of non-divided cells expressing this receptor. This indicates that further upregulation of CXCR4 is not required for encephalitogenicity. It is plausible that upregulation of CXCR4 on $CD4^+$ T cells during clonal selection in the draining LN is required for efficient activation of the T cell, but that it is not required for reactivation. This observational data is supported by the functional *in vitro* chemotaxis data in the present study. In these experiments, both naïve and PLP-sensitised cells demonstrated a marked migratory response towards the cognate ligand of CXCR4, SDF-1/CXCL12, with PLP-sensitised cells demonstrating the greatest response (although only significantly greater at one time point). Similarly to that observed for

CXCR4 expression, while restimulated cells displayed migratory capacities towards SDF-1/CXCL12, there was no significant change compared with the other cells tested. The proposed hypothesis relating to CXCR4 function on $CD4^+$ T cells will be discussed in more detail later in the chapter.

7.4.2 Elevated expression of CD4 on PLP-specific cells re-stimulated in vitro

An interesting observation was made when examining the regulation of chemokine receptors during the *in vitro* re-stimulation concerning levels of CD4 expression. When analysing CD4 expression, a bimodal pattern of CD4 was observed. Over 80% of the $CD4^+$ T cells that had divided upon re-stimulation were $CD4^{hi}$. This development of a population of $CD4^{hi}$ T cells has been observed previously both in the mouse and human systems following allogeneic activation (88, 244). Ridgeway *et al.* (1998) documented an upregulation of CD4 on murine T cells following activation *in vitro* and *in vivo* (244), and more recently, Ebert *et al.* (2001) demonstrated an upregulation of CD4 on T cells in response to cellular activation in the human MLR (88). The biological significance of CD4 upregulation is not clear at present, however, the results from the present study demonstrate that modulation of chemokine receptor expression was restricted to T cells expressing elevated levels of CD4. It is possible that the increased levels of CD4 are required for interactions distinct from those mediated by class II MHC ligation. In this regard, IL-16 is a functional ligand for CD4, and upon binding is able to induce a variety of effector functions in $CD4^+$ T cells, including chemotaxis and induction of IL-2R expression (245). Additionally, the ligation of CD4 by IL-16 in the absence of TCR triggering can result in the transmission of a negative signal, preventing subsequent activation through the TCR. Thus, upregulation of CD4 may allow the efficient binding

of IL-16 in the absence of antigen signaling, thereby regulating the degree of T cell stimulation.

7.5 Characterisation of chemokine antagonists *in vitro*

The search for chemokine antagonists began several years ago when chemokine receptor blockade was recognised as a possible therapeutic approach for the treatment of inflammatory diseases. It is well established that chemokine antagonists can be generated by modifying the N-terminal region of natural chemokines (246). The first studies focused on IL-8 and other ELR-containing chemokines, which yielded antagonists for CXCR1 and CXCR2 (247). As discussed in Chapter 1, chemokines have two main sites of interaction with their receptors – one in the N-terminal region prior to the first cysteine and another within an exposed loop of the backbone that extends between the second and third cysteine residues (160). It has been suggested that chemokines initially bind to receptors via interactions between the exposed loop region and the receptor. Subsequent interactions between the N-terminal region and the receptor facilitate receptor activation (21, 51). Therefore, progressive N-terminal truncation, or mutation, results in a molecule that cannot activate its receptor, but can compete with endogenous ligand binding. Subsequent studies have revealed that similar truncations to CC chemokines results in effective chemokine antagonists (161, 163, 165, 214). However, N-terminal truncation has not always yielded derivatives with antagonistic properties. This was the case when mutants of IP-10 and eotaxin were made. Deletion of N-terminal amino acids in these molecules resulted in simultaneous loss of activation and receptor binding (51).

The initial experiments in Chapter 5 were performed in order to determine whether N-terminal modifications to the CXC chemokines SDF-1/CXCL12 and I-TAC/CXCL11, and the CC chemokine RANTES/CCL5 produced antagonists that could subsequently be used *in vivo* in the mouse. As previously mentioned, an antagonistic role for both SDF-1 P2G and RANTES 9-68 has previously been described in terms of binding capacities and chemotactic inhibition of cultured human cells. However, with the exception of preliminary studies involving RANTES 9-68 in a model of arthritis (cited in (165)), this is the first study to use these molecules in a model of inflammation. Since the model of EAE employed in the present study involved mice, the mutants were first assessed for their capacity to act as antagonists against murine chemokine ligand/receptor interactions. *In vitro* tests of the SDF-1 P2G and RANTES 9-68 mutants clearly demonstrated their lack of ability to effectively function directly as chemotactic agents for PLP-specific lymphocytes. When added to constant sub-optimal concentrations of the wild-type chemokines, both SDF-1 P2G and RANTES 9-68 dose-dependently inhibited SDF-1/CXCL12- and RANTES/CCL5-mediated chemotaxis of $PLP_{139-151}$-stimulated lymphocytes and *Salmonella enteritidis*-reactive T lymphocytes, respectively, albeit to different extents. RANTES 9-68 also dose-dependently inhibited the migration of *Salmonella enteritidis*-reactive T lymphocytes to the CCR5 ligand, MIP-1β/CCL4.

In recent years, several publications have revealed that the CXC chemokine I-TAC is the dominant ligand for CXCR3 (248-250). Those studies demonstrated that I-TAC has a significantly higher affinity for CXCR3, as well as higher potency and efficacy than IP-10 or Mig (248-250). Based on these findings, and also on the fact that N-terminal truncations of IP-10 lost their capacity to bind CXCR3 (51), three N-terminal truncation

mutants of mI-TAC were synthesised and tested for their ability to antagonise activation of CXCR3. Initially the I-TAC mutants were assessed for their agonistic capacities. These preliminary experiments indicated that decreased agonistic properties of the truncation mutants correlated with an increase in the number of amino acids removed. Thus, the molecule that possessed the poorest chemotactic potential was the 5-79 truncation mutant of I-TAC. With regard to inhibition assays, however, the opposite was observed. In these experiments, using a sub-optimal concentration of wild-type mI-TAC/CXCL11 as an agonist, it became apparent that the progressive removal of the N-terminal amino acids resulted in a diminished capacity of the mutant to act as an antagonist. I-TAC 3-79 displayed the greatest potential to inhibit the I-TAC-induced migration, followed by I-TAC 4-79, whereas I-TAC 5-79 only inhibited migration at very high concentrations. Based on the above results, the I-TAC 4-79 mutant was selected for subsequent use *in vivo* since it displayed limited agonistic activity, but was still able to inhibit migration at lower concentrations than I-TAC 5-79.

As mentioned above, ligand-binding assays showed that I-TAC/CXCL11 has a higher affinity for CXCR3 than either IP-10/CXCL10 or Mig/CXCL9 (248). Furthermore, calcium mobilisation assays have previously demonstrated that while low concentrations of I-TAC (50nM) completely desensitized the response of CXCR3-expressing cells to a subsequent challenge with IP-10 or Mig, high concentrations of IP-10 and Mig (1000nM and 500nM, respectively) could not completely desensitize I-TAC responses. This led to the conclusion that these three chemokines may interact differently with the receptor. Cox *et al.* (2001) confirmed these findings and concluded that the binding of IP-10 and I-TAC to the G protein-coupled state of CXCR3 is allotopic, that is, each chemokine binds to different sites of the coupled receptor (249). However, although wild-type I-TAC is

capable of fully displacing IP-10 and Mig binding to CXCR3 in the human system, the results from the *in vitro* chemotaxis assays performed in the present study indicate that the mI-TAC 4-79 antagonist is not. While I-TAC 4-79 dose-dependently inhibited I-TAC-, IP-10- and Mig-mediated chemotaxis of PLP-specific cells, the analyses revealed that I-TAC 4-79 did not completely inhibit IP-10- and Mig-mediated migration. These results suggest two possibilities. Firstly, it is possible that the first 3 amino acids are in some way implicated in the high-affinity binding of the I-TAC to G protein-coupled CXCR3, and that loss of these results in a decreased ability to compete with IP-10. Alternatively, since the majority of binding assays involving CXCR3 and its ligands have used human molecules, it is possible that the results observed in the present study reflect the differences between the murine and human species.

7.6 Determination of a functional role of specific chemokine/ receptor interactions during EAE

7.6.1 A role for SDF-1/CXCR4 in the activation of $CD4^+$ T cells

Administration of SDF-1 P2G inhibited clinical EAE and markedly decreased histological evidence of the disease. SDF-1 P2G significantly reduced the maximum clinical disease score and the number of days over which the mice were displaying neurological signs compared with control-treated mice. Although the treatment did not completely prevent all signs of clinical disease, the changes observed at the level of paralysis were significant. For example, the mice from the control-treated cohorts consistently showed signs of

severe hindlimb paralysis with limited mobility at the peak of clinical disease, whereas mean maximum clinical scores mice from the SDF-1 P2G-treatment groups indicated that the level of paralysis rarely exceeded tail flaccidity. In addition, treatment with SDF-1 P2G afforded some mice complete protection from disease, which contrasted to that observed in the control-treated animals. This is the first study to demonstrate a role for the interaction between SDF-1/CXCL12 and its receptor during EAE.

The observed upregulation of CXCR4 on neuroantigen-specific T cells during EAE, together with the finding that inhibition of the ligand/receptor interaction results in inhibition of disease, indicates that the SDF-1/CXCR4 interaction plays more than just developmental and homeostatic roles in the immune system. This proposal is supported by studies examining the role of SDF-1/CXCR4 in the pathogenesis of arthritis. Matthys *et al.* (2001) demonstrated a role for CXCR4 in autoimmune collagen-induced arthritis (CIA) in IFN-γ receptor-deficient mice. In that study, a non-peptide inhibitor of the SDF-1/CXCR4 interaction inhibited autoimmune joint inflammation when treatment was initiated between the time of immunisation and the appearance of clinical symptoms (251). In addition, CXCR4 has been implicated in the accumulation of T cells in the synovium during rheumatoid arthritis (252, 253). Buckley *et al.* (2000) observed TGF-β1-induced high expression levels of CXCR4 on $CD45RO^{+}$ $CD45RB^{dull}$ T cells in the synovium, which was similar to that observed on activated T cells in the present study. Like the present study, these cells were not expected to express the homeostatic receptor (based on reported SDF-1/CXCR4 involvement in naïve cell migration). However, based on their findings, Buckley *et al.* (2000) suggested that persistent induction of CXCR4 on synovial T cells by TGF-β1 leads to their active, SDF-1/CXCL12-mediated retention in a perivascular distribution within the rheumatoid synovium (252).

Since TGF-β1 has been documented in the CNS during EAE (referenced in (254)), and SDF-1/CXCL12 is constitutively expressed on neuroepithelial cells and has been detected in the CSF of MS patients (255: Pashenkov, 2003 #400)), upregulation of CXCR4 by TGF-β1 may be a potential mechanism by which encephalitogenic T cells cross the BBB and subsequently accumulate in the CNS, and that inhibition of the SDF-1/CXCR4 interaction could interfere with this transendothelial migration. The observed decrease in the number of cellular infiltrates observed in the spinal cords of SDF-1 P2G-treated mice certainly supports this possibility. However, analyses examining the proportion of CXCR4-expressing $CD4^+$ T cells in the CNS of SDF-1 P2G-treated mice revealed that SDF-1 P2G treatment did not specifically retard the entry of CXCR4-expressing cells into the CNS, since there were similar percentages of these cells in the CNS of both the SDF-1 P2G- and control-treated mice. In addition, throughout the course of EAE it was demonstrated that CXCR4-expressing $CD4^+$ T cells were not specifically selected for entry and accumulation in the CNS. This is in contrast to that observed with respect to CXCR3- and CCR5-expressing $CD4^+$ T cells. Furthermore, as demonstrated by lack of disease inhibition in adoptive transfer experiments, SDF-1 P2G-treatment did not inhibit the entry and accumulation of effector cells in the CNS. Thus, while the above proposal cannot be eliminated, it appears that the interaction between SDF-1 and CXCR4 is not essential during the effector phase of EAE.

The results of the present study revealed a potential role for SDF-1/CXCR4 in the sensitisation phase of the immune response. In order to determine whether the observed decrease in clinical disease severity and CNS cellular infiltration in the SDF-1 P2G-treated mice was due to a reduction in antigen-specific priming, the proliferative response of

$PLP_{139-151}$-specific lymphocytes was analysed using bulk lymphocyte cultures. Lymphocytes from SDF-1 P2G-treated mice proliferated less robustly in response to $PLP_{139-151}$ compared with lymphocytes from control-treated mice. Analysis of the $CD4^+$ T cell population revealed that the reduced proliferation was attributable to a significant decrease in the number of $CD4^+$ T cells dividing in response to the antigen, thus indicating that inhibition of disease in SDF-1 P2G-treated mice was associated with a decreased PLP-specific $CD4^+$ T cell response. This decrease may be the result of fewer antigen-specific T cells recruited into the draining lymph nodes, an impaired T cell proliferative response in SDF-1 P2G-treated mice, or a combination of both. Initial analysis of cell numbers indicated that there were equivalent numbers of cells recruited to the draining LNs across the treatment groups, indicating that the reduction in proliferation in the SDF-1 P2G-treated mice was most likely due to less efficient T cell activation in the draining LN.

It is proposed that in addition to regulating leukocyte trafficking, chemokines also play a role in leukocyte activation. It is well established that chemokines can induce granule release from monocytes, neutrophils, eosinophils, and basophils (16). However, data are also accumulating demonstrating that chemokines participate in lymphocyte activation. For example, a recent *in vitro* study using human T cells described SDF-1/CXCL12 as a costimulator of T cell activation (75). The identified role for SDF-1/CXCL12 and CXCR4 during T cell activation in the present study in the draining LNs is consistent with this previous *in vitro* finding. These data together with those demonstrating an increase expression of CXCR4 during T cell activation *in vivo* (present study and (140)) suggest that SDF-1/CXCL12 also costimulates murine T cells through CXCR4. The mechanism(s) by which SDF-1 may activate T cells is currently unknown. However,

previous reports provide evidence that SDF-1/CXCL12 stimulation induces phosphorylation of Pyk2 via a G-protein-coupled pathway (256, 257), which activates mitogen-activated protein (MAP) signal-related kinases (256-258). In addition, SDF-1/CXCL12 stimulation increases NF-κB activity (258). These molecules, and others, have been implicated in CD28 signalling (259, 260). Further investigation into this mechanism of SDF-1-mediated costimulation requires experiments examining the direct effect of SDF-1 P2G on the proliferative response of PLP-specific cells *in vitro*, and also determining whether lymphocytes from SDF-1 P2G-treated mice possess the ability to transfer EAE.

MBP-specific effector cells are reactivated within the CNS parenchyma following adoptive transfer (140) and this local reactivation correlates with the pathogenic potential of the cells. The results from the adoptive transfer experiments in the present study suggest that CXCR4 stimulation is not required for the reactivation of encephalitogenic cells in the CNS. Thus, it appears that SDF-1-mediated activation of CXCR4 is required for efficient activation of naïve $CD4^+$ T cells in the draining LNs, but that it is not required during the reactivation of $CD4^+$ T cells in the target organ. This proposal is similar to the prevailing theory that the threshold for activation of memory/effector cells is lower than that of naïve cells, as demonstrated by a lack of requirement for costimulatory molecules such as CD28 and B7 for reactivation of memory/effector cells (82). To further investigate this hypothesis, the effect of SDF-1 P2G treatment on EAE relapses will need to be examined.

7.6.2 CXCR3 expression is required for accumulation of $CD4^+$ T cells in the CNS during EAE

I-TAC 4-79 treatment during active EAE induction in the SJL/J mouse significantly ameliorated EAE, with the most beneficial effects being observed at the onset of disease. In all experiments conducted, treatment with I-TAC 4-79 resulted in a significant delay in disease onset by at least 1 day, and as a result, disease length was reduced by more than 1 ½ days. Whilst disease scores were significantly lower than the control-treated animals on a number of days throughout disease, the difference in mean maximal clinical disease scores was not as great as that seen in either the SDF-1 P2G- or RANTES 9-68-treated animals. This may be due to reduced antagonistic potency compared with the SDF-1 P2G and RANTES 9-68, as was observed in the *in vitro* chemotaxis assays. Alternatively, the requirement for I-TAC/CXCR3 interactions during disease pathogenesis may not be as vital as interactions involving SDF-1 and RANTES. The observed inhibition of clinical disease was associated with decreased recruitment of lymphocytes into the CNS, as determined by histological analysis and flow cytometry. Furthermore, treatment of recipient mice with I-TAC 4-79 prior to the transfer of encephalitogenic cells significantly reduced clinical symptoms of EAE, indicating that the I-TAC/CXCR3 interaction is important during the effector phase of this T cell-mediated immune response.

Although it has been demonstrated *in vitro* that I-TAC binds to CCR3 (51), the major receptor for this molecule is CXCR3, a receptor that has been shown in the present study to be upregulated in both the draining lymph nodes and spinal cord during EAE. In contrast, CCR3 expression was not detected at either site. It therefore seems highly likely that I-TAC 4-79 is mediating its effects through CXCR3 blockade. Moreover, I-TAC is a

natural antagonist of CCR3, a Th2 receptor (51). Thus, even if CCR3 were expressed during the course of EAE, and I-TAC 4-79 was binding to it, this would theoretically further skew the immune response towards a Th1 phenotype, thereby exacerbating EAE. This is clearly not the case as I-TAC 4-79 inhibits EAE.

Experiments described in Chapter 4 indicated that CXCR3-expressing $CD4^+$ T cells are specifically selected for entry into the CNS during EAE and that antigen-activated cells upregulate expression levels of CXCR3. Therefore, attempts were made to determine whether the reduction in inflammation observed in the CNS of I-TAC 4-79-treated mice at the peak of clinical disease was a result of reduced proportion of CXCR3-expressing neuroantigen-specific $CD4^+$ T cells accumulating in the CNS. This analysis revealed that I-TAC 4-79 specifically inhibited the influx and accumulation of CXCR3-expressing $CD4^+$ T cells into the CNS, findings that are in accordance with those seen following anti-CXCR3 mAb treatment during EAE in the SJL/J mouse, in which neutralisation of CXCR3 alleviated the severity of EAE (158).

The prevailing model of CNS T cell entry suggests that while activated T cells have the capacity to enter the CNS, only antigen-specific T cells are retained (127). In addition, it has previously been demonstrated that CNS-specific inflammatory chemokine expression follows, rather than precedes the earliest infiltration of leukocytes at the onset of EAE (referenced in (136)). Taken together, these observations suggest that initial CNS antigen-specific T cell transendothelial migration does not require inflammatory chemokine expression by the resident CNS cells. However, based on the present findings, it is hypothesised that CXCR3 expression on neuroantigen-specific T cells is required for the accumulation of these cells in the CNS, and the subsequent accumulation of non-specific

inflammatory cells, during EAE. These findings are consistent with those of Fife *et al.* (2001) who demonstrated reduced mononuclear cell infiltration in the CNS of SJL/J mice following adoptive transfer of EAE and treatment with neutralising anti-IP-10/CXCL10 (141). It was proposed that IP-10/CXCL10 (a CXCR3 ligand) expression is required for antigen-specific T cells and other mononuclear cells to accumulate in the CNS during EAE, and that in the absence of T cell accumulation, inflammatory signals that amplify the pathogenic response are not present (141). Furthermore, in agreement with that observed in the present study, accompanying the reduction in cellular infiltration into the CNS tissue was a decrease in disease severity and disease incidence following anti-IP-10 treatment (141). Therefore, the data in the present study and those of Fife *et al.* (2001) indicate that CXCR3 ligand expression is involved in the accumulation of CXCR3-positive encephalitogenic T cells in the CNS during EAE.

A critical role for the IP-10/CXCR3 interaction has also been demonstrated in another animal model for MS involving infection of C57Bl/6 mice with mouse hepatitis virus (MHV) (159, 261). Following intracerebral infection with MHV, a vigorous immune response in the CNS ensues, followed by chronic demyelination and clinical paralysis (261). The mice develop clinical signs of paralysis, similar to those observed during EAE. The results from those studies revealed that early IP-10/CXCL10 expression is important for virus elimination, since mice treated with anti-IP-10 from days 0 to 10 post-infection had a higher mortality rate, reduced viral clearance and a significant reduction in the number of $CD4^+$ and $CD8^+$ T cells in the CNS (261). However, when MHV-infected mice were treated with the neutralizing antibody from days 12 to 20 post-infection, a significant decrease in disease severity was observed, indicating a role for IP-10/CXCL10 in virus-induced inflammatory demyelination. Similarly to the present study, a decrease in

CXCR3-expressing $CD4^+$ T cells in the CNS of anti-IP-10 treated animals was demonstrated, further indicating that later expression of IP-10/CXCL10 in the CNS is required for T cell accumulation (159). In IP-10/CXCL10 knockout mice infected with MHV, identical findings to Liu *et al.* (2000) were reported, in that there was an increased viral burden in the CNS of $IP\text{-}10^{-/-}$ mice compared with wild-type mice, which correlated with decreased T cell infiltration (149). In contrast to that observed in the present study, a potential role for the IP-10/CXCR3 interaction during T cell priming was observed in $IP\text{-}10^{-/-}$ mice (149). Whether IP-10/CXCL10 was playing a role in the recruitment of T cells into the draining LNs, in the activation of T cells, or a combination of both, was not determined in that study. Nevertheless, their *in vitro* data were consistent with those reported for the $CXCR3^{-/-}$ mice, which exhibited a decreased proliferative potential of T cells in the mixed lymphocyte reaction (MLR) (33).

More recently, the influence of anti-IP-10 mAb in EAE induced in the Lewis rat has been reported (142). In contrast to the present study and that of Fife *et al.* (2001), these investigators showed that IP-10/CXCL10 neutralisation exacerbated clinical disease by enhancing the accumulation of effector T cells in the CNS. It was demonstrated that the increase in the number of T cells entering the CNS was due to premature release of the cells from the draining lymph nodes, indicating that IP-10/CXCL10 plays a role in the retention of T cells in the LN, similar to studies by Yoneyama *et al.* (2002) (78). Expression of the three major CXCR3 ligands was measured in the draining LNs and CNS. The analyses revealed that only IP-10/CXCL10 and Mig/CXCL9 were expressed in the draining LNs (and spleen), whereas all three ligands were expressed in the CNS. This is in contrast to that observed by McColl *et al.* (manuscript submitted), who demonstrated expression of all three CXCR3 ligands in the draining LNs of rats during the development

of EAE and only of IP-10/CXCL10 and I-TAC/CXCL11 in the CNS (217). Nonetheless, Narumi *et al.* (2002) proposed that following initial activation, T cells are retained in the draining LNs by IP-10/CXCL10 expression until they become polarised Th1 cells expressing elevated levels of CXCR3, which then enables them to move towards a peripheral I-TAC/CXCL11 gradient in the CNS for subsequent accumulation (142). No evidence supporting this theory was observed in the present study. There was no difference in draining LN size between the I-TAC 4-79-treated mice and the control-treated mice, nor was there a difference in the number of cells accumulating in the draining LNs. The CXCR3 antagonist used in present study was an I-TAC analogue that did not completely inhibit *in vitro* IP-10-mediated migration of T cells (although 90% inhibition of IP-10-mediated migration was observed, and it was not shown how effective the anti-IP-10 antibody used by Narumi *et al.* was at inhibiting IP-10-induced chemotaxis). Therefore, treatment with I-TAC 4-79 may not have affected the initial IP-10-mediated retention of T cells in the LN and it may be possible that the observed reduction in the number of cells in the CNS in the present study was the result of inhibition of the I-TAC/CXCR3 interaction in the CNS and not the IP-10/CXCR3 interaction in the LN. Whilst this hypothesis is in theory plausible, the findings from other studies involving the disruption of IP-10 function do not support it scientifically (141, 149, 262). Nonetheless, further experiments involving combination treatment with anti-IP-10 and anti-I-TAC antibodies will provide important insights into this proposal.

7.6.3 RANTES interaction with CCR5 or CCR1 effects the development of EAE

RANTES 9-68 treatment resulted in a dramatic improvement in the clinical status of diseased mice. Disease onset was significantly delayed by approximately 2 ½ days, and

mean maximum clinical disease scores were markedly lower in the RANTES 9-68-treated animals than in control-treated animals. The difference in neurological symptoms between the two groups was similar to that observed between the SDF-1 P2G-treated mice and the control-treated animals. In addition, not all RANTES 9-68-treated mice were affected by clinical disease. Histological and flow cytometric analyses revealed that the observed reduction in neurological impairment was due to reduced numbers of $CD4^+$ T cells infiltrating the CNS. Importantly, the proportion of $CCR5^+CD4^+$ T cells in the CNS of RANTES 9-68-treated mice was significantly lower than that observed in the control-treated mice. This *in vivo* observation is consistent with the *in vitro* chemotaxis data demonstrating that RANTES 9-68 inhibited MIP-1β/CCL4-mediated migration. Since it was observed that $CCR5^+CD4^+$ cells are specifically selected for entry or accumulation in the CNS during EAE, it seems likely that the mechanism by which RANTES 9-68 reduces inflammation is by preventing accumulation of these cells in the CNS. Neuroantigen-specific T cells purportedly amplify the inflammatory response in the CNS, which results in the recruitment of non-specific macrophages, the proximate mediators of tissue injury (32). Therefore, prevention of the initial accumulation of T cells in the CNS may have reduced CNS inflammation and subsequent tissue damage. Furthermore, RANTES 9-68 may also directly inhibit the accumulation of macrophages, since macrophages have also been shown to express CCR5 (263).

$CCR5^{-/-}$ mice (C57Bl/6) have also been used to study the pathogenesis of EAE. In contrast to that observed in the present study using RANTES 9-68, $CCR5^{-/-}$ mice were equally susceptible to acute-monophasic MOG-induced EAE as the wild-type controls (145). It is important to note that the disparity between the separate studies underscores the variability of chemokine and chemokine receptor expression patterns in different

strains and species induced to develop EAE with different antigen priming and cell transfer regimens. This is further illustrated by the opposing results seen following EAE induction using MOG in MIP-1α-null mice (C57Bl/6) (145) versus those seen in recipient SJL/J mice treated with neutralising anti-MIP-1α antibodies (123). In these experiments, MIP-1α-null mice were fully susceptible to EAE, whereas anti-MIP-1α treatment inhibited adoptively-transferred EAE.

It is also important to note that expression of CCR1 protein was not examined in the present study. Since RANTES binds to CCR1 and CCR3 as well as CCR5, the effect mediated by RANTES 9-68 may not solely be due to the inhibition of CCR5, although ligand displacement studies using RANTES 9-68 on cell transfectants expressing either CCR1, CCR3 or CCR5 indicate a high level of selectivity of RANTES 9-68 for CCR5 (Clark-Lewis, personal communication). In the present study, PCR analyses demonstrated that CCR3 was not expressed in the spinal cord during EAE. However, CCR1 was upregulated such that peak expression correlated with peak clinical disease. In addition, both encephalitogenic T cells (144, 243) and macrophages (54) have previously been shown to express CCR1. Therefore, it is plausible that the observed inhibition of EAE, resulting from RANTES 9-68-treatment, was in part due to the blockade of CCR1. Indeed, as discussed in earlier, CCR1 has previously been shown to play a role in the pathogenesis of MOG-induced EAE in the mouse (146). In that study, mice lacking CCR1 (Bl6/129) experienced significantly milder disease than wild-type controls. However, since neither lymphocyte nor monocyte/macrophage CNS infiltration was examined, no conclusions could be drawn regarding the mechanisms by which CCR1 was involved in disease pathogenesis. In addition, a small-molecule non-peptide antagonist of CCR1 reduced the severity of monophasic EAE in rats (54, 264).

In order to definitively characterise a role for CCR5, separate from that of CCR1, in the pathogenesis of EAE, a molecule that specifically targets CCR5 is required. In this respect, an antibody to mCCR5 would be a suitable candidate, although it poses a challenge to generate and characterise. Several attempts were made to generate anti-CCR5 antibodies during the present research, to no avail. Treatment with small non-peptide antagonists is also a potential way in which to modulate chemokine receptor expression. However, generation and characterisation of those molecules was beyond the scope of the laboratory in which the present research was conducted.

The importance of RANTES interactions with its receptors in the development of MHV-induced neurologic disease and adjuvant-induced arthritis has previously been documented (242, 265). Both studies demonstrated that RANTES expression at the site of inflammation was responsible for the subsequent accumulation of $CD4^+$ T cells and macrophages. In addition, the results from the present study are supported by observations involving the use of another RANTES peptide antagonist, Met-RANTES, in EAE (199). Met-RANTES acts with nanomolar affinity on CCR1 and displays high-affinity binding to CCR5 (164). Treatment of mice with Met-RANTES significantly reduced disease severity in the acute phase and chronic plateau phase of a chronic-relapsing model of EAE (immunisation of SJL/J mice with $PLP_{139-151}$) (199). In contrast to that observed in chronic-relapsing EAE, it was revealed that Met-RANTES treatment did not significantly ameliorate acute MOG-induced monophasic EAE in C57Bl/6 mice, again highlighting potential strain differences. Further studies are required in order to determine whether similar effects would be seen with RANTES 9-68 during disease relapses in the PLP model of EAE, and during acute monophasic EAE.

7.7 A proposed model for the inflammatory response initiated during EAE

Collectively, the results of the present study and those from past studies have shown that chemokines and their receptors are important mediators involved in the regulation of T cell-mediated inflammatory diseases. Until now, investigators have only been able to postulate that differential temporal and spatial chemokine production by specific cell types serves as an important regulatory mechanism in the pathogenesis of these diseases. By separating the acute disease into two separate phases, that is sensitisation and effector, it has become possible to elucidate the mechanisms by which chemokine/chemokine receptor interactions regulate $CD4^+$ T cell function in the pathogenesis of EAE. As a consequence, the following model of $CD4^+$ T cell activation and migration during the pathogenesis of EAE is proposed (Figure 7.1). Firstly, within the draining LN, dendritic cell-naïve T cell interactions are mediated via interactions between SLC/CCL21 and/or MIP-3β/CCL19 (193, 194, 266). Second, TCR engagement following antigen presentation and costimulation results in the upregulation of CXCR4, the inflammatory receptors CXCR3 and CCR5, as well as CCR6 ((89), Liston and McColl, unpublished). The modulation of these receptors is temporally distinct. For example, expression of CXCR4 and CXCR3 is modulated early during clonal selection, whereas CCR5 and CCR6 modulation occurs after a number of cell divisions (88, 89). Efficient activation of the naïve T cell requires SDF-1/CXCL12-mediated co-stimulation through CXCR4 (present study and (75)), in addition to co-stimulation via CD28/B7 interactions (260). Newly activated T cells are retained in the LN possibly by MIP-3α/CCL20 and IP-10/CXCL10 expression until they are sufficiently polarised (43, 78), before exiting the LN through the

efferent lymphatics into the blood. Third, all activated T cells have the capacity to cross the BBB and enter the CNS tissue (127). Those $CD4^+$ T cells that recognise the antigen in the CNS (encephalitogenic T cells) begin to accumulate in significant numbers observable at disease onset (Day 9 post-immunisation), where they release proinflammatory cytokines and chemokines (32, 118, 267). Accumulation within the CNS is dependent upon expression of CXCR3, CCR5, and possibly CCR1 (146). By peak clinical disease, many of the encephalitogenic cells have undergone reactivation (140), the threshold for which is lower, and thus may not require SDF-1/CXCR4 costimulation. At the same time, inflammatory mediators released by the encephalitogenic T cells, and those released by the resident cells are responsible for the recruitment of non-specific CCR5- and CCR1-expressing monocyte/macrophages as well as non-specific T cells. This further contributes to disease pathogenesis. Lastly, as the animals enter remission, the number of CNS infiltrating cells decreases, as does the percentage of CXCR4, CXCR3 and CCR5-expressing activated $CD4^+$ T cells circulating in the peripheral blood. This is probably due to activation-induced cell death (ACID) of these cells (268). In contrast, the percentage of undivided (naïve) T cells expressing CXCR4 begins to increase during remission.

7.8 Speculation of a role for CXCR4, CXC3 and CCR5 retention on memory $CD4^+$ T cells during EAE Relapses

Although not the subject of specific investigation in the present study, the data generated allow some speculation regarding the role of CXCR4, CXCR3 and CCR5 during EAE relapse. Based on the linear differentiation model, which predicts that memory cells are the progeny of effector cells that escaped ACID (269), previous analyses of peripheral

blood lymphocytes suggest that the expression of CXCR3 is retained by activated T cells as they return to a resting, memory phenotype, as this receptor is expressed by a large proportion of peripheral blood memory T cells (23, 65, 67). Expression of CCR5 also appears to be retained to some extent by memory T cells, although a number of studies have shown that the expression of this receptor by memory T cells is more restricted than that of CXCR3 (23, 65, 67), suggesting that CCR5 is lost by some activated T cells as they return to a resting state. In the present study, analysis of divided $CD4^+$ T cells in the peripheral blood revealed that expression of all three receptors examined was retained for at least 21 days post-immunisation, although the relative proportion of divided cells expressing the receptors had decreased. Nonetheless, the observed results suggest that expression of these receptors is not restricted to a state of acute activation. This observation therefore provides support for the hypothesis that activated T cells retain CXCR3 and CCR5 as they return to a resting state. On the other hand, this is the first study to propose that CXCR4 remains elevated on memory T cells.

Collectively, these data may provide important insights into the reactivation of memory cells during relapses of EAE. Whilst not the focus of the present research, it would be pertinent to examine receptor regulation and function on memory cells during EAE relapses, since it more closely mimics the scenario following initial MS diagnosis. CCR2 has been implicated during relapse in EAE through the use of neutralizing antibodies, and CCR2 knockout mice are resistant to EAE (79, 148). However, in depth investigations into the other chemokine receptors during relapses are yet to be conducted. This may be the focus of future research within the laboratory.

7.9 Concluding remarks

Using an *in vivo* model of CNS inflammation, two inflammatory and one supposedly homeostatic chemokine receptors are upregulated on $CD4^+$ T cells during antigen-dependent clonal selection in the LN. As the $CD4^+$ T cells migrate through the blood and into the CNS tissue, expression of these receptors remains elevated such that at the peak of clinical disease, the majority of encephalitogenic $CD4^+$ T cells in the CNS express elevated levels of CXCR4, CXCR3 and CCR5. Detailed characterisation of these receptors revealed that upregulation occurs in co-ordination with cellular division. In experiments aimed at determining the biological significance of the observed patterns of chemokine receptor regulation, potential roles for each receptor were elucidated during the pathogenesis of EAE. These results, together with those from other studies, enabled the construction of a model detailing the temporal and spatial parameters of chemokine/chemokine receptor regulation of $CD4^+$ T cell activation and migration during a $CD4^+$ T cell-mediated immune response.

Given the complexity and diversity of the chemokine system, it is likely that these molecules will also play critical roles in controlling the activation and migration of other cells, as well as regulating many other biological functions, both within and outside of the immune system. Indeed, this is becoming increasingly apparent. Thus, a thorough understanding of how this family of molecules is regulated, as well as the precise roles that each member plays in the control of immunity is an important research focus. In addition to contributing to our understanding of how the immune system functions, investigations of these molecules are leading to the development of novel therapeutics for the control of autoimmunity, infectious diseases and transplantation reactions (1).

Figure 7.1 – A proposed model for the inflammatory response initiated during EAE.

1. Dendritic cell (APC)- naïve T cell interaction mediated by ELC/CCL19/CCR7 and SLC/CCL21/CCR7 interactions.
2. Clonal selection leads to temporally distinct upregulation of CXCR4, CXCR3 and CCR5. Efficient activation requires SDF-1/CXCL12-mediated costimulation through CXCR4.
3. Extravasation across the blood brain barrier.
4. Accumulation of $CD4^+$ T cells mediated by inflammatory chemokines.
5. $CD4^+$ T reactivation in the CNS leads to resident glial cell activation.
6. Release of proinflammatory chemokines by glial cells.
7. Recruitment of effector cells.
8. Demyelination.

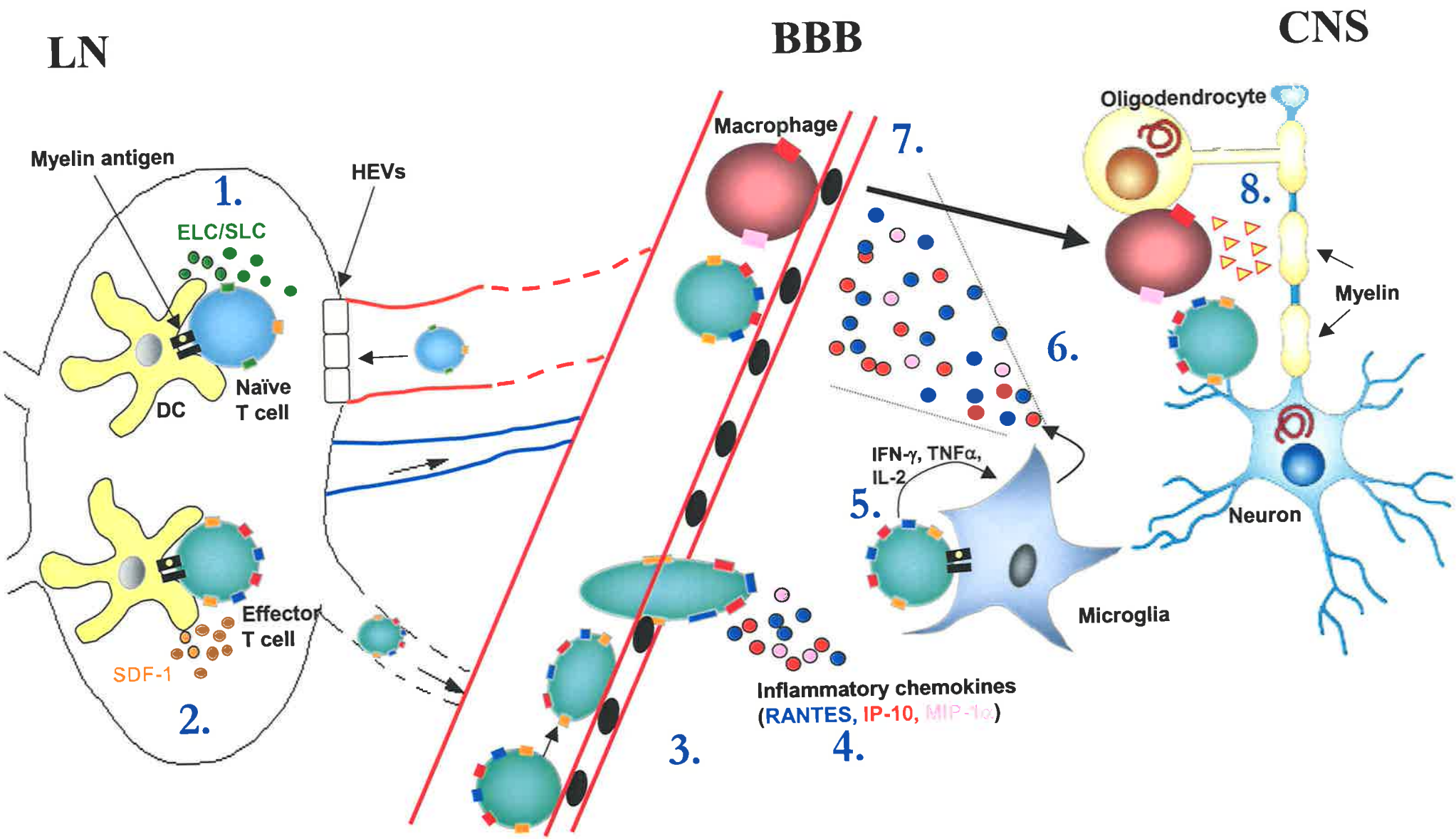
LN
BBB
CNS
Myelin antigen
1.
ELC/SLC
HEVs
Naïve
T cell
DC
Effector
T cell
SDF-1
2.
Macrophage
3.
4.
Inflammatory chemokines
(RANTES, IP-10, MIP-1α)
7.
6.
IFN-γ, TNFα,
IL-2
5.
Microglia
Oligodendrocyte
8.
Myelin
Neuron

8.1 References

1. Gerard, C., and B. J. Rollins. 2001. Chemokines and disease. *Nat Immunol 2:108.*
2. Dailey, M. O. 1998. Expression of T lymphocyte adhesion molecules: regulation during antigen-induced T cell activation and differentiation. *Crit Rev Immunol 18:153.*
3. Mackay, C., W. Marston, and L. Dudler. 1990. Naive and memory T cells show distinct pathways of lymphocyte recirculation. *J Exp Med 171:801.*
4. Butcher, E. C., and L. J. Picker. 1996. Lymphocyte homing and homeostasis. *Science 272:60.*
5. von Andrian, U. H., and C. R. Mackay. 2000. T-cell function and migration. Two sides of the same coin. *N Engl J Med 343:1020.*
6. Lichtman, A. H., and A. K. Abbas. 1997. T-cell subsets: recruiting the right kind of help. *Curr Biol 7:R242.*
7. Mosmann, T. R., H. Cherwinski, M. W. Bond, M. A. Giedlin, and R. L. Coffman. 1986. Two types of murine helper T cell clone. I. Definition according to profiles of lymphokine activities and secreted proteins. *J Immunol 136:2348.*
8. Mosmann, T. R., and R. L. Coffman. 1989. TH1 and TH2 cells: different patterns of lymphokine secretion lead to different functional properties. *Annu Rev Immunol 7:145.*
9. Abbas, A. K., K. M. Murphy, and A. Sher. 1996. Functional diversity of helper T lymphocytes. *Nature 383:787.*
10. Robinson, D. S., Q. Hamid, S. Ying, A. Tsicopoulos, J. Barkans, A. M. Bentley, C. Corrigan, S. R. Durham, and A. B. Kay. 1992. Predominant TH2-like bronchoalveolar T-lymphocyte population in atopic asthma. *N Engl J Med 326:298.*
11. Romagnani, S. 1997. The Th1/Th2 paradigm. *Immunol Today 18:263.*
12. Austrup, F., D. Vestweber, E. Borges, M. Lohning, R. Brauer, U. Herz, H. Renz, R. Hallmann, A. Scheffold, A. Radbruch, and A. Hamann. 1997. P- and E-selectin mediate recruitment of T-helper-1 but not T-helper-2 cells into inflammed tissues. *Nature 385:81.*

13. Xie, H., Y. C. Lim, F. W. Luscinskas, and A. H. Lichtman. 1999. Acquisition of selectin binding and peripheral homing properties by CD4(+) and CD8(+) T cells. *J Exp Med 189:1765.*

14. Springer, T. A. 1994. Traffic signals for lymphocyte recirculation and leukocyte emigration: the multistep paradigm. *Cell 76:301.*

15. Butcher, E. C. 1991. Leukocyte-endothelial cell recognition: three (or more) steps to specificity and diversity. *Cell 67:1033.*

16. Gale, L. M., and S. R. McColl. 1999. Chemokines: Extracellular messengers for all ocassions? *Bioessays 21:17.*

17. Rollins, B. J. 1997. Chemokines. *Blood 90:909.*

18. Streiter, R. M., J. A. Belperio, D. A. Arenberg, M. A. Smith, M. D. Burdick, and M. P. Keane. 2002. CXC chemokines in Angiogenesis. In *Universes in delicate balance: chemokines and the nervous system.* R. M. Ransohoff, ed. Elsevier Science B.V., Amsterdam, p. 129.

19. Zlotnik, A., and O. Yoshie. 2000. Chemokines: a new classification system and their role in immunity. *Immunity 12:121.*

20. Devalaraja, M. N., and A. Richmond. 1999. Multiple chemotactic factors: fine control or redundancy?

21. Baggiolini, M. 1998. Chemokines and leukocyte traffic. *Nature 392:565.*

22. Moser, B., and P. Loetscher. 2001. Lymphocyte traffic control by chemokines. *Nat Immunol 2:123.*

23. Sallusto, F., D. Lenig, C. R. Mackay, and A. Lanzavecchia. 1998. Flexible programs of chemokine receptor expression on human polarized T helper 1 and 2 lymphocytes. *J Exp Med 187:875.*

24. Hargreaves, D. C., P. L. Hyman, T. T. Lu, V. N. Ngo, A. Bidgol, G. Suzuki, Y. R. Zou, D. R. Littman, and J. G. Cyster. 2001. A coordinated change in chemokine responsiveness guides plasma cell movements. *J Exp Med 194:45.*

25. Baekkevold, E. S., T. Yamanaka, R. T. Palframan, H. S. Carlsen, F. P. Reinholt, U. H. von Andrian, P. Brandtzaeg, and G. Haraldsen. 2001. The CCR7 ligand elc (CCL19) is transcytosed in high endothelial venules and mediates T cell recruitment. *J Exp Med 193:1105.*

26. Legler, D. F., M. Loetscher, R. S. Roos, I. Clark Lewis, M. Baggiolini, and B. Moser. 1998. B cell-attracting chemokine 1, a human CXC chemokine expressed in lymphoid tissues, selectively attracts B lymphocytes via BLR1/CXCR5.

27. Pan, J., E. J. Kunkel, U. Gosslar, N. Lazarus, P. Langdon, K. Broadwell, M. A. Vierra, M. C. Genovese, E. C. Butcher, and D. Soler. 2000. A novel chemokine ligand for CCR10 and CCR3 expressed by epithelial cells in mucosal tissues. *J Immunol 165:2943.*

28. Tashiro, K., H. Tada, R. Heilker, M. Shirozu, T. Nakano, and T. Honjo. 1993. Signal sequence trap: a cloning strategy for secreted proteins and type 1 membrane proteins. *Science 261:600.*

29. Bleul, C. C., R. C. Fuhlbrigge, J. M. Casasnovas, A. Aiuti, and T. A. Springer. 1996. A highly efficacious lymphocyte chemoattractant, stromal cell-derived factor 1 (SDF-1). *J Exp Med 184:1101.*

30. Nagasawa, T., S. Hirota, K. Tachibana, N. Takakura, S. Nishikawa, Y. Kitamura, N. Yoshida, H. Kikutani, and T. Kishimoto. 1996. Defects of B-cell lymphopoiesis and bone-marrow myelopoiesis in mice lacking the CXC chemokine PBSF/SDF-1. *Nature 382:635.*

31. Alt, C., M. Laschinger, and B. Engelhardt. 2002. Functional expression of the lymphoid chemokines CCL19 (ELC) and CCL 21 (SLC) at the blood-brain barrier suggests their involvement in G-protein-dependent lymphocyte recruitment into the central nervous system during experimental autoimmune encephalomyelitis. *Eur J Immunol 32:2133.*

32. Ransohoff, R. M. 1999. Mechanisms of inflammation in MS tissue: adhesion molecules and chemokines. *J Neuroimmunol 98:57.*

33. Hancock, W. W., B. Lu, W. Gao, V. Csizmadia, K. Faia, J. A. King, S. T. Smiley, M. Ling, N. P. Gerard, and C. Gerard. 2000. Requirement of the chemokine receptor CXCR3 for acute allograft rejection. *J Exp Med 192:1515.*

34. Glabinski, A. R., M. Tani, R. M. Strieter, V. K. Tuohy, and R. M. Ransohoff. 1997. Synchronous synthesis of alpha- and beta-chemokines by cells of diverse lineage in the central nervous system of mice with relapses of chronic experimental autoimmune encephalomyelitis. *Am J Pathol 150:617.*

35. Godiska, R., D. Chantry, G. N. Dietsch, and P. W. Gray. 1995. Chemokine expression in murine experimental allergic encephalomyelitis. *J Neuroimmunol 58:167.*

36. Karpus, W. J., and R. M. Ransohoff. 1998. Chemokine regulation of experimental autoimmune encephalomyelitis: temporal and spatial expression patterns govern disease pathogenesis. *J Immunol 161:2667.*

37. Schrum, S., P. Probst, B. Fleischer, and P. F. Zipfel. 1996. Synthesis of the CC-chemokines MIP-1alpha, MIP-1beta, and RANTES is associated with a type 1 immune response. *J Immunol 157:3598.*

38. Rathanaswami, P., M. Hachicha, M. Sadick, T. J. Schall, and S. R. McColl. 1993. Expression of the cytokine RANTES in human rheumatoid synovial fibroblasts. Differential regulation of RANTES and interleukin-8 genes by inflammatory cytokines. *J Biol Chem 268:5834.*

39. Li, L., Y. Xia, A. Nguyen, L. Feng, and D. Lo. 1998. Th2-induced eotaxin expression and eosinophilia coexist with Th1 responses at the effector stage of lung inflammation.

40. Chensue, S. W., K. S. Warmington, J. H. Ruth, P. S. Sanghi, P. Lincoln, and S. L. Kunkel. 1996. Role of monocyte chemoattractant protein-1 (MCP-1) in Th1 (mycobacterial) and Th2 (schistosomal) antigen-induced granuloma formation: relationship to local inflammation, Th cell expression, and IL-12 production. *J Immunol 157:4602.*

41. Bonecchi, R., S. Sozzani, J. T. Stine, W. Luini, G. D'Amico, P. Allavena, D. Chantry, and A. Mantovani. 1998. Divergent effects of interleukin-4 and interferon-gamma on macrophage-derived chemokine production: an amplification circuit of polarized T helper 2 responses. *Blood 92:2668.*

42. Zhang, S., N. W. Lukacs, V. A. Lawless, S. L. Kunkel, and M. H. Kaplan. 2000. Cutting edge: differential expression of chemokines in Th1 and Th2 cells is dependent on Stat6 but not Stat4. *J Immunol 165:10.*

43. Kohler, R. E., A. C. Caon, D. O. Willenborg, I. Clark-Lewis, and S. R. McColl. 2003. A role for macrophage inflammatory protein-3alpha/CC chemokine ligand 20 in immune priming during T cell-mediated inflammation of the central nervous system. *J Immunol 170:6298.*

44. Dwinell, M. B., N. Lugering, L. Eckmann, and M. F. Kagnoff. 2001. Regulated production of interferon-inducible T-cell chemoattractants by human intestinal epithelial cells. *Gastroenterology 120:49.*

45. Rottman, J. B., T. L. Smith, K. G. Ganley, T. Kikuchi, and J. G. Krueger. 2001. Potential role of the chemokine receptors CXCR3, CCR4, and the integrin alphaEbeta7 in the pathogenesis of psoriasis vulgaris. *Lab Invest 81:335.*

46. Kaplan, G., A. D. Luster, G. Hancock, and Z. A. Cohn. 1987. The expression of a gamma interferon-induced protein (IP-10) in delayed immune responses in human skin. *J Exp Med 166:1098.*

47. Flier, J., D. M. Boorsma, P. J. van Beek, C. Nieboer, T. J. Stoof, R. Willemze, and C. P. Tensen. 2001. Differential expression of CXCR3 targeting chemokines CXCL10, CXCL9, and CXCL11 in different types of skin inflammation. *J Pathol 194:398.*

48. Gonzalo, J. A., C. M. Lloyd, L. Kremer, E. Finger, A. C. Martinez, M. H. Siegelman, M. Cybulsky, and J. C. Gutierrez Ramos. 1996. Eosinophil recruitment to the lung in a murine model of allergic inflammation. The role of T cells, chemokines, and adhesion receptors. *J Clin Invest 98:2332.*

49. Yang, Y., J. Loy, R. P. Ryseck, D. Carrasco, and R. Bravo. 1998. Antigen-induced eosinophilic lung inflammation develops in mice deficient in chemokine eotaxin. *Blood 92:3912.*

50. Thelen, M. 2001. Dancing to the tune of chemokines. *Nat Immunol 2:129.*

51. Loetscher, P., A. Pellegrino, J. H. Gong, I. Mattioli, M. Loetscher, G. Bardi, M. Baggiolini, and I. Clark-Lewis. 2001. The ligands of CXC chemokine receptor 3, I-TAC, Mig, and IP10, are natural antagonists for CCR3. *J Biol Chem 276:2986.*

52. Soto, H., W. Wang, R. M. Strieter, N. G. Copeland, D. J. Gilbert, N. A. Jenkins, J. Hedrick, and A. Zlotnik. 1998. The CC chemokine 6Ckine binds the CXC chemokine receptor CXCR3. *Proc Natl Acad Sci U S A 95:8205.*

53. Rappert, A., K. Biber, C. Nolte, M. Lipp, A. Schubel, B. Lu, N. P. Gerard, C. Gerard, H. W. Boddeke, and H. Kettenmann. 2002. Secondary lymphoid tissue chemokine (CCL21) activates CXCR3 to trigger a Cl- current and chemotaxis in murine microglia. *J Immunol 168:3221.*

54. Horuk, R. 2001. Chemokine receptors. *Cytokine Growth Factor Rev 12:313.*

55. Moser, B. 1997. Chemokines and HIV: a remarkable synergism. *Trends Microbiol 5:88.*

56. Littman, D. R. 1998. Chemokine receptors: keys to AIDS pathogenesis? *Cell 93:677.*

57. Horuk, R., C. E. Chitnis, W. C. Darbonne, T. J. Colby, A. Rybicki, T. J. Hadley, and L. H. Miller. 1993. A receptor for the malarial parasite Plasmodium vivax: the erythrocyte chemokine receptor. *Science 261:1182.*

58. Ding, Z., K. Xiong, and T. B. Issekutz. 2000. Regulation of chemokine-induced transendothelial migration of T lymphocytes by endothelial activation: differential effects on naive and memory T cells. *J Leukoc Biol 67:825.*

59. Adema, G. J., F. Hartgers, R. Verstraten, E. Devries, G. Marland, S. Menon, J. Foster, Y. M. Xu, P. Nooyen, T. McClanahan, K. B. Bacon, and C. G. Figdor. 1997. A dendritic-cell-derived C-C chemokine that preferentially attracts naive T cells. *Nature 387:713.*

60. Kim, C. H., L. M. Pelus, J. R. White, E. Applebaum, K. Johanson, and H. E. Broxmeyer. 1998. CK beta-11/macrophage inflammatory protein-3 beta/EBI1-ligand chemokine is an efficacious chemoattractant for T and B cells. *J Immunol 160:2418.*

61. Ngo, V. N., H. L. Tang, and J. G. Cyster. 1998. Epstein-Barr virus-induced molecule 1 ligand chemokine is expressed by dendritic cells in lymphoid tissues and strongly attracts naive T cells and activated B cells. *J Exp Med 188:181.*

62. Carr, M. W., S. J. Roth, E. Luther, S. S. Rose, and T. A. Springer. 1994. Monocyte chemoattractant protein 1 acts as a T-lymphocyte chemoattractant. *Proc Natl Acad Sci U S A 91:3652.*

63. Siveke, J. T., and A. Hamann. 1998. T helper 1 and T helper 2 cells respond differentially to chemokines. *J Immunol 160:550.*

64. Langenkamp, A., K. Nagata, K. Murphy, L. Wu, A. Lanzavecchia, and F. Sallusto. 2003. Kinetics and expression patterns of chemokine receptors in human CD4+ T lymphocytes primed by myeloid or plasmacytoid dendritic cells. *Eur J Immunol 33:474.*

65. Rabin, R. L., M. K. Park, F. Liao, R. Swofford, D. Stephany, and J. M. Farber. 1999. Chemokine receptor responses on T cells are achieved through regulation of both receptor expression and signaling. *J Immunol 162:3840.*

66. Bonecchi, R., G. Bianchi, B. Panina, D. D'Ambrosio, R. Lang, A. Borsatti, S. Sozzani, P. Allavena, P. Gray, A. Mantovani, and F. Sinigaglia. 1998. Differential expression of chemokine receptors and chemotactic responsiveness of type 1 T helper cells (Th1s) and Th2s. *J Exp Med 187:129.*

67. Sallusto, F., A. Lanzavecchia, and C. R. Mackay. 1998. Chemokines and chemokine receptors in T-cell priming and Th1/Th2-mediated responses. *Immunol Today 19:568.*

68. Imai, T., M. Nagira, S. Takagi, M. Kakizaki, M. Nishimura, J. Wang, P. W. Gray, K. Matsushima, and O. Yoshie. 1999. Selective recruitment of CCR4-bearing Th2 cells toward antigen-presenting cells by the CC chemokines thymus and activation-regulated chemokine and macrophage-derived chemokine. *Int Immunol 11:81.*

69. Sallusto, F., C. Mackay, and A. Lanzavecchia. 1998. Selective expression of the eotaxin receptor CCR3 by human T helper 2 cells. *Science 277:2005.*

70. Campbell, J. J., E. P. Bowman, K. Murphy, K. R. Youngman, M. A. Siani, D. A. Thompson, L. Wu, A. Zlotnik, and E. C. Butcher. 1998. 6-C-kine (SLC), a lymphocyte adhesion-triggering chemokine expressed by high endothelium, is an agonist for the MIP-3beta receptor CCR7. *J Cell Biol 141:1053.*

71. Pachynski, R. K., S. W. Wu, M. D. Gunn, and D. J. Erle. 1998. Secondary lymphoid-tissue chemokine (SLC) stimulates integrin alpha 4 beta 7-mediated adhesion of lymphocytes to mucosal addressin cell adhesion molecule-1 (MAdCAM-1) under flow. *J Immunol 161:952.*

72. Campbell, J. J., J. Pan, and E. C. Butcher. 1999. Cutting edge: developmental switches in chemokine responses during T cell maturation. *J Immunol 163:2353.*

73. Piali, L., C. Weber, G. LaRosa, C. R. Mackay, T. A. Springer, I. Clark Lewis, and B. Moser. 1998. The chemokine receptor CXCR3 mediates rapid and shear-resistant adhesion-induction of effector T lymphocytes by the chemokines IP10 and Mig. *Eur J Immunol 28:961.*

74. Carr, M. W., R. Alon, and T. A. Springer. 1996. The C-C chemokine MCP-1 differentially modulates the avidity of beta 1 and beta 2 integrins on T lymphocytes. *Immunity 4:179.*

75. Nanki, T., and P. E. Lipsky. 2000. Cutting edge: stromal cell-derived factor-1 is a costimulator for CD4+ T cell activation. *J Immunol 164:5010.*

76. Cerdan, C., E. Devilard, L. Xerri, and D. Olive. 2001. The C-class chemokine lymphotactin costimulates the apoptosis of human CD4(+) T cells. *Blood 97:2205.*

77. Luther, S. A., and J. G. Cyster. 2001. Chemokines as regulators of T cell differentiation. *Nat Immunol 2:102.*

78. Yoneyama, H., S. Narumi, Y. Zhang, M. Murai, M. Baggiolini, A. Lanzavecchia, T. Ichida, H. Asakura, and K. Matsushima. 2002. Pivotal role of dendritic cell-derived CXCL10 in the retention of T helper cell 1 lymphocytes in secondary lymph nodes. *J Exp Med 195:1257.*

79. Karpus, W. J., and K. J. Kennedy. 1997. MIP-1alpha and MCP-1 differentially regulate acute and relapsing autoimmune encephalomyelitis as well as Th1/Th2 lymphocyte differentiation. *J Leukoc Biol 62:681.*

80. Karpus, W. J., N. W. Lukacs, K. J. Kennedy, W. S. Smith, S. D. Hurst, and T. A. Barrett. 1997. Differential CC chemokine-induced enhancement of T helper cell cytokine production. *J Immunol 158:4129.*

81. Lu, B., B. J. Rutledge, L. Gu, J. Fiorillo, N. W. Lukacs, S. L. Kunkel, R. North, C. Gerard, and B. J. Rollins. 1998. Abnormalities in monocyte recruitment and cytokine expression in monocyte chemoattractant protein 1-deficient mice. *J Exp Med 187:601.*

82. Kuby, J. 1997. *Immunology*. W.H. Freeman and Company, New York.

83. Sallusto, F., D. Lenig, R. Forster, M. Lipp, and A. Lanzavecchia. 1999. Two subsets of memory T lymphocytes with distinct homing potentials and effector functions. *Nature 401:708.*

84. Luther, S. A., H. L. Tang, P. L. Hyman, A. G. Farr, and J. G. Cyster. 2000. Coexpression of the chemokines ELC and SLC by T zone stromal cells and deletion of the ELC gene in the plt/plt mouse. *Proc Natl Acad Sci U S A 97:12694.*

85. Gunn, M. D., S. Kyuwa, C. Tam, T. Kakiuchi, A. Matsuzawa, L. T. Williams, and H. Nakano. 1999. Mice lacking expression of secondary lymphoid organ chemokine have defects in lymphocyte homing and dendritic cell localization [see comments]. *J Exp Med 189:451.*

86. Tachibana, K., S. Hirota, H. Iizasa, H. Yoshida, K. Kawabata, Y. Kataoka, Y. Kitamura, K. Matsushima, N. Yoshida, S. Nishikawa, T. Kishimoto, and T. Nagasawa. 1998. The chemokine receptor CXCR4 is essential for vascularization of the gastrointestinal tract. *Nature 393:591.*

87. Zou, Y. R., A. H. Kottmann, M. Kuroda, I. Taniuchi, and D. R. Littman. 1998. Function of the chemokine receptor CXCR4 in haematopoiesis and in cerebellar development. *Nature 393:595.*

88. Ebert, L. M., and S. R. McColl. 2001. Coregulation of CXC chemokine receptor and CD4 expression on T lymphocytes during allogeneic activation. *J Immunol 166:4870.*

89. Ebert, L. M., and S. R. McColl. 2002. Up-regulation of CCR5 and CCR6 on distinct subpopulations of antigen-activated CD4+ T lymphocytes. *J Immunol 168:65.*

90. Zingoni, A., H. Soto, J. Hedrick, A. Stoppacciaro, C. Storlazzi, F. Sinigaglia, D. D'Ambrosio, A. O'Garra, D. Robinson, M. Rocchi, A. Santoni, A. Zlotnik, and M. Napolitano. 1998. The chemokine receptor CCR8 is preferentially expressed in Th2 but not Th1 cells. *J Immunol 161:547.*

91. Moser, B., and L. Ebert. 2003. Lymphocyte traffic control by chemokines: follicular B helper T cells. *Immunol Lett 85:105.*

92. Breitfeld, D., L. Ohl, E. Kremmer, J. Ellwart, F. Sallusto, M. Lipp, and R. Forster. 2000. Follicular B helper T cells express CXC chemokine receptor 5, localize to B cell follicles, and support immunoglobulin production. *J Exp Med 192:1545.*

93. Schaerli, P., K. Willimann, A. B. Lang, M. Lipp, P. Loetscher, and B. Moser. 2000. CXC chemokine receptor 5 expression defines follicular homing T cells with B cell helper function. *J Exp Med 192:1553.*

94. Campbell, J. J., G. Haraldsen, J. Pan, J. Rottman, S. Qin, P. Ponath, D. P. Andrew, R. Warnke, N. Ruffing, N. Kassam, L. Wu, and E. C. Butcher. 1999. The chemokine receptor CCR4 in vascular recognition by cutaneous but not intestinal memory T cells. *Nature 400:776.*

95. Zabel, B. A., W. W. Agace, J. J. Campbell, H. M. Heath, D. Parent, A. I. Roberts, E. C. Ebert, N. Kassam, S. Qin, M. Zovko, G. J. LaRosa, L. L. Yang, D. Soler, E. C. Butcher, P. D. Ponath, C. M. Parker, and D. P. Andrew. 1999. Human G protein-coupled receptor GPR-9-6/CC chemokine receptor 9 is selectively expressed on intestinal homing T lymphocytes, mucosal lymphocytes, and thymocytes and is required for thymus-expressed chemokine-mediated chemotaxis. *J Exp Med 190:1241.*

96. Kivisakk, P., C. Trebst, Z. Liu, B. H. Tucky, T. L. Sorensen, R. A. Rudick, M. Mack, and R. M. Ransohoff. 2002. T-cells in the cerebrospinal fluid express a similar repertoire of inflammatory chemokine receptors in the absence or presence of CNS inflammation: implications for CNS trafficking. *Clin Exp Immunol 129:510.*

97. Campbell, J., K. Murphy, E. Kunkel, C. Brightling, D. Soler, Z. Shen, J. Boisvert, H. Greenberg, M. Vierra, S. Goodman, M. Genovese, A. Wardlaw, E. Butcher, and L. Wu. 2001. CCR7 expression and memory T cell diversity in humans. *J Immunol 166:877.*

98. Fabry, Z., C. S. Raine, and M. N. Hart. 1994. Nervous tissue as an immune compartment: the dialect of the immune response in the CNS. *Immunol Today 15:218.*

99. Glabinski, A. R., M. Tani, S. Aras, M. H. Stoler, V. K. Tuohy, and R. M. Ransohoff. 1995. Regulation and function of central nervous system chemokines. *Int J Dev Neurosci 13:153.*

100. Hickey, W. F. 1999. Leukocyte traffic in the central nervous system: the participants and their roles. *Semin Immunol 11:125.*

101. Fife, B. T., G. B. Huffnagle, W. A. Kuziel, and W. J. Karpus. 2000. CC chemokine receptor 2 is critical for induction of experimental autoimmune encephalomyelitis. *J Exp Med 192:899.*

102. Keegan, B. M., and J. H. Noseworthy. 2002. Multiple sclerosis. *Annu Rev Med 53:285.*

103. Al Omaishi, J., R. Bashir, and H. E. Gendelman. 1999. The cellular immunology of multiple sclerosis. *J Leukoc Biol 65:444.*

104. Noseworthy, J. H. 1999. Progress in determining the causes and treatment of multiple sclerosis. *Nature 399:A40.*

105. Ranshoff, R. M., and C. Trebst. 2002. Chemokines and chemokine receptors in multiple sclerosis: A few answers and many more questions. In *Universes in delicate balance: chemokines and the nervous system.* R. M. Ranshoff, ed. Elsevier Science B.V, Amsterdam, p. 317.

106. Hillbert, J., and T. Masterman. 2001. The Genetics of Multiple Sclerosis. In *Handbook of Multiple Sclerosis.* S. D. Cook, ed. Marcel Dekker, Inc, New Youk, p. 33.

107. Oksenberg, J. R., S. E. Baranzini, L. F. Barcellos, and S. L. Hauser. 2001. Multiple sclerosis: genomic rewards. *J Neuroimmunol 113:171.*

108. Steinman, L., and P. Conlon. 2001. Antigen specific immunotherapy of multiple sclerosis. *J Clin Immunol 21:93.*

109. Hafler, D. A., and H. L. Weiner. 1987. T cells in multiple sclerosis and inflammatory central nervous system diseases. *Immunol Rev 100:307.*

110. Prineas, J. W. 2001. Pathology of Multiple Sclerosis. In *Handbook of Multiple Sclerosis*. S. D. Cook, ed. Marcel Dekker, Inc, New York, p. 289.

111. Traugott, U. 2001. Evidence for immunopathogenesis. In *Handbook of Multiple Sclerosis*. S. D. Cook, ed. Marcel Dekker, Inc, New York, p. 163.

112. Babbe, H., A. Roers, A. Waisman, H. Lassmann, N. Goebels, R. Hohlfeld, M. Friese, R. Schroder, M. Deckert, S. Schmidt, R. Ravid, and K. Rajewsky. 2000. Clonal expansions of CD8(+) T cells dominate the T cell infiltrate in active multiple sclerosis lesions as shown by micromanipulation and single cell polymerase chain reaction. *J Exp Med 192:393*.

113. Hafler, D. A., A. D. Duby, S. J. Lee, D. Benjamin, J. G. Seidman, and H. L. Weiner. 1988. Oligoclonal T lymphocytes in the cerebrospinal fluid of patients with multiple sclerosis. *J Exp Med 167:1313*.

114. Balashov, K. E., J. B. Rottman, H. L. Weiner, and W. W. Hancock. 1999. CCR5(+) and CXCR3(+) T cells are increased in multiple sclerosis and their ligands MIP-1alpha and IP-10 are expressed in demyelinating brain lesions. *Proc Natl Acad Sci U S A 96:6873*.

115. Sorensen, T. L., M. Tani, J. Jensen, V. Pierce, C. Lucchinetti, V. A. Folcik, S. Qin, J. Rottman, F. Sellebjerg, R. M. Strieter, J. L. Frederiksen, and R. M. Ransohoff. 1999. Expression of specific chemokines and chemokine receptors in the central nervous system of multiple sclerosis patients. *J Clin Invest 103:807*.

116. Sorensen, T. L., C. Trebst, P. Kivisakk, K. L. Klaege, A. Majmudar, R. Ravid, H. Lassmann, D. B. Olsen, R. M. Strieter, R. M. Ransohoff, and F. Sellebjerg. 2002. Multiple sclerosis: a study of CXCL10 and CXCR3 co-localization in the inflamed central nervous system. *J Neuroimmunol 127:59*.

117. O'Connor, K. C., A. Bar-Or, and D. A. Hafler. 2001. The neuroimmunology of multiple sclerosis: possible roles of T and B lymphocytes in immunopathogenesis. *J Clin Immunol 21:81*.

118. Karpus, W. J. 2002. Animal models of multiple sclerosis. In *Universes in delicate balance: chemokines and the nervous system*. R. M. Ransohoff, ed. Elsevier Science B.V., Amsterdam, p. 159.

119. Munoz, J. J., C. C. Bernard, and I. R. Mackay. 1984. Elicitation of experimental allergic encephalomyelitis (EAE) in mice with the aid of pertussigen. *Cell Immunol 83:92*.

120. Munoz, J. J., and I. R. Mackay. 1984. Production of experimental allergic encephalomyelitis with the aid of pertussigen in mouse strains considered genetically resistant. *J Neuroimmunol 7:91.*

121. Huang, D., Y. Han, M. R. Rani, A. Glabinski, C. Trebst, T. Sorensen, M. Tani, J. Wang, P. Chien, S. O'Bryan, B. Bielecki, Z. L. Zhou, S. Majumder, and R. M. Ransohoff. 2000. Chemokines and chemokine receptors in inflammation of the nervous system: manifold roles and exquisite regulation. *Immunol Rev 177:52.*

122. Bradl, M. 1996. Immune control of the brain. *Springer Semin Immunopathol 18:35.*

123. Karpus, W. J., N. W. Lukacs, B. L. McRae, R. M. Strieter, S. L. Kunkel, and S. D. Miller. 1995. An important role for the chemokine macrophage inflammatory protein-1 alpha in the pathogenesis of the T cell-mediated autoimmune disease, experimental autoimmune encephalomyelitis. *J Immunol 155:5003.*

124. Kennedy, K. J., R. M. Strieter, S. L. Kunkel, N. W. Lukacs, and W. J. Karpus. 1998. Acute and relapsing experimental autoimmune encephalomyelitis are regulated by differential expression of the CC chemokines macrophage inflammatory protein-1alpha and monocyte chemotactic protein-1. *J Neuroimmunol 92:98.*

125. Popovich, P. G., J. Y. Yu, and C. C. Whitacre. 1997. Spinal cord neuropathology in rat experimental autoimmune encephalomyelitis: modulation by oral administration of myelin basic protein. *J Neuropathol Exp Neurol 56:1323.*

126. Ransohoff, R. M., T. A. Hamilton, M. Tani, M. H. Stoler, H. E. Shick, J. A. Major, M. L. Estes, D. M. Thomas, and V. K. Tuohy. 1993. Astrocyte expression of mRNA encoding cytokines IP-10 and JE/MCP-1 in experimental autoimmune encephalomyelitis. *Faseb J 7:592.*

127. Hickey, W. F., B. L. Hsu, and H. Kimura. 1991. T-lymphocyte entry into the central nervous system. *J Neurosci Res 28:254.*

128. Yednock, T. A., C. Cannon, L. C. Fritz, F. Sanchez-Madrid, L. Steinman, and N. Karin. 1992. Prevention of experimental autoimmune encephalomyelitis by antibodies against alpha 4 beta 1 integrin. *Nature 356:63.*

129. Eng, L. F., R. S. Ghirnikar, and Y. L. Lee. 1996. Inflammation in EAE: role of chemokine/cytokine expression by resident and infiltrating cells. *Neurochem Res 21:511.*

130. Dore-Duffy, P., R. Balabanov, J. Rafols, and R. H. Swanborg. 1996. Recovery phase of acute experimental autoimmune encephalomyelitis in rats corresponds to development of endothelial cell unresponsiveness to interferon gamma activation. *J Neurosci Res 44:223.*

131. Krakowski, M., and T. Owens. 1996. Interferon-gamma confers resistance to experimental allergic encephalomyelitis. *Eur J Immunol 26:1641.*

132. Segal, G. M., T. D. Smith, M. C. Heinrich, F. S. Ey, and G. C. Bagby. 1992. Specific Repression of Granulocyte-Macrophage and Granulocyte Colony-Stimulating Factor Gene Expression in Interleukin-1-Stimulated Endothelial Cells with Antisense Oligodeoxynucleotides. *Blood 80:609.*

133. Willenborg, D. O., S. Fordham, C. C. Bernard, W. B. Cowden, and I. A. Ramshaw. 1996. IFN-gamma plays a critical down-regulatory role in the induction and effector phase of myelin oligodendrocyte glycoprotein-induced autoimmune encephalomyelitis. *J Immunol 157:3223.*

134. Popko, B., J. G. Corbin, K. D. Baerwald, J. Dupree, and A. M. Garcia. 1997. The effects of interferon-gamma on the central nervous system. *Mol Neurobiol 14:19.*

135. Antel, J. P., and T. Owens. 1999. Immune regulation and CNS autoimmune disease. *J Neuroimmunol 100:181.*

136. Ransohoff, R. M. 2002. The chemokine system in neuroinflammation: an update. *J Infect Dis 186:S152.*

137. Zhang, G. X., C. M. Baker, D. L. Kolson, and A. M. Rostami. 2000. Chemokines and chemokine receptors in the pathogenesis of multiple sclerosis. *Mult Scler 6:3.*

138. Ghirnikar, R. S., Y. L. Lee, and L. F. Eng. 2000. Chemokine antagonist infusion attenuates cellular infiltration following spinal cord contusion injury in rat. *J Neurosci Res 59:63.*

139. Giunti, D., G. Borsellino, R. Benelli, M. Marchese, E. Capello, M. T. Valle, E. Pedemonte, D. Noonan, A. Albini, G. Bernardi, G. L. Mancardi, L. Battistini, and A. Uccelli. 2003. Phenotypic and functional analysis of T cells homing into the CSF of subjects with inflammatory diseases of the CNS. *J Leukoc Biol 73:584.*

140. Flugel, A., T. Berkowicz, T. Ritter, M. Labeur, D. E. Jenne, Z. Li, J. W. Ellwart, M. Willem, H. Lassmann, and H. Wekerle. 2001. Migratory activity and functional changes of green fluorescent effector cells before and during experimental autoimmune encephalomyelitis. *Immunity 14:547.*

141. Fife, B. T., K. J. Kennedy, M. C. Paniagua, N. W. Lukacs, S. L. Kunkel, A. D. Luster, and W. J. Karpus. 2001. CXCL10 (IFN-gamma-inducible protein-10) control of encephalitogenic CD4+ T cell accumulation in the central nervous system during experimental autoimmune encephalomyelitis. *J Immunol 166:7617.*

142. Narumi, S., T. Kaburaki, H. Yoneyama, H. Iwamura, Y. Kobayashi, and K. Matsushima. 2002. Neutralization of IFN-inducible protein 10/CXCL10 exacerbates experimental autoimmune encephalomyelitis. *Eur J Immunol 32:1784.*

143. Serafini, B., S. Columba-Cabezas, F. Di Rosa, and F. Aloisi. 2000. Intracerebral recruitment and maturation of dendritic cells in the onset and progression of experimental autoimmune encephalomyelitis. *Am J Pathol 157:1991.*

144. Glabinski, A. R., B. Bielecki, S. O'Bryant, K. Selmaj, and R. M. Ransohoff. 2002. Experimental Autoimmune Encephalomyelitis: CC Chemokine Receptor Expression by Trafficking Cells. *J Autoimmun 19:175.*

145. Tran, E. H., W. A. Kuziel, and T. Owens. 2000. Induction of experimental autoimmune encephalomyelitis in C57BL/6 mice deficient in either the chemokine macrophage inflammatory protein-1alpha or its CCR5 receptor. *Eur J Immunol 30:1410.*

146. Rottman, J. B., A. J. Slavin, R. Silva, H. L. Weiner, C. G. Gerard, and W. W. Hancock. 2000. Leukocyte recruitment during onset of experimental allergic encephalomyelitis is CCR1 dependent. *Eur J Immunol 30:2372.*

147. Izikson, L., R. S. Klein, I. F. Charo, H. L. Weiner, and A. D. Luster. 2000. Resistance to experimental autoimmune encephalomyelitis in mice lacking the CC chemokine receptor (CCR)2. *J Exp Med 192:1075.*

148. Huang, D. R., J. Wang, P. Kivisakk, B. J. Rollins, and R. M. Ransohoff. 2001. Absence of monocyte chemoattractant protein 1 in mice leads to decreased local macrophage recruitment and antigen-specific T helper cell type 1 immune response in experimental autoimmune encephalomyelitis. *J Exp Med 193:713.*

149. Dufour, J. H., M. Dziejman, M. T. Liu, J. H. Leung, T. E. Lane, and A. D. Luster. 2002. IFN-gamma-inducible protein 10 (IP-10; CXCL10)-deficient mice reveal a role for IP-10 in effector T cell generation and trafficking. *J Immunol 168:3195.*

150. Haskell, C. A., W. W. Hancock, D. J. Salant, W. Gao, V. Csizmadia, W. Peters, K. Faia, O. Fituri, J. B. Rottman, and I. F. Charo. 2001. Targeted deletion of CX(3)CR1 reveals a role for fractalkine in cardiac allograft rejection. *J Clin Invest 108:679.*

151. Yang, A. G., X. Bai, X. F. Huang, C. Yao, and S. Chen. 1997. Phenotypic knockout of HIV type 1 chemokine coreceptor CCR-5 by intrakines as potential therapeutic approach for HIV-1 infection. *Proc Natl Acad Sci U S A 94:11567.*

152. Onai, N., Y. Zhang, H. Yoneyama, T. Kitamura, S. Ishikawa, and K. Matsushima. 2000. Impairment of lymphopoiesis and myelopoiesis in mice reconstituted with bone marrow-hematopoietic progenitor cells expressing SDF-1-intrakine. *Blood 96:2074.*

153. Dorrell, S. 1999. Blocking HIV-1 infection with intrakines [news]. *Mol Med Today 5(3): 97*

154. Huffnagle, G. B., R. M. Strieter, T. J. Standiford, R. A. McDonald, M. D. Burdick, S. L. Kunkel, and G. B. Toews. 1995. The role of monocyte chemotactic protein-1 (MCP-1) in the recruitment of monocytes and CD4+ T cells during a pulmonary Cryptococcus neoformans infection. *J Immunol 155:4790.*

155. Rand, M. L., J. S. Warren, M. K. Mansour, W. Newman, and D. J. Ringler. 1996. Inhibition of T cell recruitment and cutaneous delayed-type hypersensitivity-induced inflammation with antibodies to monocyte chemoattractant protein-1. *Am J Pathol 148:855.*

156. Lloyd, C. M., T. Delaney, T. Nguyen, J. Tian, A. C. Martinez, A. J. Coyle, and J. C. Gutierrez-Ramos. 2000. CC chemokine receptor (CCR)3/eotaxin is followed by CCR4/monocyte-derived chemokine in mediating pulmonary T helper lymphocyte type 2 recruitment after serial antigen challenge in vivo. *J Exp Med 191:265.*

157. Yoneyama, H., A. Harada, T. Imai, M. Baba, O. Yoshie, Y. Zhang, H. Higashi, M. Murai, H. Asakura, and K. Matsushima. 1998. Pivotal role of TARC, a CC chemokine, in bacteria-induced fulminant hepatic failure in mice. *J Clin Invest 102:1933.*

158. Arimilli, S., W. Ferlin, N. Solvason, S. Deshpande, M. Howard, and S. Mocci. 2000. Chemokines in autoimmune diseases. *Immunol Rev 177:43.*

159. Liu, M. T., B. P. Chen, P. Oertel, M. J. Buchmeier, T. A. Hamilton, D. A. Armstrong, and T. E. Lane. 2001. The CXC chemokines IP-10 and Mig are essential in host defense following infection with a neurotropic coronavirus. *Adv Exp Med Biol 494:323.*

160. Crump, M. P., J. H. Gong, P. Loetscher, K. Rajarathnam, A. Amara, F. Arenzana-Seisdedos, J. L. Virelizier, M. Baggiolini, B. D. Sykes, and I. Clark-Lewis. 1997. Solution structure and basis for functional activity of stromal cell-derived factor-1; dissociation of CXCR4 activation from binding and inhibition of HIV-1. *Embo J 16:6996.*

161. Loetscher, P., and I. Clark-Lewis. 2001. Agonistic and antagonistic activities of chemokines. *J Leukoc Biol 69:881.*

162. Gong, J. H., and I. Clark Lewis. 1995. Antagonists of monocyte chemoattractant protein 1 identified by modification of functionally critical NH2-terminal residues. *J Exp Med 181:631.*

163. Proudfoot, A. E., C. A. Power, A. J. Hoogewerf, M. O. Montjovent, F. Borlat, R. E. Offord, and T. N. Wells. 1996. Extension of recombinant human RANTES by the retention of the initiating methionine produces a potent antagonist. *J Biol Chem 271:2599.*

164. Proudfoot, A. E., C. A. Power, and T. N. Wells. 2000. The strategy of blocking the chemokine system to combat disease. *Immunol Rev 177:246.*

165. Gong, J. H., L. G. Ratkay, J. D. Waterfield, and I. Clark-Lewis. 1997. An antagonist of monocyte chemoattractant protein 1 (MCP-1) inhibits arthritis in the MRL-lpr mouse model. *J Exp Med 186:131.*

166. Grone, H. J., C. Weber, K. S. Weber, E. F. Grone, T. Rabelink, C. M. Klier, T. N. Wells, A. E. Proudfood, D. Schlondorff, and P. J. Nelson. 1999. Met-RANTES reduces vascular and tubular damage during acute renal transplant rejection: blocking monocyte arrest and recruitment. *Faseb J 13:1371.*

167. Kim, C. H., E. J. Kunkel, J. Boisvert, B. Johnston, J. J. Campbell, M. C. Genovese, H. B. Greenberg, and E. C. Butcher. 2001. Bonzo/CXCR6 expression defines type 1-polarized T-cell subsets with extralymphoid tissue homing potential. *J Clin Invest 107:595.*

168. Ransohoff, R. M. 1997. Chemokines in neurological disease models: correlation between chemokine expression patterns and inflammatory pathology. *J Leukoc Biol 62:645.*

169. McManus, C., J. W. Berman, F. M. Brett, H. Staunton, M. Farrell, and C. F. Brosnan. 1998. MCP-1, MCP-2 and MCP-3 expression in multiple sclerosis lesions: an immunohistochemical and in situ hybridization study. *J Neuroimmunol 86:20.*

170. Miyagishi, R., S. Kikuchi, T. Fukazawa, and K. Tashiro. 1995. Macrophage inflammatory protein-1 alpha in the cerebrospinal fluid of patients with multiple sclerosis and other inflammatory neurological diseases. *J Neurol Sci 129:223.*

171. Asensio, V. C., S. Lassmann, A. Pagenstecher, S. C. Steffensen, S. J. Henriksen, and I. L. Campbell. 1999. C10 is a novel chemokine expressed in experimental inflammatory demyelinating disorders that promotes recruitment of macrophages to the central nervous system. *Am J Pathol 154:1181.*

172. Pan, Y., C. Lloyd, H. Zhou, S. Dolich, J. Deeds, J. A. Gonzalo, J. Vath, M. Gosselin, J. Y. Ma, B. Dussault, E. Woolf, G. Alperin, J. Culpepper, J. C. Gutierrezramos, and D. Gearing. 1997. Neurotactin, a membrane-anchored chemokine upregulated in brain inflammation. *Nature 387:611.*

173. Glabinski, A. R., M. Krakowski, Y. Han, T. Owens, and R. M. Ransohoff. 1999. Chemokine expression in GKO mice (lacking interferon-gamma) with experimental autoimmune encephalomyelitis. *J Neurovirol 5:95.*

174. Gao, J. L., T. A. Wynn, Y. Chang, E. J. Lee, H. E. Broxmeyer, S. Cooper, H. L. Tiffany, H. Westphal, J. Kwon Chung, and P. M. Murphy. 1997. Impaired host defense, hematopoiesis, granulomatous inflammation and type 1-type 2 cytokine balance in mice lacking CC chemokine receptor 1. *J Exp Med 185:1959.*

175. Boring, L., J. Gosling, S. W. Chensue, S. L. Kunkel, R. V. Farese, Jr., H. E. Broxmeyer, and I. F. Charo. 1997. Impaired monocyte migration and reduced type 1 (Th1) cytokine responses in C-C chemokine receptor 2 knockout mice. *J Clin Invest 100:2552.*

176. Chvatchko, Y., A. J. Hoogewerf, A. Meyer, S. Alouani, P. Juillard, R. Buser, F. Conquet, A. E. Proudfoot, T. N. Wells, and C. A. Power. 2000. A key role for CC chemokine receptor 4 in lipopolysaccharide-induced endotoxic shock. *J Exp Med 191:1755.*

177. Zhou, Y., T. Kurihara, R. P. Ryseck, Y. Yang, C. Ryan, J. Loy, G. Warr, and R. Bravo. 1998. Impaired macrophage function and enhanced T cell-dependent immune response in mice lacking CCR5, the mouse homologue of the major HIV-1 coreceptor. *J Immunol 160:4018.*

178. Cook, D. N., D. M. Prosser, R. Forster, J. Zhang, N. A. Kuklin, S. J. Abbondanzo, X. D. Niu, S. C. Chen, D. J. Manfra, M. T. Wiekowski, L. M. Sullivan, S. R. Smith, H. B. Greenberg, S. K. Narula, M. Lipp, and S. A. Lira. 2000. CCR6 mediates dendritic cell localization, lymphocyte homeostasis, and immune responses in mucosal tissue. *Immunity 12:495.*

179. Varona, R., R. Villares, L. Carramolino, I. Goya, A. Zaballos, J. Gutierrez, M. Torres, A. C. Martinez, and G. Marquez. 2001. CCR6-deficient mice have impaired leukocyte homeostasis and altered contact hypersensitivity and delayed-type hypersensitivity responses. *J Clin Invest 107:R37.*

180. Forster, R., A. Schubel, D. Breitfeld, E. Kremmer, I. Renner-Muller, E. Wolf, and M. Lipp. 1999. CCR7 coordinates the primary immune response by establishing functional microenvironments in secondary lymphoid organs. *Cell 99:23.*

181. Chensue, S. W., N. W. Lukacs, T. Y. Yang, X. Shang, K. A. Frait, S. L. Kunkel, T. Kung, M. T. Wiekowski, J. A. Hedrick, D. N. Cook, A. Zingoni, S. K. Narula, A. Zlotnik, F. J. Barrat, A. O'Garra, M. Napolitano, and S. A. Lira. 2001. Aberrant in vivo T helper type 2 cell response and impaired eosinophil recruitment in CC chemokine receptor 8 knockout mice. *J Exp Med 193:573.*

182. Cacalano, G., J. Lee, K. Kikly, A. M. Ryan, S. Pitts Meek, B. Hultgren, W. I. Wood, and M. W. Moore. 1994. Neutrophil and B cell expansion in mice that lack the murine IL-8 receptor homolog. *Science 265:682.*

183. Voigt, I., S. A. Camacho, B. A. de Boer, M. Lipp, R. Forster, and C. Berek. 2000. CXCR5-deficient mice develop functional germinal centers in the splenic T cell zone. *Eur J Immunol 30:560.*

184. Gu, L., S. Tseng, R. M. Horner, C. Tam, M. Loda, and B. J. Rollins. 2000. Control of TH2 polarization by the chemokine monocyte chemoattractant protein-1. *Nature 404:407.*

185. Cook, D. N., M. A. Beck, T. M. Coffman, S. L. Kirby, J. F. Sheridan, I. B. Pragnell, and O. Smithies. 1995. Requirement of MIP-1 alpha for an inflammatory response to viral infection. *Science 269:1583.*

186. Rothenberg, M. E., J. A. MacLean, E. Pearlman, A. D. Luster, and P. Leder. 1997. Targeted disruption of the chemokine eotaxin partially reduces antigen-induced tissue eosinophilia. *J Exp Med 185:785.*

187. Hancock, W. W., W. Gao, V. Csizmadia, K. L. Faia, N. Shemmeri, and A. D. Luster. 2001. Donor-derived ip-10 initiates development of acute allograft rejection. *J Exp Med 193:975.*

188. Cook, D. N., S. C. Chen, L. M. Sullivan, D. J. Manfra, M. T. Wiekowski, D. M. Prosser, G. Vassileva, and S. A. Lira. 2001. Generation and analysis of mice lacking the chemokine fractalkine. *Mol Cell Biol 21:3159.*

189. Lyons, A. B., and C. R. Parish. 1994. Determination of lymphocyte division by flow cytometry. *J Immunol Methods 171:131.*

190. Foulds, K. E., L. A. Zenewicz, D. J. Shedlock, J. Jiang, A. E. Troy, and H. Shen. 2002. Cutting edge: CD4 and CD8 T cells are intrinsically different in their proliferative responses. *J Immunol 168:1528.*

191. Sallusto, F., B. Palermo, A. Hoy, and A. Lanzavecchia. 1999. The role of chemokine receptors in directing traffic of naive, type 1 and type 2 T cells. *Immunol Today. 19(12): 560*

192. Rabin, R. L., M. A. Alston, J. C. Sircus, B. Knollmann-Ritschel, C. Moratz, D. Ngo, and J. M. Farber. 2003. CXCR3 is induced early on the pathway of CD4+ T cell differentiation and bridges central and peripheral functions. *J Immunol 171:2812.*

193. Lanzavecchia, A., and F. Sallusto. 2000. Dynamics of T lymphocyte responses: intermediates, effectors, and memory cells. *Science 290:92.*

194. Cyster, J. G. 1999. Chemokines and cell migration in secondary lymphoid organs. *Science 286:2098.*

195. Kennedy, M. K., L. J. Tan, M. C. Dal Canto, V. K. Tuohy, Z. J. Lu, J. L. Trotter, and S. D. Miller. 1990. Inhibition of murine relapsing experimental autoimmune encephalomyelitis by immune tolerance to proteolipid protein and its encephalitogenic peptides. *J Immunol 144:909.*

196. Ransohoff, R. M., A. Glabinski, and M. Tani. 1996. Chemokines in immune-mediated inflammation of the central nervous system. *Cytokine Growth Factor Rev 7:35.*

197. Linthicum, D. S., and G. A. Hashim. 1984. Delayed-type hypersensitivity to myelin basic proteins in mice susceptible to allergic encephalomyelitis. *Neurochem Res 9:1467.*

198. Robbinson, D., S. Cockle, B. Singh, and G. H. Strejan. 1996. Native, but not genetically inactivated, pertussis toxin protects mice against experimental allergic encephalomyelitis. *Cell Immunol 168:165.*

199. Matsui, M., J. Weaver, A. E. Proudfoot, J. R. Wujek, T. Wei, E. Richer, B. D. Trapp, A. Rao, and R. M. Ransohoff. 2002. Treatment of experimental autoimmune encephalomyelitis with the chemokine receptor antagonist Met-RANTES. *J Neuroimmunol 128:16.*

200. Gratzner, H. G. 1982. Monoclonal antibody to 5-bromo- and 5-iododeoxyuridine: A new reagent for detection of DNA replication. *Science 218:474.*

201. Schittek, B., K. Rajewsky, and I. Forster. 1991. Dividing cells in bone marrow and spleen incorporate bromodeoxyuridine with high efficiency. *Eur J Immunol 21:235.*

202. Sallusto, F., E. Kremmer, B. Palermo, A. Hoy, P. Ponath, S. Qin, R. Forster, M. Lipp, and A. Lanzavecchia. 1999. Switch in chemokine receptor expression upon TCR stimulation reveals novel homing potential for recently activated T cells. *Eur J Immunol 29:2037.*

203. Tough, D., and J. Sprent. Measurement of T and B cell turnover with bromodeoxyuridine. In *Current Protocols in Immunology*. J. Coligan, A. Kruisbeck, D. Margulies, E. Shevach, and W. Strober, eds. Wiley Interscience, New York.

204. Ebert, L. M. 2002. The Regulation of chemokine receptor expression upon T lymphocyte activation. In *Department of Molecular Biosiences*. University of Adelaide, Adelaide, p. 230.

205. Westermann, J., S. Ronneberg, F. J. Fritz, and R. Pabst. 1989. Proliferation of lymphocyte subsets in the adult rat: a comparison of different lymphoid organs. *Eur J Immunol 19:1087.*

206. Lucas, B., F. Vasseur, and C. Penit. 1993. Normal sequence of phenotypic transitions in one cohort of 5-bromo-2'-deoxyuridine-pulse-labeled thymocytes. Correlation with T cell receptor expression. *J Immunol 151:4574.*

207. Gett, A. V., and P. D. Hodgkin. 1998. Cell division regulates the T cell cytokine repertoire, revealing a mechanism underlying immune class regulation. *Proc Natl Acad Sci U S A 95:9488.*

208. Springer, T. A. 1995. Traffic signals on endothelium for lymphocyte recirculation and leukocyte emigration. *Annu Rev Physiol 57:827.*

209. Kuchroo, V. K., C. A. Martin, J. M. Greer, S. T. Ju, R. A. Sobel, and M. E. Dorf. 1993. Cytokines and adhesion molecules contribute to the ability of myelin proteolipid protein-specific T cell clones to mediate experimental allergic encephalomyelitis. *J Immunol 151:4371.*

210. Jiang, Y., M. N. Salafranca, S. Adhikari, Y. Xia, L. Feng, M. K. Sonntag, C. M. deFiebre, N. A. Pennell, W. J. Streit, and J. K. Harrison. 1998. Chemokine receptor expression in cultured glia and rat experimental allergic encephalomyelitis. *J Neuroimmunol 86:1.*

211. Glabinski, A. R., and R. M. Ransohoff. 1999. Chemokines and chemokine receptors in CNS pathology. *J Neurovirol 5:3.*

212. Hickey, W. F., N. K. Gonatas, H. Kimura, and D. B. Wilson. 1983. Identification and quantitation of T lymphocyte subsets found in the spinal cord of the Lewis rat during acute experimental allergic encephalomyelitis. *J Immunol 131:2805.*

213. Cross, A. H., B. Cannella, C. F. Brosnan, and C. S. Raine. 1990. Homing to central nervous system vasculature by antigen-specific lymphocytes. I. Localization of 14C-labeled cells during acute, chronic, and relapsing experimental allergic encephalomyelitis. *Lab Invest 63:162.*

214. Gong, J. H., M. Uguccioni, B. Dewald, M. Baggiolini, and I. Clark-Lewis. 1996. RANTES and MCP-3 antagonists bind multiple chemokine receptors. *J Biol Chem 271:10521.*

215. Butzkueven, H., J. G. Zhang, M. Soilu-Hanninen, H. Hochrein, F. Chionh, K. A. Shipham, B. Emery, A. M. Turnley, S. Petratos, M. Ernst, P. F. Bartlett, and T. J. Kilpatrick. 2002. LIF receptor signaling limits immune-mediated demyelination by enhancing oligodendrocyte survival. *Nat Med 8:613.*

216. Mackay, C. R., W. L. Marston, and L. Dudler. 1990. Naive and memory T cells show distinct pathways of lymphocyte recirculation. *J Exp Med 171:801.*

217. McColl, S. R., S. Mahalingam, M. A. Staykova, L. A. Tylaska, K. E. Fisher, C. A. Strick, R. P. Gladue, K. Neote, and D. O. Willenborg. Expression of rat I-TAC/CXCL11/SCYA11 during central nervous system inflammation: comparison with other CXCR3 ligands. *Laboratory Investigation.*

218. Tedla, N., H. W. Wang, H. P. McNeil, N. Di Girolamo, T. Hampartzoumian, D. Wakefield, and A. Lloyd. 1998. Regulation of T lymphocyte trafficking into lymph nodes during an immune response by the chemokines macrophage inflammatory protein (MIP)-1 alpha and MIP-1 beta. *J Immunol 161:5663.*

219. Tedla, N., P. Palladinetti, M. Kelly, R. K. Kumar, N. DiGirolamo, U. Chattophadhay, B. Cooke, P. Truskett, J. Dwyer, D. Wakefield, and A. Lloyd. 1996. Chemokines and T lymphocyte recruitment to lymph nodes in HIV infection. *Am J Pathol 148:1367.*

220. Tedla, N., P. Palladinetti, D. Wakefield, and A. Lloyd. 1999. Abundant expression of chemokines in malignant and infective human lymphadenopathies. *Cytokine 11:531.*

221. Agace, W. W., A. Amara, A. I. Roberts, J. L. Pablos, S. Thelen, M. Uguccioni, X. Y. Li, J. Marsal, F. Arenzana-Seisdedos, T. Delaunay, E. C. Ebert, B. Moser, and C. M. Parker. 2000. Constitutive expression of stromal derived factor-1 by mucosal epithelia and its role in HIV transmission and propagation. *Curr Biol 10:325.*

222. Dorf, M. E., M. A. Berman, S. Tanabe, M. Heesen, and Y. Luo. 2000. Astrocytes express functional chemokine receptors. *J Neuroimmunol 111:109.*

223. Westmoreland, S. V., J. B. Rottman, K. C. Williams, A. A. Lackner, and V. G. Sasseville. 1998. Chemokine receptor expression on resident and inflammatory cells in the brain of macaques with simian immunodeficiency virus encephalitis. *Am J Pathol 152:659.*

224. Tanabe, S., M. Heesen, I. Yoshizawa, M. A. Berman, Y. Luo, C. C. Bleul, T. A. Springer, K. Okuda, N. Gerard, and M. E. Dorf. 1997. Functional expression of the CXC-chemokine receptor-4/fusin on mouse microglial cells and astrocytes. *J Immunol 159:905.*

225. McGrath, K. E., A. D. Koniski, K. M. Maltby, J. K. McGann, and J. Palis. 1999. Embryonic expression and function of the chemokine SDF-1 and its receptor, CXCR4. *Dev Biol. 213(2): 442*

226. Flynn, G., S. Maru, J. Loughlin, I. A. Romero, and D. Male. 2003. Regulation of chemokine receptor expression in human microglia and astrocytes. *J Neuroimmunol 136:84.*

227. Biber, K., I. Dijkstra, C. Trebst, C. J. De Groot, R. M. Ransohoff, and H. W. Boddeke. 2002. Functional expression of CXCR3 in cultured mouse and human astrocytes and microglia. *Neuroscience 112:487.*

228. Goldberg, S. H., P. van der Meer, J. Hesselgesser, S. Jaffer, D. L. Kolson, A. V. Albright, F. Gonzalez-Scarano, and E. Lavi. 2001. CXCR3 expression in human central nervous system diseases. *Neuropathol Appl Neurobiol 27:127.*

229. Fischer, F. R., L. Santambrogio, Y. Luo, M. A. Berman, W. W. Hancock, and M. E. Dorf. 2000. Modulation of experimental autoimmune encephalomyelitis: effect of altered peptide ligand on chemokine and chemokine receptor expression. *J Neuroimmunol 110:195.*

230. He, J., Y. Chen, M. Farzan, H. Choe, A. Ohagen, S. Gartner, J. Busciglio, X. Yang, W. Hofmann, W. Newman, C. R. Mackay, J. Sodroski, and D. Gabuzda. 1997. CCR3 and CCR5 are co-receptors for HIV-1 infection of microglia. *Nature 385:645.*

231. Horuk, R., A. W. Martin, Z. Wang, L. Schweitzer, A. Gerassimides, H. Guo, Z. Lu, J. Hesselgesser, H. D. Perez, J. Kim, J. Parker, T. J. Hadley, and S. C. Peiper. 1997. Expression of chemokine receptors by subsets of neurons in the central nervous system. *J Immunol 158:2882.*

232. Xia, M. Q., and B. T. Hyman. 1999. Chemokines/chemokine receptors in the central nervous system and Alzheimer's disease. *J Neurovirol 5:32.*

233. Qin, S., J. B. Rottman, P. Myers, N. Kassam, M. Weinblatt, M. Loetscher, A. E. Koch, B. Moser, and C. R. Mackay. 1998. The chemokine receptors CXCR3 and CCR5 mark subsets of T cells associated with certain inflammatory reactions. *J Clin Invest 101:746.*

234. Loetscher, P., M. Uguccioni, L. Bordoli, M. Baggiolini, B. Moser, C. Chizzolini, and J. M. Dayer. 1998. CCR5 is characteristic of Th1 lymphocytes. *Nature 391:344.*

235. Carroll, R. G., J. L. Riley, B. L. Levine, Y. Feng, S. Kaushal, D. W. Ritchey, W. Bernstein, O. S. Weislow, C. R. Brown, E. A. Berger, C. H. June, and D. C. St Louis. 1997. Differential regulation of HIV-1 fusion cofactor expression by CD28 costimulation of CD4+ T cells. *Science 276:273.*

236. Secchiero, P., D. Zella, S. Curreli, P. Mirandola, S. Capitani, R. C. Gallo, and G. Zauli. 2000. Engagement of CD28 modulates CXC chemokine receptor 4 surface expression in both resting and CD3-stimulated CD4+ T cells. *J Immunol 164:4018.*

237. Bleul, C. C., L. Wu, J. A. Hoxie, T. A. Springer, and C. R. Mackay. 1997. The HIV coreceptors CXCR4 and CCR5 are differentially expressed and regulated on human T lymphocytes. *Proc Natl Acad Sci U S A 94:1925.*

238. Schabath, R., G. Muller, A. Schubel, E. Kremmer, M. Lipp, and R. Forster. 1999. The murine chemokine receptor CXCR4 is tightly regulated during T cell development and activation. *J Leukoc Biol 66:996.*

239. Bermejo, M., J. Martin-Serrano, E. Oberlin, M. A. Pedraza, A. Serrano, B. Santiago, A. Caruz, P. Loetscher, M. Baggiolini, F. Arenzana-Seisdedos, and J. Alcami. 1998. Activation of blood T lymphocytes down-regulates CXCR4 expression and interferes with propagation of X4 HIV strains. *Eur J Immunol 28:3192.*

240. Potsch, C., D. Vohringer, and H. Pircher. 1999. Distinct migration patterns of naive and effector CD8 T cells in the spleen: correlation with CCR7 receptor expression and chemokine reactivity. *Eur J Immunol 29:3562.*

241. Ansel, K. M., L. J. McHeyzer-Williams, V. N. Ngo, M. G. McHeyzer-Williams, and J. G. Cyster. 1999. In vivo-activated CD4 T cells upregulate CXC chemokine receptor 5 and reprogram their response to lymphoid chemokines. *J Exp Med 190:1123.*

242. Barnes, D. A., J. Tse, M. Kaufhold, M. Owen, J. Hesselgesser, R. Strieter, R. Horuk, and H. D. Perez. 1998. Polyclonal antibody directed against human RANTES ameliorates disease in the Lewis rat adjuvant-induced arthritis model. *J Clin Invest 101:2910.*

243. Fife, B. T., M. C. Paniagua, N. W. Lukacs, S. L. Kunkel, and W. J. Karpus. 2001. Selective CC chemokine receptor expression by central nervous system-infiltrating encephalitogenic T cells during experimental autoimmune encephalomyelitis. *J Neurosci Res 66:705.*

244. Ridgway, W., M. Fasso, and C. G. Fathman. 1998. Following antigen challenge, T cells up-regulate cell surface expression of CD4 in vitro and in vivo. *J Immunol 161:714.*

245. Center, D. M., H. Kornfeld, T. C. Ryan, and W. W. Cruikshank. 2000. Interleukin 16: implications for CD4 functions and HIV-1 progression. *Immunol Today 21:273.*

246. Baggiolini, M., and B. Moser. 1997. Blocking chemokine receptors. *J Exp Med 186:1189.*

247. Moser, B., B. Dewald, L. Barella, C. Schumacher, M. Baggiolini, and I. Clark Lewis. 1993. Interleukin-8 antagonists generated by N-terminal modification. *J Biol Chem 268:7125.*

248. Cole, K. E., C. A. Strick, T. J. Paradis, K. T. Ogborne, M. Loetscher, R. P. Gladue, W. Lin, J. G. Boyd, B. Moser, D. E. Wood, B. G. Sahagan, and K. Neote. 1998. Interferon-inducible T cell alpha chemoattractant (I-TAC): a novel non-ELR CXC chemokine with potent activity on activated T cells through selective high affinity binding to CXCR3. *J Exp Med 187:2009.*

249. Cox, M. A., C. H. Jenh, W. Gonsiorek, J. Fine, S. K. Narula, P. J. Zavodny, and R. W. Hipkin. 2001. Human interferon-inducible 10-kDa protein and human interferon-inducible T cell alpha chemoattractant are allotopic ligands for human CXCR3: differential binding to receptor states. *Mol Pharmacol 59:707.*

250. Meyer, M., P. J. Hensbergen, E. M. van der Raaij-Helmer, G. Brandacher, R. Margreiter, C. Heufler, F. Koch, S. Narumi, E. R. Werner, R. Colvin, A. D. Luster, C. P. Tensen, and G. Werner-Felmayer. 2001. Cross reactivity of three T cell attracting murine chemokines stimulating the CXC chemokine receptor CXCR3 and their induction in cultured cells and during allograft rejection. *Eur J Immunol 31:2521.*

251. Matthys, P., S. Hatse, K. Vermeire, A. Wuyts, G. Bridger, G. W. Henson, E. De Clercq, A. Billiau, and D. Schols. 2001. AMD3100, a potent and specific antagonist of the stromal cell-derived factor-1 chemokine receptor CXCR4, inhibits autoimmune joint inflammation in IFN-gamma receptor-deficient mice. *J Immunol 167:4686.*

252. Buckley, C. D., N. Amft, P. F. Bradfield, D. Pilling, E. Ross, F. Arenzana-Seisdedos, A. Amara, S. J. Curnow, J. M. Lord, D. Scheel-Toellner, and M. Salmon. 2000. Persistent induction of the chemokine receptor CXCR4 by TGF-beta 1 on synovial T cells contributes to their accumulation within the rheumatoid synovium. *J Immunol 165:3423.*

253. Nanki, T., K. Hayashida, H. S. El-Gabalawy, S. Suson, K. Shi, H. J. Girschick, S. Yavuz, and P. E. Lipsky. 2000. Stromal cell-derived factor-1-CXC chemokine receptor 4 interactions play a central role in CD4+ T cell accumulation in rheumatoid arthritis synovium. *J Immunol 165:6590.*

254. Wyss-Coray, T., P. Borrow, M. J. Brooker, and L. Mucke. 1997. Astroglial overproduction of TGF-beta 1 enhances inflammatory central nervous system disease in transgenic mice. *J Neuroimmunol 77:45.*

255. Han, Y., T. He, D. R. Huang, C. A. Pardo, and R. M. Ransohoff. 2001. TNF-alpha mediates SDF-1 alpha-induced NF-kappa B activation and cytotoxic effects in primary astrocytes. *J Clin Invest 108:425.*

256. Dutt, P., J. F. Wang, and J. E. Groopman. 1998. Stromal cell-derived factor-1 alpha and stem cell factor/kit ligand share signaling pathways in hemopoietic progenitors: a potential mechanism for cooperative induction of chemotaxis. *J Immunol 161:3652.*

257. Misse, D., P. O. Esteve, B. Renneboog, M. Vidal, M. Cerutti, Y. St Pierre, H. Yssel, M. Parmentier, and F. Veas. 2001. HIV-1 glycoprotein 120 induces the MMP-9 cytopathogenic factor production that is abolished by inhibition of the p38 mitogen-activated protein kinase signaling pathway. *Blood 98:541.*

258. Ganju, R. K., S. A. Brubaker, J. Meyer, P. Dutt, Y. Yang, S. Qin, W. Newman, and J. E. Groopman. 1998. The alpha-chemokine, stromal cell-derived factor-1alpha, binds to the transmembrane G-protein-coupled CXCR-4 receptor and activates multiple signal transduction pathways. *J Biol Chem 273:23169.*

259. Schneider, H., Y. C. Cai, D. Cefai, M. Raab, and C. E. Rudd. 1995. Mechanisms of CD28 signalling. *Res Immunol 146:149.*

260. Alegre, M. L., K. A. Frauwirth, and C. B. Thompson. 2001. T-cell regulation by CD28 and CTLA-4. *Nat Rev Immunol 1:220.*

261. Liu, M. T., B. P. Chen, P. Oertel, M. J. Buchmeier, D. Armstrong, T. A. Hamilton, and T. E. Lane. 2000. The T cell chemoattractant IFN-inducible protein 10 is essential in host defense against viral-induced neurologic disease. *J Immunol 165:2327.*

262. Khan, I. A., J. A. MacLean, F. S. Lee, L. Casciotti, E. DeHaan, J. D. Schwartzman, and A. D. Luster. 2000. IP-10 is critical for effector T cell trafficking and host survival in Toxoplasma gondii infection. *Immunity 12:483.*

263. Kaufmann, A., R. Salentin, D. Gemsa, and H. Sprenger. 2001. Increase of CCR1 and CCR5 expression and enhanced functional response to MIP-1 alpha during differentiation of human monocytes to macrophages. *J Leukoc Biol 69:248.*

264. Liang, M., C. Mallari, M. Rosser, H. P. Ng, K. May, S. Monahan, J. G. Bauman, I. Islam, A. Ghannam, B. Buckman, K. Shaw, G. P. Wei, W. Xu, Z. Zhao, E. Ho, J. Shen, H. Oanh, B. Subramanyam, R. Vergona, D. Taub, L. Dunning, S. Harvey, R. M. Snider, J. Hesselgesser, M. M. Morrissey, and H. D. Perez. 2000. Identification and characterization of a potent, selective, and orally active antagonist of the CC chemokine receptor-1. *J Biol Chem 275:19000.*

265. Lane, T. E., M. T. Liu, B. P. Chen, V. C. Asensio, R. M. Samawi, A. D. Paoletti, I. L. Campbell, S. L. Kunkel, H. S. Fox, and M. J. Buchmeier. 2000. A central role for CD4(+) T cells and RANTES in virus-induced central nervous system inflammation and demyelination. *J Virol 74:1415.*

266. Banchereau, J., and R. M. Steinman. 1998. Dendritic cells and the control of immunity. *Nature 392:245.*

267. Glabinski, A. R., M. Tani, V. K. Tuohy, R. J. Tuthill, and R. M. Ransohoff. 1995. Central nervous system chemokine mRNA accumulation follows initial leukocyte entry at the onset of acute murine experimental autoimmune encephalomyelitis. *Brain Behav Immun 9:315.*

268. Opferman, J. T., B. T. Ober, and P. G. Ashton-Rickardt. 1999. Linear differentiation of cytotoxic effectors into memory T lymphocytes. *Science 283:1745.*

269. Ahmed, R., and D. Gray. 1996. Immunological memory and protective immunity: understanding their relation. *Science 272:54.*

270. Owens, T., Tran, E., Hassan-Zahraee, M. and Krakowski, M. 1998. Immune cell entry to the CNS – a focus for immunoregulation of EAE. *Res Immunol 149(9):781.*

Thesis amendments (response to reviewers' comments)

Reviewer 1:Richard M. Ransohoff

a) pg 6, line 9-10: replace '…….- ELR containing chemokines are angiogenic, …..' with '…….- ELR containing chemokines are weakly angiogenic, …..'

b) pg 12 et seq: Note that traditional and systematic nomenclature are described in Table 1.1. See pg 7, line 1 for explanation regarding use of traditional nomenclature.

c) pg 16, line 17-18: replace '……the plt/plt (paucity of lymphoid tissue) mouse, which lacks both SLC/CCL21 and ELC/CCL19, and in CCR7 knockout mice.' with '……the plt/plt (paucity of lymphoid tissue) mouse, which lacks ELC/CCL19 and one copy of SLC/CCL21, and in CCR7 knockout mice.'

d) pg 16, line 23: replace '….has been documented in the mouse since deletion of CXCR4 is embryologically lethal…..' with '….has been documented in the mouse since deletion of CXCR4 is perinatally lethal…..'

e) pg 18, line 2: replace 'Additionally, the cerebral spinal fluid (CSF) is enriched in $CD4^+$ T cells expressing CXCR3, CCR5 and CCR6, suggesting that these receptors may be involved in extravasation across the BBB (96).' with 'Additionally, the cerebral spinal fluid (CSF) is enriched in $CD4^+$ T cells expressing CXCR3, suggesting that this receptor may be involved in extravasation across the BBB (96).'

f) pg 22, line 17: replace '…..(cells capable of inducing myelitis)' with '…..(cells capable of inducing encephalitis)'

g) pg 25, line 9: proceeding 'Many studies have shown that for efficient induction, treatment with extracts of *Bordatella pertussis* is also required' cite reference Blankenhorn EP, Butterfield RJ, Rigby R, Cort L, Giambrone D, McDermott P, McEntee K, Solowski N, Meeker ND, Zachary JF, Doerge RW, and Teuscher C. 2000. Genetic analysis of the influence of pertussis toxin on experimental allergic encephalomyelitis susceptibility: an environmental agent can override genetic checkpoints. *J Immunol 164(6):3420.*

h) Table 1.5: the term 'peripheral memory' in Table 1.5 refers to T effector memory (T_{EM}) cells, see page 18, paragraph 3.

i) Table 1.6: Note that CCR1 and CCR8 are both found in MS tissues; CCR1 and CCR7 are both found on CSF cells. Also there is a reduction in CCL2/MCP-1 levels during attacks.

j) Table 1.7: Please refer to footnote 2. '…..In general, where numerous studies have used a particular knock-out mouse, only the basic characterisation of the phenotype is described. Additionally, where determined, the effect of the knock-out on the development of EAE is described.'

k) Chapter 3, section 3.2.2.2: RT-PCR experiments were preliminary studies for receptors that would be examined in further detail at the level of protein. For this purpose, the house-keeping gene GAPDH was used.

l) Fig 3.5(B): Every experimental sample had its own internal isotype control. Thus, the representative plot from the PBS/CFA has been gated according to isotype control from the same representative animal. The data are referred to on page 100, but are discussed in detail on page 69-70.

m) Fig 3.13 (B-D): In this figure, the $CD4^{hi}$ population was electronically gated. Thus, the representative density plots demonstrate chemokine receptor expression on divided and undivided $CD4^{hi}$ T cells.

n) pg 98, line 7: replace '...present in CNS that had been immunised with PLP in CFA...' with '...present in the CNS of mice that had been immunised with PLP in CFA...'

o) and p) no comment required

q) Expression of CCR1, CCR2, CCR5 and CCR8 by mononuclear phagocytes is discussed in Chapter 7, section 7.6.3.

r) Relating to Figs 4.5, 4.6 and 4.7: the predominance of CXCR4>CXCR3=CCR5 $CD4^+$ T cells in the preclinical (day 9) CNS infiltrate indicates that naïve $CD4^+$ T cells are infiltrating the CNS as effectively as effector cells. This may reflect the breakdown of the blood brain barrier. This is discussed in more detail Chapter 4, pages 100-101.

s) Relating to Fig 4.9: There was a substantial BrdU+/CD8+ infiltrate in the spinal cords of mice with EAE. CD8+ T cells have previously been observed in both EAE and MS tissue and are likely to contribute to tissue destruction. Since CD8+ T cells were not the focus of the present study, their role in CNS inflammation was not examined in further detail.

t) In 5.2.2.2 and 5.2.2.3, peptide was administered intraperitonealy every second day, as stated in detail in Section 2.2.4.

u) pg 113, line 15-16: replace 'The difference in mean maximum clinical disease score of the RANTES 9-68-treated mice was ~1.3-fold lower than that of the control-treated cohort.' with 'The mean maximum clinical disease score of the RANTES 9-68-treated mice was ~1.3-fold lower than that of the control-treated cohort.'

v) The antagonists were tested at excess and found not to stimulate cells directly (and therefore did not desensitize the cells). Furthermore, there was no sign of aggregation with respect to the antagonists

w) Chapter 5, sections 5.2.2.2-5.2.2.4 and Table 5.1: Mean maximum clinical disease score refers to the average of the highest disease score of each group during the course of the experiment, effectively indicating the degree of disease progression in each group. With respect to the values presented in Table 5.1 (column 3), these numbers represent an attempt to quantitatively compare the differences in severity of the disease in each group.

x) One-tail p values were used in certain analyses when it was predicted which group would have the larger mean prior to data collection. In those instances, the analyses confirmed the experimental hypotheses.

y) All EAE experiments were performed with an observer who was unaware of treatment status.

aa) Neutralising antibodies did not account in part for the limited efficacy of the antagonists as discussed on pages 119-121.

bb) Will be done in future experiments.

cc) no comment required.

dd) 'Importantly, however, with exception to Ebert *et al.* (2002), while these studies suggest that activated T cells expressing CCR5 and CXCR3 are associated with sites of immune activation, they do not provide evidence that these receptors are acquired during T cell activation.' with 'Importantly, however, with exception to the results presented in this thesis and Ebert *et al.* (2002), while these studies suggest that activated T cells expressing CCR5 and CXCR3 are associated with sites of immune activation, they do not provide evidence that these receptors are acquired during T cell activation.'

ee) pg 151-152: desensitisation issues addressed in point v).

ff) See new Fig 7.1.

Reviewer 2: Ranjeny Thomas

1) Fig 3.2 (B): There was no significant difference in the results obtained compared with those from CFA alone.

2) Statistics: Please refer to point x) above with respect to the use of one-tailed p values. The results referred to are biologically significant, since these data are demonstrating the difference between an animal that has partial tail paralysis and an animal that lacks the capacity to walk.

3) pg 85: Insert 'That is, only restimulated cells migrated to the lower chamber of the transwell in response to the CXCR3 ligands.' behind 'Chemotaxis assays confirmed these predictions to a certain extent, however, it appears that further restimulation *in vitro* is required for a functional response to the CXCR3 ligands, IP-10/CXCL10 and I-TAC/CXCL11.'

4) Fig 4.4 (A): Staining with the control antibodies demonstrates that there is background staining, which is discussed on page 93-94. These immunofluorescence data are not quantitative.